ATOMIC CLUSTERS: THEORY & EXPERIMENTS

EDITED BY: Ambrish Kumar Srivastava, Iwona Anusiewicz, Neeraj Misra, Suzana Velickovic and Wei-Ming Sun

PUBLISHED IN: Frontiers in Chemistry and Frontiers in Physics

frontiers Research Topics

ISSN 1664-8714
ISBN 978-2-88971-920-4
DOI 10.3389/978-2-88971-920-4

About Frontiers

Frontiers is more than just an open-access publisher of scholarly articles: it is a pioneering approach to the world of academia, radically improving the way scholarly research is managed. The grand vision of Frontiers is a world where all people have an equal opportunity to seek, share and generate knowledge. Frontiers provides immediate and permanent online open access to all its publications, but this alone is not enough to realize our grand goals.

Frontiers Journal Series

The Frontiers Journal Series is a multi-tier and interdisciplinary set of open-access, online journals, promising a paradigm shift from the current review, selection and dissemination processes in academic publishing. All Frontiers journals are driven by researchers for researchers; therefore, they constitute a service to the scholarly community. At the same time, the Frontiers Journal Series operates on a revolutionary invention, the tiered publishing system, initially addressing specific communities of scholars, and gradually climbing up to broader public understanding, thus serving the interests of the lay society, too.

Dedication to Quality

Each Frontiers article is a landmark of the highest quality, thanks to genuinely collaborative interactions between authors and review editors, who include some of the world's best academicians. Research must be certified by peers before entering a stream of knowledge that may eventually reach the public - and shape society; therefore, Frontiers only applies the most rigorous and unbiased reviews.
Frontiers revolutionizes research publishing by freely delivering the most outstanding research, evaluated with no bias from both the academic and social point of view. By applying the most advanced information technologies, Frontiers is catapulting scholarly publishing into a new generation.

What are Frontiers Research Topics?

Frontiers Research Topics are very popular trademarks of the Frontiers Journals Series: they are collections of at least ten articles, all centered on a particular subject. With their unique mix of varied contributions from Original Research to Review Articles, Frontiers Research Topics unify the most influential researchers, the latest key findings and historical advances in a hot research area! Find out more on how to host your own Frontiers Research Topic or contribute to one as an author by contacting the Frontiers Editorial Office: frontiersin.org/about/contact

ATOMIC CLUSTERS: THEORY & EXPERIMENTS

Topic Editors:
Ambrish Kumar Srivastava, Deen Dayal Upadhyay Gorakhpur University, India
Iwona Anusiewicz, University of Gdansk, Poland
Neeraj Misra, University of Lucknow, India
Suzana Velickovic, University of Belgrade, Serbia
Wei-Ming Sun, Fujian Medical University, China

Citation: Srivastava, A. K., Anusiewicz, I., Misra, N., Velickovic, S., Sun, W.-M., eds. (2021). Atomic Clusters: Theory & Experiments. Lausanne: Frontiers Media SA. doi: 10.3389/978-2-88971-920-4

Table of Contents

frontiers in Chemistry

EDITORIAL
published: 01 November 2021
doi: 10.3389/fchem.2021.795113

Editorial: Atomic Clusters: Theory & Experiments

Ambrish Kumar Srivastava[1]*, *Iwona Anusiewicz*[2], *Suzana Velickovic*[3], *Wei-Ming Sun*[4] and *Neeraj Misra*[5]

[1]Department of Physics, Deen Dayal Upadhyaya Gorakhpur University, Gorakhpur, India, [2]Department of Chemistry, University of Gdansk, Gdansk, Poland, [3]Department of Physical Chemistry, Vinča Institute of Nuclear Science, University of Belgrade, Belgrade, Serbia, [4]Department of Basic Chemistry, Fujian Medical University, Fuzhou, China, [5]Department of Physics, University of Lucknow, Lucknow, India

Keywords: atomic clusters, theory, superatom, fullerene, nanostructure

Editorial on the Research Topic

Atomic Clusters: Theory & Experiments

Atomic clusters are finite aggregates of atoms, varying in size from a few Angstrom to a few nanometers. The importance of atomic clusters lies in the fact that they possess very unique properties, which are sometimes, quite different than their bulk analogs. Due to advancements in theory and instrumentation along with the aid of powerful computers, the research and development in this field are greatly accelerated. The topic "*Atomic Clusters: Theory & Experiments*" provide a compilation of the recent progress made in this very exciting field of research. This topic consists of two review and seven research articles on various themes, which are outlined below.

Pal et al. reviewed the various aspects of atomic clusters. They discussed the structures of certain atomic clusters such as noble gas encapsulated B_{40} cage, small molecule encapsulated octa acid, $(HF)_2$ confined fullerenes, etc. using different machine learning techniques. The bonding and reactivity of these clusters were discussed with the help of the quantum theory of atoms in molecule (QTAIM) and conceptual density functional theory (CDFT). Srivastava reviewed various optimization algorithms such as genetic algorithm (GA), basin-hopping (BH) method and its variants, heuristic algorithm combined with the surface and interior operators (HA-SIO), fast annealing evolutionary algorithm (FAEA), random tunneling algorithm (RTA), and dynamic lattice searching (DLS) to obtain the global minimum structures of the different type clusters such as pure metallic clusters, bimetallic clusters, trimetallic and tetrametallic clusters, fullerene-like clusters, and dipolar clusters.

Zhou et al. introduced a newly developed NKCS python code based on xTB local optimization and BH global search algorithm. They obtained global minimum structures of the cations of phosphorus clusters, P_{2n+1}^+ for n = 1–15 in which the pnicogen bonds play an important role in the stabilization of clusters and identified P_{29}^+ and P_{31}^+ as the most stable isomers. Their results showed that the NKCS program is effective and robust in searching global minimum structures for atomic clusters. Shi et al. searched the lowest-energy structures of hydrated calcium ion clusters $Ca^{2+}(H_2O)_n$ (n = 10–18) in the whole potential energy surface by the comprehensive genetic algorithm (CGA) combined with DFT. Their theoretical results could provide useful guidance for analyzing the hydrated calcium ion clusters in experiments, and are of fundamental importance for an in-depth understanding of the microscopic interactions between Ca^{2+} and water molecules in aqueous environments.

Jiang et al. examined the stability of two transition metal boron clusters Sc_2B_8 and Y_2B_8 in the inverse sandwich configuration via first-principle calculations combined with a comprehensive genetic algorithm (CGA). It is confirmed that such novel structures are the lowest-energy isomers and can be extended to 1D nanowires (NWs). They revealed that both theoretically designed 1D-Sc_4B_{24} and 1D-Y_2B_{12} nanowires are nonmagnetic such that the former NW is a direct-band-gap

OPEN ACCESS

Edited and reviewed by:
Moyuan Cao,
Tianjin University, China

***Correspondence:**
Ambrish Kumar Srivastava
ambrishphysics@gmail.com

Specialty section:
This article was submitted to Physical Chemistry and Chemical Physics, a section of the journal Frontiers in Chemistry

Received: *14 October 2021*
Accepted: *18 October 2021*
Published: *01 November 2021*

Citation:
Srivastava AK, Anusiewicz I, Velickovic S, Sun W-M and Misra N (2021) Editorial: Atomic Clusters: Theory & Experiments. Front. Chem. 9:795113. doi: 10.3389/fchem.2021.795113

semiconductor, whereas the latter one is a metal. Tiznado et al. investigated the stability of the isolated silicon-lithium nanowire (Li_6Si_5-NW) assembled from stacking the Li_6Si_5 units as well as its electronic properties by using DFT methods and Born-Oppenheimer *ab initio* molecular dynamic simulations. They studied the possibility of using carbon nanotubes (CNTs) as an alternative way to stabilize thus obtained 1D Li_6Si_5-NW by stacking Li_6Si_5 units one above another and confirmed its metallic character. They found that finite $(Li_6Si_5)_4$ systems are stable inside both armchair and zigzag CNTs which supports the hypothesis of possible formation of Li_6Si_5-NW in CNTs.

Yu et al. reported an osmium-centered aromatic cluster of boron, OsB_9^- using DFT and QTAIM approaches. They described the structure, energetics, electron delocalization as well as photoelectron spectrum. Their findings suggested that the dual $\sigma + \pi$ aromaticity is a key factor to design highly stable borometallic molecular wheels. Meloni et al. studied Li_3F_2 superalkali encapsulated C_{60} fullerene by DFT and found that this endofullerene is stable. They noticed that the CO_2 molecule can be activated by trapping within this endofullerene. During the activation, an F atom of Li_3F_2 is bonded to the CO_2, unlike a simple electron transfer process. These findings suggested the activation of CO_2 at the nanoscale. Qasemnazhand et al. investigated the structure of sila-fulleranes (Si_nH_n; n = 20–60) and the interaction of $Si_{20}H_{20}$ with glycoprotein. They compared the electronic absorption spectrum of pure $Si_{20}H_{20}$ with those interacting with glycoproteins through O- and N-links. They suggested that the optical response of sila-fullerane changes when it interacts with viral spikes and therefore, it acts as a sensor for monitoring the environment.

Thus, the topic covers the articles on a variety of themes such as non-metallic clusters, metallic clusters, nanowires, fullerenes, etc. and introduces the readers to the current status in this rapidly growing field of research. We, the editors, thank all the authors for contributing to this topic as well as reviewers for their voluntary support. We believe that the contents of the topic will benefit the scientific community at large.

AUTHOR CONTRIBUTIONS

All authors listed have made a substantial, direct, and intellectual contribution to the work and approved it for publication.

Conflict of Interest: The authors declare that the research was conducted in the absence of any commercial or financial relationships that could be construed as a potential conflict of interest.

Publisher's Note: All claims expressed in this article are solely those of the authors and do not necessarily represent those of their affiliated organizations, or those of the publisher, the editors and the reviewers. Any product that may be evaluated in this article, or claim that may be made by its manufacturer, is not guaranteed or endorsed by the publisher.

frontiers in Chemistry

REVIEW
published: 12 March 2021
doi: 10.3389/fchem.2021.637286

Application of Optimization Algorithms in Clusters

Ruby Srivastava *†

Bioinformatics, CSIR-Centre for Cellular and Molecular Biology, Hyderabad, India

The structural characterization of clusters or nanoparticles is essential to rationalize their size and composition-dependent properties. As experiments alone could not provide complete picture of cluster structures, so independent theoretical investigations are needed to find out a detail description of the geometric arrangement and corresponding properties of the clusters. The potential energy surfaces (PES) are explored to find several minima with an ultimate goal of locating the global minima (GM) for the clusters. Optimization algorithms, such as genetic algorithm (GA), basin hopping method and its variants, self-consistent basin-to-deformed-basin mapping, heuristic algorithm combined with the surface and interior operators (HA-SIO), fast annealing evolutionary algorithm (FAEA), random tunneling algorithm (RTA), and dynamic lattice searching (DLS) have been developed to solve the geometrical isomers in pure elemental clusters. Various model or empirical potentials (EPs) as Lennard–Jones (LJ), Born–Mayer, Gupta, Sutton–Chen, and Murrell–Mottram potentials are used to describe the bonding in different type of clusters. Due to existence of a large number of homotops in nanoalloys, genetic algorithm, basin-hopping algorithm, modified adaptive immune optimization algorithm (AIOA), evolutionary algorithm (EA), kick method and Knowledge Led Master Code (KLMC) are also used. In this review the optimization algorithms, computational techniques and accuracy of results obtained by using these mechanisms for different types of clusters will be discussed.

Keywords: global optimization, potential energy landscape, clusters, empirical potentials, homotops

OPEN ACCESS

Edited by:
Suzana Velickovic,
University of Belgrade, Serbia

Reviewed by:
William Tiznado,
Andres Bello University, Chile
Wensheng Cai,
Nankai University, China

****Correspondence:***
Ruby Srivastava
amitruby1@gmail.com

†ORCID:
Ruby Srivastava
orcid.org/0000-0002-2367-0176

Specialty section:
This article was submitted to Theoretical and Computational Chemistry, a section of the journal Frontiers in Chemistry

Received: *03 December 2020*
Accepted: *21 January 2021*
Published: *12 March 2021*

Citation:
Srivastava R (2021) Application of Optimization Algorithms in Clusters. Front. Chem. 9:637286. doi: 10.3389/fchem.2021.637286

INTRODUCTION

Nanoclusters are considered as a collection of ~10 to 10^6 atoms or molecules within a nanometre size range (Lesley and Johnston, 2000; Johnston, 2002) such as fullerenes, metal clusters, molecular clusters and ionic clusters (Jellinek, 1999; Baletto and Ferrando, 2005). Nanometre-size clusters are both crystalline (face-centred cubic (fcc), octahedra or truncated octahedral (TO)) and noncrystalline (icosahedra, decahedra, polytetrahedra and polyicosahedra) structures. The small size nanoclusters exist in noncrystalline shapes. The noble and transition metals are dominated with icosahedra and Marks truncated decahedra structures (Martin, 1996). These structures are not favourable for large clusters due to the strain arising from their noncrystalline packing (Baletto and Ferrando, 2005). However the strain can be released by placing a smaller atom in the core of the nanoalloy (Rossi et al., 2004) as the strain is proportional to the cluster volume. The quantized electronic energy levels of clusters give rise to atomic-like character (Halperin, 1986; Ralph et al., 1995) and this phenomenon is used to enhance the optical and electrical properties of some clusters (Heath, 1995; Papavassiliou, 1979). Advancement in modern research occur with nanoalloy composition (Ferrando et al., 2008; Oderji and Ding, 2011; Liu et al., 2005) and chemical

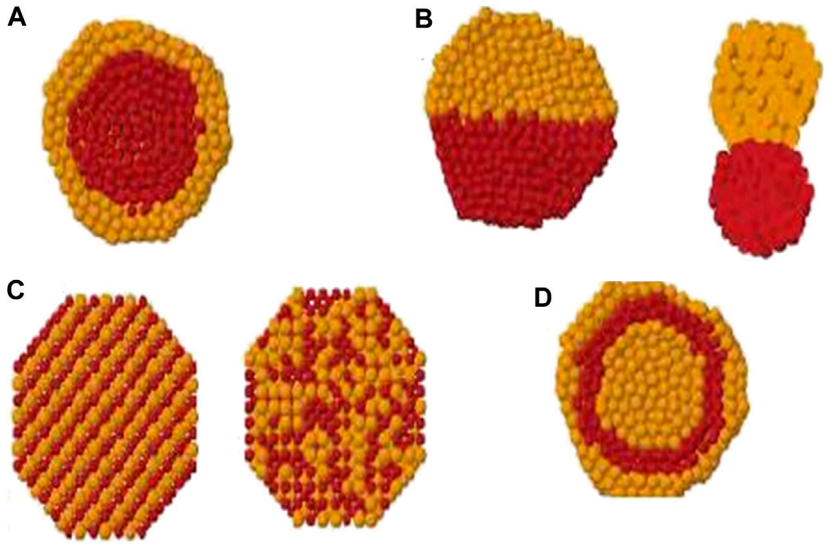

FIGURE 1 | Cross section view of **(A)** core-shell, **(B)** subcluster segregated, **(C)** mixed and **(D)** multishell patterns. (Ismail, 2012).

ordering patterns (Scott et al., 2004; Chen et al., 2005; Knudsen et al., 2007; Maksimuk et al., 2007; Ye and Crooks, 2007; Teng and Yang, 2003) in addition to the size, atomic order and structure. Chemical ordering depends upon structure, size and composition, among others (Johnston, 2003). See **Figure 1**. The theoretical studies for clusters are far cheaper than the experimental trial-and-error approaches, and led to conclusion by following parameters; heat of formation, energies, structural mechanisms, transition states (TS) mechanisms, and molecular spectra analysis (Foresman and Frisch, 1996). Various groups have explored these properties for the generation and characterization of the atomic clusters (Cabaleiro-Lago et al., 2000; Marques and Pereira, 2010a; Marques and Pereira, 2013; Marques and Pereira, 2013, Marques et al., 2018; Bartolomei et al., 2015).

The PES is explored to locate the GM for the smaller clusters by different approaches. Electronic structure of these clusters can be defined by either *ab initio* Molecular Orbital (MO) or semi-empirical atomistic potentials (Wales and Scheraga, 1999; Johnston, 2002). GM structure is the most preferred structure though other metastable structures are also observed due to kinetic effects. A*b initio* method are feasible for the smaller systems (tens of atoms) as it is based on the laws of quantum mechanics, atomic, electronic properties and few other physical constants. In this method, the system is studied either by short single-point energy calculation or by geometrically relax the system for more stable configuration. The empirical or semi-empirical methods are used for the medium sized systems. As *ab initio* methods are computationally demanding so empirical methods are used as an alternative, but empirical methods are not found to be accurate to encounter hydrogen-bonding, chemical transitions or nitrated compounds (Akutsu et al., 1991; Cook, 2005). Further compared to pure elemental clusters, the existence of homotops complicates nanoalloys studies. The conformational stability of clusters is carried out by the global minima and transition states being stationary points with zero potential gradients. Local minima is obtained by the rise in potential energy for any infinitesimal displacement of internal coordinates, where there is a Hessian with positive (second derivative matrix) eigenvalue for the transition states.

GA is considered as a better and popular choice in clusters compared to Monte Carlo (MC) and Molecular Dynamics (MD) Simulated Annealing method. The other techniques are evolution strategies, differential evolution, genetic programming, evolutionary programming, gene expression programming, neuro-evolution, learning classifier systems. Xiao and Williams (Xiao and Williams, 1993) used the GA approach for the molecular clusters (benzene, naphthalene and anthracene) in 1990's. Then Hartke (Hartke, 1993) reported the genetic algorithms for global optimization of molecular clusters. The binary encoded geometries and bitwise acting genetic operators on binary strings were reported by Xiao et al. (Xiao and Williams, 1993). Further these binary encoding and decoding were replaced by applying cartesian coordinates on GA approach (Zeiri, 1995). A significant contribution was made by Deaven and Ho (Deaven and Ho, 1995) in which gradient-driven local minimization was implemented for the cluster energy. Birmingham Cluster Genetic Algorithm (BCGA) in house GA was developed by Wales group for Morse clusters (Roberts et al., 2000), fullerenes (Johnston, 2003), ionic clusters (Roberts and Johnston, 2001), water clusters (Guimaraes et al., 2002), metal clusters (Lloyd et al., 2002) and bimetallic clusters (Bailey et al., 2003; Lordeiro et al., 2003). BHMC algorithm is based on the MC minimization or BH algorithm (Li and Scheraga, 1987) in which PES is simplified by the transformation of energy which results in a smoother landscape. So these methods are also known as hypersurface deformation (Stillinger and Weber, 1988). In 2005 Karaboga (Karaboga, 2005) proposed artificial bee colony (ABC) algorithm which was very efficient in locating global minima for long range potentials. The ABC algorithm was successfully

TABLE 1 | Gupta potential parameters used for the four (Pt, Pd, Ag, Au) coinage metals. (Srivastava, 2017b).

Compositions	A_{ij} (eV)	ξ_{ij} (eV)	p_{ij}	q_{ij}	$r_{ij}^{(0)}$ (Å)
Pt-Pt	0.2975	2.6950	10.612	4.004	2.7747
Pt-Pd	0.2300	2.2000	10.740	3.870	2.7600
Pd-Pd	0.1746	1.7180	10.867	3.742	2.7485
Ag-Ag	0.1028	1.1780	10.928	3.139	2.8885
Ag-Au	0.1490	1.4874	10.494	3.607	2.8864
Au-Au	0.2061	1.7900	10.229	4.036	2.8843
Au-Pt	0.2500	2.2000	10.420	4.020	2.8300
Ag-Pd	0.1607	1.5597	10.895	3.492	2.8230
Ag-Pt	0.1750	1.7900	10.730	3.590	2.8330
Au-Pd	0.2764	2.0820	10.569	3.913	2.8160

applied to the atomic clusters (Zhang and Dolg, 2015) and rigid molecules with corresponding ABCluster software (Zhang and Dolg, 2016). Particle swarm optimization (Call et al., 2007), stochastic surface walking (Shang and Liu, 2013), kick method (Saunders, 1987; Bera et al., 2007; Addicoat and Metha, 2009; Zhai et al., 2015) and GIGA (Jäger et al., 2019) have shown good performance for various chemical systems.

Various model or empirical potentials (EPs) are used to describe the bonding in these clusters. It was observed that global minimum configurations show different symmetries for Sutton Chen potentials and Lennard-Jones potentials. The Sutton-Chen potential is a Finnis-Sinclair type potential with two terms providing the pair-wise repulsive and approximate many-body cohesive contributions separately. Gupta potential is a semi-empirical potential derived within the tight-binding second-moment approximation. It is highly recommended for metallic systems (Gupta, 1981) with inter-atomic interactions. This potential function is applied to describe homonuclear and heteronuclear interactions. The parameters used for this potential is given in **Table 1** from the work carried out by Srivastava (Srivastava, 2017a) for (Au_m-Ag_n-Pd_o-Pt_p) (m = 10 and n + o + p = 10) tetrametallic clusters. A, ξ, p and q potential parameters are used to fit the experimental properties as cohesive energy, lattice parameters, elastic constants, among others), while r_0 can either be average of the pure bulk distances or can be taken by specific ordered bulk alloy. See **Figure 2**.

Due to high computational costs, a combined empirical-*ab initio* approach is used to carry out the unbiased searches at empirical level for global and local minima structures. These structures were optimized at *ab initio* level and GO technique was used at EP level to build a database of structural motifs. Global searches were performed with the BCGA and BHMC algorithms by employing Gupta and Gupta-derives potentials. Then the selected minima are locally optimized at the DFT level using various softwares as the Northwest Computational Chemistry (NWChem) (Aprà et al., 2020), Quantum ESPRESSO (QE) (Giannozzi et al., 2020), Gaussian 09 package (Frisch, 2009), VASP (Kresse and Furthmüller, 1996) and ADF (TeVelde et al., 2001; Baerends et al., 2003) etc.

OGOLEM (Hartke, 1993; Dieterich and Hartke, 2017), GMIN (Wales and Scheraga, 1999; Wales, 2010), BCGA (Johnston, 2003; Shayeghi et al., 2015), Gradient Embedded Genetic Algorithm or GEGA (Alexandrova and Boldyrev, 2005), Global Reaction Route Mapping (GRRM) (Ohno and Maeda, 2006; Ohno and Maeda, 2019), Evolutionary Algorithm for Molecular Clusters or EA_MOL (Llanio-Trujillo et al., 2011; Marques and Pereira, 2011), Automated Mechanisms and Kinetics (AutoMeKin) (Martínez-Núñez, 2015a; Martínez-Núñez, 2015b; Martínez-Núñez et al., 2020), ABCluster (Zhang and Dolg, 2015), Genetic Algorithm fitting (GAFit) (Rodríguez-Fernández et al., 2017; Rodríguez-Fernández et al., 2020), AUTOMATON (Yañez et al., 2019; Yañez et al., 2020) and NWPEsSe (Zhang et al., 2020) are some of the computational tools which have included many of these methods.

The energetic analysis of clusters is carried out by average binding energy (pure clusters), second difference in binding energy and excess (or mixing) energy for nanoalloys by both EP and DFT levels. The mixing effect is studied by various factors as size, cohesive energy, surface energy, electronegativity among many others. Radial distribution function (RDF), pair distribution function (PDF) and average nearest-neighbour distance (ANND) are also calculated for bonding analysis. Further chemical ordering and symmetry are studied for the cluster structure analysis. Compositional Mixing Degree is calculated to give emphasis to the mixed bonds (Srivastava, 2017a; Srivastava, 2018a).

In next section, we will discuss the use of these optimization algorithms in various types of clusters.

PURE METALLIC CLUSTERS

Spherical shell model was used to determine the electronic structures of "magic numbers" in Na_n and K_n alkali-metal clusters (Brack, 1993; de Heer, 1993). Åkeby et al. (Åkeby et al., 1990) used the configuration interaction (CI) method with an effective core potential for small clusters (n ≤ 10). Full-potential muffin-tin orbitals (FP-LMTO) technique was used for small Cu_n clusters (Kabir et al., 2003). Tight-binding (TB) approach with quasi-empirical potential was used to study the molecular dynamics for nearly 1,300 atoms (D'Agostino, 1993). A minimal parameter TBMD method was used for transition metal (Ni_n and Fe_n) clusters (Menon et al., 1994; Lathiotakis et al., 1996). Random search method has been adopted by Johnston group on (Al, Ca, Fe, Ni, Pd and Pt) bound 17–19 atoms clusters by Murrell–Mottram 2 + 3 body potentials. Results indicated similar structural patterns but different positions of elements for both Murrell–Mottram and Sutton–Chen potentials.

A previous studies indicated amorphous structures for 13 atoms (Au, Ag, Cu) clusters (Oviedo and Palmer, 2002) and large Au_n clusters (n = 38, 55, 75) (Michaelian et al., 1999; Li et al., 2000; Wilson and Johnston, 2000). *Ab initio* studies showed that most of the copper clusters adopt icosahedral structure for (10 ≤ n ≤ 55), derived from the 13 atom icosahedron; polyicosahedral (19, 23, and 26) atom; and icosahedron (55 atoms) clusters by adding or removing atoms (Moore, 2013). Small anionic gold clusters were studied by Häkkinen et al. (Häkkinen et al., 2002) with PBE (Perdew et al., 1996) functional in which Au_7^- formed a

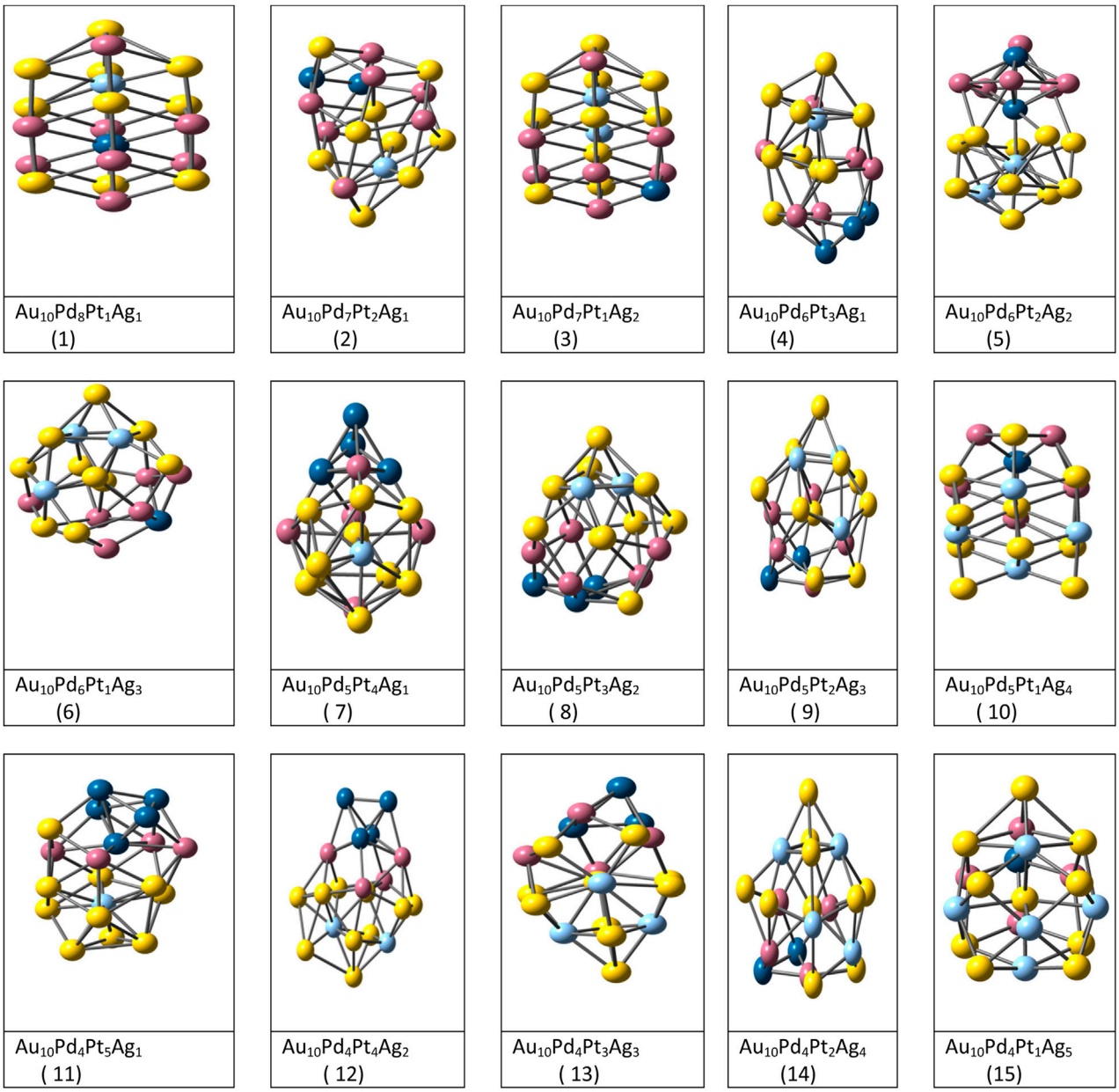

FIGURE 2 | Optimized structures of Fifteen tetrametallic clusters complexes by DFT method. (Srivastava, 2017b).

planar structure, whereas both Cu_7^- and Ag_7^- form 3D structure. Furche et al. (Furche et al., 2002) found planar structures for Au_n^- up to n = 15. DFT calculations find stable planar gold clusters (Jain, 2005), while *Fa et al.* (Fa et al., 2005) predicted 2D→3D transition between n = 13 and n = 15 for neutral gold clusters.

Large magic number Cu clusters tend to adopt close-packed structures such as icosahedron or cuboctahedron (Massobrio et al., 1998). Jackson used local-spin-density approximation for even-numbered Cu clusters, while other study (Winter et al., 1991) predicted jellium model like icosahedral geometrical closure effects for small copper clusters. Density functional theory (DFT) within generalized gradient approximation and BFGS algorithm on Cu_{20}, Ag_{20}, and Au_{20} clusters study also showed tetrahedral structures with T_d symmetry for Ag_{20} and Au_{20} clusters (Wang et al., 2003). Li et al. (Li et al., 2003) predicted tetrahedral structure with T_d symmetry for Au_{20}; similar to alkali-metal cluster Na_{20} (Solov'yov et al., 2002). Recently Asenjo et al. (Asenjo et al., 2013) showed that L-BFGS as well as FIRE algorithm is also a fastest minimizer and it led to less fragmented basins of attraction. As these magic number clusters are stable and have closed electronic and/or geometric shell, they can be used as building block in nanoscale materials and devices.

TABLE 2 | Parameters Used in Dynamic Lattice Searching Method. For the magic numbers (38, 75–77, 98, 102–104). N_{runs} 10,000. (Shao et al., 2004b).

N	N_{mov}	N_P	N_{try}	N_{best}	N_{runs}[a]
13–49	10	92	100	4	1,000
50–79	15	162	200	4	1,000
80–119	15	252	300	5	1,000
120–149	20	362	350	5	1,000
150–169	20	492	400	5	1,000
170–189	20	492	450	8	2000
190–199	20	492	500	10	2000
200–229	20	492	550	10	2000
230–251	20	642	550	10	2000
252–309	25	642	700	10	2000
500	40	812	1,000	10	10,000

38, 75, and 98 atom Lennard-Jones clusters, truncated octahedron for LJ_{38} (Doye et al., 1999), tetrahedral symmetry for LJ_{98} (Leary and Doye, 1999a), Marks decahedra for $LJ_{75–77}$ (Doye et al., 1995) and $LJ_{102–104}$ (Doye and Wales, 1995) which are all multiple-funnel systems of the corresponding energy landscapes (Wales et al., 1998, Wales, 2004; Doye et al., 1999) were studied by GMIN optimization code by Wales Group (Wales, 2012; Oakley et al., 2013). Adaptive immune optimization algorithm (AIOA) search algorithm has been used for the structural optimization of monatomic LJ clusters (up to 200 atoms) (Ye et al., 2011; Cheng et al., 2004). Studies on the geometrical optimization of Lennard-Jones clusters within 250 atoms and Ag clusters (within 150 atoms) were carried out by adaptive immune optimization algorithm (AIOA) with dynamic lattice searching (DLS) operation (AIOA-DLS) using many-body Gupta potential (Wu and Wu, 2014a). Dynamic searching approach reduces the searching space and runs at a very high efficiency, especially for larger size clusters. This approach can be effectively used for other molecular or atomic clusters. The performance of DLS for the optimization of LJ clusters with $13 \leq N \leq 309$ with different parameters are listed in **Table 2**. DLS method showed a very fast convergence speed compared with monotonic sequence basin-hopping (MSBH). Recently KLMC

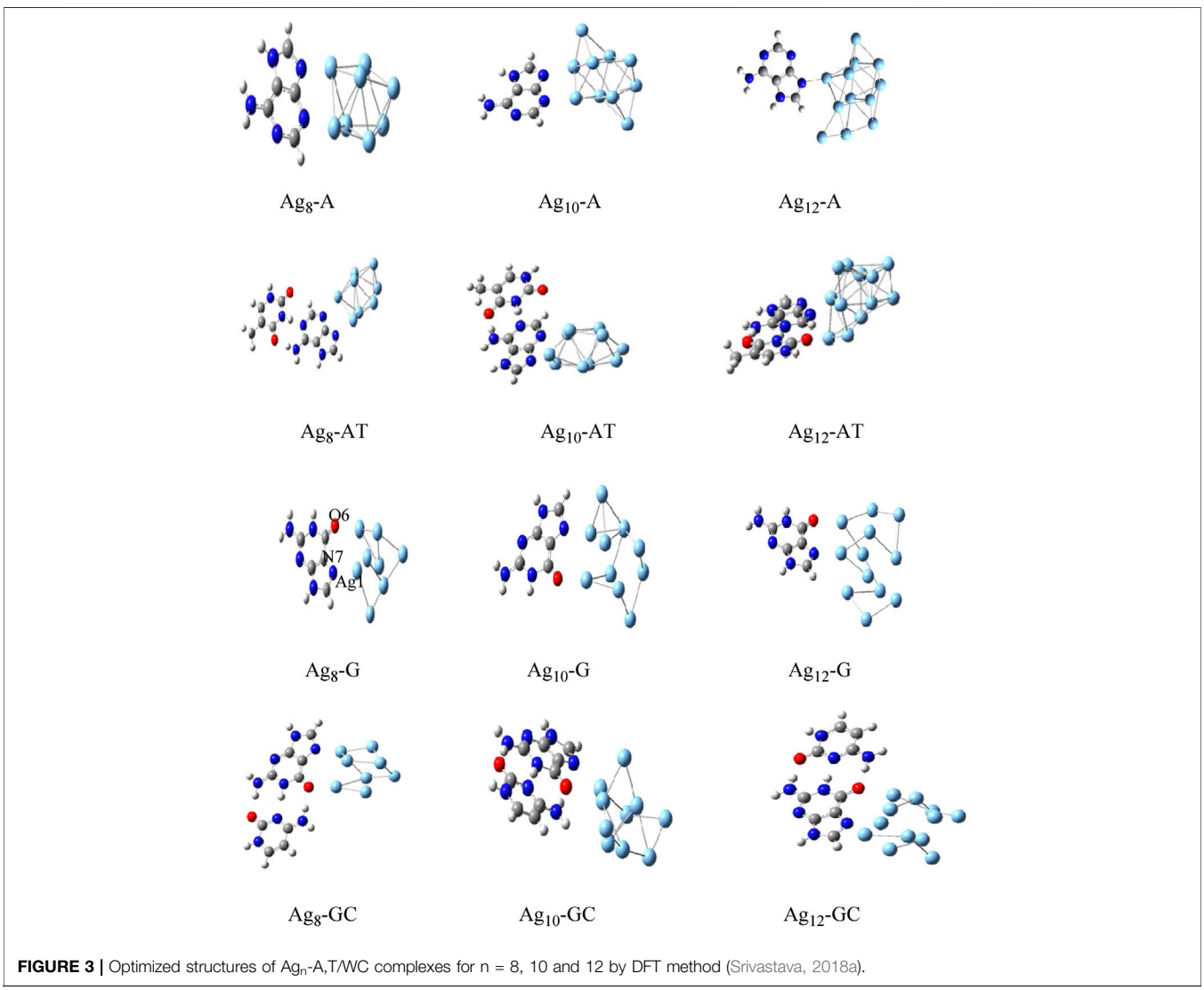

FIGURE 3 | Optimized structures of Ag_n-A,T/WC complexes for n = 8, 10 and 12 by DFT method (Srivastava, 2018a).

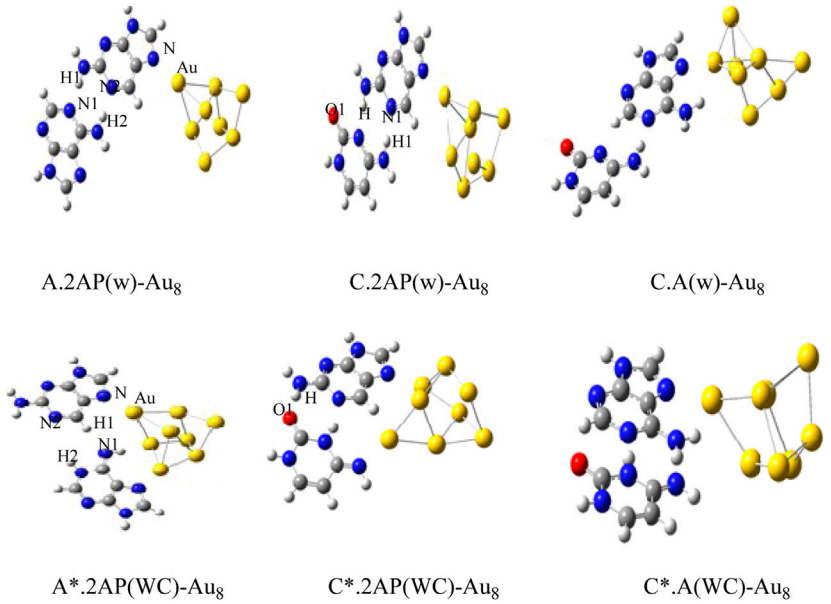

FIGURE 4 | Optimized structures of Au_8-wobble/WC mispair Complexes by DFT method. (Srivastava, 2018a).

method is used to locate and explore double funnel landscape of LJ_{38} atom system (Lazauskas et al., 2017).

The Gupta potential parameters with GMIN code were used for the gold and silver clusters for Cystene-coinage metal interactions (Srivastava, 2017a). The clusters were optimized using basin hopping algorithms within higher temperature and the structures validated the experimental studies. Results indicated that basin hopping algorithm based on the Monte Carlo minimization is appropriate for these clusters. The same GMIN code has been used for the structural optimization of silver clusters (Ag_8, Ag_{10} and Ag_{12}) in Ag_n-A,T/WC complexes interactions (Srivastava, 2018a). See **Figure 3**. In Mutagen-Au_8 complexes, the gold clusters were optimized using Gupta potential parameters and BH algorithm and the electronic and optical properties of the Mutagen-Au_8 complexes (Srivastava 2017c) were studied with G09 software. See **Figure 4**.

Bimetallic Clusters

In bimetallic clusters, four different types of chemical ordering are possible as core-shell, subcluster segregated (Janus nanoparticles), mixed and multiple shells. See **Figure 1**. The design of nanoalloys can be changed by fine tuning the mixing pattern. The chemical arrangement of these clusters are influenced by many factors as relative strengths of homo and heteronuclear bonds, atomic sizes, electronic/magnetic effects and many others (Ferrando et al., 2008; Oderji and Ding, 2011).

The highly efficient unbiased optimization methods used for nanoalloys are the genetic algorithm (GA) (Daven et al., 1996; Xiang et al., 2004; Curley et al., 2007), basin hopping (BH) method and its variants (Wales and Doye, 1997; Wales et al., 1998; Leary and Doye, 1999b), self-consistent basin-to-deformed-basin mapping, heuristic algorithm (Leary and Doye, 1999b) with surface and interior operators (HA-SIO) (Takeuchi, 2006), fast annealing evolutionary algorithm (FAEA) (Cai and Shao, 2002), evolutionary algorithm (EA) (Hartke, 2000), random tunneling algorithm (RTA) (Shao et al., 2004a), dynamic lattice searching (DLS) methods (Pillardy et al., 1999; Shao et al., 2004b), modified adaptive immune optimization algorithm (AIOA) (Shao et al., 2004c) and Knowledge Led Master Code (KLMC) (Woodley, 2013) due to larger number of homotops. In a previous study Spin polarized density-functional theory (SP-DFT) (Pant and Rajagopal, 1972) with B3 (Becke, 1993) exchange functional and PW91 (Perdew and Wang, 1992) correlation functional was used to investigate small Ag_xPt_{10-x} ($1 \leq x \leq 10$) nanoalloys and global reactivity descriptors were used to determine the activity of these bimetallic clusters (Erlinda del et al., 2009). The LANL2DZ pseudo-potential with corresponding double- ζ basis set was used for Ag and Pt atoms (Hay and Wadt, 1985). Nanoalloys as iron and silver are of immense interest as they have distinct properties compared to the pure elemental clusters and corresponding bulk alloys due to finite size effects. These nanoalloys may show both magic sizes and magic compositions (Baletto and Ferrando, 2005). Paz Borbón et al. (Paz Borbón et al., 2008) used combined empirical potential (EP)/density functional (DF) method to study the structural properties and segregation effects for 38 atom binary clusters (combination of Pt-Ag, Ag-Au, Pd-Au and Ag-Pt) metals. Results favored mixed five-fold-symmetric/close-packed or decahedral arrangements for Pt-Pd, Ag-Pt and Ag-Au pairs. We have also used the combined EP-DF approach for structural optimization of nineteen bimetallic $Au_{38-x}Pt_x$ and $Au_{38-x}Ag_x$ clusters. The basin-hopping procedures with accept/reject strategies (10,000 Steps) were used and the studied structures were compared to the reference Au_{38} (theoretical and experimental) structure. Further the geometrical, thermal and other properties were studied for these binary structures (Srivastava, 2018b). See **Figure 5**.

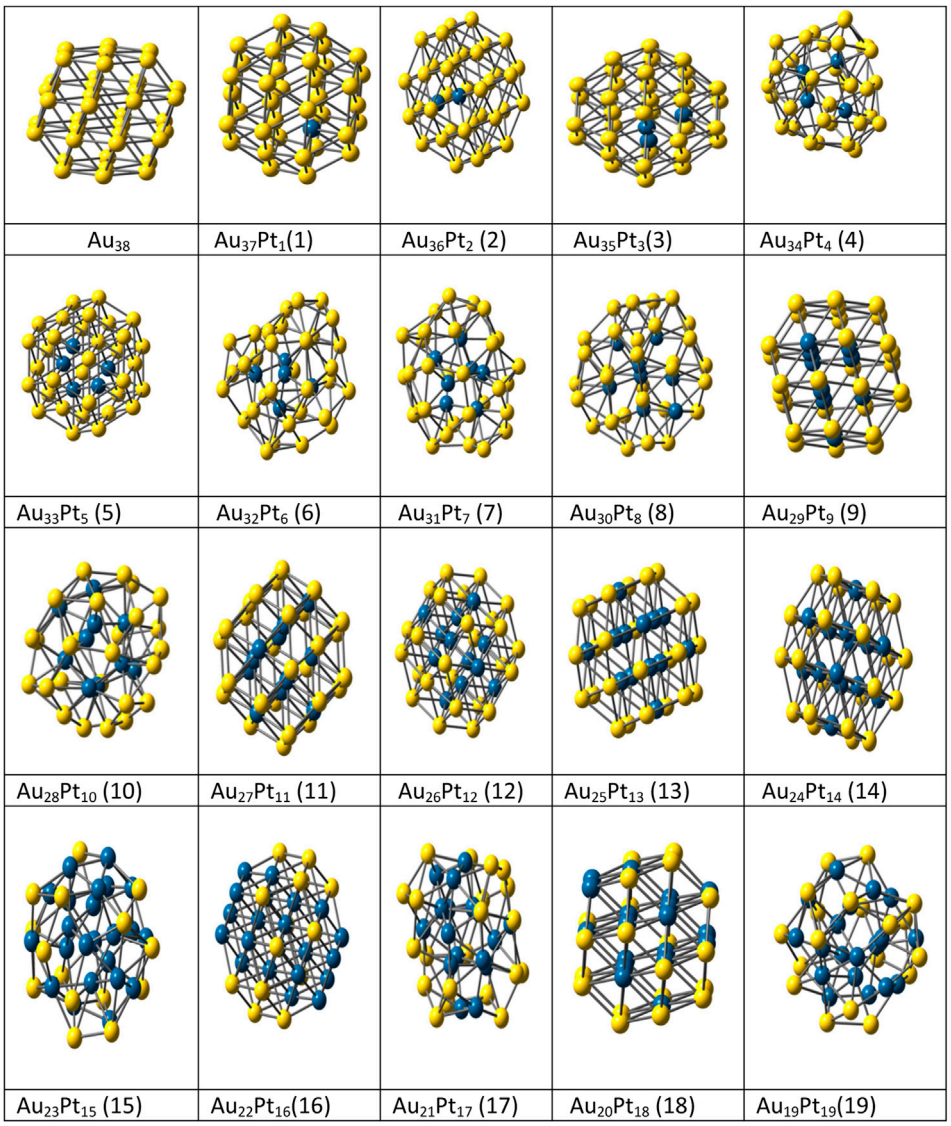

FIGURE 5 | Optimized structures of $Au_{38-x}Pt_x$ bimetallic (x = 1–19) clusters. (Srivastava, 2018b).

A general tight-binding (TB) total energy scheme has been used to calculate the structural properties of the smaller bimetallic coinage metal compounds: Cu_3Au, CuAu, $CuAu_2$, $CuAu_3$, and Cu_6Au_8 clusters (Metadjer et al., 2001). The structural and electronic properties of bimetallic gold-silver clusters (Bonacic et al., 2002) and Au_nX_m+ (X = Cu, Al, Y, In) (Bouwen et al., 1999) were studied by the TB energy scheme. *Heinebrodt el al.* (Heinebrodt el al., 1999) used DFT method for Au_nX_m (X = Cu, Al, Y, In, Cs) clusters and found the electronic shell effects separately in the clusters. *Yuan et al.* investigated the geometric and electronic structures of Au_nM (n = 1–7, M = Ni, Pd, Pt) by employing the first-principles method (Yuan et al., 2005). The structures and electronic properties of Cu_nO_n (n = 1–8) clusters (Bae et al., 2011) were also carried out by DFT.

The structural stability and electronic properties of Pd_nSi_q (n = 1–7 and q = 0, 1, −1) clusters were studied by DFT within GGA (Begum et al., 2014) framework. The chemical ordering in magic-size Ag–Pd clusters were carried out for global optimization searches with DFT based atomistic potential developed within the second-moment approximation to the tight-binding model (Cyrot-Lackmann and Ducastelle, 1971) using the BH algorithm (Wales and Doye, 1997; Rossi and Ferrando, 2009). BH algorithm consists of Metropolis Monte Carlo simulations in which local minimization are performed after each move. In this study exchange moves were only allowed to search the best homotops for the most favourable chemical ordering patterns. Thermodynamic parameters of surface configurations for the corresponding bulk alloys were studied by Strohl and King et al. (Strohl and King, 1989). In another study different chemical ordering patterns were analyzed for Ag–Pd nanoparticles up to 60 atoms (Bochicchio et al., 2014).

The embedded-atom method was used to study the structural stability of Cu_mAg_n nanoalloys with BH algorithm for all (m,n) with N = m + n from 2 to 60 atoms. Most of the structures were icosahedra, polyicosahedra, truncated octahedral and 5-fold pancakes (Molayem et al., 2010). The studies were compared to the Ni_mAg_n (Molayem et al., 2011) clusters using the similar approaches. Electronic shell closure effects have been observed for magic size N = 40 for Cu-Ag nanoalloys (Barcaro et al., 2006).

The second moment approximation to the tight binding (SMATB) method with Gupta potential and genetic algorithms (GA) were employed for the global optimization (Rossi et al., 2004; Barcaro et al., 2006; Nu_nez and Johnston, 2010) for CuAg clusters using three different algorithms; basin-hopping (BH) method, the energy-landscape paving method, and the parallel excitable walkers method. The predicted most stable clusters have core shell polyicosahedra structures (Rossi et al., 2004; Nu_nez and Johnston, 2010). Another study has been carried out for $Au_{19}X$ doped (X = Li, Na, K, Rb, Cs, Ag and Cu) clusters by *ab initio* scalar relativistic DFT method using ADF package based on zero-order regular approximation (ZORA) (vanLenthe et al., 1993; vanLenthe et al., 1994). Perdew-Wang 1991 (PW91) (Perdew, 1991) exchange-correlation (XC) functional within GGA with triple-STO basis set added with two polarization functions at the frozen core approximation level were used for the studies (Ghanty et al., 2010).

KLMC method (Woodley, 2013; Farrow et al., 2014) was used to study the nanocluster structures of binary heteropolar compounds; ZnO, MgO, KF, and CdSe, (Farrow et al., 2014) using interatomic potentials (IP) (within GULP (Gale, 1997; Gale and Rohl, 2003) and density functional theory (DFT) (within FHI-aims (Blum et al., 2009) respectively. The study showed that improved Lamarckian evolutionary algorithm within KLMC proves to be a useful tool for structural prediction for nanoclusters (Woodley, 2013). These algorithms were used for $(BaO)_n$ nanoclusters (Escher et al., 2017) and it showed great resemblance for $(KF)_n$ clusters, while $(MgO)_n$ nanoclusters have barrel shape LM for n = 6. Interestingly $(BaO)_n$ for n = (4, 6, 8, 10, 16) were considered to be the magic number clusters (Lazauskas et al., 2017). The similar code has been used to study the ionic semiconductor $(ZnO)_{1-32}$ and CdSe (Farrow et al., 2014) to explore the energy landscape using interatomic potentials.

Trimetallic and Tetrametallic Clusters

Trimetallic (or ternary) coinage metal clusters have shown potential applications in optics, electronics, magnetic, and catalytic field (Stucky et al., 1989; Teo et al., 1993; Hungria et al., 2006; Fang et al., 2011). These clusters are highly catalytic and selective, yet the studies are very complex (Toshima and Yonezawa, 1998). Various global optimization techniques are used for the structural analysis for these clusters. (See Introduction section paragraph 3).

The interactions of Cu-Ag-Au trimetallic clusters were described by the second-moment approximation of the tight-binding (TB) potentials (N-body Gupta potential) with AIOA method. AIOA is an adaptive heuristic GA based algorithm which is used in the biological applications also. Another modified algorithm, MAIOA is used for the structural optimization of bimetallic (Wu et al., 2009; Wu et al., 2017) and ternary clusters. The immune clone selection and a mutation operation were the basic steps of MAIOA algorithms (Wu et al., 2011). AIOA method was also approved for $A_{(l)}B_{(m)}C_{(n)}$ (l + m + n = 9–55) clusters and $A_{(l)}B_{(m)}C_{(n)}$ (l = 13, m + n = 42) clusters (Wu et al., 2011). Further an improved adaptive immune optimization algorithm (AIOA-IC method) was found to be suitable for $Cu_8Au_nPt_{30-n}$ (n = 1–29), $Cu_8Au_nPt_{47-n}$ (n = 1–46), and partial 75, 79, 100, and 147 atom clusters (Wu et al., 2017). The structures, properties and interatomic interactions of trimetallic M–Pd–Pt (M = Ag and Au) upto 75 atoms were optimized using AIOA with the tight-binding Gupta potential (Wu et al., 2015). The Stacking fault (sf) and twin defects in Pd, Au–Pd, and Au–Pd–Pt clusters were studied with Gupta potential using DFT and fitted averaged parameters (Wu and Dong, 2014b). It was seen that the Gupta and Murrell Mottram potentials (Lloyd and Johnston, 2000) were found to be a good choice for the 19 atom trimetallic Double-icosahedra (DI) clusters (Farges et al., 1985). In another studies, random selection of bimetallic atom pairs were made with their exchanged location (Calvo and Yurtsever, 2004) based on the fact that the atoms with lower number of nearest neighbor contacts have higher potential energies in energy based mutations. Mutation and updating operation were performed for MAIOA runs till the achievement of maximal iteration number (LOOP), as the larger LOOP is needed for the structural optimization of unknown clusters. Limited memory quasi-Newton algorithm (L-BFGS) (Liu and Nocedal, 1989b) was used for local minimization (LM) for the clusters.

Au@Pd@Pt NPs were studied by DFT total-energy with VASP software (Zhou and Lee, 2007). The projector augmented wave method (PAW) and the Perdew–Burke–Ernzerhof generalized gradient approximation (GGA-PBE) was used for the exchange–correlation functional with an energy cut-off of 400 eV. A dipole correction (Neugebauer and Scheffler, 1992; Makov and Payne, 1995) was employed to use the induced dipole moment. Interestingly the theoretical results match well with the experimental values. In one of the Agpdpt alloys study, both empirical investigation and the theoretical analysis has given strong evidence that these nanoparticles are composed by an AgPd alloy core with Pt atoms lied on the surface (Wang and Yamauchi, 2011).

The structural optimization of $(Au_m\text{-}Ag_n\text{-}Pd_o\text{-}Pt_p)$ (m = 10 and n + o + p = 10) tetrametallic coinage metal clusters (Srivastava, 2017b) were carried out using combined EP-DF method. Completely random starting configuration was taken subjected to the lowest DF energy minimizations within GMIN code. In this work, the thermal and chemical stability of thirty eight tetrametallic clusters were measured by various parameters. Mixing/segregation effect results indicated that the surface sites are occupied by Au and Ag atoms while inner and middle shell are occupied by Pt and Pd atoms. See **Figure 2**.

INORGANIC FULLERENES AND FULLERENE-LIKE CLUSTERS

The stability, electronic and mechanical properties of fullerenes has been used broadly in nanotechnological and biomedical

applications. The discovery of buckyball C_{60} (Kroto et al., 1985) has launched a new era and stimulated the search for other related allotropes of carbon as nanotubes, nanopeapods, nanocones, etc. Detailed information about the structure, synthesis, and properties of carbon fullerenes are published in books and reviews (Dresselhaus et al., 1996; Hirsch, 1999, 2002; Hirsch and Brettreich, 2005). In 1970s, the first articles about C_{20} and C_{60} cages and their boron derivatives using quantum-mechanical method was published by Bochvar et al. (Bochvar and Galpern, 1973; Bochvar and Galpern, 1974). There are other well-known fullerene-like and fullerenic allotropes, chalcogenides, halides and oxides (Bar-Sadan et al., 2007; Tenne and Seifert, 2009). Small cage-like clusters Si_n ($n < 60$) doped by endohedral metal atoms (Kumar, 2003) showed stable cage structures. The elemental fullerenes based on boron particles form pure boron and mixed borocarbide structures (Albert, 2009). In 1912 Stock reported his pioneering work on boranes (Stock and Massanez, 1912), which led to the identification of neutral boron hydrides (B_2H_6, B_4H_{10}, B_5H_9, B_5H_{11}, and B_6H_{10}). Further, Lipscomb and co-workers (Eberhardt et al., 1954) introduced the concept of three-center two-electron (3c-2e) bonding B_2H_6 diborane. The existence of regular octahedra of boron atoms in several metal hexaborides with general formula MB_6 was demonstrated experimentally by Allard et al. (Allard, 1932; Pauling et al., 1934). Longuet-Higgins and Roberts show that the $[B_6]^{2-}$ unit has a highly stable closed-shell electronic arrangement (Longuet-Higgins and Roberts, 1954) and B_{12} icosahedron is a dominant structure of various allotropes of boron (Longuet-Higgins and Roberts, 1955). The existence of other deltahedral boranes, $B_{11}H_{11}^{2-}$, $B_9H_9^{2-}$, $B_8H_8^{2-}$, $B_7H_7^{2-}$, and $B_6H_6^{2-}$ were demonstrated in experimental studies (Klanberg and Muetterties, 1966; Klanberg et al., 1967; Boone, 1964). In another study to search global minima for the B_nH_{n+2} ($n = 2–5$) series, it was found that classical structures composed of 2c-2e B—H and B—B bonds become progressively less stable. The reason for this might be that the boron atoms are trying to avoid sp^2 hybridization and trigonal structure at the boron atoms, which is highly unfavourable as in that case one 2p-AO is empty (Osorio et al., 2012). These studies play a very important role to emulate structures analogous to the C allotropes (i.e., C_{60}), such as in systems containing N-B replacing an isoelectronic C-C fragment. A lot more about boron cluster studies is covered in an extensive review by Alexandrova et al. (Alexandrova et al., 2006). The most stable allotropes of boron exists as B_{12} (boron polyhedral) while sandwich-like hexagonal-structured "metal" atoms between boron atomic structure is seen in layered borides MgB_2, AlB_2, and TiB_2 (Chernozatonskii, 2001; Ivanovskaya et al., 2004). The most stable crystalline form of binary boron nitride is the hexagonal one, which is held by weak van der Waals interaction. Semi-empirical Hückel Austin Model (AM1) and *ab initio* Hartree–Fock (HF) methods have predicted possible configurations for BN nanoalloys. Similar approach with coupled-cluster theory (CCSD) method showed stable cage structures for $(BN)_n$ ($n = 8–11$) clusters. DFT tight-binding method (DFTB) was performed to study the structural stability of $(BN)_n$ fullerenes with $n = 4–30$ (Fowler et al., 1996) and $(BN)_n$ fullerenes with $n = 13–35$ (Rogers et al., 2000). Octahedron-like fullerenes structures were found for $B_{12}N_{12}$, $B_{16}N_{16}$, and $B_{28}N_{28}$ (Seifert et al., 1997). *Ab initio* calculations have been performed for energetically stable small cages $B_{13}N_{13}$, $B_{14}N_{14}$, $B_{16}N_{16}$ clusters (Strout, 2004) and B_nN_m fullerenes for $20 < (n + m) < 288$ (Alexandre et al., 2001; Batista et al., 2006). Semi-empirical PM5 and discrete-variational calculations were carried out for $B_{12}N_{12}$, $B_{28}N_{28}$, $B_{36}N_{36}$ (Oku et al., 2004a; Oku et al., 2004b; Oku et al., 2004c) and $B_{24}N_{24}$ (Oku et al., 2003) clusters, while semi-empirical AM1 and discrete-variational (DV) calculations were used to study the stability of single atom doped $B_{36}N_{36}$ fullerene clusters (Nishiwaki et al., 2004). First principle calculations were carried out for boron-carbon nanocages ($B_{12}C_{48}$, $B_{12}C_{50}$) and it was found that these structural motifs showed aggregated boron atoms at one location in the form of a patch. These studies have violated all the other previous suggested empirical rules for constructing low-energy fullerenes. Also the energetic stabilities of these two clusters predicted that the structures derived from the C_{60} (buckminsterfullerene) are not necessarily magic sizes for heterofullerene structures (Mohr et al., 2014).

Ab initio projector-augmented wave (PAW) spin-polarized calculations were performed on La@B36N36 endofullerene, tetrahedral Fe_4, Co_4, and Ni_4 clusters encapsulated into $B_{36}N_{36}$ fullerene (Nigam and Majumder, 2007), while spin polarized DFT–GGA pseudo-potential calculations were performed for $B_{36}N_{36}$ fullerene doped by (Fe, Co, and W) and FeO molecule (Batista et al., 2007). The stability of BN tubular structures were studied by DFT calculations, while the sphericity of BN cap models (squares, and pentagon–pentagon and pentagon–heptagon pairs) (Fowler et al., 1999) and octahedral fullerenes $B_{12}N_{12}$ inside (14,0), (8,8), and (12,4) BN nanotubes (Enyashin and Ivanovskii, 2008) were studied by DFTB method. Different lattice parameters of $B_{12}N_{12}$ and $B_{24}N_{24}$ (Pokropivny and Bekenev, 2006, 2007) have been studied by semi-empirical MNDO and *ab initio* FLAPW methods (Pokropivny et al., 2000) and the results indicated that $B_{12}N_{12}$ fullerites were the most stable diamond-like lattice structure.

In a latest study entirely unusual derivatives of boron clusters doped with lithium, $LiB_n^{0/-}$ ($n = 10–20$) clusters were studied through Crystal structure AnaLYsis by Particle Swarm Optimization (CALYPSO) structural search approach alongwith the DFT calculations. Three (half-sandwich-type, quasi-planar and drum-type) structures were found for the studied clusters (Shi et al., 2020). The lowest-energy minima of the pure B_{22} cluster and the capacity of its isomers to form endohedrally doped cages with two transition metal atoms M (M = Sc and Ti) were carried out with genetic search algorithm using DFT calculations (Celaya et al., 2020). Recent reviews on boron clusters (Yan et al., 2020; Axtell et al., 2018; Zhu and Hosmane, 2018; Núñez et al., 2016a; Núñez et al., 2016b) are recommended for the interested readers.

DFTB method was used to investigate the properties of sulfide fullerene-like particles and sulfide MoS_2 nanotubes, while DFTB calculations with a derived continuum approach (Bar-Sadan et al., 2006.; Enyashin et al., 2007) was used to investigate WS_2, MoS_2, and $MoSe_2$ polyhedral nanoclusters (Margulis et al., 1996; Parilla et al., 2004). The semi-empirical Extended

Hückel Theory (EHT) level was used to study $(MoS_2)_n$ upto (n = 64), $(MoS_2)_n$ upto (n = 576), imperfect MoS_2 fullerenes and nanoseashells (Enyashin et al., 2009). Halide fullerenes was studied by *ab initio* spin-polarized DV method without geometry optimization for $(NiCl_2)_{48}$, $(FeCl_2)_{48}$, and $(CdCl_2)_{48}$ clusters (Enyashin and Ivanovskii, 2005a; Enyashin et al., 2005b), while $(TiO_2)_n$ nanooctahedra with n upto 108 (Enyashin and Seifert, 2007) were studied by DFTB method. Recently KLMC is used to investigate the metallic Ni_{13} and covalently bonded C_{60} (buckminsterfullerene) potential energy surfaces (Lazauskas et al., 2017).

P, As, Sb, and Bi, are the few elements among all the variety of periodic table which can appear as hexagonal atomic layers assembled using covalently bounded sp^3 hybridized atoms. The possibility of stable non-carbon fullerenes as phosphorus fullerene-like cage structures was studied on the basis of Density Functional Tight Binding calculations (Seifert et al., 2001). DFT calculations showed that P_{20} (dodecahedron) is the most stable structure and P_n hollow cages corresponds to the metastable structures. It was observed that with increasing nuclearity these metastable structures become less stable with respect to separate molecular P_4 units.

DIPOLAR CLUSTERS

Dipolar interactions form chains with a low coordination number, while spherical particle clusters with isotropic attraction form close-packed structures. The dipolar clusters favor strongly distinguished nearest-neighbour interactions. The combination of both isotropic and dipolar interactions form intricate knot, link and coil structures. The global minima of these interconverted self-organize structures are bound by the Stockmayer potential (Lennard-Jones plus point dipole). The Stockmayer model with dipolar fluids has been summarized in a good review (Teixeira et al., 2000). For these particles, the energy landscape for low-lying minima was obtained by the basin-hopping global optimization. The isotropic Lennard-Jones part of the potential is used to drive the compact structures toward highly-coordinated arrangements for the frustrated Stockmayer clusters, while chain-like motifs are favored by dipolar interactions. The studies of these idealized model systems are useful as it give insight for the knot systems as biomolecules and synthetic organic molecules.

The global optimization calculations for the Stockmayer particle have been carried out for the energetically favorable structures (knots, links, and coils) with a permanent dipole plus anisotropic soft core and alluring tail by Miller et al. (Miller and Wales, 2005). These particles have anisotropic point dipole with five degrees of freedom and cylindrical symmetry. Further, the PES is characterized by scaling out local minima which corresponds to the locally stable structures, connected *via* first-order saddle points (transition states). The clusters of spherical particles are bound by Lennard-Jones and Morse type of simple isotropic potentials, while the anisotropic Stockmayer potential differs from these potentials as the particles' have the tendency to form chains (Farrell et al., 2013).

ENERGY LANDSCAPE FOR KAGOME LATTICE FROM SOFT ANISOTROPIC PARTICLES

Studies were carried out for the energetically stabilized kagome structures, which are the simple model of triblock Janus particles based on the discoidal building blocks. Basin-hopping global optimization was used for these particles. The three nearest neighbors were detected by an algorithm based on the interparticle distances. Further it was seen that the energetic stabilization is enhanced with the occurrence of sedimentation. The interaction of each ellipsoid of two building blocks occured via the Paramonov–Yaliraki (PY) potential (Paramonov and Yaliraki, 2005). The Paramonov-Yaliraki (PY) potential is used to study the collection of both homomolecular and heteromolecular pyrene, coronene, and circumcoronene below 1000 K within a stochastic Monte Carlo framework (Hernandez-Rojas and Calvo, 2019). This elliptic potential is also applicable for mixtures of any (size, orientation) ellipsoids and/or spheres, hard and soft particles.

ENERGY LANDSCAPE FOR PLANAR COLLOIDAL SYSTEMS

Short-ranged pairwise Morse potential is more appropriate method to study the structural optimization of colloidal clusters with planar morphologies. The PES, global minima, rearrangement paths with discrete path sampling and free energy landscapes are visualized by the disconnectivity graphs. Here the number of nearest neighbor contacts control the short range potential. It was found that the free energy global minimum differs from the potential energy GM in quasi-degeneracy state due to the symmetry effects, which results in higher entropic lower symmetry structures. BH steps were taken as random Cartesian displacements (Wales, 2004) and the possible nominee for the transition states are selected between the minima's by the doubly-nudged (Trygubenko and Wales, 2004; Carr et al., 2005) elastic band (Henkelman et al., 2000a; Henkelman and Jónsson, 2000b; Henkelman and Jónsson, 2001) method.

ENERGY LANDSCAPES FOR WATER DIMER

The understanding of the structure and thermodynamics of water is very important as water is used in the wide range of applications from biomolecular solvation to the atmospheric chemistry. The angle axis framework with TIP4P potential was used for the water clusters containing eight molecules. In these clusters the energy landscape was mapped with the basin-hopping global optimization and a modified limited-memory Broyden-

Fletcher-Goldfarb Shanno (L-BFGS) algorithm to find the global minima and a database for the low energy minima. The combined doubly-nudged elastic band and a hybrid eigenvector-following method (Henkelman and Jónsson, 2000b; Kumeda et al., 2001.) was used to obtain minimum-transition state-minimum triplets. The intermolecular and intramolecular forces were studied over the larger amplitudes to get a connectivity PES graph by exploring the local minima. Recently artificial bee colony (ABC) algorithm with "ABCluster" was used to find the successful location of global minima for TIP4P water clusters $(H2O)_N$ ($N \leq 20$). The similar methodology was further applied to various clusters of different chemical nature: 10 microhydration clusters, 4 methanol microsolvation clusters, 4 nonpolar clusters and 2 ion–aromatic clusters (Zhang and Dolg, 2016).

ENERGY LANDSCAPES OF HYDRATED SULFATE CLUSTERS

These clusters were optimized using BHMC simulations with a rigid-body EP and a move set, which included the cycle inversions to inquire the hydrogen bond topologies with the sulfate ion, belonging to the Hofmeister series. As the system has large size so the bond parameters (length, angle) of the sulfate clusters were held rigid. The water molecules were described by four-site rigid-body TIP4P water potential (Jorgensen et al., 1983a; Jorgensen et al., 1983b; Jorgensen et al., 1983c; Kazachenko and Thakkar, 2010) to describe the water phase diagram with certain modifications. The TS connecting the minima on the PES were located by doubly nudged elastic band method. Translational (linear interpolation) and rotational coordinates (spherical interpolation) were used for the endpoints interpolation and the artificial frustration was removed by connecting the minima to the global minimum (Małolepsza et al., 2010) with the visualization of disconnectivity graphs (Becker and Karplus, 1997; Morgan and Wales, 2014; Smeeton et al., 2014).

CONCLUSION

The rise of machine learning (ML) has explored the use of these algorithms in atomistic modeling and inference techniques and led it toward the data-driven approaches in the recent years. The machine learning landscape can easily analyze the most fitted functions that exhibit multiple solutions as local minima. Supervised as well as the unsupervised learning methods in combination to the fundamental mathematical concepts are mostly used for the machine learning techniques (Ceriott, 2019). These studies are mainly focused toward clusters, biomaterials, crystals and self-organized structures (Ballard et al., 2017). ML can use the algorithms more effectively to get a new and useful insight about the corresponding predictions, so that the directions for new interdisciplinary research will be explored. Though certain limitations regarding the use of machine-learning techniques in atomistic modeling are still needed to be rectified for materials, chemical, and biomolecular clusters, we hope that machine learning techniques and computational chemical physics will collaborate in highly efficient manner to show great productivity for different models in near future.

AUTHOR CONTRIBUTIONS

The author confirms being the sole contributor of this work and has approved it for publication.

FUNDING

RS acknowledges the financial assistance by DST WOSA project (SR/WOS-A/CS-69/2018). This work is funded by DST WOSA project (SR/WOS-A/CS-69/2018). The author is thankful to Dr Shrish Tiwari, Bioinformatics, CSIR-Centre for Cellular and Molecular Biology and Dr G. Narahari Sastry, Director, CSIR-NEIST for the technical support.

REFERENCES

Addicoat, M. A., and Metha, G. F. (2009). Kick: constraining a stochastic search procedure with molecular fragments. *J. Comput. Chem.* 30, 57–64. doi:10.1002/jcc.21026

Åkeby, H., Panas, I., Pettersson, L. G., Seigbahn, M. P., and Wahlgren, U. (1990). Electronic and geometric structure of the copper (Cun) cluster anions (n ≤ 10). *J. Chem. Phys.* 94, 5471–5477. doi:10.1021/j100377a010

Akutsu, Y., Tahara, S.-Y., Tamura, M., and Yoshida, T. (1991). Calculations of heats of formation for nitro compounds by semi-empirical mo methods and molecular mechanics. *J. Energetic Mat.* 1991 (9), 161–171. doi:10.1080/07370659108019862

Albert, B. (2009). Boron: elementary challenge for experimenters and theoreticians. *Angew. Chem. Int. Ed.* 48 (46), 8640–8668. doi:10.1002/anie.200903246

Alexandre, S. S., Chacham, H., and Nunes, R. W. (2001). Structure and energetics of boron nitride fullerenes: the role of stoichiometry. *Phys. Rev. B* 63, 045402. doi:10.1103/PhysRevB.63.045402

Alexandrova, A. N., and Boldyrev, A. I. (2005). Search for the Lin0/+1/-1 (n = 5–7) lowest-energy structures using the ab initio gradient embedded genetic algorithm (GEGA). Elucidation of the chemical bonding in the lithium clusters. *J. Chem. Theor. Comput.* 1, 566–580. doi:10.1021/ct050093g

Alexandrova, A. N., Boldyrev, A. I., Zhai, H.-J., and Wang, L.-S. (2006). All-boron aromatic clusters as potential new inorganic ligands and building blocks in chemistry. *Coord. Chem. Rev.* 250, 2811–2866. doi:10.1016/j.ccr.2006.03.032

Allard, A. (1932). X-ray study of some borides, bull. Soc. Chim. *Fr.* 51, 1213–1215. doi:10.1361/105497199770335974

Aprà, E., Bylaska, E. J., de Jong, W. A., Govind, N., Kowalski, K., Straatsma, T. P., et al. (2020). NWChem: past, present, and future. *J. Chem. Phys.* 152, 184102. doi:10.1063/5.0004997

Asenjo, D., Stevenson, J. D., Wales, D. J., and Frenkel, D. (2013). Visualizing basins of attraction for different minimization algorithms, *J. Phys. Chem. B* 117, 12717–12723. doi:10.1021/jp312457a

Axtell, J. C., Saleh, L. M. A., Qian, E. A., Wixtrom, A. I., and Spokoyny, A. M. (2018). Synthesis and applications of perfunctionalized boron clusters. *Inorg. Chem.* 57, 2333–2350. doi:10.1021/acs.inorgchem.7b02912

Bae, G.-T., Dellinger, B., and Hall, R. W. (2011). Density functional calculation of the structure and electronic properties of CunOn(n= 1–8) clusters. *J. Phys. Chem. A.* 115 (11), 2087–2095. doi:10.1021/jp104177q

Baerends, E. J., Autscbach, J., and Berces, A. (2003). *Amsterdam density functional.* Amsterdam, Netherlands: VirjeUniversiteit.

Bailey, M. S., Wilson, N. T., Roberts, C., and Johnston, R. L. (2003). Structures, stabilities and ordering in Ni-Al nanoalloy clusters. *Eur. Phys. J. D* 25, 41–55. doi:10.1140/epjd/e2003-00218-2

Baletto, F., and Ferrando, R. (2005). Structural properties of nanoclusters: energetic, thermodynamic, and kinetic effects. *Rev. Mod. Phys.* 77, 371–423. doi:10.1103/RevModPhys.77.371

Ballard, A. J., Das, R., Martiniani, S., MehtaD.Sagun, L., Stevenson, J. D., et al. (2017). Energy landscapes for machine learning. *Phys. Chem. Chem. Phys.* 19, 12585–12603. doi:10.1039/c7cp01108c

Bar-Sadan, M., Enyashin, A. N., Gemming, S., Popovitz- Biro, R., Hong, S. Y., Prior, Y., et al.(2006). Structure and stability of molybdenum sulfide fullerenes†. *J. Phys. Chem. B* 110, 25399–25410. doi:10.1021/jp0644560

Bar-Sadan, M., Kaplan-Ashiri, I., and Tenne, R. (2007). Inorganic fullerenes and nanotubes: wealth of materials and morphologies. *Eur. Phys. J. Spec. Top.* 149, 71–101. doi:10.1140/epjst/e2007-00245-1

Barcaro, G., Fortunelli, A., Rossi, G., Nita, F., and Ferrando, R. (2006). Electronic and structural shell closure in AgCu and AuCu nanoclusters. *J. Phys. Chem. B* 110, 23197. doi:10.1021/jp064593x

Bartolomei, M., Pirani, F., and Marques, J. M. C. (2015). Low-energy structures of benzene clusters with a novel accurate potential surface. *J. Comput. Chem.* 36 (31), 2291–2301. doi:10.1002/jcc.24201

Batista, R. J. C., Mazzoni, M. S. C., and Chacham, H. (2007). Boron nitride fullerene B36N36 doped with transition metal atoms: first-principles calculations. *Phys. Rev. B* 75, 035417. doi:10.1103/PhysRevB.75.035417

Batista, R. J. C., Mazzoni, M. S. C., and Chacham, H. (2006). A theoretical study of the stability trends of boron nitride fullerenes. *Chem. Phys. Lett.* 421, 246–250. doi:10.1016/j.cplett.2005.12.097

Becke, A. D. (1993). A new mixing of Hartree-Fock and local density-functional theories. *J. Chem. Phys.* 98 (1372), 1372. doi:10.1063/1.464304

Becker, O. M., and Karplus, M. (1997). The topology of multidimensional potential energy surfaces: theory and application to peptide structure and kinetics. *J. Chem. Phys.* 106, 1495. doi:10.1063/1.473299

Begum, P., Bhattacharjee, D., Mishra, B. K., and Deka, R. C. (2014). Density functional study on structures, stabilities, and electronic properties of size-selected PdnSiq (n 5 1–7 and q 5 0, +1, 21) clusters. *TheorChemAcc* 133, 1418. doi:10.1007/s00214-013-1418-9

Bera, P. P., Schleyer, P. v. R., and Schaefer, H. F. (2007). Periodane: a wealth of structural possibilities revealed by the kick procedure. *Int. J. Quan. Chem.* 107, 2220–2223. doi:10.1002/qua.21322

Blum, V., Gehrke, R., Hanke, F., Havu, P., Havu, V., Ren, X., et al. (2009). Ab initio molecular simulations with numeric atom-centered orbitals. *Comput. Phys. Commun.* 2009 (180), 2175–2196. doi:10.1016/j.cpc.2009.06.022

Bochicchio, D., Ferrando, R., Novakovic, R., Panizona, E., and Rossia, G. (2014). Chemical ordering in magic-size Ag-Pd nanoparticles. *Phys. Chem. Chem. Phys.* 16, 26478–26484. doi:10.1039/C4CP02143F

Bochvar, D. A., and Galpern, E. G. (1974). Calculation of hypothetical systems: carbododecahedron (C_{20}) and various diboracarbododecahedrons (B_2C_{18}) by the expanded Huckel method. *Russ. Chem. Bull.* 23, 2282–2284. doi:10.1007/BF00921307

Bochvar, D. A., and Galpern, E. G. (1973). Hypothetical systems carbododecahedron, s-icosahedrone and carbo-s-icosahedron. *Proc. Acad. Sci. USSR* 209, 610–612.

Bonacic, K. V., Burda, J., Mitric, R., Ge, M., Zampella, G., and Fantucci, P. (2002). Density functional study of structural and electronic properties of bimetallic silver–gold clusters: comparison with pure gold and silver clusters, *J. Chem. Phys* 117, 3120–3131. doi:10.1063/1.1492800

Boone, J. L. (1964). Isolation of the hexahydroclovohexaborate(2^-) anion, $B_6H_6^{2-}$. *J. Am. Chem. Soc.* 86, 5036. doi:10.1021/ja01076a082

Bouwen, W., Vanhoutte, F., Despa, F., Bouckaert, S., Neukermans, S., Kuhn, L. T., et al. (1999). Stability effects of AunXm+ (X=Cu, Al, Y, In) clusters. *Chem. Phys. Lett.* 314, 227–233. doi:10.1016/S0009-2614(99)01150-1

Brack, M. (1993). The physics of simple metal clusters: self-consistent jellium model and semiclassical approaches. *Rev. Mod. Phys.* 65, 677–732. doi:10.1103/RevModPhys.65.677

Cabaleiro-Lago, E. M., Hermida-Ramón, J. M., and Pena-Gallego, A. (2000). Intermolecular interactions and cooperative effects in acetonitrile clusters. An ab initio molecular orbital study. *J. Mol. Struct. Theochem* 498 (1-3), 21–28. doi:10.1016/S0166-1280(99)00207-9

Cai, W., and Shao, X. (2002). A fast annealing evolutionary algorithm for global optimization. *J. Comput. Chem.* 23, 427–435. doi:10.1002/jcc.10029

Call, S. T., Zubarev, D. Y., and Boldyrev, A. I. (2007). Global minimum structure searches via particle swarm optimization. *J. Comput. Chem.* 28, 1177–1186. doi:10.1002/jcc.20621

Calvo, F., and Yurtsever, E. (2004). Composition-induced structural transitions in mixed rare-gas clusters. *Phys. Rev. B* 70, 045423. doi:10.1103/PhysRevB.70.045423

Carr, J. M., Trygubenko, S. A., and Wales, D. J. (2005). Finding pathways between distant local minima. *J. Chem. Phys.* 122, 234903. doi:10.1063/1.1931587

Celaya, C. A., Buendía, F., Miralrio, A., Paz-Borbón, L. O., Beltran, M., Nguyen, M. T., et al. (2020). Structures, stabilities and aromatic properties of endohedrally transition metal doped boron clusters M@B22, M = Sc and Ti: a theoretical study. *Phys. Chem. Chem. Phys.* 22, 8077–8087. doi:10.1039/D0CP00307G

Ceriott, M. (2019). Unsupervised machine learning in atomistic simulations, between predictions and understanding. *J. Chem. Phys.* 150, 150901. doi:10.1063/1.5091842

Chen, M., Kumar, D., Yi, C.-W., and Goodman, D. W. (2005). The promotional effect of gold in catalysis by palladium-gold. *Science* 310, 291–293. doi:10.1126/science.1115800

Cheng, L., Cai, W., and Shao, X. (2004). A connectivity table for cluster similarity checking in the evolutionary optimization method. *Chem. Phys. Lett.* 389, 309–314. doi:10.1016/j.cplett.2004.03.125

Chernozatonskii, L. A. (2001). Diboride bifullerenes and binanotubes. *JETP Lett.* 74, 335–339. doi:10.1134/1.1421411

Cook, D. B. (2005). *Handbook of computational quantum Chemistry (dover books on Chemistry)*. Mineola, NY: Dover Publications.

Curley, B. C., Johnston, R. L., YoungP.Li, N., Di Vece, Z., Palmer, Y. M. R. E., et al. (2007). Combining theory and experiment to characterize the atomic structures of surface-deposited Au309 clusters. *J. Phys. Chem. C* 2007 (111), 17846–17851. doi:10.1021/jp0713099

Cyrot-Lackmann, F., and Ducastelle, F. (1971). Self-consistent theory of clusters in disordered alloys. *Phys. Rev. Lett.* 27, 429–431. doi:10.1103/PhysRevLett.27.429

Daven, D. M., Tit, N., Morris, J. R., and Ho, K. M. (1996). Structural optimization of Lennard-Jones clusters by a genetic algorithm. *Chem. Phys. Lett.* 256, 195–200. doi:10.1016/0009-2614(96)00406-X

De Heer, W. A. (1993). The physics of simple metal clusters: experimental aspects and simple models. *Rev. Mod. Phys.* 65, 611–676. doi:10.1103/RevModPhys.65.611

Deaven, D. M., and Ho, K. M. (1995). Molecular geometry optimization with a genetic algorithm. *Phys. Rev. Lett.* 75, 288–291. doi:10.1103/PhysRevLett.75.288

Dieterich, J. M., and Hartke, B. (2017). OGOLEM: framework for GA-based global optimization. Available at: https://www.ogolem.org/ (Accessed March 13, 2020).

Doye, J. P. K., Miller, M. A., and Wales, D. J. (1999). The double-funnel energy landscape of the 38-atom Lennard-Jones cluster. *J. Chem. Phys.* 110, 6896–6906. doi:10.1063/1.480217

Doye, J. P. K., Wales, D. J., and Berry, R. S., (1995). The effect of the range of the potential on the structures of clusters. *J. Chem. Phys.* 103, 4234–4249. doi:10.1063/1.470729

Doye, J. P. K., and Wales, D. J. (1995). Magic numbers and growth sequences of small face-centered-cubic and decahedral clusters. *Chem. Phys. Lett.* 247, 339–347. doi:10.1016/S0009-2614(95)01223-0

Dresselhaus, M. S., Dresselhaus, G., and Eklund, P. C. (1996). *Science of fullerenes and carbon nanotubes*. San Diego, CA: Academic Press, 965.

D'Agostino, G. (1993). Copper clusters simulated by a many-body tight-binding potential. *Philos. Mag. B* 68, 903–911. doi:10.1080/13642819308217948

Eberhardt, W. H., Crawford, B., and Lipscomb, W. N. (1954). The valence structure of the boron hydrides. *J. Chem. Phys.* 22, 989–1001. doi:10.1063/1.1740320

Enyashin, A. N., and Ivanovskii, A. L. R. (2005a). Calculating the atomic and electronic structure and magnetic properties of inorganic fullerenes. *Russian J. Phys. Chem.* 79, 940–945.

Enyashin, A. N., Bar-Sadan, M., Sloan, J., Houben, L., and Seifert, G. (2009). Nanoseashells and nanooctahedra of MoS_2: routes to inorganic fullerenes. *Chem. Mater.* 21, 5627–5636. doi:10.1021/am404843b

Enyashin, A. N., Gemming, S., Bar-SadanPopovitz-Biro, M., Hong, R., Y.Prior, S., Tenne, Y., et al. (2007). Struktur und Stabilität von Molybdänsulfid-Fullerenen. *Angew. Chem.* 119 (119), 631–635. doi:10.1002/ange.200602136

Enyashin, A. N., and Ivanovskii, A. L. (2008). Atomic and electronic structures and thermal stability of boron-nitrogen nanopeapods: $B_{12}N_{12}$ fullerenes in BN nanotubes. *Phys. Solid State* 50, 390–396. doi:10.1134/S1063783408020285

Enyashin, A. N., Medvedeva, N. I., Medvedeva, Y. E., and Ivanovskii, A. L. (2005b). Electronic structure and magnetic states of crystalline and fullerene-like forms of nickel dichloride NiCl[sub 2]. *Phys. Solid State* 47, 527–530. doi:10.1134/1.1884717

Enyashin, A. N., and Seifert, G. (2007). Titanium oxide fullerenes: electronic structure and basic trends in their stability. *Phys. Chem. Chem. Phys.* 9, 5772–5775. doi:10.1039/B712094J

Erlinda del, V. O., María, B., López, B., and Castroc, E. A. (2009). Spin polarized density functional theory applied to the study of nanoalloys. *Mecánica Computacional* XXVIII, 2435–2443.

Escher, S. G. E. T., Lazauskas, T., Zwijnenburg, M. A., and Woodley, S. M. (2017). Structure prediction of (BaO) n nanoclusters forn⩽24using an evolutionary algorithm. *Comput. Theor. Chem.* 1107, 74–81. doi:10.1016/j.comptc.2017.01.010

Fa, W., Luo, C., and Dong, J. (2005). Bulk fragment and tube like structures of AuN (N=2–26). *Phys. Rev. B* 72, 205428. doi:10.1103/PhysRevB.72.205428

Fang, P. P., Duan, S., Lin, X. D., Anema, J. R., Li, J. F., et al. (2011). Tailoring Au-core Pd-shell Pt-cluster nanoparticles for enhanced electrocatalytic activity. *Chem. Sci.* 2, 531–539. doi:10.1039/C0SC00489H

Farges, J., Feraudy De, M. F., Raoult, B., and Torchet, G. (1985). Cluster models made of double icosahedron units. *Surf. Sci.* 156, 370–378. doi:10.1016/0039-6028(85)90596-5

Farrell, J. D., Lines, C., Shepherd, J. J., Chakrabarti, D., Miller, M. A., and Wales, D. J. (2013). Energy landscapes, structural topologies and rearrangement mechanisms in clusters of dipolar particles. *Soft Matter* 9 (22), 5407–5416. doi:10.1039/C3SM50711D

Farrow, M. R., Chow, Y., and Woodley, S. M. (2014). Structure prediction of nanoclusters; a direct or a pre-screened search on the DFT energy landscape? *Phys. Chem. Chem. Phys.* 16, 21119–21134. doi:10.1039/C4CP01825G

Ferrando, R., Jellinek, J., and Johnston, R. L. (2008). Nanoalloys: from theory to applications of alloy clusters and nanoparticles. *Chem. Rev.* 108 (108), 845–910. doi:10.1021/cr040090g

Foresman, J. B., and Frisch, A. (1996). *Exploring chemistry with electronic structure methods*. Wallingford, CT: Gaussian Inc.

Fowler, P. W., Heine, T., Mitchell, D., Schmidt, R., and Seifert, G. (1996). Boron-nitrogen analogues of the fullerenes: the isolated-square rule. *J. Chem. Soc. Faraday Trans.* 92 (92), 2197–2201. doi:10.1039/FT9969202197

Fowler, P. W., Rogers, K. M., Seifert, G., Terrones, M., and Terrones, H. (1999). Pentagonal rings and nitrogen excess in fullerene-based BN cages and nanotube caps. *Chem. Phys. Lett.* 299, 359–367. doi:10.1016/S0009-2614(98)01265-2

Frisch, M. J. (2009). *Gaussian 09, revision*. Wallingford, CT: Gaussian Inc.

Furche, F., Ahlrichs, R., Weis, P. J., Gilb, C., Bierweiler, S. T., and Kappes, M. (2002). The structures of small gold cluster anions as determined by a combination of ion mobility measurements and density functional calculations. *J. Chem. Phys.* 117, 6982–6990. doi:10.1063/1.1507582

Gale, J. D. J. (1997). GULP: a computer program for the symmetry-adapted simulation of solids. *Faraday Trans.* 93, 629–637. doi:10.1039/A606455H

Gale, J. D., and Rohl, A. L. (2003). The general utility lattice program (GULP). *Mol. Simul.* 29, 291–341. doi:10.1080/0892702031000104887

Ghanty, T. K., Banerjee, A., and Chakrabarti, A. (2010). Structures and the electronic properties of $Au_{19}X$ clusters (X = Li, Na, K, Rb, Cs, Cu, and Ag). *J. Phys. Chem. C* 114, 20–27. doi:10.1021/jp906400t

Giannozzi, P., Baseggio, O., Bonfà, P., Brunato, D., Car, R., Carnimeo, I., et al. (2020). Quantum ESPRESSO toward the exascale. *Chem. Phys.* 152, 154105. doi:10.1063/5.0005082

Guimaraes, F. F., Belchior, J. C., Johnston, R. L., and Roberts, C. (2002). Global optimization analysis of water clusters $(H_2O)_n$ $(11 \leqslant n \leqslant 13)$ through a genetic evolutionary approach. *J. Chem. Phys.* 116, 8327–8333. doi:10.1063/1.1471240

Gupta, R. P. (1981). Lattice relaxation at a metal surface. *Phys. Rev. B* 23, 6265–6270. doi:10.1103/PhysRevB.23.6265

Häkkinen, H., Moseler, M., and Landman, U. (2002). Bonding in Cu, Ag, and Au clusters: relativistic effects, trends, and surprises. *Phys. Rev. Lett.* 89, 033401. doi:10.1103/PhysRevLett.89.033401

Halperin, W. P. (1986). Quantum size effects in metal particles. *Rev. Mod. Phys.* 58, 533–606. doi:10.1103/RevModPhys.58.533

Hartke, B. (2000). Global geometry optimization of molecular clusters: TIP4P water. *Z. Phys. Chem.* 214, 1251–1264. doi:10.1002/(SICI)1096-987X10.1524/zpch.2000.214.9.1251

Hartke, B. (1993). Global geometry optimization of clusters using genetic algorithms *J. Phys. Chem.* 97, 9973–9976. doi:10.1021/j100141a013

Hay, P. J., and Wadt, W. R. (1985). Ab initio effective core potentials for molecular calculations. Potentials for the transition metal atoms Sc to Hg. *J. Chem. Phys.* 82, 270. doi:10.1063/1.448799

Heath, J. R. (1995). Monolayer/bilayer transition in Langmuir films of derivatized gold nanoparticles at the gas/water interface: an x-ray scattering study. *Science* 270, 1315. doi:10.1063/1.1640334

Heinebrodt, M., Malinowski, N., Tast, F., Branz, W., Billas, I. M. L., and Martin, T. P. (1999). Bonding character of bimetallic clusters AunXm (X=Al, In, Cs). *J. Chem. Phys.* 110, 9915–9921. doi:10.1063/1.478865

Henkelman, G., and Jónsson, H. (2000b). Improved tangent estimate in the nudged elastic band method for finding minimum energy paths and saddle points. *J. Chem. Phys.* 113, 9978–9985. doi:10.1063/1.1323224

Henkelman, G., and Jónsson, H. (2001). Long time scale kinetic Monte Carlo simulations without lattice approximation and predefined event table. *J. Chem. Phys.* 115, 9657–9666. doi:10.1063/1.1415500

Henkelman, G., Uberuaga, B. P., and Jónsson, H. (2000a). A climbing image nudged elastic band method for finding saddle points and minimum energy paths. *J. Chem. Phys.* 113, 9901–9904. doi:10.1063/1.1329672

Hernandez-Rojas, J., and Calvo, F. (2019). Coarse-grained modeling of the nucleation of polycyclic aromatic hydrocarbons into soot precursors. *Phys. Chem. Chem. Phys.* 21 (9), 5123–5132. doi:10.1039/C8CP07724J

Hirsch, H. (2002). *The Chemistry of the fullerenes*. Weinheim, Germany: Wiley-VCH, 215.

Hirsch, H., and Brettreich, M. (2005). *Fullerenes: Chemistry and reactions*. Weinheim, Germany: Wiley-VCH, 440.

Hirsch, H. (1999). *Fullerenes and related structures*. Berlin, Germany: Springer, 246.

Hungria, A. B., Raja, R., Adams, R. D., Captain, B., Thomas, J. M., Midgley, P. A., et al. (2006). Single-step conversion of dimethyl terephthalate into cyclohexanedimethanol with Ru_5PtSn, a trimetallic nanoparticle catalyst. *Angew. Chem.* 118, 4900–4903. doi:10.1002/anie.200702407

Ismail, R. (2012). Theoretical studies of free and supported nanoalloy clusters. PhD thesis. Birmingham (England): The University of Birmingham.

Ivanovskaya, V. V., Enyashin, A. N., and Ivanovskii, A. L. (2004). Structure, electronic spectrum, and chemical bonding of fullerene-like nanoparticles based on MB_2(M = Mg, Al, Sc, Ti) layered diborides. *Inorg. Mater. Struct.* 40, 134–143. doi:10.1023/B:INMA.0000016087.31732.b0

Jäger, M., Schafer, R., and Johnston, R. L. (2019). GIGA: a versatile genetic algorithm for free and supported clusters and nanoparticles in the presence of ligands. *Nanoscale* 11, 9042–9052. doi:10.1039/C9NR02031D

Jain, P. K. (2005). A DFT-based study of the low-energy electronic structures and properties of small gold clusters. *Struct. Chem.* 16, 421–426. doi:10.1007/s11224-005-6350-8

Jellinek, J. (1999). *Theory of atomic and molecular clusters: with a glimpse at experiments*. Berlin, Germany: Springer.

Johnston, R. L. (2002). *Atomic and molecular clusters*. London, England: Taylor and Francis.

Johnston, R. L. (2003). Evolving better nanoparticles: genetic algorithms for optimising cluster geometries. *Dalton Trans.* 22, 4193–4207. doi:10.1039/B305686D

Jorgensen, W. L., Chandrasekhar, J., and Klein, M. L. (1983c). Comparison of simple potential functions for simulating liquid water. *J. Chem. Phys.* 79, 926–935. doi:10.1063/1.445869

Jorgensen, W. L., Chandrasekhar, J., Madura, J. D., Impey, R. W., and Klein, M. L. (1983a). Comparison of simple potential functions for simulating liquid water. *J. Chem. Phys.* 79, 926–935. doi:10.1063/1.445869

Jorgensen, W. L., Chandrasekhar, J., Madura, J. D., Impey, R. W., and Klein, M. L. (1983b). Comparison of simple potential functions for simulating liquid water. *J. Chem. Phys.* 79, 926–935. doi:10.1063/1.445869

Kabir, M., Mookerjee, A., Datta, R., Banerjea, A., and Bhattacharya, A. K. (2003). Study of small metallic nanoparticles an ab-initio full-potential muffin-tin orbitals based molecular dynamics study of small Cu clusters. *Int. J. Mod. Phys. B* 17, 2061–2075. doi:10.1142/S0217979203018181

Karaboga, D. (2005). *An idea based on honey bee swarm for numerical optimization: technical report TR06*. Kayseri, Turkey: Erciyes University.

Kazachenko, S., and Thakkar, A. J. (2010). Are there any magic numbers for water nanodroplets, $(H_2O)_n$, in the range 36 ≤n≤ 50? *Mol. Phys.* 108, 2187–2193. doi:10.1063/1.445869

Klanberg, F., Eaton, D. R., Guggenberger, L. J., and Muetterties, E. L. (1967). Chemistry of boranes. XXVIII. New polyhedral borane anions, B8H82-, B8H8-, and B7H72-. *Inorg. Chem.* 6, 1271–1281. doi:10.1016/S0040-4020(01)90682-9

Klanberg, F., and Muetterties, E. L. (1966). Chemistry of boranes. XXVII. new polyhedral borane anions, B9H92-and B11H112-. *Inorg. Chem.* 5, 1955–1960. doi:10.1021/ic50045a027

Knudsen, J., Nilekar, A. U., Vang, R. T., Schnadt, J., Kunkes, E. L., and Dumesic, J. A. (2007). A Cu/PtNear-Surface alloy for Water−Gas shift catalysis. *J. Am. Chem. Soc.* 129, 6485–6490. doi:10.1021/ja0700855

Kresse, G., and Furthmüller, J. (1996). Efficient iterative schemes forab initiototal-energy calculations using a plane-wave basis set. *Phys. Rev. B* 54 (16), 11169–11186. doi:10.1103/physrevb.54.11169

Kroto, H. W., Heath, J. R., OBrien, S. C., Curl, R. F., and Smalley, R. E. (1985). C60: buckminsterfullerene. *Nature* 318, 162–163. doi:10.1038/318162a0

Kumar, V. (2003). Novel metal-encapsulated caged clusters of silicon and germanium. *Eur. Phys. J. D-At. Mol. Opt. Phys.* 24, 227–232. doi:10.1140/epjd/e2003-00194-5

Kumeda, Y., Munro, L. J., and Wales, D. J. (2001). Transition states and rearrangement mechanisms from hybrid eigenvector-following and density functional theory. *Chem. Phys. Lett.* 341, 185–194. doi:10.1016/S0009-2614(01)00334-7

Lathiotakis, N. N., Andriotis, A. N., Menon, M., and Connolly, J. (1996). Tight binding molecular dynamics study of Ni clusters. *J. Chem. Phys.* 104, 992–1003. doi:10.1063/1.470823

Lazauskas, T., Sokol, A. A., and Woodley, S. M. (2017). An efficient genetic algorithm for structure prediction at the nanoscale. *Nanoscale* 9, 3850–3864. doi:10.1039/C6NR09072A

Leary, R. H., and Doye, J. P. K. (1999a). Tetrahedral global minimum for the 98-atom Lennard-Jones cluster. *Phys. Rev. E* 60, R6320–R6322. doi:10.1063/1.480465

Leary, R. H., and Doye, J. P. K. (1999b). Tetrahedral global minimum for the 98-atom Lennard-Jones cluster. *Phys. Rev. E* 60, R6320–R6322. doi:10.1103/PhysRevE.60.R6320

Lesley, D. L., and Johnston, R. L. (2000). Theoretical analysis of 17–19-atom metal clusters using many-body potentials. *J. Chem. Soc. Dalton Trans.*, 307–316. doi:10.1039/A908003A

Li, J., Li, X., Zhai, H., and Wang, L. (2003). Au20: a tetrahedral cluster. *Science* 299, 864–867. doi:10.1126/science.1079879

Li, T., Yin, S., Ji, Y., Wang, G., and Zhao, J. (2000). A genetic algorithm study on the most stable disordered and ordered configurations of Au38-55. *Phys. Lett. A* 267, 403–407. doi:10.1016/S0375-9601(00)00120-1

Li, Z., and Scheraga, H. A. (1987). Monte Carlo-minimization approach to the multiple-minima problem in protein folding. *Proc. Natl. Acad. Sci. U.S.A.* 84, 6611–6615. doi:10.1073/pnas.84.19.6611

Liu, D. C., and Nocedal, J. (1989b). On the limited memory BFGS method for large scale optimization. *Math. Programming* 45, 503–528. doi:10.1007/BF01589116

Liu, H. B., Pal, U., Medina, A., Maldonado, C., and Ascencio, J. A. (2005). Structural incoherency and structure reversal in bimetallicAu−Pdnanoclusters. *Phys. Rev. B* 71, 075403–2. doi:10.1103/PhysRevB.71.075403

Llanio-Trujillo, J. L., Marques, J. M. C., and Pereira, F. B. (2011). An evolutionary algorithm for the global optimization of molecular clusters: application to water, benzene, and benzene cation. *J. Phys. Chem. A.* 115, 2130–2138. doi:10.1021/jp1117695

Lloyd, L. D., Johnston, R. L., Roberts, C., and Mortimer-Jones, T. V. (2002). Geometry Optimisation of Aluminium Clusters Using a Genetic Algorithm. *ChemPhysChem* 3, 408–415. doi:10.1002/1439-7641(20020517)3

Lloyd, L. D., and Johnston, R. L. (2000). Theoretical analysis of 17-19-atom metal clusters using many-body potentials †. *J. Chem. Soc. Dalton Trans.* 2000, 307–316. doi:10.1039/A908003A

Longuet-Higgins, H. C., and Roberts, M. D. (1955). The electronic structure of an icosahedron of boron atoms. *Proc. R. Soc.* 230A, 110–119. doi:10.1098/rspa.1955.0115

Longuet-Higgins, H. C., and Roberts, M. D. (1954). The electronic structure of the borides MB 6. *Proc. R. Soc.* 224A, 336–347. doi:10.1098/rspa.1954.0162

Lordeiro, R. A., Guimaraes, F. F., Belchior, J. C., and Johnston, R. L. (2003). Determination of main structural compositions of nanoalloy clusters of CuxAuy (x + y ≤ 30) using a genetic algorithm approach. *Int. J. Quan. Chem.* 95, 112–125. doi:10.1002/qua.10660

Makov, G., and Payne, M. C. (1995). Periodic boundary conditions inab initiocalculations. *Phys. Rev. B* 51, 4014–4022. doi:10.1103/PhysRevB.51.4014

Maksimuk, S., Yang, S., Peng, Z., and Yang, H. (2007). Synthesis and Characterization of Ordered Intermetallic PtPb Nanorods. *J. Am. Chem. Soc.* 129, 8684–8685. doi:10.1021/ja071980r

Margulis, L., Tenne, R., and Iijima, S. (1996). Nucleation of WS2Fullerenes at Room Temperature. *Microsc. Microanal. Microstruct.* 7, 87–89. doi:10.1051/mmm:1996107

Marques, J. M. C., Jesus, W. S., Prudente, F. V., and Pereira, F. B. (2018). Revealing Energy Landscapes of Atomic Clusters by Applying Adaptive Bioinspired Algorithms. *Phys. Chem. Chemist. Chem. Enginee.* 3, 28. doi:10.1201/b22413

Marques, J. M. C., and Pereira, F. B. (2010a). An evolutionary algorithm for global minimum search of binary atomic clusters. *Chem. Phys. Lett.* 485 (1–3), 211–221. doi:10.1016/j.cplett.2009.11.059

Marques, J. M. C., and Pereira, F. B. (2011). EA_MOL: evolutionary algorithm for the global minimum search of molecular clusters. Available at: https://apps.uc.pt/mypage/faculty/qtmarque/en/software/ (Accessed Feburary 20, 2020).

Marques, J. M. C., and Pereira, F. B. (2013). A detailed investigation on the global minimum structures of mixed rare-gas clusters: Geometry, energetics, and site occupancy. *J. Comput. Chem.* 34 (6), 505–517. doi:10.1002/jcc.23161

Marques, J. M. C., and Pereira, F. B. (2015). Colloidal clusters from a global optimization perspective. *J. Mol. Liquids* 210, 51–63. doi:10.1016/j.molliq.2015.03.009

Martínez-Núñez, E., Barnes, G. L., Glowacki, D. R., Kopec, S., Pelaez-Ruiz, D., Rodriguez, A., et al. (2020). AutoMeKin: automated mechanisms and kinetics. Available at: https://rxnkin.usc.es/index.php/AutoMeKin (Accessed January 14, 2020).

Martin, T. P. (1996). Shells of atoms. *Phys. Rep.* 273, 199–241. doi:10.1016/0370-1573(95)00083-6

Martínez-Núñez, E. (2015a). An automated method to find transition states using chemical dynamics simulations. *J. Comput. Chem.* 36, 222–234. doi:10.1002/jcc.23790

Martínez-Núñez, E. (2015b). An automated transition state search using classical trajectories initialized at multiple minima. *Phys. Chem. Chem. Phys.* 17, 14912. doi:10.1039/C5CP02175H

Massobrio, C., PasquarelloDal Corso, A., and Dal Corso, A. (1998). Structural and electronic properties of small CunCun clusters using generalized-gradient approximations within density functional theory. *J. Chem.Phys.* 109, 6626–6630. doi:10.1063/1.477313

Małolepsza, E., Strodel, B., Khalili, M., Trygubenko, S., Fejer, S. N., and Wales, D. J. (2010). Symmetrization of the AMBER and CHARMM force fields. *J. Comput. Chem.* 31, 1402–1409. doi:10.1002/jcc.21425

Menon, M., Connolly, J., Lathiotakis, N., and Andriotis, A. (1994). Tight-binding molecular-dynamics study of transition-metal clusters. *Phys. Rev. B* 50, 8903–8906. doi:10.1103/PhysRevB.50.8903

Metadjer, N., Laref, A., and Khelifa, B. (2001). TightTight-binding calculation of structural properties of bulk Cu_3Au and its corresponding clusters. *Superlatti. Microstru.* 30, 21–28. doi:10.1006/spmi.2001.0988

Michaelian, K., Rendon, N., and Garz_on, I. L. (1999). Structure and energetics of Ni, Ag, and Au nanoclusters. *Phys. Rev. B* 60, 2000–2010. doi:10.1103/PhysRevB.60.2000

Miller, M. A., and Wales, D. J. (2005). Novel structural motifs in clusters of dipolar spheres: knots, links, and coils. *J. Phys. Chem. B* 109, 23109. doi:10.1021/jp0549632

Mohr, S., Pochet, P., Amsler, M., Schaefer, B., Sadeghi, A., Genovese, L., et al. (2014). Boron aggregation in the ground states of boron-carbon fullerenes. *Phys. Rev. B* 89, 041404(R). doi:10.1103/PhysRevB.89.041404

Molayem, M., Grigoryan, V. G., and Springborg, M. (2010). Theoretical studies of structural and electronic properties of clusters. *J. Phys. Chem. C* 115, 7179–7192. doi:10.1021/jp1094678

Molayem, M., Grigoryan, V. G., and Springborg, M. (2011). Global Minimum Structures and Magic Clusters of CumAgn Nanoalloys. *J. Phys. Chem. C* 115, 22148–22162. doi:10.1021/jp2050417

Moore, J. M. (2013). molecular dynamics simulations of supported Pt nanoclusters with sutton-chen potentials. *J. Phys. Chem* 120, 14883–14891. doi:10.1021/acs.jpcc.6b03074

Morgan, J. W. R., and Wales, D. J. (2014). Energy landscapes of planar colloidal clusters. *Nanoscale.* 6, 10717–10726. doi:10.1039/C4NR02670E

Neugebauer, J., and Scheffler, M. (1992). Adsorbate-substrate and adsorbate-adsorbate interactions of Na and K adlayers on Al(111). *Phys. Rev. B* 46, 16067. doi:10.1103/physrevb.46.16067

Nigam, S., and Majumder, C. (2007). Magnetic needles encapsulated inside (BN)36 cage: Prediction of atomic, electronic, and magnetic structure from first principle calculations. *Appl. Phys. Lett.* 91, 223112. doi:10.1063/1.2815922

Nishiwaki, A., Oku, T., and Suganuma, K. (2004). Atomic and electronic structures of endohedral B36N36 clusters with doping elements studied by molecular orbital calculations. *Physica B: Condensed Matter* 349, 254–259. doi:10.1016/j.physb.2004.03.308

Nu_nez, S., and Johnston, R. L. (2010). Structures and Chemical Ordering of Small Cu–Ag Clusters.J. *Phys. Chem. C* 114, 13255–13266. doi:10.1021/jp1048088

Núñez, R., Tarrés, M., Ferrer-Ugalde, A., de Biani, F. F., and Teixidor, F. (2016a). Electrochemistry and photoluminescence of icosahedral carboranes, boranes, metallacarboranes, and their derivatives. *Chem. Rev.* 116, 14307–14378. doi:10.1021/acs.chemrev.6b00198

Núñez, R., Romero, I., Teixidor, F., and Viñas, C. (2016b). Icosahedral boron clusters: A perfect tool for the enhancement of polymer features. *Chem. Soc. Rev.* 45, 5147–5173. doi:10.1039/C6CS00159A

Oakley, M. T., Johnston, R. L., and Wales, D. J. (2013). Symmetrisation schemes for global optimisation of atomic clusters. *Phys. Chem. Chem. Phys.* 15, 3965–3976. doi:10.1039/C3CP44332A

Oderji, H. Y., and Ding, H. (2011). Determination of melting mechanism of $Pd_{24}Pt_{14}$ nanoalloy by multiple histogram method via molecular dynamics simulations. *Chem. PhysicsChem. Phys.* 388, 23–30. doi:10.1016/j.chemphys.2011.07.011

Ohno, K., and Maeda, S. (2019). Distribution of GRRM. Available at: https://iqce.jp/GRRM/index_e.shtml (Accessed October 5, 2020).

Ohno, K., and Maeda, S. (2006). global reaction route mapping on potential energy surfaces of formaldehyde, formic acid, and their metal-substituted analogues. *J. Phys. Chem. A.* 110, 8933–8941. doi:10.1021/jp061149l

Oku, T., Nishiwaki, A., and Narita, I. (2004a). Formation and atomic structure of $B_{12}N_{12}$ nanocage clusters studied by mass spectrometry and cluster calculation. *Sci. Tech. Adv. Mater.* 5, 635–638. doi:10.1016/j.stam.2004.03.017

Oku, T., Nishiwaki, A., and Narita, I. (2004b). Formation and structure of B28N28 clusters studied by mass spectrometry and molecular orbital calculation. *Solid State. Commun.* 130, 171–173. doi:10.1016/j.ssc.2004.02.004

Oku, T., Nishiwaki, A., and Narita, I. (2004c). Formation and structures of B36N36 and Y@B36N36 clusters studied by high-resolution electron microscopy and mass spectrometry clusters studied by high-resolution electron microscopy and mass spectrometry. *J. Phys. Chem. Sol.* 65, 369–372. doi:10.1016/j.jpcs.2003.09.010

Oku, T., Nishiwaki, A., Narita, I., and Gonda, M. (2003). Formation and structure of. $B_{24}N_{24}$ clusters. *Chem. Phys. Lett.* 380, 620–623. doi:10.1016/j.stam.2004.03.017

Osorio, E., Olson, J. K., Tiznado, W., and Boldyrev, A. I. (2012). Analysis of why boron avoids sp^2 hybridization and classical structures in the B_nH_{n+2} Series. *Chem. Eur. J.* 18 (31), 9677–9681. doi:10.1002/chem.201200506

Oviedo, J., and Palmer, R. E. (2002). Amorphous structures of Cu, Ag, and Au nanoclusters from first principles calculations. *J. Chem. Phys.* 117, 9548–9551. doi:10.1063/1.1524154

Pant, M. M., and Rajagopal, A. K. (1972). Theory of inhomogeneous magnetic electron gas. *Solid State. Commun.* 10, 1157–1160. doi:10.1016/0038-1098(72)90934-9

Papavassiliou, G. C. (1979). Optical properties of small inorganic and organic metal particles. *Prog. Solid State. Chem.* 12, 185–271. doi:10.1016/0079-6786(79)90001-3

Paramonov, L., and Yaliraki, S. N. (2005). The directional contact distance of two ellipsoids: coarse-grained potentials for anisotropic interactions. *J. Chem. Phys.* 123, 194111–194122. doi:10.1063/1.2102897

Parilla, P. A., Dillon, A. C., Parkinson, B. A., Jones, K. M., Alleman, J., Riker, G., et al. (2004). Formation of nanooctahedra in molybdenum disulfide and molybdenum diselenide using pulsed laser vaporization. *J. Phys. Chem. B* 108, 6197–6207. doi:10.1021/jp036202

Pauling, L., and Weinbaum, S. (1934). The structure of calcium boride. *Z. Kristallogr.* 87, 181–183. doi:10.1007/BF00802582

Paz Borbón, L. O., Johnston, R. L., Barcaro, G., and Fortunelli, A. (2008). Structural motifs, mixing, and segregation effects in 38-atom binary clusters. *J. Chem. Phys.* 128, 134517. doi:10.1063/1.2897435

Perdew, J. P. (1991). " in *Electronic structure of solids '91*. Editors P. Ziesche and H. Eschriq (Berlin, Germany: AkademieVerlag), 11–20.

Perdew, J. P., Burke, K., and Ernzerhof, M. (1996). Generalized Gradient Approximation Made Simple. *Phys. Rev. Lett.* 77, 3865–3868. doi:10.1103/PhysRevLett.77.3865

Perdew, J. P., and Wang, Y. (1992). Accurate and simple analytic representation of the electron-gas correlation energy. *Phys. Rev. B* 45, 13244–13249. doi:10.1103/PhysRevB.45.13244

Pillardy, J., Liwo, A., and Scheraga, H. A. (1999). An efficient deformation-based global optimization method (self-consistent basin-to-deformed-basin mapping (SCBDBM)). application to lennard-jones atomic clusters. *J. Phys. Chem. A.* 103, 9370–9377. doi:10.1021/jp992741w

Pokropivny, V. V., and Bekenev, V. L. (2006). Electronic properties and bulk moduli of new boron nitride polymorphs, i.e., hyperdiamond $B_{12}N_{12}$ and simple cubic $B_{24}N_{24}$, $B_{12}N_{12}$ fulborenites. *Semiconductors* 40, 636–641. doi:10.1134/S1063782606060042

Pokropivny, V. V., Skorokhod, V. S., Oleinik, G. S., Kurdyumov, A. V., Bartnitskaya, T. S., Pokropivny, A. V., et al. (2000). Boron nitride analogs of fullerenes (the Fulborenes), nanotubes, and fullerites (the fulborenites. *J. Solid State. Chem.* 154, 214–222. doi:10.1006/jssc.2000.8838

Pokropivny, V. V., Smolyar, A. S., and Pokropivny, A. V. (2007). Fluid synthesis and structure of a new boron nitride polymorph-hyperdiamond fulborenite $B_{12}N_{12}$ (E phase). *Phys. Solid State* 49, 591–598. doi:10.1134/S1063783407030365

Ralph, D. C., Black, C. T., and Tinkham, M. (1995). Spectroscopic measurements of discrete electronic states in single metal particles. *Phys. Rev. Lett.* 74, 3241–3244. doi:10.1103/PhysRevLett.74.3241

Roberts, C., and Johnston, R. L. (2001). Investigation of the structures of MgO clusters using a genetic algorithm. *Phys. Chem. Chem. Phys.* 2001 (3), 5024–5034. doi:10.1039/B106507F

Roberts, C., Johnston, R. L., and Wilson, N. T. (2000). A genetic algorithm for the structural optimization of Morse clusters. *Theor. Chem. Acc.* 104, 123–130. doi:10.1007/s002140000117

Rodríguez-Fernández, R., Pereira, F. P., Marques, J. M. C., Vázquez-Rodríguez, S., and Martinez-Nunez, E. (2020). GAFit, version 1.6. Available at: https://rxnkin.usc.es/index.php/GAFit (Accessed January 29, 2020).

Rodríguez-Fernández, R., Pereira, F. B., Marques, J. M. C., Martínez-Núñez, E., and Vázquez, S. A. (2017). GAFit: A general-purpose, user-friendly program for fitting potential energy surfaces. *Comput. Phys. Commun.* 217, 89. doi:10.1016/j.cpc.2017.02.008

Rogers, K. M., Fowler, P. W., and Seifert, G. (2000). Chemical versus steric frustration in boron nitride heterofullerene polyhedra. *Chem. Phys. Lett.* 332, 43–50. doi:10.13005/ojc/300247

Rossi, G., and Ferrando, R. (2009). Searching for low-energy structures of nanoparticles: a comparison of different methods and algorithms. *J. Phys. Condens. Matter* 21, 084208. doi:10.1088/0953-8984/21/8/084208

Rossi, G., Rapallo, A., Mottet, C., Fortunelli, A., Baletto, F., and Ferrando, R. (2004). Magic polyicosahedral core-shell clusters. *Phys. Rev. Lett.* 93, 105503–105507. doi:10.1103/PhysRevLett.93.105503

Saunders, M. (1987). stochastic exploration of molecular mechanics energy surfaces. hunting for the global minimum. *J. Am. Chem. Soc.* 109, 3150–3152. doi:10.1021/ja00244a051

Scott, R. W. J., Wilson, O. M., Oh, S.-K., Kenik, E. A., and Crooks, R. M. (2004). Bimetallic palladium–gold dendrimer-encapsulated Catalysts. *J. Am. Chem. Soc.* 126, 15583–15591. doi:10.1021/ja0475860

Seifert, G., Fowler, P. W., Mitchell, D., Porezag, D., and Frauenheim, T. (1997). Boron-nitrogen analogues of the fullerenes: electronic and structural properties. *Chem. Phys. Lett.* 268, 352–358. doi:10.1016/S0009-2614(97)00214-5

Seifert, G., Heine, T., and Fowler, P. W. (2001). Inorganic nanotubes and fullerenes - Structure and properties of hypothetical phosphorus fullerenes. *Eur. Phys. J. D* 16 (1–3), 341–343. doi:10.1007/s100530170125

Shang, C., and Liu, Z.-P. (2013). Stochastic Surface Walking Method for Structure Prediction and Pathway Searching. *J. Chem. Theor. Comput.* 9, 1838–1845. doi:10.1021/ct301010b

Shao, X., Jiang, H., and Cai, W. (2004a). Parallel Random Tunneling Algorithm for Structural Optimization of Lennard-Jones Clusters up toN= 330. *J. Chem. Inf. Comput. Sci.* 44 (1), 193–199. doi:10.1021/ci0340862

Shao, X., Cheng, L., and Cai, W. (2004b). A dynamic lattice searching method for fast optimization of Lennard-Jones clusters. *J. Comput. Chem.* 25, 1693–1698. doi:10.1002/jcc.20096

Shao, X., Cheng, L., and Cai, W. (2004c). An adaptive immune optimization algorithm for energy minimization problems. *J. Chem. Phys.* 120, 11401–11406. doi:10.1063/1.1753257

Shayeghi, A., Götz, D., Davis, J. B. A., Schäfer, R., and Johnston, R. L. (2015). Pool-BCGA: a parallelised generation-free genetic algorithm for the ab initio global optimisation of nanoalloy clusters. *Phys. Chem. Chem. Phys.* 17, 2104–2112. doi:10.1039/C4CP04323E

Shi, H., Kuang, X., and Lu, C. (2020). LiB_{13}: a new member of tetrahedral-typed B_{13} ligand half-surround cluster. *Sci. Rep.* 10, 1642–1651. doi:10.1038/s41598-020-57769-2

Smeeton, L. C., Oakley, M. T., and Johnston, R. L. (2014). Visualizing energy landscapes with metric disconnectivity graphs. *J. Comput. Chem.* 35, 1481–1490. doi:10.1002/jcc.23643

Solov'yov, I. A., Solov'yov, A. V., and Greiner, W. (2002). Structure and properties of small sodium clusters. *Phys. Rev. B* 65, 053203–053222. doi:10.1103/PhysRevA.65.053203

Srivastava, R. (2018b). Theoretical analysis of Au_{38}-xPtx and $Au_{38-x}Ag_x$ (x=1−19) bimetallic clusters. *AASCIT J. Mater.* 4 (2), 33–42.

Srivastava, R. (2018a). Complexes of DNA bases and Watson-Crick base pairs interaction with neutral silver Ag_n (n = 8, 10, 12) clusters: a DFT and TDDFT study. *J. Biomol. Struct. Dyn.* 36 (4), 1050–1062. doi:10.1080/07391102.2017.1310059

Srivastava, R. (2017a). Interaction of cysteine with Au_n (n =8, 10, 12) even neutral clusters: a theoretical study. *ChemistrySelect* 2, 2789–2796. doi:10.1002/slct.201700041

Srivastava, R. (2017b). Structural Optimization of (Au_m-Ag_n-Pd_o-Pt_p) (m=10 and n+o+p=10) Tetrametallic Clusters Using a Combined Empirical Potential-Density Functional (EP-DF) Approach. *ChemistrySelect* 2, 8063–8071. doi:10.1002/slct.201701145

Srivastava, R. (2017c). Theoretical studies on the electronic and optoelectronic properties of [A.2AP(w)/A*.2AP(WC)/C.2AP(w)/C*.2AP(WC)/C.A(w)/C*.A(WC)]-Au_8 mismatch nucleobase complexes. *Mol. Phys.* 116 (2), 263–272. doi:10.1080/00268976.2017.1382737

Stillinger, F. H., and Weber, T. A. (1988). Nonlinear optimization simplified by hypersurface deformation. *J. Stat. Phys.* 52, 1429–1445. doi:10.1007/bf01011658

Stock, A., and Massanez, C. (1912). Borwasserstoffe. *Chem. Ber* 45 (1912), 3539–3568. doi:10.1002/cber.191204503113

Strohl, J., and King, T. (1989). A multicomponent, multilayer model of surface segregation in alloy catalysts. *J. Catal.* 118, 53–67. doi:10.1016/0021-9517(89)90300-X

Strout, D. L. (2004). Fullerene-like cages versus alternant cages: isomer stability of $B_{13}N_{13}$, $B_{14}N_{14}$, and $B_{16}N_{16}$. *Chem. Phys. Lett.* 383, 95–98. doi:10.1016/j.cplett.2003.10.141

Stucky, G. D., Herron, N., Wang, Y., Eddy, M., Cox, D., Moller, K., et al. (1989). Structure and optical properties of cadmium sulfide superclusters in zeolite hosts. *J. Am. Chem. Soc.* 111, 530–540. doi:10.1021/ja00184a021

Takeuchi, H. (2006). Clever and efficient method for searching optimal geometries of Lennard-Jones clusters. *J. Chem. Inf. Model.* 46, 2066–2070. doi:10.1021/ci600206k

Teixeira, P. I. C., Tavares, J. M., and Gama, M. M. T. d. (2000). The effect of dipolar forces on the structure and thermodynamics of classical fluids. *J. Phys. Condens. Matter* 12, R411–R434. doi:10.1088/0953-8984/12/33/201

Teng, X., and Yang, H. (2003). Synthesis of face-centered tetragonal FePt nanoparticles and granular films from Pt@Fe_2O_3 core–shell nanoparticless. *J. Am. Chem. Soc.* 125, 14559–14563. doi:10.1021/ja0376700

Tenne, R., and Seifert, G. (2009). Recent Progress in the Study of Inorganic Nanotubes and Fullerene-Like Structures. *Annu. Rev. Mater. Res.* 39, 387–413. doi:10.1146/annurev-matsci-082908-145429

Teo, B. K., Zhang, H., and Shi, X. (1993). Design, synthesis, and structure of the largest trimetallic cluster, [$(Ph_3P)10Au_{12}Ag_{12}PtC_{l7}$]Cl: the first example of a trimetallic biicosahedral supracluster and its implication for the vertex-sharing polyicosahedral growth of the gold/silver/platinum ternary cluster system. *J. Am. Chem. Soc.* 115, 8489–8490. doi:10.1021/ja00071a085

TeVelde, G., Bickelhaupt, F. M., Baerends, E. J., Fonseca Guerra, C., van Gisbergen, S. J. A., Snijders, J. G., et al. (2001). Chemistry with ADF. *J. Comput. Chem.* 22, 931–967. doi:10.1002/jcc.1056

Toshima, N., and Yonezawa, T. (1998). Bimetallic nanoparticles-novel materials for chemical and physical applications. *New J. Chem.* 22, 1179–1201. doi:10.1039/A805753B

Trygubenko, S. A., and Wales, D. J. (2004). A doubly nudged elastic band method for finding transition states. *J. Chem. Phys.* 120, 2082–2094. doi:10.1063/1.1636455

vanLenthe, E., Baerends, E. J., and Snijders, J. G. (1993). Relativistic regular two-component Hamiltonians. *J. Chem. Phys.* 99, 4597–4610. doi:10.1063/1.466059

vanLenthe, E., Baerends, E. J., and Snijders, J. G. (1994). Relativistic total energy using regular approximations. *Chem. Phys.* 101, 9783–9792. doi:10.1063/1.467943

Wales, D. J. (2004). Some further applications of discrete path sampling to cluster isomerization. *Mol. Phys.* 102, 891–908. doi:10.1080/00268970410001703363

Wales, D. J. (2012). Decoding the energy landscape: extracting structure, dynamics and thermodynamics. *Phil. Trans. R. Soc. A.* 370, 2877–2899. doi:10.1021/acs.jctc.5b00962

Wales, D. J., and Doye, J. P. K. (1997). Global optimization by basin-hopping and the lowest energy structures of Lennard-Jones clusters containing up to 110 atoms. *J. Phys. Chem. A.* 101, 5111–5116. doi:10.1021/jp970984n

Wales, D. J. (2010). Energy landscapes of clusters bound by short-ranged potentials. *Chem. Eur. J. Chem. Phys.* 11, 2491–2494. doi:10.1002/cphc.201000233

Wales, D. J., Miller, M. A., and Walsh, T. R. (1998). Archetypal energy landscapes. *Nature* 394, 758–760. doi:10.1038/29487

Wales, D. J., and Scheraga, H. A. (1999). Global optimization of clusters, crystals, and biomolecules. *Science* 285, 1368–1372. doi:10.1126/science.285.5432.1368

Wang, J., Wang, G., and Zhao, J. (2003). Structures and electronic properties of Cu_{20}, Ag_{20}, and Au_{20} clusters with density functional method. *Chem. Phys. Lett.* 380, 716–720. doi:10.1016/j.cplett.2003.09.062

Wang, L., and Yamauchi, Y. (2011). Tailoring Au-core Pd-shell Pt-cluster nanoparticles for enhancedelectrocatalytic activity. *Chem. Sci.* 2, 531–539. doi:10.1039/C0SC00489H

Wilson, N. T., and Johnston, R. L. (2000). Modelling gold clusters with an empirical many-body potential. *Eur. Phys. J. D* 12, 161–169. doi:10.1007/s100530070053

Winter, B. J., Parks, E. K., and Riley, S. J. (1991). Copper clusters: The interplay between electronic and geometrical structure. *J. Chem. Phys.* 94, 8618–8621. doi:10.1063/1.460046

Woodley, S. M. (2013). knowledge led master code search for atomic and electronic structures of LaF_3 nanoclusters on hybrid rigid ion–shell model–DFT landscapes. *J. Phys. Chem. C* 117, 24003–24014. doi:10.1021/jp406854j

Wu, G., Sun, Y., Wu, X., Chen, R., and Wang, Y. (2017). Large scale structural optimization of trimetallic Cu-Au-Pt clusters up to 147 atoms. *Chem. Phys. Lett.* 686, 103–110. doi:10.1016/j.cplett.2017.08.049

Wu, X., Wu, G., and Youcun, C. (2011). structural optimization of Cu-Ag-Au trimetallic clusters by adaptive immune optimization algorithmstructural optimization of CuAgAu trimetallic clusters by adaptive immune optimization algorithm. *J. Phys. Chem. A.* 115, 13316–13323. doi:10.1021/jp208514m

Wu, X., Cai, W., and Shao, X. (2009). Optimization of bimetallic Cu-Au and Ag-Au clusters by using a modified adaptive immune optimization algorithm. *J. Comput. Chem.* 30, 1992–2000. doi:10.1063/1.4896152

Wu, X., and Dong, Y. (2014b). Theoretical studies of structures and energies of Pd, Au-Pd, and Au-Pd-Pt clusters. *New J. Chem.* 38, 4893–4900. doi:10.1039/C4NJ00984C

Wu, X., Liu, Q., Sun, Y., and Wu, G. (2015). Structural characterization of metal dopants (M = Ag or Au) in trimetallic M-Pd-Pt clusters. *RSC Adv.* 5, 51142–51148. doi:10.1039/C5RA06457K

Wu, X., and Wu, G. (2014a). An adaptive immune optimization algorithm with dynamic lattice searching operation for fast optimization of atomic clusters. *Chem. Phys.* 440, 94–98. doi:10.1016/j.chemphys.2014.06.002

Xiang, Y., Cheng, L., Cai, W., and Shao, X. (2004). structural distribution of lennard-jones clusters containing 562 to 1000 atoms. *J. Phys. Chem. A.* 108, 9516–9520. doi:10.1021/jp047807o

Xiao, Y., and Williams, D. E. (1993). Genetic algorithm: a new approach to the prediction of the structure of molecular clusters. *Chem. Phys. Lett.* 215, 17–24. doi:10.1016/0009-2614(93)89256-H

Yan, J., Yang, W., Zhang, Q., and Yan, Y. (2020). Introducing borane clusters into polymeric frameworks: architecture, synthesis, and applications. *Chem. Commun.* 56, 11720–11734. doi:10.1039/D0CC04709K

Yañez, O., Báez-Grez, R., Inostroza, D., Rabanal-León, W. A., Pino-Rios, R., Garza, J., et al. (2019). Automaton: a program that combines a probabilistic cellular automata and a genetic algorithm for global minimum search of clusters and molecules. *J. Chem. Theor. Comput.* 15, 1463–1475. doi:10.1021/acs.jctc.8b00772

Yañez, O., Inostroza, D., Usuga-Acevedo, B., Pino-Rios, R., Tabilo-Sepulveda, M., Garza, J., et al. (2020). Evaluation of restricted probabilistic cellular automata on the exploration of the potential energy surface of Be_6B_{11}−. *Theor. Chem. Acc.* 139, 41. doi:10.1007/s00214-020-2548-5

Ye, H., and Crooks, R. M. (2007). effect of elemental composition of PtPd bimetallic nanoparticles containing an average of 180 atoms on the kinetics of the electrochemical oxygen reduction reaction. *J. Am. Chem. Soc.* 129 (129), 3627–3633. doi:10.1021/ja068078o

Ye, T., Xu, R., and Huang, W. (2011). global optimization of binary lennard-jones clusters using three perturbation operators. *J. Chem. Inf. Model.* 51 (3), 572–577. doi:10.1021/ci1004256

Yuan, D. W., Wang, Y., and Zeng, Z. (2005). Geometric, electronic, and bonding properties of AuNM (N=1–7, M=Ni, Pd, Pt) clusters. *J. Chem. Phys.* 122, 114310. doi:10.1063/1.1862239

Zeiri, Y. (1995). Prediction of the lowest energy structure of clusters using a genetic algorithm. *Phys. Rev. E* 51, R2769. doi:10.1103/PhysRevE.51.R2769

Zhai, H., Ha, M.-A., and Alexandrova, A. N. (2015). AFFCK: adaptive force-field-assistedab initiocoalescence kick method for global minimum search. *J. Chem. Theor. Comput.* 11, 2385–2393. doi:10.1021/acs.jctc.5b00065

Zhang, J., and Dolg, M. (2015). ABCluster: the artificial bee colony algorithm for cluster global optimization. *Phys. Chem. Chem. Phys.* 17, 24173–24181. doi:10.1039/c5cp04060d

Zhang, J., and Dolg, M. (2016). Global optimization of clusters of rigid molecules using the artificial bee colony algorithm. *Phys. Chem. Chem. Phys.* 18, 3003–3010. doi:10.1039/c5cp06313b

Zhang, J., Glezakou, V.-A., Rousseau, R., and Nguyen, M.-T. (2020). NWPEsSe: an adaptive-learning global optimization algorithm for nanosized cluster systems. *J. Chem. Theor. Comput.* 16 (6), 3947–3958. doi:10.1021/acs.jctc.9b01107

Zhou, W., and Lee, J. Y. (2007). Highly active core-shell Au@Pd catalyst for formic acid electrooxidation. *Electrochemistry Commun.* 9 (9), 1725–1729. doi:10.1016/j.elecom.2007.03.016

Zhu, Y., and Hosmane, N. S. (2018). Nanostructured boron compounds for cancer therapy. *Pure Appl. Chem.* 90, 653–663. doi:10.1515/pac-2017-0903

Conflict of Interest: The author declares that the research was conducted in the absence of any commercial or financial relationships that could be construed as a potential conflict of interest.

frontiers in Physics

ORIGINAL RESEARCH
published: 15 June 2021
doi: 10.3389/fphy.2021.691034

Optical Response of Sila-Fulleranes in Interaction With Glycoproteins for Environmental Monitoring

Mohammad Qasemnazhand[1], *Farhad Khoeini*[1]* *and Farah Marsusi*[2]

[1]Department of Physics, University of Zanjan, Zanjan, Iran, [2]Department of Physics and Energy Engineering, Amirkabir University of Technology, Tehran, Iran

In this paper, we introduce new features of silicon in fullerane structures. Silicon, when placed in a fullerane structure, increases its electron affinity and electrophilicity index, compared to placement in a diamondoids structure. These nanoparticles can be used to make optical sensors to detect viral environments. In this work, we theoretically examine the changes in the UV-Visible spectrum of sila-fulleranes by interacting with viral spikes. As a result, we find out how the color of silicon nanoparticles changes when they interact with viruses. We apply N- and O-Links for viral glycoprotein structures, and $Si_{20}H_{20}$ silicon dodecahedrane, respectively. Our computational method to obtain optimal structures and their energy in the ground and excited states, is density functional theory (DFT). Besides, to get the UV-Visible spectrum, time-dependent density functional theory (TD-DFT) approach has been used. Our results show that the color of sila-dodecahedrane is white, and turns green in the face of viral spikes. We can use the optical sensitivity of silicon nanoparticles, especially to identify environments infected with the novel coronavirus.

Keywords: sila-fullerane, electrophilicity index, density functional theory, novel coronavirus, glycoproteins

OPEN ACCESS

Edited by:
Ambrish Kumar Srivastava,
Deen Dayal Upadhyay Gorakhpur University, India

Reviewed by:
Ruby Srivastava,
Centre for Cellular and Molecular Biology (CCMB), India
Abhishek Kumar,
University of Lucknow, India

***Correspondence:**
Farhad Khoeini
khoeini@znu.ac.ir

Specialty section:
This article was submitted to Physical Chemistry and Chemical Physics, a section of the journal Frontiers in Physics

Received: *05 April 2021*
Accepted: *31 May 2021*
Published: *15 June 2021*

Citation:
Qasemnazhand M, Khoeini F and Marsusi F (2021) Optical Response of Sila-Fulleranes in Interaction With Glycoproteins for Environmental Monitoring. Front. Phys. 9:691034. doi: 10.3389/fphy.2021.691034

INTRODUCTION

If environmental health can reduce the role of viruses, the complex issue of treating viral patients will be removed from its critical state. But with the spread of human societies, can old methods clean the environment from microbial contamination? These methods are based on disinfecting suspicious, susceptible, and busy places. These are very costly due to the large statistical target population; as a result, it is sometimes impossible to do so [1]. Therefore, the need for substances that detect microbial contamination of the environment, whether viral or bacterial, etc., is felt more and more.

Nanoparticles can be sensitive to the viral environment. This sensitivity can appear as changes in color, light or even electrical properties. Metal nanoparticles have previously been studied to identify a variety of microbes. However, they usually have high chemical softness, which not only causes them to be unstable, but also causes unpredictable changes in biological systems [2, 3]. From non-metallic nanoparticles, carbon can be affected by the environment, if it is located in a structure with sp^2 orbital hybridization, such as graphene, fullerenes, etc., due to the resonance of unlocated electrons, and so can be used as a sensor [4–7]. But graphene-based nanoparticles also always tend to oxidize [8].

Silicon, as the most popular metalloid, exhibits significant properties when placed in the form of nanoparticles. In 2013, Moore et al. showed that silicon nanoparticles can be used as optical sensors [9]. Biocompatibility and sensitivity to surface factors make silicon nanoparticles more attractive to therapeutic agents in biological systems [10–12]. In this study, we investigate the sensitivity of silicon nanoparticles to biological contamination, and introduce a type of nanoparticles as a virus-sensitive

identifier [13–16]. We indicate that when silicon is placed in a fullerane structure, its electron sensitivity increases, so that we do our study on sila-fulleranes [17–21]. Since the electronic properties of sila-fulleranes with sizes between 1 and 2 nm, are very close to each other, we focus on our smallest samples to save on computational costs [22]. Also, to remove the edge factors, we have selected the most symmetric sila-fullerane for this purpose [23–25]. As a result, we select the sila-dodecahedrane with the chemical formula $Si_{20}H_{20}$, which has icosahedral (Ih) symmetry [26, 27]. Finally, we generalize the results to a set of sila-fulleranes.

COMPUTATIONAL METHOD

Our calculations are based on density functional theory. We obtain the optimal and stable geometry of the structures and their energy in the ground and excited states, by B3LYP hybrid functional [28–30]. Using time-dependent density functional theory, we obtained the UV-visible spectrum for the studied structures [31, 32]. We describe the orbitals of the atoms by basis set, which include the split valence, polarized and diffuse functions, that is 6-31 + G (d,p) basis set [33, 34, 35]. The calculations are performed by the Gaussian package [36, 37]. We also used AIM2000 software to analyze the interaction between the structure of the sensor and the glycoproteins studied [38].

RESULTS

Virus spikes are usually made up of glycoproteins. Glycoprotein is a combination of protein and carbohydrate. There are different types of glycoproteins, however, the most common glycoproteins that make virus spikes, like the spike of the coronaviruses, are O-Link and N-Link types [39–43]. If the causative of carbohydrate-binding to protein is oxygen atoms, it is called O-Link, and if it is nitrogen atoms, it is called N-Link. The structure of these two types of glycoproteins is shown in **Figure 1**.

In this study, we propose that silicon nanoparticles have the ability to sense N-Link and O-Link glycoproteins. Because, in addition to biocompatibility, they are also electron sensitive. Although silicon is usually placed in the diamond structure, but when silicon placed in a fullerane structure, the rate of quantum confinement effect will be smaller. Unlike sila-diamondoids, sila-fulleranes does not consist of pure sp^3 hybridization structure. Especially if fulleranes structures consist of a number of fused hexagon rings (NFHR), deviation from sp^3 hybridization occurs more frequently [22]. Finally, this deviation causes difference in the electronic properties of sila-fullerans and sila-diamondoids.

Using the following equations [44–47], we can obtain electronic information, such as the HOMO-LUMO gap, chemical potential, chemical hardness, and finally an estimate of electron affinity:

$$E_{Gap} = E_{LUMO} - E_{HOMO}. \quad (1)$$

$$\mu = \frac{(E_{HOMO} + E_{LUMO})}{2}. \quad (2)$$

TABLE 1 | A list of some of the electronic features of the first six structures of Sila-fullerane (in unit eV).

Nanoparticle	HOMO	LUMO	E_{Gap}	μ	η	EA	IP	ω
$Si_{20}H_{20}$	−6.83	−2.36	4.48	−4.60	2.24	2.36	6.83	4.72
$Si_{24}H_{24}$	−6.70	−2.39	4.31	−4.54	2.16	2.39	6.70	4.78
$Si_{28}H_{28}$	−6.88	−2.49	4.39	−4.69	2.20	2.49	6.88	5.00
$Si_{30}H_{30}$	−6.86	−2.48	4.39	−4.67	2.20	2.48	6.86	4.97
$Si_{36}H_{36}$	−6.78	−2.49	4.29	−4.64	2.14	2.49	6.78	5.02
$Si_{60}H_{60}$	−7.05	−2.59	4.46	−4.82	2.23	2.59	7.05	5.20

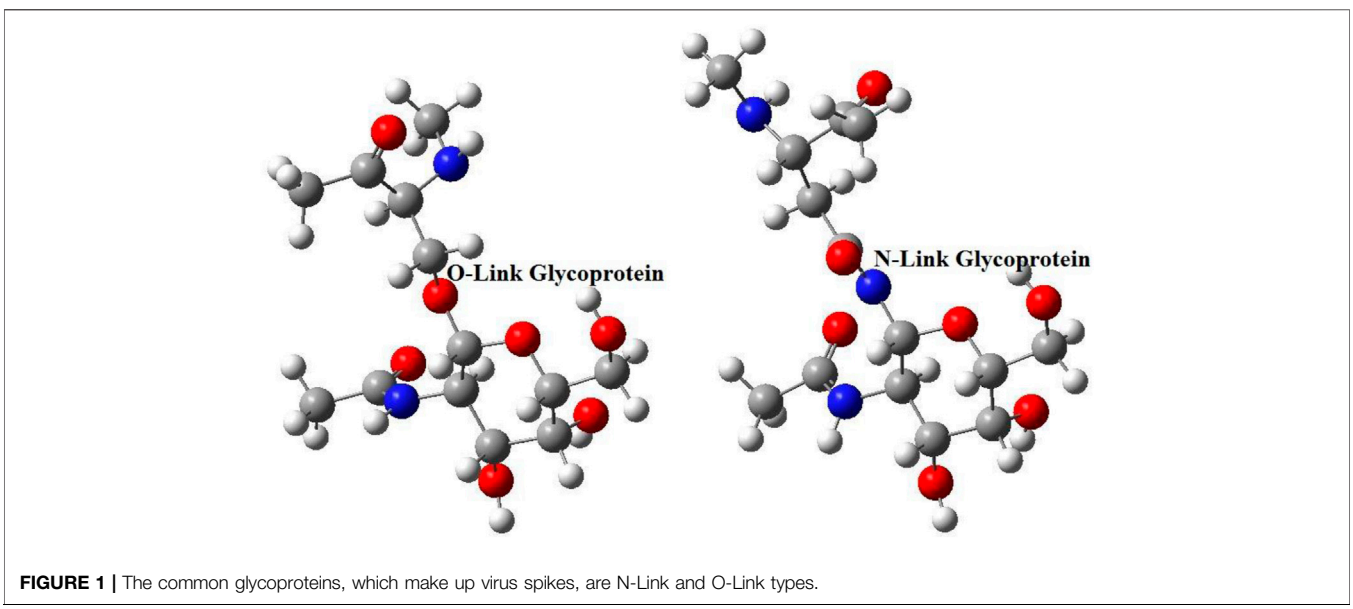

FIGURE 1 | The common glycoproteins, which make up virus spikes, are N-Link and O-Link types.

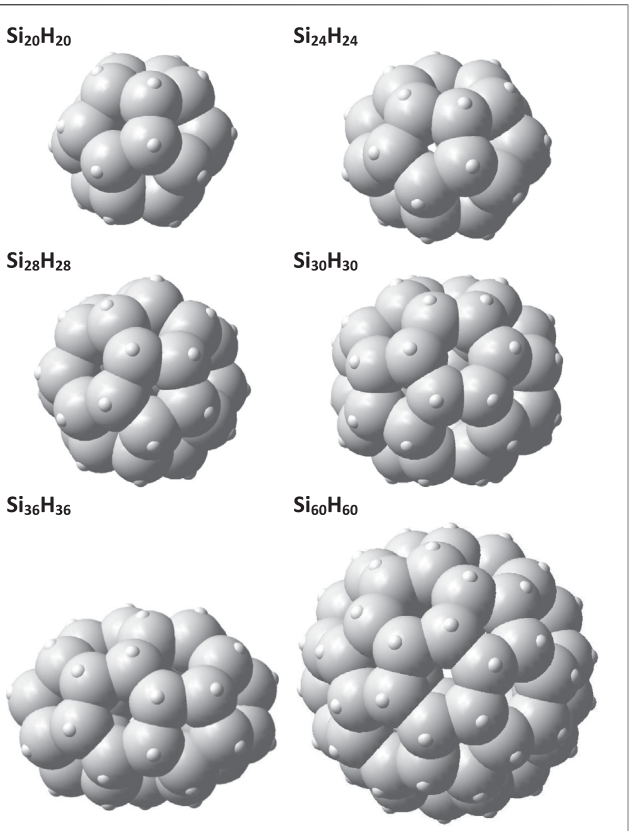

FIGURE 2 | The first six structures of Sila-fulleranes.

$$\eta = \frac{(E_{HOMO} - E_{LUMO})}{2}. \tag{3}$$

$$EA = -E_{LUMO}. \tag{4}$$

$$IP = -E_{HOMO}. \tag{5}$$

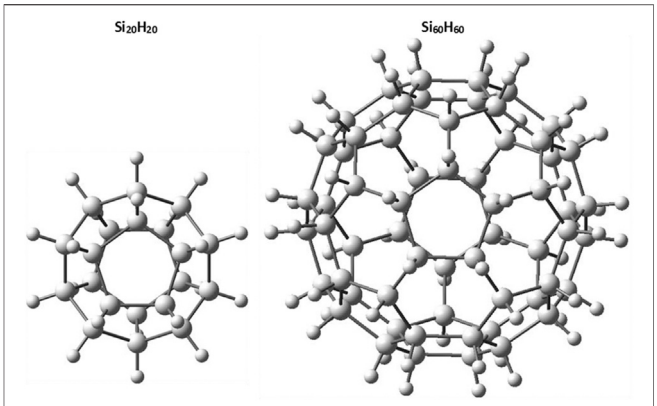

FIGURE 4 | $Si_{20}H_{20}$ and $Si_{60}H_{60}$ structures, which have icosahedral symmetry.

The new index, electrophilicity, can be obtained using chemical potential and chemical hardness through **Eq. 6**. Regarding electrophilicity, the difference between the type of structures is clearly visible [48, 49].

$$\omega = \frac{\mu^2}{2\eta}. \tag{6}$$

We calculated the above electronic information for the six structures of sila-fulleranes. You can see the electronic information of them in **Table 1**.

Our previous researches on silicon nanoparticles shows that diagram of quantum confinement effect (QCE) for sila-fulleranes smoothly change than sila-diamondoids, especially in the range of 1–2 nm [22]. As a result, the HOMO-LUMO gap of fulleranes close to each other in this range, and because many properties such as chemical hardness, chemical potential and indexes such as electrophilicity are derived from this gap, so the properties of

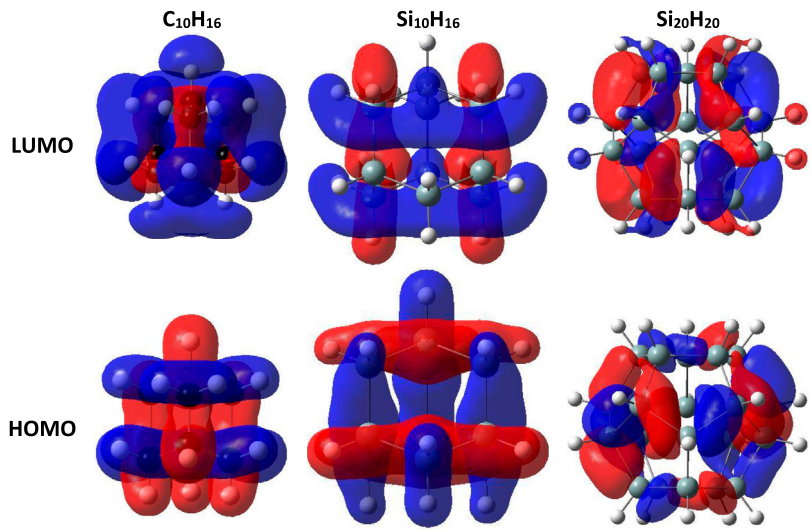

FIGURE 3 | The HOMO and LUMO orbitals for diamondoids, sila-diamondoids and sila-fulleranes (Isovalue = 0.02).

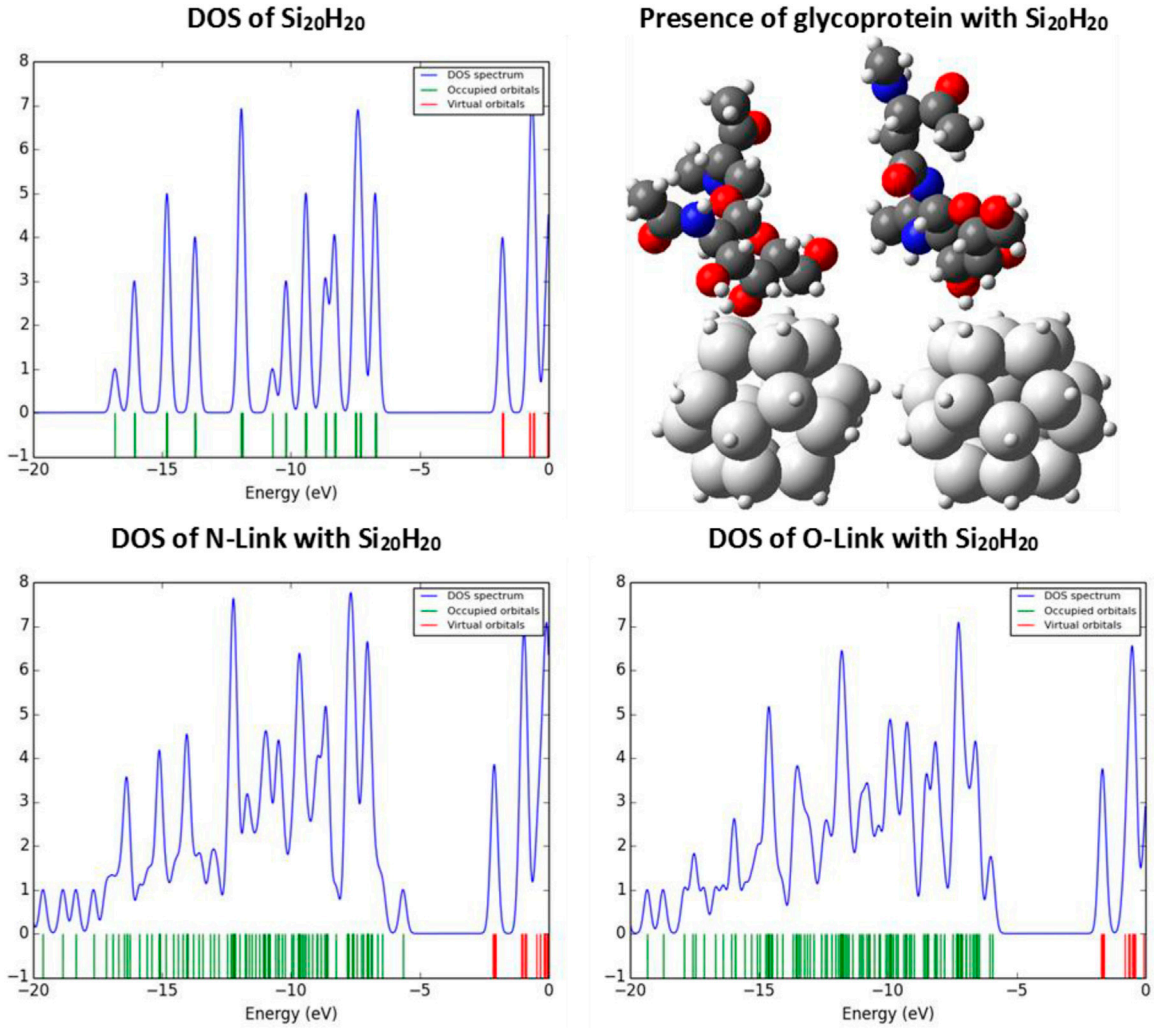

FIGURE 5 | The DOS diagrams of the $Si_{20}H_{20}$ in the absence and presence of N- and O-Link glycoproteins.

these two fullerenes will be similar. For this reason, comparing the values of the above specifications for the $Si_{20}H_{20}$ and $Si_{60}H_{60}$ structures, it cannot be concluded that these two structures have different electronic properties. Despite the different values of electrophilicity, even this sensitive index does not classify the two structures studied in different types. In the following, the structures of the studied sila-fulleranes are shown in **Figure 2**.

According to the data in **Table 1**. It can be concluded that the high chemical hardness combined with significant electron affinity of the sila-fulleranes, make them a good candidate for chemical sensors due to increased electronic interaction with the environment. To determine the advantage of fullerane structures over diamond structures, **Figure 3** shows the HOMO and LUMO orbitals in the smallest diamondoids, sila-diamondoids, and sila-fulleranes. The localized orbitals of HOMO and LUMO in diamonds and their silicon analogues mean that the electrons in their structure have less impact on the environment.

As mentioned earlier, we used the most symmetrical structures, to remove the effect of the edges. The formulas for our structures are $Si_{20}H_{20}$ and $Si_{60}H_{60}$, which have an icosahedral symmetry. The geometry of these two types of structures is shown in **Figure 4**.

Now, according to the data given in **Table 1**, our selected sample to save time in calculations, is the sila-dodecahedrane with the chemical formula $Si_{20}H_{20}$. We investigate the ability of the $Si_{20}H_{20}$ to see if it can sense the presence of the desired glycoproteins. We examine the reaction of $Si_{20}H_{20}$ to the presence of the desired glycoproteins with the probable changes in the density of states (DOS) diagram. **Figure 5** shows the changes in the diagram of the density of states of the $Si_{20}H_{20}$, due to the presence of N- and O-Link glycoproteins. The diagrams of this study are plotted with Gauss Sum software [50].

Silicon nanostructures have a very sensitive surface, so that in the face of high electronegative factors such as oxygen, its HOMO energy level increases, which is also confirmed by the density of states diagram, which it is confirmed by the density of states

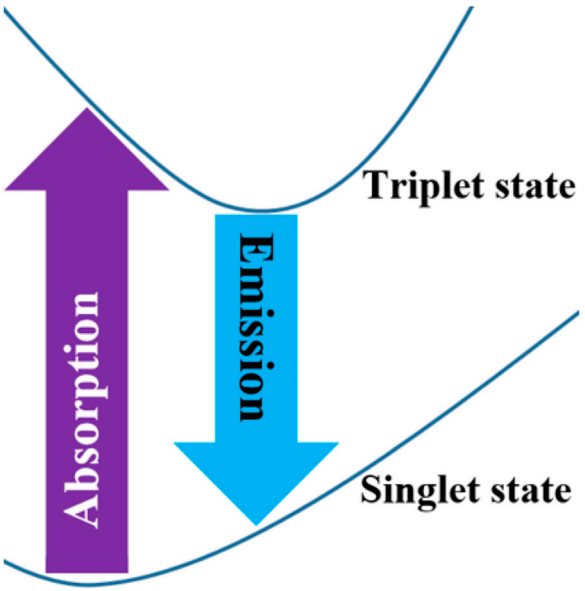

FIGURE 6 | The absorption and emission gaps of the system.

diagram. This is because the presence of oxygen increases the chemical potential of the structure and causes the electron to ionize or excite with less energy than before. So, changes in the DOS indicate differences in properties related to the electronic behaviors, such as optical properties. Now, we want to show how the color of the $Si_{20}H_{20}$ changes due to the presence of N- and O-Link glycoproteins?

Due to its large E_{Gap} of about 4.5 eV, the color of our nanoparticle should be white. In other words, since the spectrum of visible light, about 1.6–3.2 eV, does not have enough energy to act on the electrons of the $Si_{20}H_{20}$, the total radiation returned to space at each wavelength, without any absorption.

The calculation of the optical gap also confirms our results. Optical gaps are usually smaller than HOMO-LUMO gaps. The optical absorption gap can be calculated by subtracting the total energy of the optimized-ground state from the total energy of the excited state in the same ground state geometry, as shown in **Figure 6**.

Because the number of electrons of the $Si_{20}H_{20}$ is even, its spin state will be singlet, in the ground state. The lower-energy triplet excited-state is optically inactive, according to the $\Delta S = 0$ selection rule. Therefore, the lowest-energy allowed optical transition excites the system into the singlet excited state [51–55].

The energy of the singlet excited state is higher than the triplet state, due to larger repulsive Coulomb interactions between antiparallel spins. Therefore, the excited system may relax from the singlet state into the triplet one. Therefore, we calculate the emission bandgap from the relaxed excited triplet state to the ground state at the same energy, as shown in **Figure 6**. In **Table 2**, we present the calculated absorption and emission gaps of the $Si_{20}H_{20}$. The difference between the absorption and emission gaps shows the Stokes shift.

The calculated absorption and emission gaps confirm our prediction, that the color of the $Si_{20}H_{20}$ is white. Because the absorption gap is about 3.7 eV, and also, the emission gap is about 3.3 eV, none of them are in the range of the visible spectrum.

Our investigates show, the optimal distance between glycoprotein and sila-dodecahedrane depends on the condition and orientation of the glycoprotein relative to the sensor structure. But in general, it can be concluded that when the distance of hydrogens of both strucures have more than 2 Å of together, the energy of the correlation between them is close to zero. **Table 3** shows the electron properties of sila-dodecahedrane intracted to the studied glycoproteins.

Our calculations using AIM software analysis show that intermolecular interactions can take place between sila-dodecahedrane and glycoproteins in four zones (see **Figure 7**):

Zone (a): Between the hydroxyl oxygen of carbohydrate part of glycoprotein and the hydrogen sila-dodecahedrane, the distance between which is about 7.8 Å. At the critical point of this interaction, the electron density is about 0.0001 e.bohr^{-3} and the Laplacein density is about −0.0001 e.bohr^{-5}.

Zone (b): Between the carbonyl oxygen of carbohydrate part of glycoprotein and the hydrogen sila-dodecahedrane, the distance between which is about 2.2 Å. At the critical point of this

TABLE 2 | The absorption and emission gaps for the $Si_{20}H_{20}$ (in unit eV).

Spin state	Singlet (ground)	Triplet	Absorption gap	Singlet	Triplet (ground)	Emission Gap	Stoke shift
E_{Total}	−1,57,889.48	−1,57,885.77	3.71	−1,57,889.26	−1,57,885.94	3.32	0.39

TABLE 3 | A list of HOMO, LUMO and the H-L Gap for O and N-Link glycoproteins, $Si_{20}H_{20}$ and their complex systems together (in unit eV).

Structures	HOMO	LUMO	H-L gap
O-Link	−6.20	−0.98	5.22
N-Link	−6.13	−1.05	5.07
$Si_{20}H_{20}$	−6.83	−2.36	4.48
O-Link and $Si_{20}H_{20}$	−6.32	−2.07	4.25
N-Link and $Si_{20}H_{20}$	−6.06	−2.67	3.39

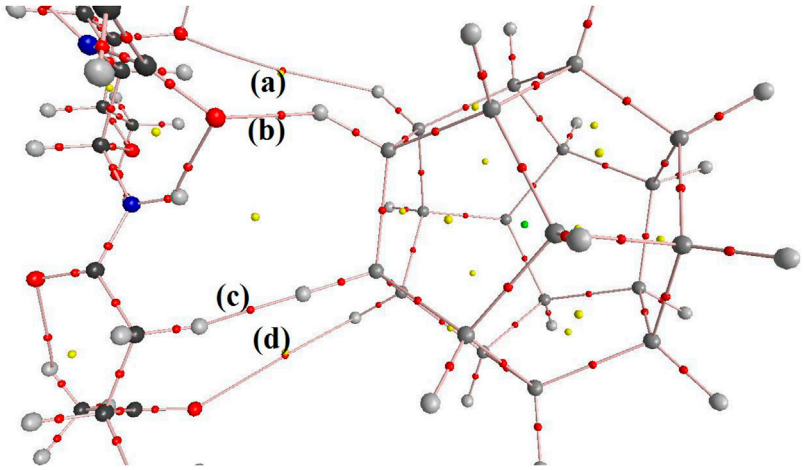

FIGURE 7 | AIM software analysis show that intermolecular interactions can take place between sila-dodecahedrane and glycoproteins in four zones.

interaction, the electron density is about 0.0179 e.bohr^{-3} and the Laplacein density is about −0.0147 e.bohr^{-5}.

Zone (c): Between the nearest hydrogens of glycoprotein and sila-dodecahedrane, the distance between which is about 2.0 Å. At the critical point of this interaction, the electron density is about 0.0112 e.bohr^{-3} and the Laplacein density is about −0.0080 e.bohr^{-5}.

Zone (d): Between the carbonyl oxygen of protein part of glycoprotein and the hydrogen sila-dodecahedrane, the distance between which is about 7.8 Å. At the critical point of this interaction, the electron density is about 0.0003 e.bohr^{-3} and the Laplacein density is about −0.0003 e.bohr^{-5}.

The following **Figure 8** shows the distance between atoms that interact with each other:

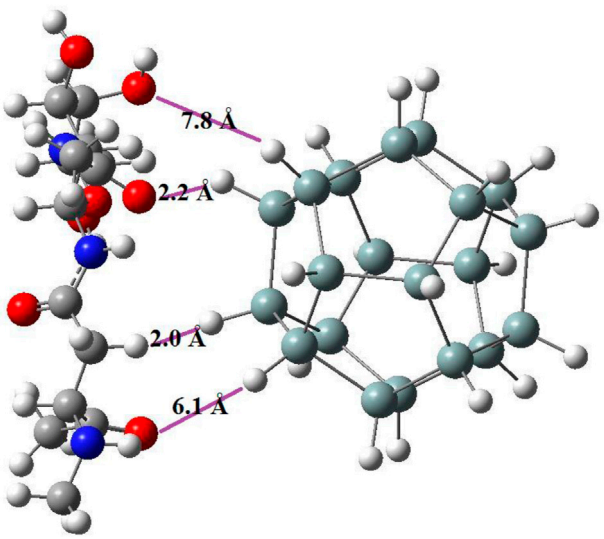

FIGURE 8 | The distance between the two structures of sila-dodecahedrane and glycoprotein in four zones that have intermolecular interaction.

Now, by obtaining the UV-Visible spectrum for the desired glycoproteins, we see that these structures also have no absorption in the visible spectrum [56]. The absorption range of N-Link and O-Link glycoproteins is in the ultraviolet part. But, interestingly, when van der Waals interaction between the $Si_{20}H_{20}$ and the desired glycoproteins is established, the absorption of the new combined system enters the visible region, as shown in **Figure 9**.

The details of our final absorption spectra for the complex system of sila-dodecahedrane and O and N-Linke glycoproteins are given below in **Table 4** using Gauss Sum software.

Since the absorption spectrum of the combined system of $Si_{20}H_{20}$ and desired glycoproteins also includes violet light, we expect to see the composite system in yellowish-green, based on the complementary wavelength [57–64].

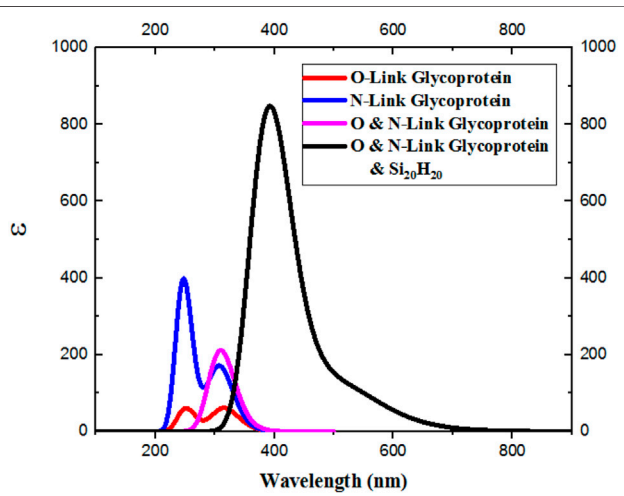

FIGURE 9 | Van der Waals interactions are established between the $Si_{20}H_{20}$ and N- and O-Link glycoproteins, the absorption in the new system also enters the visible spectrum.

TABLE 4 | The details of absorption spectra for the sila-dodecahedrane and O and N-Link glycoproteins.

Wavelength (nm)	Major contribs	Minor contribs
518.54	H-1→LUMO (21%), HOMO→LUMO (74%)	
432.10	H-1→LUMO (72%), HOMO→LUMO (21%)	HOMO→L+1 (4%)
405.45	HOMO→L+1 (88%)	H-2→LUMO (3%), H-1→LUMO (4%)
392.04	H-2→LUMO (78%)	H-9→LUMO (4%), H-6→LUMO (3%), H-3→LUMO
386.13	H-1→L+1 (92%)	HOMO→L+2 (2%)

Our investigations show that what is effective in changing the spectrum of optical absorption is the distance of oxygen of the protein part or the carbohydrate part of the glycoprotein from the surface of silicon nanoparticles. Because the presence of oxygen changes the electron density around the silicon nanoparticles, and it increases the dipole moment of the system from 0.002 about to 10 debye.

Since the electronic properties of silicon nanoparticles can be easily engineered, significant changes and desired color can be achieved by functionalizing the Si-nanoparticle surface. It should be noted that in 2015, Wagner et al. synthesized silicon dodecahedrane as a sila-fullerane with an endohedral chlorideIon [65].

CONCLUSION

The present study includes two crucial applications. First, the diagnosis of viral diseases by using diagnostic kits based on silicon nanoparticles, which are biocompatible, in addition to high electrical and optical sensitivity. Second, for environmental hygiene in the facades of houses, schools, etc. or urban structures, or at least handles or gloves, the coating of silicon nanoparticles can be used to detect viral contamination. Coronavirus (COVID-19) is an example of a viral infection that becomes a global problem today.

DATA AVAILABILITY STATEMENT

The raw data supporting the conclusions of this article will be made available by the authors, without undue reservation.

AUTHOR CONTRIBUTIONS

All authors listed have made a substantial, direct, and intellectual contribution to the work and approved it for publication.

ACKNOWLEDGMENTS

We gratefully acknowledge from Arshia Alaii, Mahdi Tavangar and Mohammad Parham Jafari for computational collaboration. The authors would also like to thank, Pedram and Parham Fathali Brothers, the young researchers of Rey1's Razi Pazhooheshsara's Nano Simulation Laboratory, because of their creative ideas.

REFERENCES

1. O'Neill MS. Helping Schoolchildren with Asthma Breathe Easier: Partnerships in Community-Based Environmental Health Education. *Environ Health Perspect* (1996) 104(5):464–6. doi:10.1289/ehp.96104464
2. Omar NAS, Fen YW, Abdullah J, Anas NAA, Ramdzan NSM, and Mahdi MA. Optical and Structural Properties of Cadmium Sulphide Quantum Dots Based Thin Films as Potential Sensing Material for Dengue Virus E-Protein. *Results Phys* (2018) 11:734–9. doi:10.1016/j.rinp.2018.10.032
3. Khalkhali M, Rostamizadeh K, Sadighian S, Khoeini F, Naghibi M, and Hamidi M. The Impact of Polymer Coatings on Magnetite Nanoparticles Performance as MRI Contrast Agents: a Comparative Study. *DARU J Pharm Sci* (2015) 23(1):1–12. doi:10.1186/s40199-015-0124-7
4. Hong SW, Kim DY, Lee JU, and Jo WH. Synthesis of Polymeric Temperature Sensor Based on Photophysical Property of Fullerene and Thermal Sensitivity of Poly(N-Isopropylacrylamide). *Macromolecules* (2009) 42(7):2756–61. doi:10.1021/ma802862h
5. Haino T, Araki H, Fujiwara Y, Tanimoto Y, and Fukazawa Y. Fullerene Sensors Based on Calix[5]arene. *Chem Commun* (2002)(18) 2148–9. doi:10.1039/b205048j
6. Cheng Z, Li Q, Li Z, Zhou Q, and Fang Y. Suspended Graphene Sensors with Improved Signal and Reduced Noise. *Nano Lett* (2010) 10(5):1864–8. doi:10.1021/nl100633g
7. Yavari F, and Koratkar N. Graphene-based Chemical Sensors. *J Phys Chem Lett* (2012) 3(13):1746–53. doi:10.1021/jz300358t
8. Robinson JT, Perkins FK, Snow ES, Wei Z, and Sheehan PE. Reduced Graphene Oxide Molecular Sensors. *Nano Lett* (2008) 8(10):3137–40. doi:10.1021/nl8013007
9. Romero JJ, Llansola-Portolés MJ, Dell'Arciprete ML, Rodríguez HB, Moore AL, and Gonzalez MC. Photoluminescent 1-2 Nm Sized Silicon Nanoparticles: A Surface-dependent System. *Chem Mater* (2013) 25(17):3488–98. doi:10.1021/cm401666a
10. Popplewell JF, King SJ, Day JP, Ackrill P, Fifield LK, Cresswell RG, et al.Kinetics of Uptake and Elimination of Silicic Acid by a Human Subject: a Novel Application of 32Si and Accelerator Mass Spectrometry. *J Inorg Biochem* (1998) 69(3):177–80. doi:10.1016/s0162-0134(97)10016-2
11. Park J-H, Gu L, Von Maltzahn G, Ruoslahti E, Bhatia SN, and Sailor MJ. Biodegradable Luminescent Porous Silicon Nanoparticles for *In Vivo* Applications. *Nat Mater* (2009) 8(4):331–6. doi:10.1038/nmat2398
12. Yu MK, Park J, and Jon S. Targeting Strategies for Multifunctional Nanoparticles in Cancer Imaging and Therapy. *Theranostics* (2012) 2(1):3–44. doi:10.7150/thno.3463
13. Connétable D, Timoshevskii V, Artacho E, and Blase X. Tailoring Band Gap and Hardness by Intercalation: An Ab Initio Study of I 8@ S I– 46 and Related Doped Clathrates. *Phys Re-view Lett* (2001) 87(20):206405. doi:10.1103/physrevlett.87.206405
14. Tournus F, Masenelli B, Mélinon P, Connétable D, Blase X, Flank AM, et al.Guest Displacement in Silicon Clathrates. *Phys Rev B* (2004) 69(3):035208. doi:10.1103/physrevb.69.035208
15. Kumar V, and Kawazoe Y. Hydrogenated Caged Clusters of Si, Ge, and Sn and Their Endohedral Doping with Atoms: Ab Initio Calculations. *Phys Rev B* (2007) 75(15):155425. doi:10.1103/physrevb.75.155425

16. Hao SG, Zhang DB, and Dumitrică T. Effect of Small Shape Changes on the Optical Response of Highly Symmetric Silicon Quantum Dots. *Phys Rev B* (2007) 76(8):081305. doi:10.1103/physrevb.76.081305
17. Fthenakis ZG, Havenith RW, Menon M, and Fowler PW. Structural and Electronic Properties of the Fullerene Isomers of Si 38: A Systematic Theoretical Study. *Phys Rev B* (2007) 75(15):155435. doi:10.1103/physrevb.75.155435
18. Zdetsis AD. One-nanometer Luminous Silicon Nanoparti-Cles: Possibility of a Fullerene Interpretation. *Phys Rev B* (2009) 79(19):195437. doi:10.1103/physrevb.79.195437
19. Kumar V, and Kawazoe Y. Hydrogenated Silicon Fullerenes: Effects of H on the Stability of Metal-Encapsulated Silicon Clusters. *Phys Rev Lett* (2003) 90(5):055502. doi:10.1103/physrevlett.90.055502
20. Zdetsis AD. Stabilization of Large Silicon Fullerenes and Re-lated Nanostructures through Puckering and Poly (Oligo) Merization. *Phys Rev B* (2009) 80(19):195417. doi:10.1103/physrevb.80.195417
21. Palagin D, and Reuter K. Evaluation of Endohedral Doping of Hydrogenated Si Fullerenes as a Route to Magnetic Si Building Blocks. *Phys Rev B* (2012) 86(4):045416. doi:10.1103/physrevb.86.045416
22. Marsusi F, and Qasemnazhand M. Sila-fulleranes: Promising Chemically Active Fullerene Analogs. *Nanotechnology* (2016) 27(27):275704. doi:10.1088/0957-4484/27/27/275704
23. Xie RH, Bryant GW, Zhao J, Kar T, and Smith VH, Jr. Tunable Optical Properties of Icosahedral, Dodecahedral, and Tetra-Hedral Clusters. *Phys Rev B* (2005) 71(12):125422. doi:10.1103/physrevb.71.125422
24. Karttunen AJ, Linnolahti M, and Pakkanen TA. Icosahedral Polysilane Nanostructures. *J Phys Chem C* (2007) 111(6):2545–7. doi:10.1021/jp067700w
25. Zdetsis AD. High-symmetry High-Stability Silicon Fuller-Enes: A First-Principles Study. *Phys Rev B* (2007) 76(7):075402. doi:10.1103/physrevb.76.075402
26. Sun Q, Wang Q, Briere TM, Kumar V, Kawazoe Y, and Jena P. First-principles Calculations of Metal Stabilized Si 20 Cages. *Phys Rev B* (2002) 65(23):235417. doi:10.1103/physrevb.65.235417
27. Palagin D, and Reuter K. MSi20H20 Aggregates: From Simple Building Blocks to Highly Magnetic Functionalized Materials. *ACS nano* (2013) 7(2):1763–8. doi:10.1021/nn3058888
28. Zhang IY, Wu J, and Xu X. Extending the Reliability and Applicability of B3LYP. *Chem Commun* (2010) 46(18):3057–70. doi:10.1039/c000677g
29. Lee C, Yang W, and Parr RG. Development of the Colle-Salvetti Correlation-Energy Formula into a Functional of the Electron Density. *Phys Rev B* (1988) 37(2):785–9. doi:10.1103/physrevb.37.785
30. Stephens PJ, Devlin FJ, Chabalowski CF, and Frisch MJ. Ab Initio calculation of Vibrational Absorption and Circular Dichroism Spectra Using Density Functional Force fields. *J Phys Chem* (1994) 98(45):11623–7. doi:10.1021/j100096a001
31. Cysewski P, Jeliński T, Przybyłek M, and Shyichuk A. Color Prediction from First Principle Quantum Chemistry Computations: a Case of Alizarin Dissolved in Methanol. *New J Chem* (2012) 36(9):1836–43. doi:10.1039/c2nj40327g
32. Castro A, Marques MAL, Alonso JA, and Rubio A. Optical Properties of Nanostructures from Time-dependent Density Functional Theory. *J Comput Theor Nanosci* (2004) 1(3):231–55. doi:10.1166/jctn.2004.2931
33. Tirado-Rives J, and Jorgensen WL. Performance of B3LYP Density Functional Methods for a Large Set of Organic Molecules. *J Chem Theor Comput.* (2008) 4(2):297–306. doi:10.1021/ct700248k
34. Hehre WJ, Ditchfield R, and Pople JA. Self-Consistent Molecular Orbital Methods. XII. Further Extensions of Gaussian-type Basis Sets for Use in Molecular Orbital Studies of Organic Molecules. *J Chem Phys* (1972) 56(5):2257–61. doi:10.1063/1.1677527
35. Ditchfield R, Hehre WJ, and Pople JA. Self-Consistent Molecular-Orbital Methods. IX. An Extended Gaussian-Type Basis for Molecular-Orbital Studies of Organic Molecules. *J Chem Phys* (1971) 54(2):724–8. doi:10.1063/1.1674902
36. Binkley JS, Whiteside R, Hariharan PC, Seeger R, Heh-re WJ, Lathan WA, et al.*GAUSSIAN 76: An Ab Initio Molecular Orbital Program (No. BNL-24136).* Upton, NY (USA): Brookhaven National Lab. (1978). doi:10.2172/6738000
37. Petersson GA, Malick DK, Wilson WG, Ochterski JW, Montgomery JA, Jr, and Frisch MJ. Calibration and Comparison of the Gaussian-2, Complete Basis Set, and Density Functional Methods for Computational Thermochemistry. *J Chem Phys* (1998) 109(24):10570–9. doi:10.1063/1.477794
38. Bader RFW. *AIM2000 Program, v. 2.0*. Hamilton, Canada: McMaster University (2000)
39. Andersen KG, Rambaut A, Lipkin WI, Holmes EC, and Garry RF. The Proximal Origin of SARS-CoV-2. *Nat Med* (2020) 26(4):450–2. doi:10.1038/s41591-020-0820-9
40. Khalkhali M, Mohammadinejad S, Khoeini F, and Rostamizadeh K. Vesicle-like Structure of Lipid-Based Nanoparticles as Drug Delivery System Revealed by Molecular Dynamics Simulations. *Int J pharmaceutics* (2019) 559:173–81. doi:10.1016/j.ijpharm.2019.01.036
41. Watanabe Y, Berndsen ZT, Raghwani J, Seabright GE, Allen JD, Pybus OG, et al.Vulnerabilities in Coronavirus Glycan Shields Despite Extensive Glycosylation. *Nat Commun* (2020) 11(1):1–10. doi:10.1038/s41467-020-16567-0
42. Goutham S, Kumari I, Pally D, Singh A, Ghosh S, Akhter Y, et al.Mutually Exclusive Locales for N-Linked Gly-Cans and Disorder in Human Glycoproteins. *Scientific Rep* (2020) 10(1):1–12. doi:10.1038/s41598-020-61427-y
43. Amin M, Sorour MK, and Kasry A. Comparing the Binding Interactions in the Receptor Binding Domains of SARS-CoV-2 and SARS-CoV. *J Phys Chem Lett* (2020)
44. Qasemnazhand M, Khoeini F, and Marsusi F Fulleryne, a New Member of the Carbon Cages Family. arXiv preprint arXiv. 2020, 2003.09835.
45. Wang T, Lu J, Zhu H, Liu J, Lin X, Liu Y, et al.The Electronic Properties of Chiral Silicon Nanotubes. *Superlattices and Microstructures* (2017) 109:457–62. doi:10.1016/j.spmi.2017.05.034
46. Tavakol H, and Shahabi D. DFT, QTAIM, and NBO Study of Adsorption of Rare Gases into and on the Surface of Sulfur-Doped, Single-Wall Carbon Nanotubes. *J Phys Chem C* (2015) 119(12):6502–10. doi:10.1021/jp510508y
47. Zhan C-G, Nichols JA, and Dixon DA. Ionization Potential, Electron Affinity, Electronegativity, Hardness, and Electron Excitation Energy: Molecular Properties from Density Functional Theory Orbital Energies. *J Phys Chem A* (2003) 107(20):4184–95. doi:10.1021/jp0225774
48. Parr RG, Szentpály LV, and Liu S. Electrophilicity index. *J Am Chem Soc* (1999) 121(9):1922–4. doi:10.1021/ja983494x
49. Qasemnazhand M, Khoeini F, and Marsusi F. Predicting the New Carbon Nanocages, Fullerynes: A DFT Study. Scientific reports (2021) 11. doi:10.1038/s41598-021-82142-2
50. O'boyle NM, Tenderholt AL, and Langner KM. Cclib: A Library for Package-independent Computational Chemistry Algorithms. *J Comput Chem* (2008) 29(5):839–45. doi:10.1002/jcc.20823
51. Patrick CE, and Giustino F. Quantum Nuclear Dynamics in the Photophysics of Diamondoids. *Nat Commun* (2013) 4:2006. doi:10.1038/ncomms3006
52. Marsusi F, Sabbaghzadeh J, and Drummond ND. Compar-ison of Quantum Monte Carlo with Time-dependent and Static Densi-Ty-Functional Theory Calculations of Diamondoid Excitation Energies and Stokes Shifts. *Phys Rev B* (2011) 84(24):245315. doi:10.1103/physrevb.84.245315
53. Shu Y, Fales BS, and Levine BG. Defect-induced Conical Intersections Promote Nonradiative Recombination. *Nano Lett* (2015) 15(9):6247–53. doi:10.1021/acs.nanolett.5b02848
54. Marsusi F. Nuclear Dynamic Effects on Electronic Properties of Functionalized Diamondoids. *Physica E: Low-dimensional Syst Nanostructures* (2018) 103:435–43. doi:10.1016/j.physe.2018.05.010
55. Qasemnazhand M, Khoeini F, and Shekarforoush S. Electronic Transport Properties in the Stable Phase of a cumulene/B7/cumulene Molecular Bridge Investigated Using Density Functional Theory and a Tight-Binding Method. *New J Chem* (2019) 43(42):16515–23. doi:10.1039/c9nj02860a
56. Alrikabi A. Theoretical Study of the Design Dye-Sensitivity for Usage in the Solar Cell Device. *Results Phys* (2017) 7:4359–63. doi:10.1016/j.rinp.2017.07.022
57. Pickering C, Beale MIJ, Robbins DJ, Pearson PJ, and Greef R. Optical Studies of the Structure of Porous Silicon Films Formed in P-type Degenerate and Non-degenerate Silicon. *J Phys C: Solid State Phys* (1984) 17(35):6535–52. doi:10.1088/0022-3719/17/35/020
58. Canham LT. Silicon Quantum Wire Array Fabrication by Electrochemical and Chemical Dissolution of Wafers. *Appl Phys Lett* (1990) 57(10):1046–8. doi:10.1063/1.103561

59. Belomoin G, Therrien J, Smith A, Rao S, Twesten R, Chaieb S, et al.Observation of a Magic Discrete Family of Ultrabright Si Nanoparticles. *Appl Phys Lett* (2002) 80(5):841–3. doi:10.1063/1.1435802
60. Kanemitsu Y. Light Emission from Porous Silicon and Related Materials. *Phys Rep* (1995) 263(1):1–91. doi:10.1016/0370-1573(95)00021-4
61. Veinot JGC. Synthesis, Surface Functionalization, and Properties of Freestanding Silicon Nanocrystals. *Chem Commun* (2006)(40) 4160–8. doi:10.1039/b607476f
62. Yang L, Liu Y, Zhong Y-L, Jiang X-X, Song B, Ji X-Y, et al.Fluorescent Silicon Nanoparticles Utilized as Stable Color Converters for white Light-Emitting Diodes. *Appl Phys Lett* (2015) 106(17):173109. doi:10.1063/1.4919526
63. Fu YH, Kuznetsov AI, Miroshnichenko AE, Yu YF, and Luk'yanchuk B. Directional Visible Light Scattering by Silicon Nanoparticles. *Nat Commun* (2013) 4(1):1–6. doi:10.1038/ncomms2538
64. Harun K, Salleh NA, Deghfel B, Yaakob MK, and Mohamad AA. DFT + U Calculations for Electronic, Structural, and Optical Properties of ZnO Wurtzite Structure: A Review. *Results Phys* (2020) 16:102829. doi:10.1016/j.rinp.2019.102829
65. Tillmann J, Wender JH, Bahr U, Bolte M, Lerner H-W, Holthausen MC, et al.One-Step Synthesis of a [20]Silafullerane with an Endohedral Chloride Ion. *Angew Chem Int Ed* (2015) 54(18):5429–33. doi:10.1002/anie.201412050

Conflict of Interest: The authors declare that the research was conducted in the absence of any commercial or financial relationships that could be construed as a potential conflict of interest.

frontiers in Chemistry

ORIGINAL RESEARCH
published: 30 June 2021
doi: 10.3389/fchem.2021.637750

Ground-State Structures of Hydrated Calcium Ion Clusters From Comprehensive Genetic Algorithm Search

Ruili Shi[1,2], *Zhi Zhao*[1,2], *Xiaoming Huang*[3], *Pengju Wang*[2], *Yan Su*[2]*, *Linwei Sai*[4], *Xiaoqing Liang*[5], *Haiyan Han*[1] and *Jijun Zhao*[2]

[1]School of Mathematics and Physics, Hebei University of Engineering, Handan, China, [2]Key Laboratory of Materials Modification by Laser, Ion and Electron Beams, Ministry of Education, Dalian University of Technology, Dalian, China, [3]School of Ocean Science and Technology, Dalian University of Technology, Panjin Campus, Panjin, China, [4]Department of Mathematics and Physics, Hohai University, Changzhou, China, [5]School of Electronics and Information Engineering, Taizhou University, Taizhou, China

We searched the lowest-energy structures of hydrated calcium ion clusters $Ca^{2+}(H_2O)_n$ (n = 10–18) in the whole potential energy surface by the comprehensive genetic algorithm (CGA). The lowest-energy structures of $Ca^{2+}(H_2O)_{10–12}$ clusters show that Ca^{2+} is always surrounded by six H_2O molecules in the first shell. The number of first-shell water molecules changes from six to eight at n = 12. In the range of n = 12–18, the number of first-shell water molecules fluctuates between seven and eight, meaning that the cluster could pack the water molecules in the outer shell even though the inner shell is not full. Meanwhile, the number of water molecules in the second shell and the total hydrogen bonds increase with an increase in the cluster size. The distance between Ca^{2+} and the adjacent water molecules increases, while the average adjacent O-O distance decreases as the cluster size increases, indicating that the interaction between Ca^{2+} and the adjacent water molecules becomes weaker and the interaction between water molecules becomes stronger. The interaction energy and natural bond orbital results show that the interaction between Ca^{2+} and the water molecules is mainly derived from the interaction between Ca^{2+} and the adjacent water molecules. The charge transfer from the lone pair electron orbital of adjacent oxygen atoms to the empty orbital of Ca^{2+} plays a leading role in the interaction between Ca^{2+} and water molecules.

Keywords: hydrated calcium ion cluster, genetic algorithm, hydrogen bond, coordination number, natural bond orbital

OPEN ACCESS

Edited by:
Wei-Ming Sun,
Fujian Medical University, China

Reviewed by:
Chang Q. Sun,
Nanyang Technological University, Singapore
Yongli Huang,
Xiangtan University, China

***Correspondence:**
Yan Su
su.yan@dlut.edu.cn

Specialty section:
This article was submitted to Theoretical and Computational Chemistry, a section of the journal Frontiers in Chemistry

Received: *04 December 2020*
Accepted: *02 June 2021*
Published: *30 June 2021*

Citation:
Shi R, Zhao Z, Huang X, Wang P, Su Y, Sai L, Liang X, Han H and Zhao J (2021) Ground-State Structures of Hydrated Calcium Ion Clusters From Comprehensive Genetic Algorithm Search. Front. Chem. 9:637750. doi: 10.3389/fchem.2021.637750

INTRODUCTION

It is well acknowledged that most of the biochemistry reactions accomplished by ions happen in the water environment. The activation of water by metal ions and charge transfer to solvent originating from a metal ion are of fundamental importance for understanding the hydrogen bond formation in aqueous environments (Kistenmacher et al., 1974; Rudolph and Irmer, 2013; Chen and Ruckenstein, 2015; Hadad et al., 2019). By the end of the last century, a series of works used molecular dynamics (MD) or density functional theory (DFT) to study the hydrated ion clusters. These research focused on the structures, the coordination number (CN) of the metal ion, the interaction of ion–solvent or

solvent–solvent, and the influential factors of hydration bond structures (Caldwell et al., 1990; Hall et al., 2000; Hofer et al., 2005; Fujiwara et al., 2010; Boda et al., 2012; Yoo et al., 2016; Delgado et al., 2020). For example, Fujiwara et al. used the fragment molecular orbital–based molecular dynamics (FMO-MD) method to investigate the hydration structure of the droplet containing a divalent zinc ion and 64 water molecules and provided the CN of 6 (Fujiwara et al., 2010). Hofer et al. made the comparison of *ab initio* quantum mechanical/molecular mechanical (QM/MM) molecular dynamics (MD) simulations with those of classical simulations based on the pair potential added by three-body interaction potentials to accentuate the difference of the "quantum effect" in the hydrated Ba (II) ion (Hofer et al., 2005). The investigation from microhydration to bulk hydration of the Sr^{2+} ion has been accomplished by Anil Boda et al. using DFT, MP2, and the molecular dynamics study (Boda et al., 2012). The experimental studies could yield considerable results and make the structural and physical properties obtained from theoretical studies more credible (Misaizu et al., 1995; Siu et al., 2002; Buck et al., 2007; Gao and Liu, 2007; Carrera et al., 2009; Zhang and Liu, 2011). All these make us understand much deeper the actual reactions outside the laboratory and inside organisms.

Calcium, as one of the most important ions in the tissue fluid, participates in many biochemical reactions such as exocytosis, neurotransmitter release, and many vital movements such as muscle contraction or electrical conduction of the heart (Prendergast and Mann, 1977; Hewish et al., 1982; Chizhik et al., 2016). The fundamental study is to describe the CN and microstructures of the hydrated calcium ion clusters since the biological or chemical properties are determined by the structures of hydrated calcium ion clusters (Bakó et al., 2002; González et al., 2005).

In experiments, the CN of the calcium ion varies largely from 5 to 10 by using X-ray diffraction, neutron diffraction, extended X-ray absorption fine structure spectroscopy, and other techniques (Hewish et al., 1982; Probst et al., 1985; Marcus, 1988; Yamaguchi et al., 1989; Peschke et al., 1998; Jalilehvand et al., 2001; Fulton et al., 2003; Megyes et al., 2004). It should be ascribed to the different conditions and environments of water molecules. The ratio between water molecules and ions also could change the CN. For example, when the ion concentration is smaller, the number of first-shell water molecules will be larger (Hewish et al., 1982; Yamaguchi et al., 1989; Jalilehvand et al., 2001; Megyes et al., 2004). Moreover, infrared (IR) spectra could help provide the evolution information of the structures of the hydrated calcium ion clusters (Butler et al., 2014). Williams and colleagues conducted a series of IR spectroscopy of $Ca^{2+}(H_2O)_n$ with n = 4–69 in experiments (Bush et al., 2007; Bush et al., 2008; Bush et al., 2009). Their results revealed that there are six water molecules adjacent to the calcium dication for $Ca^{2+}(H_2O)_n$ with n = 6–10 clusters (Bush et al., 2007), and the number of water molecules in the first hydration shell changes from six to eight at $n \approx 12$ (Bush et al., 2008). Recently, the binding energy of hydrated calcium ion clusters with up to n = 20 was measured by Bruzzi and Stace using the pick-up technique in conjunction with finite heat bath theory to characterize the interaction between calcium ions with the multi-outer shell water molecules (Bruzzi and Stace, 2017). Their results showed that there are six water molecules in the first hydration shell, and the 2+ charge on the calcium cation has an influence on the molecular interactions that extends far beyond the first hydration shell.

Meanwhile, the CN of the calcium ion and the structures of the hydrated calcium ion attracted lots of attention on the theoretical side. Using a semiempirical coupling method with a basin-hopping global optimization approach, Wales and co-workers searched the low-lying structures of $Ca^{2+}(H_2O)_n$ with n = 1–20 clusters, showing that Ca^{2+} prefers to locate at the center of the cluster surrounded by eight adjacent water molecules (González et al., 2005). The CN of the calcium ion attained by Monte Carlo (MC) (Bernal-Uruchurtu and Ortega-Blake, 1995) and MD (Obst and Bradaczek, 1996; Tongraar et al., 1997; Todorova et al., 2008; Wanprakhon et al., 2011; León-Pimentel et al., 2018) studies varies from 6 to 10. However, the results from DFT calculations showed that there are six water molecules in the first hydration shell (Megyes et al., 2004; Peschke et al., 2000; Carl et al., 2007; Lei and Pan, 2010). For example, the work by Lei and Pan at the BLYP/6-311+G(d,p) level of theory showed that the first and second hydration shells of the lowest-energy structures of $Ca^{2+}(H_2O)_n$ with n = 1–20 and 27 are fully occupied by six and nine water molecules, respectively (Lei and Pan, 2010). The discrepancy may be caused by the different computational methods. All the studies imply that still there is some controversy about the ground state structures of medium-sized hydrated calcium ion clusters, especially for the influence of the interaction between Ca^{2+} and the second- or even the third-shell water molecules on the number of first-shell water molecules. The evolution process of the first and second hydration shells mainly occurs in the range of n = 10–18. Therefore, more efforts are needed to search the potential energy surface (PES) of $Ca^{2+}(H_2O)_n$ clusters with n = 10–18.

In this work, we use the comprehensive genetic algorithm (CGA) (Zhao et al., 2016) combined with DFT to globally search the PES of hydrated calcium ion clusters $Ca^{2+}(H_2O)_n$ with n = 10–18. The contrast with the structures given by precedent works and the evolution of the structures with the growth of size is also shown. Finally, we present the interaction between Ca^{2+} and the water molecules using natural bond orbital (NBO) analyses. This work concentrates on the competition between the first- and second-shell water molecules and shows some new low-energy structures of hydrated calcium ion clusters. Our theoretical results provide useful guidance for analyzing the hydrated calcium ion clusters in experiments.

METHOD

The CGA (Zhao et al., 2016) has been proved to be outstanding for searching the lowest-energy structures of protonated water clusters and fluoride anion–water clusters (Shi et al., 2017; Shi et al., 2018a; Shi et al., 2018b). We used the CGA combined with the DMol^3 program (Delley, 1990; Delley, 2000) based on DFT to globally search the PES of $Ca^{2+}(H_2O)_n$ with n = 10–18. All structures generated by the CGA were fully relaxed with DFT

without any symmetry constraint. The double-numerical basis including *p*- and *d*-polarization functions (DNP) and the Becke's exchange functional (Becke, 1988) and the correlation functional by Lee, Yang, and Parr (BLYP) (Lee et al., 1988) were adopted. The self-consistent field (SCF) density calculations were carried out with a convergence criterion of 10^{-6} a.u. on the total energy.

BLYP and B3LYP (Stephens et al., 1994) as well as 6-311++G(d,p), 6-311+G(d,p), or 6-31+G(d,p) basis set are usually used to describe the hydrated calcium ion clusters (Bakó et al., 2002; Bush et al., 2008; Bush et al., 2009; Lei and Pan, 2010). Meanwhile, MP2 (Møller and Plesset, 1934) is treated as a replacement of CCSD(T) to get more accurate results with low cost for hydrogen bond systems (Shi et al., 2017; Wang et al., 2019; Shi et al., 2020). Thus, we choose MP2 combined with high-level basis set 6-311++G(2d,2p) to evaluate these methods and basis set for describing the geometries of hydrated calcium ion clusters. All the calculations were done with Gaussian 09 package (Frisch et al., 2009). The differences of average adjacent O-O distances and average adjacent O-Ca distances of $Ca^{2+}(H_2O)_{10}$ cluster isomers between several methods and MP2/6-311++G(2d,2p) results are shown in **Supplementary Table S1**. First, the results of MP2 with 6-311++G(d,p), 6-311+G(d,p), and 6-31+G(d,p) basis set show that the 6-311+G(d,p) basis set could give the most similar results to the 6-311++G(2d,2p) basis set. Thus, we choose 6-311+G(d,p) basis set to optimize hydrated calcium ion clusters. Then the results from BLYP/6-311+G(d,p) and B3LYP/6-311+G(d,p) reveal that B3LYP is outstanding. Finally, we evaluated the dispersion correction on the B3LYP method. We can see from the results of B3LYP/6-311+G(d,p) and B3LYP-D3/6-311+G(d,p) that B3LYP-D3 could give a better geometry of $Ca^{2+}(H_2O)_{10}$ clusters. Considering the computational cost and accuracy, we chose B3LYP-D3/6-311+G(d,p) to optimize the structures of hydrated calcium ion clusters.

Frequency calculations were carried out at the B3LYP-D3/6-311+G(d,p) level of theory, which is same with optimization to ensure each cluster is the true local minimum without imaginary frequency as well as to obtain the zero-point energy (ZPE) and thermal correction at 298 K. Furthermore, the single-point energy (SPE) was calculated at the MP2/6-311++G(2d,2p) level of theory to get more accurate energy. The basis set superposition error (BSSE) correction is considered for the interaction energy. The BSSE correction (ΔE_{BSSE}) is based on the site–site function counterpoise method proposed by Wells and Wilson (1983), which is defined as:

$$\Delta E_{BSSE} = \sum_{i=1}^{m} \left[E^{full}(fragm) - E^{fragm}(fragm) \right], \quad (1)$$

where superscript *full* or *fragm* is the energy calculated in the full basis set or in the fragment basis set, and *m* is the number of fragment for a given cluster. Moreover, NBO analyses were performed at the MP2/6-311++G(2d,2p) level of theory based on the B3LYP-D3/6-311+G(d,p) optimization to obtain the charge transfer between calcium ion and water molecules as well as the natural charge of the clusters.

RESULTS AND DISCUSSION

Lowest-Energy Structures

Figure 1 shows the lowest-energy structures and symmetry of $Ca^{2+}(H_2O)_n$ clusters with n = 10–18 obtained from the CGA global search. The number of water molecules in the first (N_1), second (N_2), and third (N_3) hydration shells and the number of hydrogen bonds of the lowest-energy structures are listed in **Table 1**. For comparison, the lowest-energy structures of $Ca^{2+}(H_2O)_n$ with n = 10–18 taken from Lei and Pan (2010) as well as Wales and co-workers (González et al., 2005) optimized at the B3LYP-D3/6-311+G(d,p) level of theory are shown in **Supplementary Figure S1**. The structures taken from Lei and Pan as well as Wales and co-workers are described as *n*-Lei and *n*-Wales, respectively.

From **Figure 1**, we can see that, for all the lowest-energy structures, there are no hydrogen bonds between the water molecules in the first hydration shell and Ca^{2+} prefers to stay inside the cluster, in agreement with *n*-Lei, *n*-Wales, and the results of molecular dynamics simulations (Egorov et al., 2003; González et al., 2005; Lei and Pan, 2010). The relatively intensive electronic field makes the water molecules more relaxed and more difficult to form hydrogen bonds (González et al., 2005). For n = 10, there are no hydrogen bonds between the water molecules in the second shell. While from n = 11, there are hydrogen bonds between the water molecules in the second hydration shell. Meanwhile, only $Ca^{2+}(H_2O)_{15}$ and $Ca^{2+}(H_2O)_{16}$ have a water molecule in the third hydration shell.

As shown in **Table 1**, in the beginning, the first hydration shell of the calcium ion is fully occupied with six water molecules, which is a distorted octahedral core. As the number of water molecules increases, N_1 increases to eight. The transition of N_1 from six to eight begins at about n = 12, which is corresponding to the experimental results of Bush et al. (2008). As the number of water molecules increases, N_1 fluctuates between seven and eight. The number of water molecules in the second shell increases monotonously with the number of water molecules increasing. Like the number of water molecules in the second shell, the number of hydrogen bonds increases as the number of water molecules increases. Thus, in the range of n = 10–18, N_1 and N_2 are not exactly six and nine, respectively, which is not the same as the simulation of Lei and Pan (2010). There is a strong competition between the first and second hydration shell water molecules.

The average adjacent O-O distance and the average Ca-O distance between Ca^{2+} and oxygen atoms of the water molecules in the first, second, and third hydration shells of the lowest-energy structures of $Ca^{2+}(H_2O)_{10-18}$ clusters are shown in **Table 2**. As the number of water molecules increases, the average adjacent O-O distance decreases, meaning that as the cluster size increases, the average interaction between water molecules becomes stronger. The average distance between Ca^{2+} and O in the first hydration shell water molecules varies from 2.38 to 2.521 Å, which are consistent with the results of MD simulation (Schwenk et al., 2001). Meanwhile, the variation trends of the coordination number of the first hydration shell

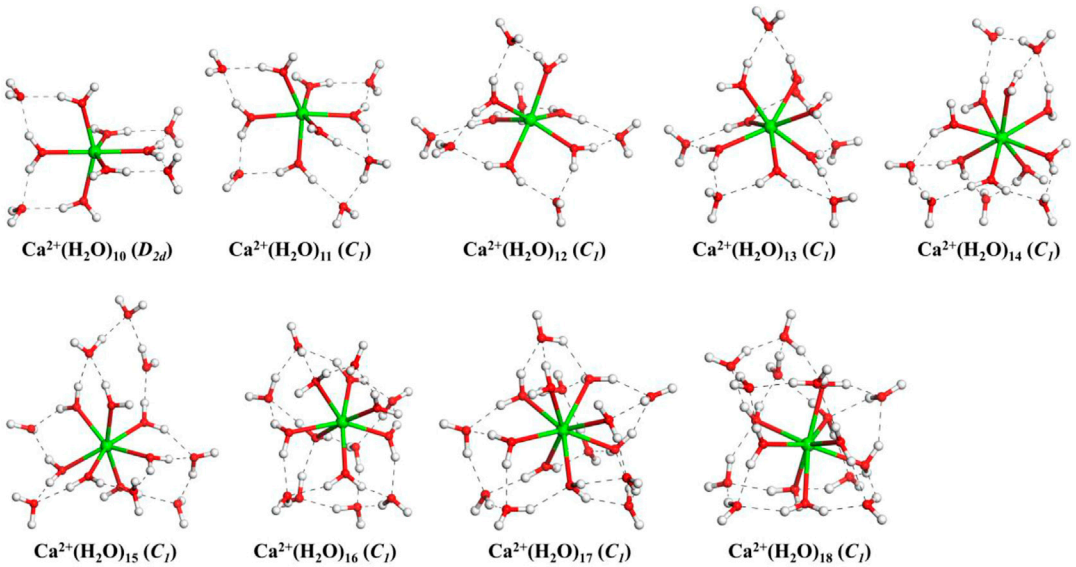

FIGURE 1 | The lowest-energy structures of $Ca^{2+}(H_2O)_n$ clusters with n = 10–18. The symmetries in parentheses are the symmetries of clusters without hydrogen atoms. The green, red, and white balls denote Ca, O, and H atoms, respectively. The dashed black lines represent the hydrogen bonds.

TABLE 1 | The number of water molecules in the first (N_1), second (N_2), and third (N_3) hydrated shells, and the number of hydrogen bonds (N_{HB}) of the lowest-energy structures of $Ca^{2+}(H_2O)_{10-18}$ clusters.

n	N_1	N_2	N_3	N_{HB}
10	6	4	0	8
11	6	5	0	10
12	6	6	0	12
13	7	6	0	12
14	8	6	0	12
15	7	7	1	15
16	7	8	1	20
17	8	9	0	23
18	8	10	0	25

TABLE 2 | Average adjacent O-O distance ($\overline{R}_{O-O}$) and the average Ca-O distance between Ca^{2+} and oxygen atoms in the first ($\overline{R}^1_{Ca-O}$), second ($\overline{R}^2_{Ca-O}$), and third ($\overline{R}^3_{Ca-O}$) shell water molecules of the lowest-energy structures of $Ca^{2+}(H_2O)_{10-18}$ clusters.

n	$\overline{R}_{O-O}$Å	$\overline{R}^1_{Ca-O}$Å	$\overline{R}^2_{Ca-O}$Å	$\overline{R}^3_{Ca-O}$Å
10	2.818	2.385	4.257	—
11	2.825	2.381	4.275	—
12	2.839	2.380	4.281	—
13	2.852	2.426	4.350	—
14	2.822	2.477	4.528	—
15	2.843	2.425	4.411	6.149
16	2.791	2.446	4.169	5.005
17	2.775	2.518	4.083	—
18	2.781	2.521	4.106	—

as well as the average distance between Ca^{2+} and O in the first hydration shell with the cluster size are the same, as shown in **Figure 2**. Thus, the average distance between Ca^{2+} and O in the

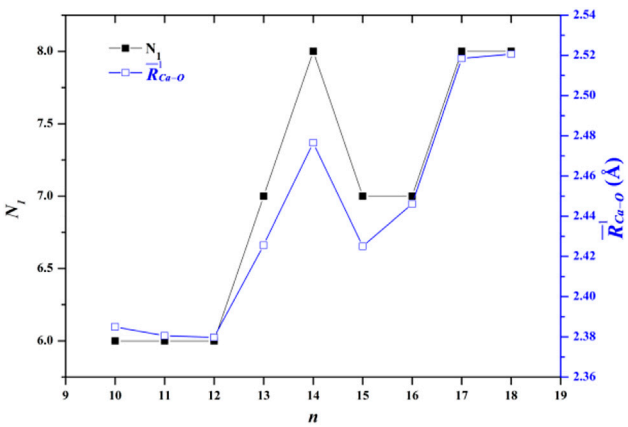

FIGURE 2 | Comparison between the number of water molecules in the first hydration shell (N_1) and the average adjacent Ca-O distance as a function of the number of water molecules.

water molecules of the first hydration shell increases as the number of first-shell water molecules increases, which have the same trend with the previous works (Bakó et al., 2002; Carl et al., 2007; Lei and Pan, 2010). The average distance between Ca^{2+} and O in the second hydration shell increases as the cluster size increases for n = 10–14, while it decreases as the cluster size increases for 14 < n ≤ 18. Thus, the distance between the first and second hydration shells decreases as the number of water molecules increases. Meanwhile, from n = 14, when the number of water molecules in the first hydration shell remains seven or eight, the number of water molecules in the second hydration shell still increases, and the water molecules in the second hydration shell generate hydrogen bonds. The geometric

TABLE 3 | The energy differences (in units of kJ/mol) between the structures obtained from the CGA and *n*-Lei as well as *n*-Wales calculated at MP2/6–311++G(2d,2p)//B3LYP-D3/6–311+G(d, p) level of theory with thermal correction at different temperature.

n	0K			298K		
	GA	Lei	Wales	GA	Lei	Wales
10	0	3.87	3.87	0	3.41	5.40
11	0	1.70	8.77	0	2.24	12.91
12	0	0	6.69	0	0	9.25
13	0	−2.10	7.31	0	−5.67	7.31
14	0	−1.87	−0.12	0	−5.01	−0.22
15	0	0.17	−0.11	0	−5.90	−2.96
16	0	0.33	−3.57	0	8.93	7.28
17	0	2.83	−7.22	0	17.25	5.41
18	0	9.75	−2.22	0	27.04	14.26

TABLE 4 | The sequential water binding energy ($\Delta E_{seq.}$, in units of kJ/mol) and the average interaction energy (E_i/N_1, in units of kJ/mol) of the lowest-energy structures of $Ca^{2+}(H_2O)_{10-18}$ clusters.

n	ΔE_{seq}	E_{exp}	E_i/N_1
10	—	—	−227.7
11	56.3	48 ± 7[a] 55.7[b]	−235.3
12	57.0	44 ± 6.4[a] 54.4[b]	−245.7
13	55.2	43 ± 2.4[a] 51.9[b]	−221.0
14	49.1	46 ± 4.3[a] 49.8[b]	−198.4
15	51.8	40 ± 5.9[a]	−234.4
16	46.7	38 ± 3.2[a]	−211.0
17	47.7	41 ± 5.9[a]	−179.4
18	51.5	48 ± 4.1[a]	−182.4

[a]*Taken from Bruzzi and Stace, 2017.*
[b]*Taken from Peschke et al., 1998.*

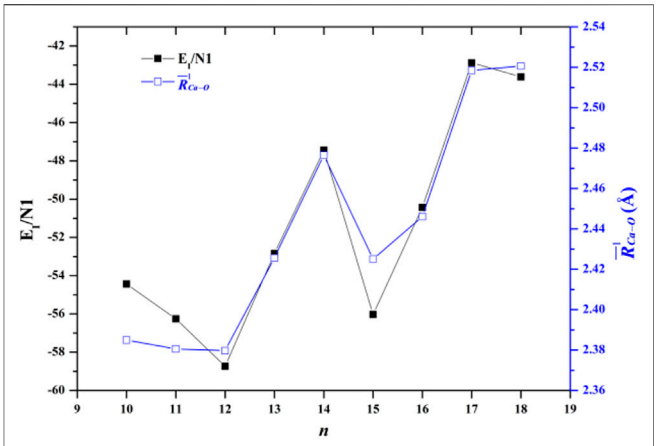

FIGURE 3 | Comparison between the average interaction energy and the average adjacent Ca-O distance as a function of the number of water molecules.

TABLE 5 | Average natural charge of the calcium ion $\delta(Ca^{2+})$ and the oxygen atoms in the first $\delta(O_1)$, second $\delta(O_2)$, and third $\delta(O_3)$ solvation shells of the lowest-energy structures of $Ca^{2+}(H_2O)_{10-18}$ clusters.

	$\delta(Ca^{2+})$	$\delta(O_1)$	$\delta(O_2)$	$\delta(O_3)$
10	1.900	−1.047	−0.988	—
11	1.899	−1.050	−0.990	—
12	1.898	−1.055	−0.987	—
13	1.886	−1.038	−0.982	—
14	1.880	−1.023	−0.990	—
15	1.885	−1.040	−0.988	−0.979
16	1.883	−1.052	−1.009	−1.014
17	1.873	−1.053	−1.013	—
18	1.873	−1.056	−1.013	—

characteristic of $Ca^{2+}(H_2O)_{10-18}$ clusters reveals that as the cluster size increases, the interaction between Ca^{2+} and water molecules decreases and the interaction between water molecules increases.

Relative Energy and Stability

The energy differences at the MP2/6-311++G(2d,2p) level of theory between the structures obtained from the CGA and *n*-Lei and *n*-Wales are shown in **Table 3**. As shown in **Figure 1**, **Supplementary Figure S1**, and **Table 3**, for $Ca^{2+}(H_2O)_{10}$, the number of first hydration shell water molecules is six. The structure is different from 10-Lei and 10-Wales, while has the same number of hydrogen bonds with 10-Lei. $Ca^{2+}(H_2O)_{10}$ has higher symmetry and lower total energy by 3.87 kJ/mol compared with 10-Lei and 10-Wales. $Ca^{2+}(H_2O)_{11}$ is also different from 11-Lei and 11-Wales with lower energy. There are hydrogen bonds between the water molecules in the second shell. $Ca^{2+}(H_2O)_{12}$ is the same with 12-Lei, which is 6.69 kJ/mol lower in energy than 12-Wales. For $Ca^{2+}(H_2O)_{13}$, there are seven water molecules in the first hydration shell. $Ca^{2+}(H_2O)_{13}$ is 2.10 kJ/mol higher in energy than 13-Lei and 7.31 kJ/mol lower in energy than 13-Wales, respectively. $Ca^{2+}(H_2O)_{14}$ has eight water molecules in the first shell and is 1.87 kJ/mol higher in energy than 14-Lei as well as 0.12 kJ/mol higher in energy than 14-Wales. For $Ca^{2+}(H_2O)_{15}$, the third-shell water molecule appears. Meanwhile, $Ca^{2+}(H_2O)_{15}$ is 0.17 kJ/mol lower in energy than 15-Lei and 0.11 kJ/mol higher in energy than 15-Wales. $Ca^{2+}(H_2O)_{16}$ is 0.33 kJ/mol lower in energy than 16-Lei, while is 3.57 kJ/mol higher in energy than 16-Wales. $Ca^{2+}(H_2O)_{17}$ and $Ca^{2+}(H_2O)_{18}$ only have two hydration shells, and several water molecules in the second shell hydrogen bonded to three water molecules in the first shell. $Ca^{2+}(H_2O)_{17}$ and $Ca^{2+}(H_2O)_{18}$ are both more stable than the corresponding ones taken from the work of Lei and Pan, and higher in energy than the ones taken from the work of Wales and co-workers.

The above-mentioned energy differences are all at 0 K, while the thermal effect could change the relative stability of clusters (Lei and Pan, 2010; Shi et al., 2018b). Thus, we also provide the energy difference at room temperature in **Table 3**. For $n = 10–12$, the structures obtained from the CGA are the most stable ones both at 0 K and room temperature. For $n = 13$, 13-Lei are the most stable ones both at 0 and 298 K. The structures obtained from the CGA are more stable than the 13-Wales. However, for $n = 14$ and 15, *n*-Lei and *n*-Wales become more stable than $Ca^{2+}(H_2O)_n$ from the CGA at room temperature. For $n = 16–18$, the structures obtained from the CGA are more stable than the *n*-Lei, while more unstable than the *n*-Wales at 0 K. As the temperature arises

TABLE 6 | Average second-order perturbation energy (in units of kcal/mol) of several kinds of charge transfer of the lowest-energy structures of $Ca^{2+}(H_2O)_{10-18}$ clusters.[a]

n	LP(O)-LP*(Ca)	BD(O-H)-LP*(Ca)	LP*(Ca)-RY*(O)	LP*(Ca)-RY*(H)	LP*(Ca)-BD*(O-H)	LP*(Ca)-RY*(Ca)
10	86.98	16.96	—	—	—	—
11	87.44	17.63	—	—	—	—
12	86.80	18.05	—	—	—	—
13	106.19	22.04	—	—	—	—
14	118.65	25.12	305.52	34.54	--	58.56
15	105.86	22.28	—	—	—	—
16	101.11	23.73	—	—	—	—
17	109.36	29.72	267.95	17.35	43.87	92.48
18	108.12	31.26	170.70	21.08	54.17	90.04

[a]*LP and LP* represent the lone pair electron orbital and the empty orbital, respectively. BD and BD* represent the bonding orbital and antibonding orbital, respectively. RY* is the Rydberg orbital.*

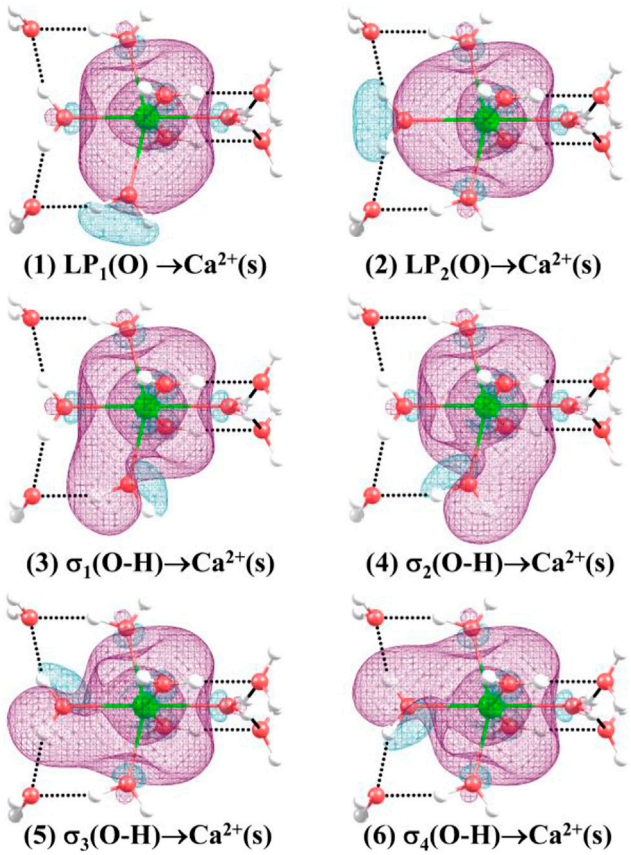

FIGURE 4 | Three-dimensional schematics of the charge transfer from (1) to (2): the lone pair electron orbital of adjacent oxygen atoms, and (3)–(6): the bonding orbital of adjacent O-H to the empty orbital of Ca^{2+} for the lowest-energy structure of $Ca^{2+}(H_2O)_{10}$.

to 298 K, the structures obtained from the CGA become the most stable structures. In general, as the temperature increases as well as the cluster size increases, the number of water molecules in the first hydration shell is more favored between seven and eight, which is opposite with the trend derived by Bai and co-workers using *ab initio* molecular dynamic simulation (Bai et al., 2013). Meanwhile, as shown in **Table 3**, such small energy differences indicate that the structures obtained from the CGA, *n*-Lei, and *n*-Wales are concomitant both at 0 K and at room temperature.

The sequential water binding energy ($\Delta E_{seq.}$) of a $Ca^{2+}(H_2O)_n$ cluster is defined as follows:

$$\Delta E_{seq.} = E(H_2O) + E\left[Ca^{2+}(H_2O)_{n-1}\right] - E\left[Ca^{2+}(H_2O)_n\right]. \quad (2)$$

As shown in **Table 4**, the simulated sequential water binding energy of the lowest-energy structures of $Ca^{2+}(H_2O)_n$ clusters with n = 11–18 is almost overlapped in the error bar though slightly larger than the corresponding experimental results with the same cluster size (Peschke et al., 1998; Bruzzi and Stace, 2017).

Another significant energetic property of the $Ca^{2+}(H_2O)_n$ cluster is the interaction energy between the calcium ion and water molecules. The average interaction energy between the calcium ion and adjacent water molecules of a $Ca^{2+}(H_2O)_n$ cluster (E_I/N_1) is defined as follows:

$$E_I/N_1 = \left[E\left[Ca^{2+}(H_2O)_n\right] - E\left(Ca^{2+}\right) - E\left[(H_2O)_n\right]\right]/N_1, \quad (3)$$

where $E[(H_2O)_n]$ is the energy of all the water molecules in the same geometry as in the cluster. The E_I/N_1 of the lowest-energy structures of $Ca^{2+}(H_2O)_{10-18}$ clusters are listed in **Table 4**. **Figure 3** also shows the comparison between the E_I/N_1 and the average adjacent Ca-O distances as a function of the number of water molecules. As the average distance between Ca^{2+} and oxygen atoms in the first-shell water molecules increases, the interaction between Ca^{2+} and water molecules decreases. Furthermore, the trends of the E_I/N_1 and the average adjacent Ca-O distances as a function of the number of water molecules are similar, indicating that the interaction between Ca^{2+} and water molecules mainly originates from Ca^{2+} and water molecules in the first-shell water molecules (Lei and Pan, 2010).

Natural Bond Orbital

NBO analyses could give the information about the natural charge of every atom and charge transfer between different units and so on. **Table 5** provides the average natural charge of the calcium ion and the oxygen atoms in the first, second, and third solvation shells.

The average natural charge of Ca^{2+} becomes smaller as the number of first-shell water molecules increases. The average natural charge of the oxygen atoms in the first-shell water molecules is smaller than that in the second- and third-shell water molecules. Meanwhile, the average natural charge of the oxygen atoms in the second and third hydration shells remains almost unchanged. Therefore, the interaction between Ca^{2+} and water molecules mainly focuses on the interplay between the calcium ion and the first hydration shell (Lei and Pan, 2010).

Table 6 shows the second-order perturbation energy of the charge transfer between Ca^{2+} and water molecules, which results in the interaction between Ca^{2+} and adjacent water molecules. The charge transfer from the lone pair electron orbital of adjacent oxygen atoms and the bonding orbital of adjacent O-H to the empty orbital of Ca^{2+} occurs in all the lowest-energy structures of $Ca^{2+}(H_2O)_{10-18}$ clusters. **Figure 4** provides the schematic diagrams of these two kinds of charge transfer in the lowest-energy structure of $Ca^{2+}(H_2O)_{10}$ clusters. Among them, the charge transfer from the lone pair electron orbital of adjacent oxygen atoms to the empty orbital of Ca^{2+} plays a leading role. Moreover, for the lowest-energy structures of $Ca^{2+}(H_2O)_n$ clusters with n = 14, 17, and 18, the empty orbital of Ca^{2+} is not exactly empty. There is charge transfer from the empty orbital of Ca^{2+} to the Rydberg orbital of adjacent oxygen atoms, adjacent hydrogen atoms, and Ca^{2+} as well as to the antibonding orbital of adjacent O-H. Thus, the electron of Ca^{2+} becomes more diffused as the number of first-shell water molecules is eight.

CONCLUSION

By means of CGA combined with DMol^3 package, we search the potential energy surface of the hydrated calcium ion clusters $Ca^{2+}(H_2O)_n$ with n = 10–18. The low-lying structures of $Ca^{2+}(H_2O)_n$ clusters obtained from the CGA are re-optimized at the B3LYP-D3/6-311+G(d,p) level of theory. The lowest-energy structures of $Ca^{2+}(H_2O)_{10-18}$ clusters reveal that Ca^{2+} prefers to locate at the center of the cluster. Meanwhile, the lowest-energy structures of $Ca^{2+}(H_2O)_{10-12}$ clusters revalidate the conclusion that the coordination number of first-shell water molecules is six. The switch of the N_1 from six to eight is with up to n = 12. As the cluster size rises to n = 18, the N_1 fluctuates between seven and eight, indicating that there is a strong competition between the first and second hydration shell water molecules. The complexity of the lowest-energy structures of $Ca^{2+}(H_2O)_{10-18}$ clusters increases as the cluster size increases since the number of the water molecules in the second shell and the total hydrogen bonds becomes more.

As the cluster size increases, the distance between Ca^{2+} and the adjacent water molecules increases while the average adjacent O-O distance decreases, implying that the interaction between Ca^{2+} and the adjacent water molecules becomes weaker and the interaction between water molecules becomes stronger. The interaction energy between Ca^{2+} and the water molecules, the natural charge, certifies that the interaction is mainly derived from the interaction between Ca^{2+} and the adjacent water molecules. Furthermore, the charge transfer from the lone pair electron orbital of adjacent oxygen atoms to the empty orbital of Ca^{2+} plays a leading role in the interaction between Ca^{2+} and water molecules.

DATA AVAILABILITY STATEMENT

The original contributions presented in the study are included in the article/**Supplementary Material**; further inquiries can be directed to the corresponding author.

AUTHOR CONTRIBUTIONS

RS contributed to conceptualization, methodology, formal analysis, writing—original draft, project administration, and funding acquisition. ZZ performed formal analysis, writing—original draft, and funding acquisition. XH performed data curation and investigation. PW contributed to data curation and formal analysis. YS performed conceptualization, methodology, investigation, writing—original draft, project administration, supervision, and funding acquisition. LS carried out the formal analysis, validation, and funding acquisition. XL contributed to data curation, investigation, and funding acquisition. HH performed formal analysis, writing-original draft, and investigation. JZ contributed to conceptualization, methodology, writing— review and editing, funding acquisition, project administration, and supervision.

FUNDING

This work was supported by the National Natural Science Foundation of China (Nos. 91961204, 11674046, 11804076, 11904251, 12004094, 12004095, 21976049), the Science Challenge Project (No. TZ2016001), and the Supercomputing Center of Dalian University of Technology.

SUPPLEMENTARY MATERIAL

The Supplementary Material for this article can be found online at: https://www.frontiersin.org/articles/10.3389/fchem.2021.637750/full#supplementary-material

REFERENCES

Bai, G., Yi, H.-B., Li, H.-J., and Xu, J.-J. (2013). Hydration Characteristics of Ca^{2+} and Mg^{2+}: a Density Functional Theory, Polarized Continuum Model and Molecular Dynamics Investigation. *Mol. Phys.* 111, 553–568. doi:10.1080/00268976.2012.737035

Bakó, I., Hutter, J., and Pálinkás, G. (2002). Car-Parrinello Molecular Dynamics Simulation of the Hydrated Calcium Ion. *J. Chem. Phys.* 117, 9838–9843. doi:10.1063/1.1517039

Becke, A. D. (1988). Density-functional Exchange-Energy Approximation with Correct Asymptotic Behavior. *Phys. Rev. A.* 38, 3098–3100. doi:10.1103/physreva.38.3098

Bernal-Uruchurtu, M. I., and Ortega-Blake, I. (1995). *J. Chem. Phys.* 103, 1588.
Boda, A., De, S., Ali, S. M., Tulishetti, S., Khan, S., and Singh, J. K. (2012). From Microhydration to Bulk Hydration of Sr^{2+} Metal Ion: DFT, MP2 and Molecular Dynamics Study. *J. Mol. Liquids* 172, 110–118. doi:10.1016/j.molliq.2012.05.006
Bruzzi, E., and Stace, A. J. (2017). Experimental Measurements of Water Molecule Binding Energies for the Second and Third Solvation Shells of $[Ca(H_2O)_N]^{2+}$ Complexes. *R. Soc. Open Sci.* 4, 160671. doi:10.1098/rsos.160671
Buck, U., Dauster, I., Gao, B., and Liu, Z.-f. (2007). Infrared Spectroscopy of Small Sodium-Doped Water Clusters: Interaction with the Solvated Electron†. *J. Phys. Chem. A.* 111, 12355–12362. doi:10.1021/jp075717o
Bush, M. F., O'Brien, J. T., Prell, J. S., Wu, C.-C., Saykally, R. J., and Williams, E. R. (2009). Hydration of Alkaline Earth Metal Dications: Effects of Metal Ion Size Determined Using Infrared Action Spectroscopy. *J. Am. Chem. Soc.* 131, 13270–13277. doi:10.1021/ja901011x
Bush, M. F., Saykally, R. J., and Williams, E. R. (2007). Hydration of the Calcium Dication: Direct Evidence for Second Shell Formation from Infrared Spectroscopy. *ChemPhysChem* 8, 2245–2253. doi:10.1002/cphc.200700404
Bush, M. F., Saykally, R. J., and Williams, E. R. (2008). Infrared Action Spectra of $Ca^{2+}(H_2O)_{11-69}$ Exhibit Spectral Signatures for Condensed-phase Structures with Increasing Cluster Size. *J. Am. Chem. Soc.* 130, 15482–15489. doi:10.1021/ja804621r
Butler, M., Mañez, P. A., Cabrera, G. M., and Maître, P. (2014). Gas Phase Structure and Reactivity of Doubly Charged Microhydrated Calcium(II)-Catechol Complexes Probed by Infrared Spectroscopy. *J. Phys. Chem. A.* 118, 4942–4954. doi:10.1021/jp503789j
Caldwell, J., Dang, L. X., and Kollman, P. A. (1990). Implementation of Nonadditive Intermolecular Potentials by Use of Molecular Dynamics: Development of a Water-Water Potential and Water-Ion Cluster Interactions. *J. Am. Chem. Soc.* 112, 9144–9147. doi:10.1021/ja00181a017
Carl, D. R., Moision, R. M., and Armentrout, P. B. (2007). Binding Energies for the Inner Hydration Shells of Ca^{2+}: An Experimental and Theoretical Investigation of $Ca^{2+}(H_2O)_X$ Complexes (X = 5-9). *Int. J. Mass Spectrom.* 265, 308–325. doi:10.1016/j.ijms.2007.03.008
Carrera, Á., Mobbili, M., and Marceca, E. (2009). Electric Susceptibility of Sodium-Doped Water Clusters by Beam Deflection. *J. Phys. Chem. A.* 113, 2711–2714. doi:10.1021/jp809411p
Chen, H., and Ruckenstein, E. (2015). Hydrated Ions: From Individual Ions to Ion Pairs to Ion Clusters. *J. Phys. Chem. B* 119, 12671–12676. doi:10.1021/acs.jpcb.5b06837
Chizhik, V. I., Egorov, A. V., Pavlova, M. S., Egorova, M. I., and Donets, A. V. (2016). Structure of Hydration Shell of Calcium Cation by NMR Relaxation, Car-Parrinello Molecular Dynamics and Quantum-Chemical Calculations. *J. Mol. Liquids* 224, 730–736. doi:10.1016/j.molliq.2016.10.035
Delgado, A. A. A., Sethio, D., Munar, I., Aviyente, V., and Kraka, E. (2020). Local Vibrational Mode Analysis of Ion-Solvent and Solvent-Solvent Interactions for Hydrated Ca^{2+} Clusters. *J. Chem. Phys.* 153, 224303. doi:10.1063/5.0034765
Delley, B. (1990). An All-electron Numerical Method for Solving the Local Density Functional for Polyatomic Molecules. *J. Chem. Phys.* 92, 508–517. doi:10.1063/1.458452
Delley, B. (2000). From Molecules to Solids with the $DMol^3$ Approach. *J. Chem. Phys.* 113, 7756–7764. doi:10.1063/1.1316015
Egorov, A. V., Brodskaya, E. N., and Laaksonen, A. (2003). The Effect of Ions on Solid-Liquid Phase Transition in Small Water Clusters. A Molecular Dynamics Simulation Study. *J. Chem. Phys.* 118, 6380–6386. doi:10.1063/1.1557523
Frisch, M., Trucks, G., Schlegel, H., Scuseria, G., Robb, M., Cheeseman, J., et al. (2009). *Gaussian, Inc., Wallingford CT*.
Fujiwara, T., Mochizuki, Y., Komeiji, Y., Okiyama, Y., Mori, H., Nakano, T., et al. (2010). Fragment Molecular Orbital-Based Molecular Dynamics (FMO-MD) Simulations on Hydrated Zn(II) Ion. *Chem. Phys. Lett.* 490, 41–45. doi:10.1016/j.cplett.2010.03.020
Fulton, J. L., Heald, S. M., Badyal, Y. S., and Simonson, J. M. (2003). Understanding the Effects of Concentration on the Solvation Structure of Ca^{2+} in Aqueous Solution. I: The Perspective on Local Structure from EXAFS and XANES. *J. Phys. Chem. A.* 107, 4688–4696. doi:10.1021/jp0272264
Gao, B., and Liu, Z.-F. (2007). Ionization Induced Relaxation in Solvation Structure: A Comparison between $Na(H_2O)_n$ and $Na(NH_3)_n$. *J. Chem. Phys.* 126, 084501. doi:10.1063/1.2464109
González, B. S., Hernández-Rojas, J., and Wales, D. J. (2005). Global Minima and Energetics of $Li^+(H_2O)_n$ and $Ca^{2+}(H_2O)_n$ Clusters for $n \leqslant 20$. *Chem. Phys. Lett.* 412, 23–28. doi:10.1016/j.cplett.2005.06.090
Hadad, C., Florez, E., Acelas, N., Merino, G., and Restrepo, A. (2019). Microsolvation of Small Cations and Anions. *Int. J. Quan. Chem.* 119, e25766. doi:10.1002/qua.25766
Hall, R. J., Hillier, I. H., and Vincent, M. A. (2000). Which Density Functional Should Be Used to Model Hydration? *Chem. Phys. Lett.* 320, 139–143. doi:10.1016/s0009-2614(00)00218-9
Hewish, N. A., Neilson, G. W., and Enderby, J. E. (1982). Environment of Ca^{2+} Ions in Aqueous Solvent. *Nature* 297, 138–139. doi:10.1038/297138a0
Hofer, T. S., Rode, B. M., and Randolf, B. R. (2005). Structure and Dynamics of Solvated Ba(II) in Dilute Aqueous Solution - an Ab Initio QM/MM MD Approach. *Chem. Phys.* 312, 81–88. doi:10.1016/j.chemphys.2004.11.023
Jalilehvand, F., Spångberg, D., Lindqvist-Reis, P., Hermansson, K., Persson, I., and Sandström, M. (2001). Hydration of the Calcium Ion. An EXAFS, Large-Angle X-ray Scattering, and Molecular Dynamics Simulation Study. *J. Am. Chem. Soc.* 123, 431–441. doi:10.1021/ja001533a
Kistenmacher, H., Popkie, H., and Clementi, E. (1974). Study of the Structure of Molecular Complexes. VIII. Small Clusters of Water Molecules Surrounding Li^+, Na^+, K^+, F^-, and Cl^- Ions. *J. Chem. Phys.* 61, 799–815. doi:10.1063/1.1682019
Lee, C., Yang, W., and Parr, R. G. (1988). Development of the Colle-Salvetti Correlation-Energy Formula into a Functional of the Electron Density. *Phys. Rev. B* 37, 785–789. doi:10.1103/physrevb.37.785
Lei, X. L., and Pan, B. C. (2010). Structures, Stability, Vibration Entropy and IR Spectra of Hydrated Calcium Ion Clusters $[Ca(H_2O)_n]^{2+}$ (n = 1–20, 27): A Systematic Investigation by Density Functional Theory. *J. Phys. Chem. A.* 114, 7595–7603. doi:10.1021/jp102588m
León-Pimentel, C. I., Amaro-Estrada, J. I., Hernández-Cobos, J., Saint-Martin, H., and Ramírez-Solís, A. (2018). Aqueous Solvation of Mg(ii) and Ca(ii): A Born-Oppenheimer Molecular Dynamics Study of Microhydrated Gas Phase Clusters. *J. Chem. Phys.* 148, 144307. doi:10.1063/1.5021348
Marcus, Y. (1988). Ionic Radii in Aqueous Solutions. *Chem. Rev.* 88, 1475–1498. doi:10.1021/cr00090a003
Megyes, T., Grósz, T., Radnai, T., Bakó, I., and Pálinkás, G. (2004). Solvation of Calcium Ion in Polar Solvents: An X-ray Diffraction and Ab Initio Study. *J. Phys. Chem. A.* 108, 7261–7271. doi:10.1021/jp048838m
Misaizu, F., Tsukamato, K., Sanekata, M., and Fuke, K. (1995). Photoelectron Spectroscopy of Mass-Selected Copper-Water Cluster Negative Ions. *Laser Chem.* 15, 195–207. doi:10.1155/1995/68042
Møller, C., and Plesset, M. S. (1934). Note on an Approximation Treatment for Many-Electron Systems. *Phys. Rev.* 46, 618. doi:10.1103/PhysRev.46.618
Obst, S., and Bradaczek, H. (1996). Molecular Dynamics Study of the Structure and Dynamics of the Hydration Shell of Alkaline and Alkaline-Earth Metal Cations. *J. Phys. Chem.* 100, 15677–15687. doi:10.1021/jp961384b
Peschke, M., Blades, A. T., and Kebarle, P. (2000). Binding Energies for Doubly-Charged Ions $M^{2+} = Mg^{2+}$, Ca^{2+} and Zn^{2+} with the Ligands L = H_2O, Acetone and N-Methylacetamide in Complexes M for n = 1 to 7 from Gas Phase Equilibria Determinations and Theoretical Calculations. *J. Am. Chem. Soc.* 122, 10440–10449. doi:10.1021/ja002021z
Peschke, M., Blades, A. T., and Kebarle, P. (1998). Hydration Energies and Entropies for Mg^{2+}, Ca^{2+}, Sr^{2+}, and Ba^{2+} from Gas-phase Ion–Water Molecule Equilibria Determinations. *J. Phys. Chem. A.* 102, 9978–9985. doi:10.1021/jp9821127
Prendergast, F. G., and Mann, K. G. (1977). Differentiation of Metal Ion-Induced Transitions of Prothrombin Fragment 1. *J. Biol. Chem.* 252, 840–850. doi:10.1016/s0021-9258(19)75174-6
Probst, M. M., Radnai, T., Heinzinger, K., Bopp, P., and Rode, B. M. (1985). Molecular Dynamics and X-ray Investigation of an Aqueous Calcium Chloride Solution. *J. Phys. Chem.* 89, 753–759. doi:10.1021/j100251a007
Rudolph, W. W., and Irmer, G. (2013). Hydration of the Calcium(ii) Ion in an Aqueous Solution of Common Anions (ClO_4^-, Cl^-, Br^-, and NO_3^-). *Dalton Trans.* 42, 3919. doi:10.1039/c2dt31718d
Schwenk, C. F., Loeffler, H. H., and Rode, B. M. (2001). Molecular Dynamics Simulations of Ca^{2+} in Water: Comparison of a Classical Simulation Including Three-Body Corrections and Born-Oppenheimer Ab Initio and Density Functional Theory Quantum Mechanical/molecular Mechanics Simulations. *J. Chem. Phys.* 115, 10808–10813. doi:10.1063/1.1419057

Shi, R., Huang, X., Su, Y., Lu, H.-G., Li, S.-D., Tang, L., et al. (2017). Which Density Functional Should Be Used to Describe Protonated Water Clusters? *J. Phys. Chem. A.* 121, 3117–3127. doi:10.1021/acs.jpca.7b00058

Shi, R., Li, K., Su, Y., Tang, L., Huang, X., Sai, L., et al. (2018a). Revisit the Landscape of Protonated Water Clusters $H^+(H_2O)_n$ with n = 10-17: An Ab Initio Global Search. *J. Chem. Phys.* 148, 174305. doi:10.1063/1.5026383

Shi, R., Wang, P., Tang, L., Huang, X., Chen, Y., Su, Y., et al. (2018b). Structures and Spectroscopic Properties of $F^-(H_2O)_n$ with n = 1-10 Clusters from a Global Search Based on Density Functional Theory. *J. Phys. Chem. A.* 122, 3413–3422. doi:10.1021/acs.jpca.7b08872

Shi, R., Zhao, Z., Liang, X., Su, Y., Sai, L., and Zhao, J. (2020). Structures and Vertical Detachment Energies of Water Cluster Anions $(H_2O)_n^-$ with n = 6-11. *Theor. Chem. Acc.* 139, 66. doi:10.1007/s00214-020-2567-2

Siu, C.-K., Liu, Z.-F., and Tse, J. S. (2002). Ab Initio Studies on $Al^+(H_2O)_n$, $HAlOH^+(H_2O)_{n-1}$, and the Size-dependent H_2 Elimination Reaction. *J. Am. Chem. Soc.* 124, 10846–10860. doi:10.1021/ja0117579

Stephens, P. J., Devlin, F. J., Chabalowski, C. F., and Frisch, M. J. (1994). Ab Initio Calculation of Vibrational Absorption and Circular Dichroism Spectra Using Density Functional Force Fields. *J. Phys. Chem.* 98, 11623–11627. doi:10.1021/j100096a001

Todorova, T., Hünenberger, P. H., and Hutter, J. (2008). Car-Parrinello Molecular Dynamics Simulations of $CaCl_2$ Aqueous Solutions. *J. Chem. Theor. Comput.* 4, 779–789. doi:10.1021/ct700302m

Tongraar, A., Liedl, K. R., and Rode, B. M. (1997). Solvation of Ca^{2+} in Water Studied by Born–Oppenheimer Ab Initio QM/MM Dynamics. *J. Phys. Chem. A.* 101, 6299–6309. doi:10.1021/jp970963t

Wang, P., Shi, R., Su, Y., Tang, L., Huang, X., and Zhao, J. (2019). Hydrated Sodium Ion Clusters $[Na^+(H_2O)_n$ (n = 1–6)]: An ab initio Study on Structures and Non-covalent Interaction. *Front. Chem.* 7. doi:10.3389/fchem.2019.00624

Wanprakhon, S., Tongraar, A., and Kerdcharoen, T. (2011). Hydration Structure and Dynamics of K^+ and Ca^{2+} in Aqueous Solution: Comparison of Conventional QM/MM and ONIOM-XS MD Simulations. *Chem. Phys. Lett.* 517, 171–175. doi:10.1016/j.cplett.2011.10.048

Wells, B. H., and Wilson, S. (1983). van der Waals interaction potentials: Many-body basis set superposition effects. *Chem. Phys. Lett.* 101, 429–434. doi:10.1016/0009-2614(83)87508-3

Yamaguchi, T., Hayashi, S., and Ohtaki, H. (1989). X-ray Diffraction Study of Calcium(II) Chloride Hydrate Melts: $CaCl_2.RH_2O$ (R = 4.0, 5.6, 6.0, and 8.6). *Inorg. Chem.* 28, 2434–2439. doi:10.1021/ic00311a036

Yoo, J., Wilson, J., and Aksimentiev, A. (2016). Improved Model of Hydrated Calcium Ion for Molecular Dynamics Simulations Using Classical Biomolecular Force fields. *Biopolymers* 105, 752–763. doi:10.1002/bip.22868

Zhang, H., and Liu, Z.-F. (2011). The Identification of a Solvated Electron Pair in the Gaseous Clusters of $Na^-(H_2O)_n$ and $Li^-(H_2O)_n$. *J. Chem. Phys.* 135, 064309. doi:10.1063/1.3622562

Zhao, J., Shi, R., Sai, L., Huang, X., and Su, Y. (2016). Comprehensive Genetic Algorithm for Ab initio global Optimisation of Clusters. *Mol. Simulation* 42, 809–819. doi:10.1080/08927022.2015.1121386

Conflict of Interest: The authors declare that the research was conducted in the absence of any commercial or financial relationships that could be construed as a potential conflict of interest.

frontiers in Chemistry

ORIGINAL RESEARCH
published: 14 July 2021
doi: 10.3389/fchem.2021.712960

CO_2 Activation Within a Superalkali-Doped Fullerene

Giovanni Meloni[1,2]*, *Andrea Giustini*[2] *and Heejune Park*[1]

[1]Department of Chemistry, University of San Francisco, San Francisco, CA, United States, [2]Department of Physical and Chemical Sciences, Università degli Studi de L'Aquila, L'Aquila, Italy

With the aim of finding a suitable synthesizable superalkali species, using the B3LYP/6-31G* density functional level of theory we provide results for the interaction between the buckminsterfullerene C_{60} and the superalkali Li_3F_2. We show that this endofullerene is stable and provides a closed environment in which the superalkali can exist and interact with CO_2. It is worthwhile to mention that the optimized Li_3F_2 structure inside C_{60} is not the most stable C_{2v} isomer found for the "free" superalkali but the D_{3h} geometry. The binding energy at 0 K between C_{60} and Li_3F_2 (D_{3h}) is computed to be 119 kJ mol^{-1}. Once CO_2 is introduced in the endofullerene, it is activated, and the $\widehat{OCO}$ angle is bent to 132°. This activation does not follow the previously studied CO_2 reduction by an electron transfer process from the superalkali, but it is rather an actual reaction where a F (from Li_3F_2) atom is bonded to the CO_2. From a thermodynamic analysis, both CO_2 and the encapsulated [Li_3F_2·CO_2] are destabilized in C_{60} with solvation energies at 0 K of 147 and < −965 kJ mol^{-1}, respectively.

Keywords: CO_2 activation, superalkali, endofullerene, ionization energy, solvation energy

OPEN ACCESS

Edited by:
Ambrish Kumar Srivastava, Deen Dayal Upadhyay Gorakhpur University, India

Reviewed by:
Gourhari Jana, Indian Institute of Technology Bombay, India
Amlan Kusum Roy, Indian Institute of Science Education and Research Kolkata, India

***Correspondence:**
Giovanni Meloni
gmeloni@usfca.edu

Specialty section:
This article was submitted to Theoretical and Computational Chemistry, a section of the journal Frontiers in Chemistry

Received: *21 May 2021*
Accepted: *28 June 2021*
Published: *14 July 2021*

Citation:
Meloni G, Giustini A and Park H (2021) CO_2 Activation Within a Superalkali-Doped Fullerene. Front. Chem. 9:712960. doi: 10.3389/fchem.2021.712960

INTRODUCTION

In 1985, Kroto and co-workers discovered an extremely stable cluster consisting of 60 carbon atoms during a study of long-chain carbon molecules. (Kroto et al., 1985). This cluster, called fullerene, has a football shape with 12 pentagonal and 20 hexagonal rings. (Kroto et al., 1985). Shortly after, a study presenting successful formation of fullerenes with a lanthanum atom trapped in the cavity of C_{60}, called endofullerene, $C_{60}La$, was published. (Heath et al., 1985). Another consequent experiment proved the stability of $C_{60}La^+$ against H_2, O_2, NO, and NH_3. (Weiss et al., 1988). This suggested that the lanthanum atom can be "protected" by being encapsulated in the fullerene. Since then, a number of studies focusing on novel properties of C_{60} and its interactions with other species have been carried out. (Ruoff et al., 1993; Diederich and Gómez-López, 1999; Bakry et al., 2007; Mignolet et al., 2013; Wang et al., 2014; Elliott et al., 2018; Kouřil et al., 2018) Some investigations concentrated on medical applications, hydrogen storage, and various endofullerene. (Wang et al., 2013; Srivastava et al., 2016; Srivastava et al., 2017; Elliott et al., 2018; Kouřil et al., 2018). Due to the fullerene's unique cage-like cavity, a procedure called molecular surgery can be performed to entrap an atom or molecule. (Murata et al., 2006; Krachmalnicoff et al., 2016). Utilizing this technique, encapsulation of molecular hydrogen and HF were successfully achieved. (Murata et al., 2006; Krachmalnicoff et al., 2016). In addition, a recent paper by Jana and Chattaraj (2020) describes the effects of a molecular reaction environment, dodecahedrane, on the He dimer bonding. Also, theoretical studies of a new type of endofullerenes with superalkali have been performed. (Srivastava et al., 2016; Srivastava et al., 2017) Superalkalis are clusters with very low adiabatic ionization energies. (Gutsev and Boldyrev, 1982; Gutsev and Boldyrev, 1983; Gutsev and Boldyrev, 1987; Lia et al., 1988; Gutsev and Boldyrev, 1990;

Tong et al., 2013a; Tong et al., 2013b). The first and most common superalkalis have the formula $M_{k+1}L$, where M is an alkali atom with valence k and L is an electronegative atom. (Gutsev and Boldyrev, 1985; Gutsev and Boldyrev, 1987; Zhao et al., 2017). Nambiar et al. (2021) showed the importance of these compounds through a density functional computational study to improve the efficacy of redox reactions.

The concentration of carbon dioxide (CO_2) in the atmosphere has been increasing constantly since the early 20th century with rapid industrialization. (D'Amato and Akdis, 2020; Kuzovkin and Semenov, 2020). This is a globally recognized issue as CO_2 contributes significantly to the greenhouse effect and the acidification of the oceans. (Crowley and Berner, 2001; Hönisch et al., 2012). Increment of atmospheric temperature causes climate change that threatens the overall ecosystem. To capture CO_2 molecules present in the air, various methods have been employed such as packed column of monoethanolamine and metal-organic frameworks. (Lv et al., 2015; Li et al., 2019; Li et al., 2020). The next step is activating CO_2 molecules and converting them to value-added chemicals such as hydrocarbon fuels. (Hu et al., 2013). The activation of CO_2 is extremely complex due to its stability and much efforts have been made by researchers to directly convert it into liquid hydrocarbons, useful for the aviation sector as novel jet fuels (Boreriboon et al., 2018; Vogt et al., 2019; Yao et al., 2020) or into oxygenates, such as ethanol. (Song et al., 2016; Bai et al., 2017; Wang et al., 2018). This conversion, whether it involves a direct CO_2 hydrogenation route or not, entails the usage of metal-based catalysts to ensure an overall reasonable efficiency. (Yao et al., 2020).

In our previous studies, successful activation of CO_2 with a superalkali species, Li_3F_2, were presented. (Park and Meloni, 2017). The computational study showed charge transfer from Li_3F_2 to CO_2, which indicates migration of the unpaired electron from Li_3F_2 to CO_2. The activated CO_2 showed geometric change such as bent $\widehat{OCO}$ angle. The activated CO_2 then can be transformed to other organic molecules with catalysis. (Liu et al., 2016; Luc et al., 2017). Removing the unpaired electron from $[Li_3F_2{\cdot}CO_2]$ cluster weakens the interaction between Li_3F_2 and CO_2 and geometry of CO_2 returns back to the linear form. (Park and Meloni, 2017). The superalkali Li_3F_2 was observed and characterized experimentally. (Yokoyama et al., 2000; Haketa et al., 2002). They also confirmed three stable Li_3F_2 structures through a computational density functional approach. (Haketa et al., 2002). In this investigation, the Li_3F_2-doped fullerene and its endo-reaction with CO_2 has been characterized using the B3LYP/6-31G* level of theory. These results are explained in terms of energetics and molecular orbitals of the species involved. In addition, these findings will be beneficial in providing insights for CO_2 reduction and in helping the exploration of new materials with tailored properties.

Computational Methods

Geometries and total electronic energies of the investigated species were calculated at the B3LYP/6-31G* level of theory (Becke, 1988; Lee et al., 1988) using the computational software Gaussian09. (Frisch et al., 2016). B3LYP is one of the most commonly used density functional theory (DFT) methods that employs a three-parameter exchange functional developed by Becke (1992) and Becke (1993) with a correlational functional proposed by Lee, Yang, and Parr (LYP) Becke (1988) to approximate the exchange-correlation energy. The B3LYP/6-31G* level has been employed to study endofullerene systems because it yields reliable geometries and energies. (Wang et al., 2013; Srivastava et al., 2016; Srivastava et al., 2017). Partial atomic charges are calculated based on the Mulliken population analysis (Mulliken, 1955) and natural bond orbital (NBO) population analysis. (Reed et al., 1985).

The adiabatic ionization energy (AIE) is calculated by taking the zero-point energy corrected electronic energy difference between the optimized neutral and cation, whereas the adiabatic electron affinity (AEA) is obtained by subtracting the zero-point-energy corrected electronic energy of the optimized anion and neutral. All the optimized structures have real vibrational frequencies and their Cartesian coordinates have been reported in the **Supplementary Material**.

RESULTS AND DISCUSSION

The main intent of this computational investigation is to study the interactions relevant to the reduction of CO_2 by the superalkali Li_3F_2 inside our molecular reaction vessel, i.e., C_{60}, and see how this environment affects the CO_2 activation. The system is fairly large and, therefore, computationally challenging to investigate. We have analyzed the possible interactions between the fullerene and the two reactants, CO_2 and Li_3F_2. All the computed energetics are reported in **Table 1** together with the available literature (experimental and computed) values.

Figure 1 reports the optimized geometries for CO_2 and CO_2^-, $Li_3F_2(C_{2v})$, $Li_3F_2(D_{3h})$ and their cations. The structures of CO_2 and CO_2^- reproduce well the literature experimental values for both bond distances and bond angles. In fact, for CO_2 we have $r_{C\text{-}O}$ = 1.17 Å (1.16 Å) (Herzberg, 1966) and for CO_2^- we have $r_{C\text{-}O}$ = 1.25 Å (1.25 Å) (Hartman and Hisatsune, 1966) and ∠OCO° = 134° (127 ± 7°) . (Hartman and Hisatsune, 1966). Both the geometries of the lowest energy $Li_3F_2(C_{2v})$ isomer, trigonal bipyramidal $Li_3F_2(D_{3h})$, and their cations are in agreement with our previous work. (Park and Meloni, 2017; Cochran and Meloni, 2014). **Figure 2** shows the two superalkali isomers reducing the CO_2. The geometry for the previously studied C_{2v} isomer interacting with CO_2 is in agreement with our previous results, (Park and Meloni, 2017), whereas the $D_{3h}{\cdot}CO_2$ species is reported for the first time. When the D_{3h} structure reacts with CO_2, the trigonal bipyramidal geometry is distorted by increasing two "equatorial" Li-Li distances, maintaining only the Li(1)-Li(2) distance of 2.30 Å, with Li(3) being closer to the CO_2, Li(3)-O(7) = Li(3)-O(8) = 2.03 Å and increasing the axial F-F distance from 2.40 to 2.68 Å. The ∠OCO° bond angle is 128° and the C-O bond length is 1.26 Å. The Li_3F_2 isomers have similar binding energy with CO_2, with the C_{2v} isomer

TABLE 1 | Energetics of all the species relevant to this study calculated at the B3LYP/6-31G* level of theory. The zero-point-energy corrected total electronic energy (E_0) is in Hartree, the adiabatic ionization energy (AIE) and adiabatic electron affinity are in eV, and the binding energy at 0 K is in kJ mol^{-1}. [SA·CO_2] stays for the endo superalkali·CO_2 complex.

Species	E_0	AIE	AIE liter	AEA	AEA liter	BE	BE liter
CO_2	−188.569349	13.6	13.78 Herzberg (1966)	−1.27	−0.60 Wang et al. (1988) −1.60 de Vries et al. (1992)	–	–
$Li_3F_2(C_{2v})$	−222.473494	3.91	3.80 Hartman and Hisatsune (1966)	0.63	0.59 Hartman and Hisatsune (1966)	–	–
$Li_3F_2(D_{3h})$	−222.459703	4.24	3.86 Hartman and Hisatsune (1966)	0.36	0.75 Hartman and Hisatsune (1966)	–	–
C_{60}	−2285.799198	7.08	7.54 Sikorska and Gaston (2020)	2.25	2.68 Knapp et al. (1986)	–	–
$Li_3F_2(C_{2v})·CO_2$	−411.112817	5.42	5.21 Park and Meloni, (2017)	0.97	0.36 Park and Meloni (2017)	184	163 Park and Meloni (2017)
$Li_3F_2(D_{3h})·CO_2$	−411.096882	5.25	–	0.80	–	178	–
$C_{60}·CO_2$	−2474.312373	7.08	–	2.27	–	−147[a]	–
$C_{60}·Li_3F_2(D_{3h})$	−2508.304346	5.64	–	2.45	–	119[a]	–
$C_{60}·[SA·CO_2]$	−2696.601627	5.73	–	2.56	–	[a]	–

[a]*This binding energy at 0 K corresponds to the negative solvation energy at 0 K that C_{60} exerts on the encapsulated species, reactants, Li_3F_2 and CO_2, and product SA·CO_2 (see text).*

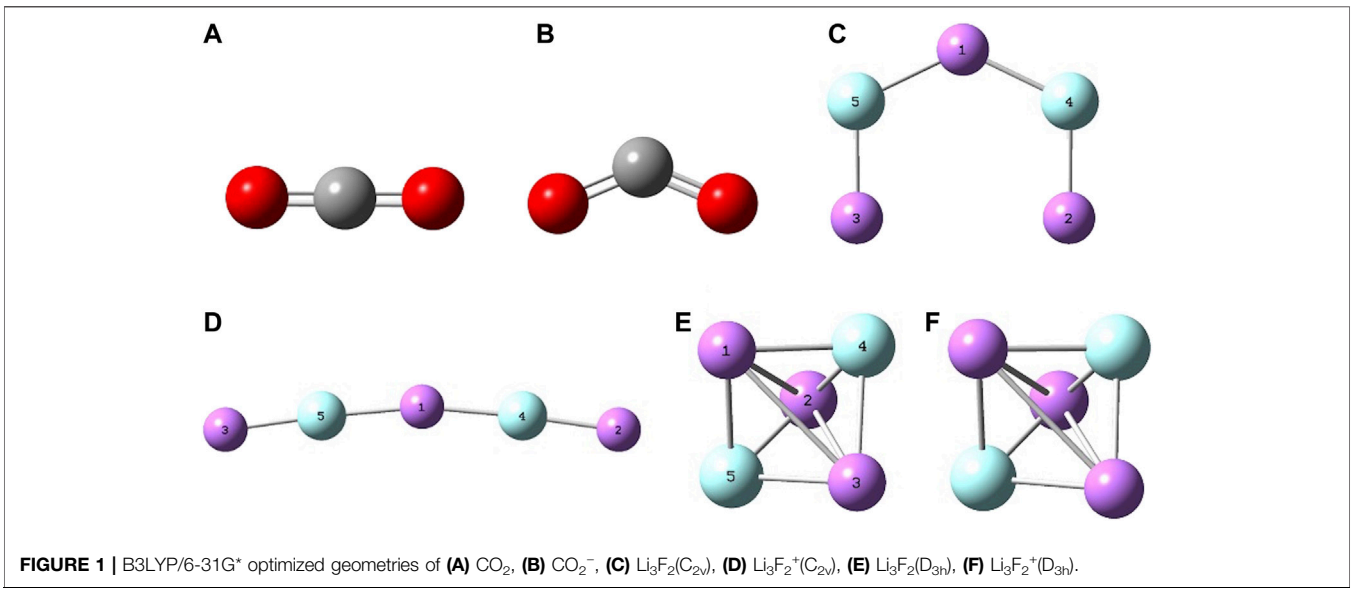

FIGURE 1 | B3LYP/6-31G* optimized geometries of **(A)** CO_2, **(B)** CO_2^-, **(C)** $Li_3F_2(C_{2v})$, **(D)** $Li_3F_2^+(C_{2v})$, **(E)** $Li_3F_2(D_{3h})$, **(F)** $Li_3F_2^+(D_{3h})$.

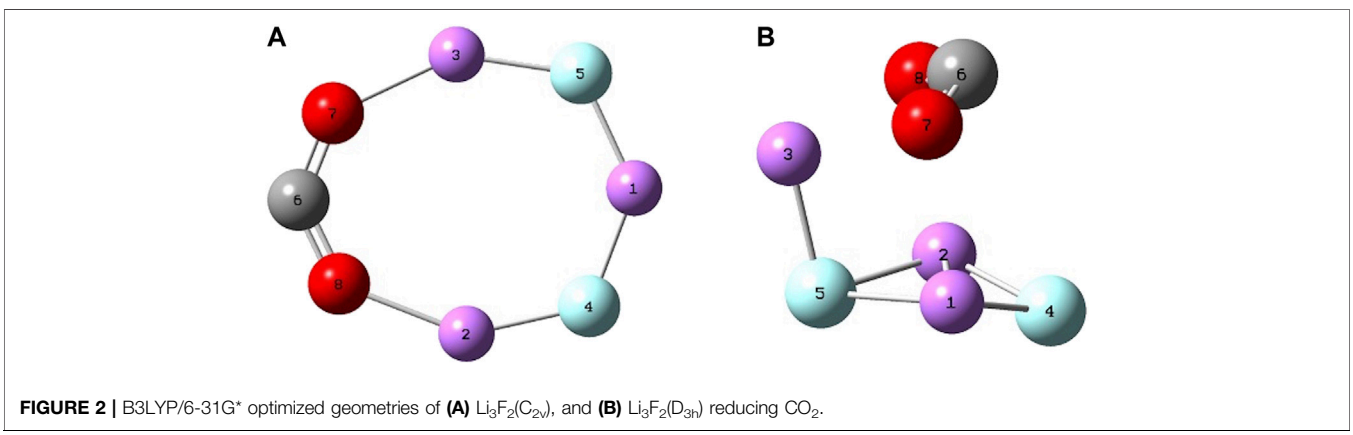

FIGURE 2 | B3LYP/6-31G* optimized geometries of **(A)** $Li_3F_2(C_{2v})$, and **(B)** $Li_3F_2(D_{3h})$ reducing CO_2.

presenting a stronger interaction of 184 kJ mol^{-1}. These clusters can be defined as "free" or "naked" because they are isolated in the gas phase. The presented energy values are calculated at the B3LYP/6-31G* level and are within 10% from the literature reported quantities, whether they are experimental or computed at very high level of theory.

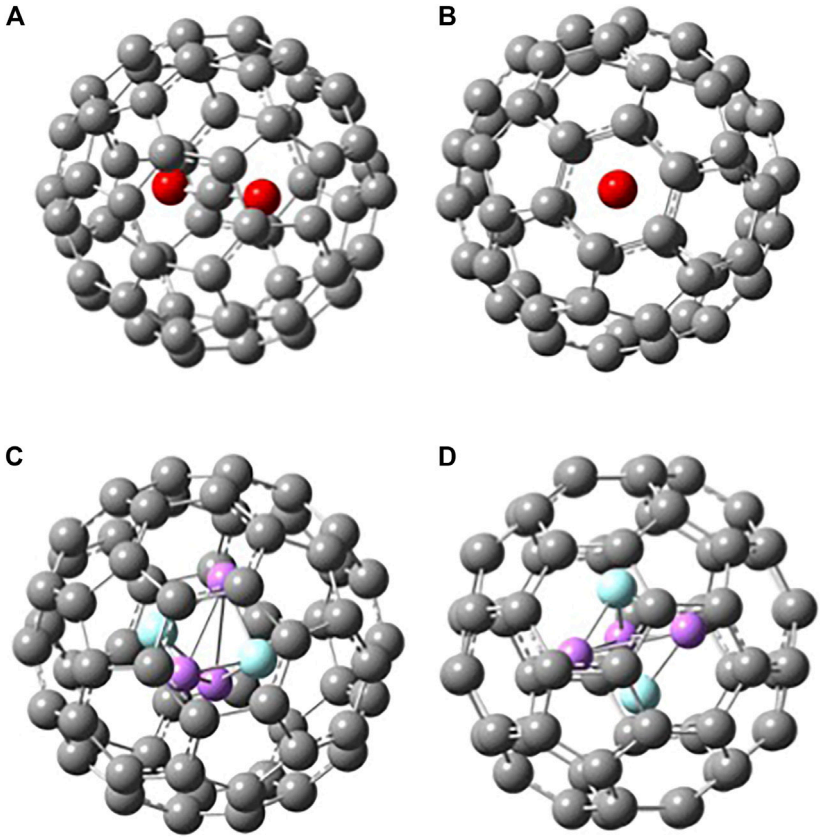

FIGURE 3 | Two different views of B3LYP/6-31G* optimized structures of **(A)**-**(B)** $C_{60} \cdot CO_2$ and **(C)**-**(D)** $C_{60} \cdot Li_3F_2(D_{3h})$.

When a molecule is inserted in the fullerene (yielding an endofullerene), the chemical system is not free, but it will be subjected to the interactions with the carbon cage ("solvation effects"). In **Figure 3**, the two endofullerenes with CO_2 and Li_3F_2 are shown. In the case of carbon dioxide, it is clear from the energetics presented in **Table 1** that CO_2 is destabilized by C_{60} having a negative binding energy at 0 K of −147 kJ mol^{-1} or a solvation energy at 0 K of 147 kJ mol^{-1}, calculated as $E_0(CO_2) + E_0(C_{60})—E_0(C_{60}{\cdot}CO_2)$. The CO_2 occupies the center of the C_{60}, aligned with the C_3 axis passing through a hexagonal face, minimizing its interactions with the C cage. The solvation energy is more properly defined as the Gibbs free energy change associated with the transfer of a molecule from the gas phase into a solvent, i.e., it provides the relative equilibrium populations of a species between gas phase and the solvent. Therefore, we should also know the entropy change connected with this process. The values that we are reporting in this investigation are at 0 K, so that $\Delta_{solv}H_0^o = \Delta_{solv}G_0^o = -\,\mathrm{BE}\,(\mathrm{solvent} - \mathrm{species})$, from which we can see that negative binding energies correspond to positive solvation energies (destabilizing effect). For the encapsulated superalkali two main findings can be noticed. First, the superalkali inside the fullerene is "forced" to assume a D_{3h}

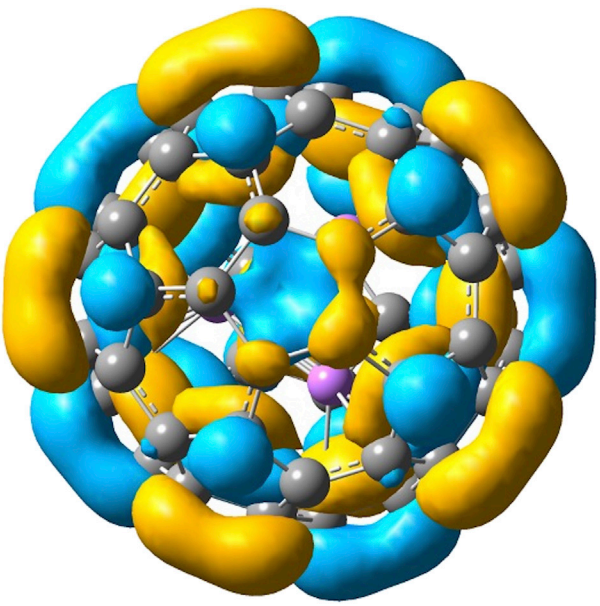

FIGURE 4 | HOMO of $C_{60} \cdot Li_3F_2(D_{3h})$.

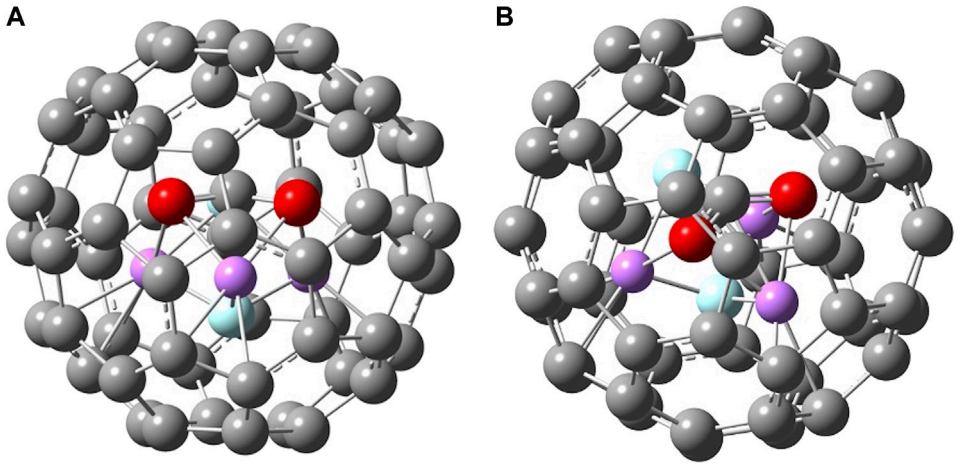

FIGURE 5 | Two different views of B3LYP/6-31G* optimized geometry of $C_{60} \cdot Li_3F_2(D_{3h}) \cdot CO_2$.

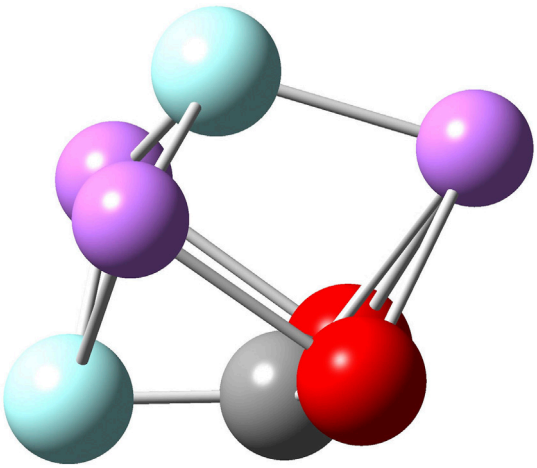

FIGURE 6 | B3LYP/6-31G* optimized geometry of the $Li_3F_2{\cdot}CO_2$ complex inside C_{60}.

geometry, a structure almost identical to the free D_{3h} cluster but less stable than the free C_{2v} cluster. Despite having started the Li_3F_2 geometry optimization from different initial configurations, the optimized structure inside the fullerene resulted in the trigonal bipyramidal geometry. The Li-F distances are shortened in C_{60} from 1.83 (free superalkali) to 1.77 Å, which corresponds to a compression along the F-F distance from 2.40 to 2.21 Å, and the two Li-Li bonds elongate to 2.40 Å. The second result is that C_{60} interacts strongly with Li_3F_2 with a binding energy at 0 K of 119 kJ mol^{-1} or solvation energy at 0 K of −119 kJ mol^{-1}, calculated as $E_0(Li_3F_2(D_{3h})) + E_0(C_{60})—E_0(C_{60}{\cdot}Li_3F_2(D_{3h}))$. This interaction is not a reduction of C_{60}, where the electron from the superalkali is transferred to the fullerene. In fact, upon ionization of $C_{60}{\cdot}Li_3F_2$, the encapsulated Li_3F_2 retains its trigonal bipyramidal structure, just slightly distorted (as described above) due to the interactions with C_{60}. In addition, looking at the Mulliken population and the natural orbital population neither the endo-$Li_3F_2(D_{3h})$ nor the C_{60} show an increase or change of electron charges. The $C_{60}{\cdot}Li_3F_2$ HOMO, the main contribution of which is given by C 2p AO's, is delocalized almost entirely on the fullerene (**Figure 4**). The fact that the $C_{60}{\cdot}Li_3F_2$ AIE is much lower than C_{60} AIE, 5.64 vs. 7.08 eV, respectively, can be explained using a molecular orbital character argument. The interaction of C_{60} with the superalkali makes the HOMO of fullerene less bonding, and consequently, most of the C-C bonds are elongated by 0.1–0.2 Å. Upon ionization, the C-C bonds in $C_{60}{\cdot}Li_3F_2$ are shortened on average by 0.1 Å, which can be interpreted as the removal of an electron from a HOMO with antibonding character.

The insertion of CO_2 within $C_{60}{\cdot}Li_3F_2(D_{3h})$ produces an unexpected result (**Figure 5**). In previous computational studies, (Zhao et al., 2017; Park and Meloni, 2017; Sikorska and Gaston, 2020), naked superalkali have been shown to be capable of reducing carbon dioxide by transferring an electron and yielding an activated bent CO_2^-. In this investigation, we show that our molecular vessel C_{60} forces the reaction to proceed in a different way (**Figure 6**). From an analysis of the optimized geometries inside fullerene, it is clear that CO_2 is activated by showing a ∠OCO° bond angle of 132° and C-O bond lengths of 1.20 Å, 0.03 Å longer than $r_{C\text{-}O}$ in CO_2 but 0.06 Å shorter than $r_{C\text{-}O}$ in the free $Li_3F_2(D_{3h}){\cdot}CO_2$ species. The activation of CO_2 is achieved by a F transfer from Li_3F_2 to CO_2 with the formation of a C-F bond of 1.38 Å, almost identical to the $r_{C\text{-}F}$ of 1.382 Å in CH_3F. (Demaison et al., 1999). This moiety FCO_2 does not resemble either the fluorocarboxyl radical FCO_2 for which $r_{C\text{-}O}$ is 1.234 Å, $r_{C\text{-}F}$ is 1.310 Å, and ∠OCO° bond angle is 118.8°, (Zelinger et al., 2003), or the fluoroformate ion FCO_2^- for which $r_{C\text{-}O}$ is 1.234 Å, $r_{C\text{-}F}$ is 1.46 Å, and ∠OCO° bond angle is 135.9°. (Arnold et al., 1995; Thomas et al., 2018). In addition, both fluorocarboxyl radical and fluoroformate ion are planar, whereas the endo-reaction species (**Figure 6**) resembles a non-planar

(trigonal pyramidal) FCO_2 that interacts with what it looks like a FLi_3 species. All the attempts to optimize this structure outside C_{60} as free endo-$Li_3F_2{\cdot}CO_2$ returned a $Li_3F_2(D_{3h}){\cdot}CO_2$ geometry. Unfortunately, this prevents us from quantifying the interaction of $Li_3F_2(D_{3h})$ with CO_2 inside C_{60}. In fact, the reaction we need is

$$C_{60} \cdot [SA \cdot CO_2] + C_{60} \rightarrow C_{60} \cdot Li_3F_2(D_{3h}) + C_{60} \cdot CO_2 \quad (1)$$

from which the interaction of $Li_3F_2(D_{3h})$ with CO_2 can be derived if we were able to find the $[SA{\cdot}CO_2]$ reaction product as a free species and then its binding energy (or negative solvation energy) with C_{60}, i.e.,

$$C_{60} \cdot [SA \cdot CO_2] \rightarrow C_{60} + [SA \cdot CO_2] \quad (2)$$

In fact, the interaction of $Li_3F_2(D_{3h})$ with CO_2 inside fullerene can be calculated as:

$$\Delta_r H^o(1) - BE(C_{60} \cdot CO_2) - BE(C_{60} \cdot Li_2F_3(D_{3h})) + BE(C_{60} \cdot [SA \cdot CO_2]) \quad (3)$$

In other words, this expression tells us that the interaction between endo-$Li_3F_2(D_{3h})$ and endo-CO_2, i.e., the BE of superalkali-CO_2 in fullerene, is equal to the enthalpy of reaction (1) plus the solvation energies of CO_2 and $Li_3F_2(D_{3h})$ minus the solvation energy of $[SA{\cdot}CO_2]$. Because we cannot derive this last solvation energy absolute value due to the impossibility of optimizing the free endo-$[SA{\cdot}CO_2]$ species, we can estimate this interaction by performing a single-point energy calculation of the free $[SA{\cdot}CO_2]$ optimized inside C_{60}. This structure necessarily represents a higher energy structure than a real minimum and, therefore, the estimated BE of superalkali-CO_2 in fullerene would denote an upper bound providing us some insights on this interaction. From this computation we get an upper bound for $BE(C_{60} \cdot [SA \cdot CO_2])$ of $-965\ kJ\ mol^{-1}$, which tells us that this endo-product is highly destabilized by C_{60}!

CONCLUSION

The activation of CO_2 by the Li_3F_2 superalkali within C_{60} has been investigated at the B3LYP/6-31G* level of theory. C_{60} has been utilized as a reaction vessel and its interaction with the reactants, superalkali and carbon dioxide, have been computed. C_{60} is capable of forcing a superalkali geometry, which does not present the global minimum in the gas phase. Specifically, Li_3F_2 takes the D_{3h} structure. C_{60} has a stabilizing effect on the superalkali but a destabilizing effect on the CO_2, as it can be deduced by the binding energies of these two systems, $BE(C_{60}{\cdot}CO_2) = -147\ kJ\ mol^{-1}$ and $BE(C_{60}{\cdot}Li_3F_2) = 119\ kJ\ mol^{-1}$. Upon interaction of $Li_3F_2(D_{3h})$ with CO_2 inside fullerene, CO_2 is clearly activated showing a $\angle OCO^{\circ}$ bond angle of 132° and C-O bond lengths of 1.20 Å, 0.03 Å longer than $r_{C\text{-}O}$ in CO_2 but 0.06 Å shorter than $r_{C\text{-}O}$ in the free $Li_3F_2(D_{3h}){\cdot}CO_2$ species. The activation of CO_2 is achieved by a F transfer from Li_3F_2 to CO_2 with the formation of a C-F bond of 1.38 Å. Due to the impossibility of optimizing a free superalkali-CO_2 complex, $[SA{\cdot}CO_2]$, resembling the one optimized within the C_{60}, a single-point energy calculation has been performed on the free $[SA{\cdot}CO_2]$. This energy has been utilized to provide an upper bound for the binding energy of $Li_3F_2(D_{3h})$ with CO_2 within C_{60} of $-965\ kJ\ mol^{-1}$, showing that C_{60} destabilizes the reaction product.

DATA AVAILABILITY STATEMENT

The original contribution presented in the study are included in the article/**Supplementary Material**, further inquiries can be directed to the corresponding author.

AUTHOR CONTRIBUTIONS

All authors listed have made a substantial, direct, and intellectual contribution to the work and approved it for publication.

FUNDING

This research was supported by the American Chemical Society Petroleum Research under the fund grant number #56067-UR6.

SUPPLEMENTARY MATERIAL

The Supplementary Material for this article can be found online at: https://www.frontiersin.org/articles/10.3389/fchem.2021.712960/full#supplementary-material

REFERENCES

Arnold, D. W., Bradforth, S. E., Kim, E. H., and Neumark, D. M. (1995). Study of Halogen–Carbon Dioxide Clusters and the Fluoroformyloxyl Radical by Photodetachment of $X^-(CO_2)$ (X=I,Cl,Br) and FCO_2^-. *J. Chem. Phys.* 102 (9), 3493–3509. doi:10.1063/1.468575

Bai, S., Shao, Q., Wang, P., Dai, Q., Wang, X., and Huang, X. (2017). Highly Active and Selective Hydrogenation of CO2 to Ethanol by Ordered Pd–Cu Nanoparticles. *J. Am. Chem. Soc.* 139 (20), 6827–6830. doi:10.1021/jacs.7b03101

Bakry, R., Vallant, R. M., Najam-ul-Haq, M., Rainer, M., Szabo, Z., Huck, C. W., et al. (2007). Medicinal Applications of Fullerenes. *Int. J. Nanomed.* 2 (4), 639–649.

Becke, A. D. (1992). A New Mixing of Hartree-Fock and Local Density-Functional Theories. *J. Chem. Phys.* 98, 1372–1377.

Becke, A. D. (1988). Density-functional Exchange-Energy Approximation with Correct Asymptotic Behavior. *Phys. Rev. A.* 38, 3098–3100. doi:10.1103/physreva.38.3098

Becke, A. D. (1993). Density-functional Thermochemistry. III. The Role of Exact Exchange. *J. Chem. Phys.* 98, 5648–5652. doi:10.1063/1.464913

Boreriboon, N., Jiang, X., Song, C., and Prasassarakich, P. (2018). Higher Hydrocarbons Synthesis from CO_2 Hydrogenation over K- and La-Promoted Fe–Cu/TiO_2 Catalysts. *Top. Catal.* 61 (15), 1551–1562. doi:10.1007/s11244-018-1023-1

Cochran, E., and Meloni, G. (2014). Hypervalence in Monoxides and Dioxides of Superalkali Clusters. *J. Chem. Phys.* 140, 204319. doi:10.1063/1.4879658

Crowley, T. J., and Berner, R. A. (2001). CO2 and Climate Change. *Science* 292870 (5518).

D'Amato, G., and Akdis, C. A. (2020). Global Warming, Climate Change, Air Pollution and Allergies. *Allergy* 75 (9), 2158–2160.

de Vries, J., Steger, H., Kamke, B., Menzel, C., Weisser, B., Kamke, W., et al. (1992). Single-photon Ionization of C_{60}^- and C_{70}^-Fullerene with Synchrotron Radiation: Determination of the Ionization Potential of C_{60}. *Chem. Phys. Lett.* 188 (3), 159–162. doi:10.1016/0009-2614(92)90001-4

Demaison, J., Breidung, J., Thiel, W., and Papousek, D. (1999). The Equilibrium Structure of Methyl Fluoride. *Struct. Chem.* 10 (2), 129–133. doi:10.1023/a:1022085314343

Diederich, F., and Gómez-López, M. (1999). Supramolecular Fullerene Chemistry. *Chem. Soc. Rev.* 28, 263–277. doi:10.1039/a804248i

Elliott, S. J., Bengs, C., Kouril, K., Meier, B., Alom, S., Whitby, R. J., et al. (2018). NMR Lineshapes and Scalar Relaxation of the Water-Endofullerene $H_2{}^{17}O@C_{60}$. *ChemPhysChem* 19, 251–255. doi:10.1002/cphc.201701330

Frisch, M. J., Trucks, G. W., Schlegel, H. B., Scuseria, G. E., Robb, M. A., Cheeseman, J. R., et al. (2016). Gaussian 09., *Revision A.02*. Wallingford, CT.: Gaussian. Inc.

Gutsev, G. L., and Boldyrev, A. I. (1983). An Explanation of the High Electron Affinities of the 5d-Metal Hexafluorides. *Chem. Phys. Lett.* 101, 441–445. doi:10.1016/0009-2614(83)87510-1

Gutsev, G. L., and Boldyrev, A. I. (1982). DVM Xα Calculations on the Electronic Structure of "Superalkali" Cations. *Chem. Phy. Lett.* 92, 262–266. doi:10.1016/0009-2614(82)80272-8

Gutsev, G. L., and Boldyrev, A. I. (1987). The Electronic Structure of Superhalogens and Superalkalies. *Russ. Chem. Rev.* 56, 519–531. doi:10.1070/rc1987v056n06abeh003287

Gutsev, G. L., and Boldyrev, A. I. (1985). The Theoretical Investigation of the Electron Affinity of Chemical Compounds. *Adv. Chem. Phys.* 61, 169–221.

Gutsev, G. L., and Boldyrev, A. I. (1990). Theoretical Estimation of the Maximal Value of the First, Second and Higher Electron Affinity of Chemical Compounds. *J. Phys. Chem.* 94, 2256–2259. doi:10.1021/j100369a012

Haketa, N., Yokoyama, K., Tanaka, H., and Kudo, H. (2002). Theoretical Study on the Geometric and Electronic Structure of the Lithium-Rich $Li_nF_{(n-1)}$ (N=2-5) Clusters. *J. Mol. Struct. THEOCHEM.* 577, 55–67. doi:10.1016/s0166-1280(01)00655-8

Hartman, K. O., and Hisatsune, I. C. (1966). Infrared Spectrum of Carbon Dioxide Anion Radical. *J. Chem. Phys.* 44 (5), 1913–1918. doi:10.1063/1.1726961

Heath, J. R., O'Brien, S. C., Zhang, Q., Liu, Y., Curl, R. F., Tittel, F. K., et al. (1985). Lanthanum Complexes of Speroidal Carbon Shells. *J. Am. Chem. Soc.* 107, 7779–7780. doi:10.1021/ja00311a102

Herzberg, G. (1966). *Electronic Spectra and Electronic Structure of Polyatomic Molecules*. New York: Van Nostrand.

Hönisch, B., Ridgwell, A., Schmidt, D. N., Thomas, E., Gibbs, S. J., Sluijs, A., et al. (2012). The Geological Record of Ocean Acidification. *Science* 335 (6072), 1058–1063. doi:10.1126/science.1208277

Hu, B., Guild, C., and Suib, S. L. (2013). Thermal, Electrochemical, and Photochemical Conversion of CO_2 to Fuels and Value-Added Products. J. Co_2 Util. 1, 18–27. doi:10.1016/j.jcou.2013.03.004

Jana, G., and Chattaraj, P. K. (2020). Effect of Substitution on the Bonding in He Dimer Confined within Dodecahedrane: A Computational Study. *J. Comput. Chem.* 41, 2398–2405. doi:10.1002/jcc.26403

Knapp, M., Echt, O., Kreisle, D., Märk, T. D., and Recknagel, E. (1986). Formation of long-lived CO_2^-, N_2O^-, and their dimer anions, by electron attachment to van der waals clusters. *Chem. Phys. Lett.* 126 (3), 225–231. doi:10.1016/s0009-2614(86)80074-4

Kouřil, K., Meier, B., Alom, S., Whitby, R. J., and Levitt, M. H. (2018). Alignment of ^{17}O-Enriched Water–Endofullerene $H_2O@C_{60}$ in a Liquid crystal Matrix. *Faraday Discuss.* 212, 517–532. doi:10.1039/c8fd00095f

Krachmalnicoff, A., Bounds, R., Mamone, S., Alom, S., Concistrè, M., Meier, B., et al. (2016). The Dipolar Endofullerene $HF@C_{60}$. *Nat. Chem.* 8, 953–957. doi:10.1038/nchem.2563

Kroto, H. W., Heath, J. R., O'Brien, S. C., Curl, R. F., and Smalley, R. E. (1985). C_{60} : Buckminsterfullerene. *Nature* 318, 162–163. doi:10.1038/318162a0

Kuzovkin, V. V., and Semenov, S. M. (2020). Growth Rate of Carbon Dioxide Concentration in the Atmospheric Surface Layer in the Late 20th Century and Early 21st Century. *Russ. Meteorol. Hydrol.* 45 (3), 207–210. doi:10.3103/s1068373920030097

Lee, C., Yang, W., and Parr, R. G. (1988). Development of the Colle-Salvetti Correlation-Energy Formula into a Functional of the Electron Density. *Phys. Rev. B* 37, 785–789. doi:10.1103/physrevb.37.785

Li, K., Feron, P. H. M., Jones, T. W., Jiang, K., Bennett, R. D., and Hollenkamp, A. F. (2020). Energy Harvesting from Amine-Based CO2 Capture: Proof-Of-Concept Based on Mono-Ethanolamine. *Fuel* 263, 116661. doi:10.1016/j.fuel.2019.116661

Li, Z., Wang, L., Li, C., Cui, Y., Li, S., Yang, G., et al. (2019). Absorption of Carbon Dioxide Using Ethanolamine-Based Deep Eutectic Solvents. *ACS Sustain. Chem. Eng.* 7 (12), 10403–10414. doi:10.1021/acssuschemeng.9b00555

Lia, S. G., Bartmess, J. E., Liebman, J. F., Homes, J. L., Levin, R. D., and Mallard, W. G., Gas-Phase Ion and Neutral Thermochemistry. *J. Phys. Chem. Ref. Data*, Suppl, 1. 1988, 17, 1–861.

Liu, X., Song, Y., Geng, W., Li, H., Xiao, L., and Wu, W. (2016). Cu-Mo2C/MCM-41: An Efficient Catalyst for the Selective Synthesis of Methanol from CO_2. *Catalysts* 6 (5). doi:10.3390/catal6050075

Luc, W., Collins, C., Wang, S., Xin, H., He, K., Kang, Y., et al. (2017). Ag–Sn Bimetallic Catalyst with a Core–Shell Structure for CO2 Reduction. *J. Am. Chem. Soc.* 139 (5), 1885–1893. doi:10.1021/jacs.6b10435

Lv, B., Guo, B., Zhou, Z., and Jing, G. (2015). Mechanisms of CO_2 Capture into Monoethanolamine Solution with Different CO_2 Loading during the Absorption/Desorption Processes. *Environ. Sci. Technol.* 49 (17), 10728–10735. doi:10.1021/acs.est.5b02356

Mignolet, B., Johansson, J. O., Campbell, E. E. B., and Remacle, F. (2013). Probing Rapidly-Ionizing Super-atom Molecular Orbitals in C_{60} : A Computational and Femtosecond Photoelectron Spectroscopy Study. *ChemPhysChem* 14, 3332–3340. doi:10.1002/cphc.201300585

Mulliken, R. S. (1955). Electronic Population Analysis on LCAO-MO Molecular Wave Functions. I. *J. Chem. Phys.* 23 (10), 1833–1840. doi:10.1063/1.1740588

Murata, M., Murata, Y., and Komatsu, K. (2006). Synthesis and Properties of Endohedral C_{60} Encapsulating Molecular Hydrogen. *J. Am. Chem. Soc.* 128, 8024–8033. doi:10.1021/ja061857k

Nambiar, S. R., Jana, G., and Chattaraj, P. K. (2021). Can Superalkalis and Superhalogens Improve the Efficacy of. Redox Reactions? *Chem. Phys. Lett.* 762, 138131. doi:10.1016/j.cplett.2020.138131

Park, H., and Meloni, G. (2017). Reduction of Carbon Dioxide with a Superalkali. *Dalton Trans.* 46, 11942–11949. doi:10.1039/c7dt02331f

Reed, A. E., Weinstock, R. B., and Weinhold, F. (1985). Natural Population Analysis. *J. Chem. Phys.* 83, 735–746. doi:10.1063/1.449486

Ruoff, R. S., Tse, D. S., Malhotra, R., and Lorents, D. C. (1993). Solubility of C_{60} in a Variety of Solvents. *J. Phys. Chem.* 97, 3379–3383. doi:10.1021/j100115a049

Sikorska, C., and Gaston, N. (2020). N4Mg6M (M = Li, Na, K) Superalkalis for CO2 Activation. *J. Chem. Phys.* 153 (14), 144301. doi:10.1063/5.0025545

Song, Y., Peng, R., Hensley, D. K., Bonnesen, P. V., Liang, L., Wu, Z., et al. (2016). High-Selectivity Electrochemical Conversion of CO_2 to Ethanol Using a Copper Nanoparticle/N-Doped Graphene Electrode. *ChemistrySelect* 1 (19), 6055–6061. doi:10.1002/slct.201601169

Srivastava, A. K., Kumar, A., and Misra, N. (2017). Superalkali@C_{60}-superhalogen: Structure and Nonlinear Optical Properties of a New Class of Endofullerene Complexes. *Chem. Phys. Lett.* 682, 20–25. doi:10.1016/j.cplett.2017.05.070

Srivastava, A. K., Pandey, S. K., and Misra, N. (2016). Prediction of superalkali@C_{60} Endofullerenes, Their Enhanced Stability and Interesting Properties. *Chem. Phys. Lett.* 655-656, 71–75. doi:10.1016/j.cplett.2016.05.039

Thomas, D. A., Mucha, E., Gewinner, S., Schöllkopf, W., Meijer, G., and von Helden, G. (2018). Vibrational Spectroscopy of Fluoroformate, FCO_2^-, Trapped in Helium Nanodroplets. *J. Phys. Chem. Lett.* 9 (9), 2305–2310. doi:10.1021/acs.jpclett.8b00664

Tong, J., Wu, D., Li, Y., Wang, Y., and Wu, Z. (2013). Superalkali Character of Alkali-Monocyclic (pseudo)Oxocarbon Clusters. *Dalton Trans.* 42, 9982–9989. doi:10.1039/c3dt50224d

Tong, J., Wu, Z., Li, Y., and Wu, D. (2013). Prediction and Characterization of Novel Polynuclear Superalkali Cations. *Dalton Trans.* 42, 577–584. doi:10.1039/c2dt31429k

Vogt, C., Monai, M., Kramer, G. J., and Weckhuysen, B. M. (2019). The Renaissance of the Sabatier Reaction and its Applications on Earth and in Space. *Nat. Catal.* 2 (3), 188–197. doi:10.1038/s41929-019-0244-4

Wang, K., Liu, Z., Wang, X., and Cui, X. (2014). Enhancement of Hydrogen Binding Affinity with Low Ionization Energy Li_2F Coating on C_{60} to Improve Hydrogen Storage Capacity. *Int. J. Hydrog. Energ.* 39, 15639–15645. doi:10.1016/j.ijhydene.2014.07.132

Wang, L.-S., Reutt, J. E., Lee, Y. T., and Shirley, D. A. (1988). High Resolution UV Photoelectron Spectroscopy of CO_2^+, COS^+ and CS_2^+ Using Supersonic

Molecular Beams. *J. Electron. Spectros. Relat. Phenomena* 47, 167–186. doi:10.1016/0368-2048(88)85010-2

Wang, L., Wang, L., Zhang, J., Liu, X., Wang, H., Zhang, W., et al. (2018). Selective Hydrogenation of CO_2 to Ethanol over Cobalt Catalysts. *Angew. Chem. Int. Ed.* 57 (21), 6104–6108. doi:10.1002/anie.201800729

Wang, S.-J., Li, Y., Wang, Y.-F., Wu, D., and Li, Z.-R. (2013). Structures and Nonlinear Optical Properties of the Endohedral Metallofullerene-Superhalogen Compounds Li@C_{60}-BX_4 (X=F, Cl, Br). *Phys. Chem. Chem. Phys.* 15, 12903–12910. doi:10.1039/c3cp51443a

Weiss, F. D., Elkind, J. L., O'Brien, S. C., Curl, R. F., and Smalley, R. E. (1988). Photophysics of Metal Complexes of Spheroidal Carbon Shells. *J. Am. Chem. Soc.* 110, 4464–4465. doi:10.1021/ja00221a085

Yao, B., Xiao, T., Makgae, O. A., Jie, X., Gonzalez-Cortes, S., Guan, S., et al. (2020). Transforming Carbon Dioxide into Jet Fuel Using an Organic Combustion-Synthesized Fe-Mn-K Catalyst. *Nat. Commun.* 11 (1), 6395. doi:10.1038/s41467-020-20214-z

Yokoyama, K., Haketa, N., Tanaka, H., Furukawa, K., and Kudo, H. (2000). Ionization Energies of Hyperlithiated Li_3F Molecule and $Li_nF_{(n-1)}$ (N=3, 4) Clusters. *Chem.Phys. Lett.* 330, 339–346. doi:10.1016/s0009-2614(00)01109-x

Zelinger, Z., Dréan, P., Walters, A., Moreno, J. R. A., Bogey, M., Pernice, H., et al. (2003). Gas-phase Detection of the FCO_2 Radical by Millimeter Wave and High Resolution Infrared Spectroscopy Assisted by Ab Initio Calculations. *J. Chem. Phys.* 118 (3), 1214–1220. doi:10.1063/1.1528607

Zhao, T., Wang, Q., and Jena, P. (2017). Rational Design of Super-alkalis and Their Role in CO_2 Activation. *Nanoscale* 9, 4891–4897. doi:10.1039/c7nr00227k

Conflict of Interest: The authors declare that the research was conducted in the absence of any commercial or financial relationships that could be construed as a potential conflict of interest.

frontiers in Chemistry

ORIGINAL RESEARCH
published: 26 July 2021
doi: 10.3389/fchem.2021.694156

Search for Global Minimum Structures of P^+_{2n+1} (n = 1–15) Using xTB-Based Basin-Hopping Algorithm

Min Zhou[1,2], Yicheng Xu[2], Yongliang Cui[2], Xianyi Zhang[1] and Xianglei Kong[2,3]**

[1]School of Physics and Electronic Information, Anhui Normal University, Wuhu, China, [2]The State Key Laboratory and Institute of Elemento-Organic Chemistry, Collage of Chemistry, Nankai University, Tianjin, China, [3]Collaborative Innovation Center of Chemical Science and Engineering, Nankai University, Tianjin, China

A new program for searching global minimum structures of atomic clusters using basin-hopping algorithm based on the xTB method was developed here. The program can be performed with a much higher speed than its replacement directly based on DFT methods. Considering the structural varieties and complexities in finding their global minimum structures, phosphorus cluster cations were studied by the program. The global minimum structures of cationic P^+_{2n+1} (n = 1–15) clusters are determined through the unbiased structure searching method. In the last step, further DFT optimization was performed for the selected isomers. For P^+_{2n+1} (n = 1–4, 7), the found global minimum structures are in consistent with the ones previously reported; while for P^+_{2n+1} (n = 5, 6, 8–12), newly found isomers are more energy-favorable than those previously reported. And those for P^+_{2n+1} (n = 13–15) are reported here for the first time. Among them, the most stable isomers of P^+_{2n+1} (n = 4–6, 9) are characterized by their C_{3v}, C_s, C_{2v} and C_s symmetry, in turn. But those of P^+_{2n+1} (n = 7, 8, 10–12), no symmetry has been identified. The most stable isomers of P^+_{29} and P^+_{31} are characterized by single P-P bonds bridging units inside the clusters. Further analysis shows that the pnicogen bonds play an important role in the stabilization of these clusters. These results show that the new developed program is effective and robust in searching global minimum structures for atom clusters, and it also provides new insights into the role of pnicogen bonds in phosphorus clusters.

Keywords: global optimization, atomic clusters, basin-hopping algorithm, phosphorus cluster cations, xTB method, pnicogen bond

OPEN ACCESS

Edited by:
Ambrish Kumar Srivastava, Deen Dayal Upadhyay Gorakhpur University, India

Reviewed by:
Ruby Srivastava, Centre for Cellular and Molecular Biology (CCMB), India
Wei-Ming Sun, Fujian Medical University, China

****Correspondence:***
Xianyi Zhang
xyzhang@ahnu.edu.cn
Xianglei Kong
kongxianglei@nankai.edu.cn

Specialty section:
This article was submitted to Physical Chemistry and Chemical Physics, a section of the journal Frontiers in Chemistry

Received: *12 April 2021*
Accepted: *15 July 2021*
Published: *26 July 2021*

Citation:
Zhou M, Xu Y, Cui Y, Zhang X and Kong X (2021) Search for Global Minimum Structures of P^+_{2n+1} (n = 1–15) Using xTB-Based Basin-Hopping Algorithm. Front. Chem. 9:694156. doi: 10.3389/fchem.2021.694156

INTRODUCTION

Clusters bridge atoms, molecules and bulk matter (Johnstom, 2002; Castleman and Jena, 2006; Fehlner et al., 2007; Ha et al., 2019), showing their great potentials for applications in many research fields such as catalysis (Liu and Corma, 2018; Du et al., 2020) and energy storage (VanGelder et al., 2018; VanGelder et al., 2019). They are also characterized by their geometries and electronic structures in many cases (Johnstom, 2002; Fehlner et al., 2007; Ferrando, 2015; Luo et al., 2016; Jena and Sun, 2018; Ha et al., 2019). There are many wonderful examples, including the cage-like fused-ring structure (truncated icosahedron) of C_{60} fullerene (Kroto et al., 1985), the tetrahedral structure of Au_{20} (Li et al., 2003), C_{6v} symmetry boron cluster of B_{36} (Piazza et al., 2014), the borospherene cluster of B_{40} (Zhai et al., 2014; Li et al., 2017), and the protonated serine octamer (Cooks et al., 2001; Kong et al., 2006; Scutelnic et al., 2018). In lots of cases, the structural information of the clusters can

hardly be obtained directly from experiments, and theoretical calculations are very important to provide structural candidates whose predicted properties should be further compared with the experimental results, in order to make the identification stable (Zhang and Glezakou, 2020).

Although the structural determination of small molecules based on density functional theory (DFT) or other methods has become a relatively routine task for computational chemists, the identification of the global minimum structures for clusters, especially those with large sizes, is still a great challenge. The reason is that the complexity of the searching space in their potential energy surface (PES) grows exponentially with the increasing number of atoms inside the clusters. Since the numbers of local minima grow quickly with the size of clusters, the global optimization becomes a very difficult task to overcome. Thus, different search algorithms and methodologies, including the genetic algorithm (GA) (Hartke, 1993; Deaven and Ho, 1995; Hartke, 1995; Daven et al., 1996; Rogan et al., 2013; Kanters and Donald, 2014; Shayeghi et al., 2015; Lazauskas et al., 2017; Rabanal-León et al., 2018; Jäger et al., 2019; Yañez et al., 2019) and relative evolutionary algorithm (EA) (Zhou et al., 2020), the swarm intelligence algorithm (Wang et al., 2012; Jana et al., 2019) and others, have been proposed and applied in the past decades (Zhang and Glezakou, 2020).

It is now accepted that the choosing of a suitable method for a special system based on its properties is very important. Usually, for clusters with tens of atoms, a very detailed investigation on their potential energy surfaces is still too difficult to be performed with reasonable computational cost. The Basin-Hopping (BH) algorithm, has been suggested as a good choice to solve global minima of Lennard–Jones clusters (Wales and Doye, 1997; Wales and Scheraga, 1999). Programs based on the BH algorithm have been developed based on empirical potentials (Zhan et al., 2005; Paz-Borbón et al., 2007) and DFT methods (Yoo et al., 2004.; Bai et al., 2006; Bulusu and Zeng, 2006; Huang et al., 2010; Jiang et al., 2012; Chen et al., 2017; Zhao et al., 2017; Chen et al., 2019). And the self-consistent charge density functional tight binding (SCC-DFTB) methods, including DFTB2, DFTB2-γh, DFTB2-γh + gaus and others, have been also applied (Choi et al., 2013).

Considering the success of the method of GFN-xTB, which was a DFTB3 variant developed by Grimme et al. (2017) (Bannwarth et al., 2019), the current work presents a new BH program named NKCS based on the Python, in conjunction with the xTB method for searching global minima of atomic clusters. Phosphorus clusters are selected to be studied, due to the two facts. The first one is that phosphorus exhibits a variety of structural phases, such as orthorhombic black, rhombohedral, violet, metallic, fibrous red, white, and amorphous. Thus, a better understanding about phosphorus clusters can deepen our knowledge about its structures and properties. The second fact is that although phosphorus cluster ions with wide size distributions have been observed in the laser ablation experiments for a long time (Martin, 1986; Mu et al., 2015; Yang et al., 2016; Kong et al., 2019), its structural studies are still limited for small to medium-sized clusters (Guo et al., 2004; Xue et al., 2010; Mu et al., 2015; Kong et al., 2019). And searching for the global minima in their PES is still a challenging task due to the diverse bonding patterns of the element.

METHODS

The newly developed program NKCS described here is written in Python language. The procedure of the program is shown in **Figure 1**. It couples the xTB-based local optimization and BH global search algorithm. For all initially generated or distorted structures through the BH processes, xTB-based local optimization was applied. Then these structures were ranked according to their energies. In the last step, the selected isomers were further sent to high-level DFT calculations. The procedure of the program is shown in the middle part of the picture. According to the input parameters set by the user, initial structures of the clusters are randomly built for xTB optimization. Then the BH algorithm are employed to some selected isomers and during the process, the criteria to accept newly distorted isomers are judged according to their energies calculated by the xTB method. At last, some local minima are further selected to perform high-level DFT calculations to identify the global minimum.

To improve the efficiency of the program, the randomly generated or distorted geometries should be instantly checked according to their inter-atomic distances. Unreasonable structures with inter-atomic distances much smaller than the sum of their covalent radii are directly discarded. After that, a similarity check algorithm is applied to avoid duplicated structures. In this process, the ultrafast shape recognition (USR) algorithm is applied to compare the similarities of the randomly generated or distorted structures and the ones stored in the database (Ballester and Richards, 2007a; Ballester and Richards, 2007b; Ballester et al., 2009). For the homo atomic clusters studied here, the previously suggested 12 descriptors were applied here. The set of intra-cluster atomic distances from four locations are considered: the molecular centroid (*ctd*), the closest atom to *ctd* (*cst*), the farthest atom from *ctd* (*fct*) and the farthest atom from *fct* (*ftf*). So a molecule can be described as: $\overrightarrow{M} = (\mu_1^{ctd}, \mu_2^{ctd}, \mu_3^{ctd}, \mu_1^{cst}, \mu_2^{cst}, \mu_3^{cst}, \mu_1^{fct}\ \mu_2^{fct}, \mu_3^{fct}, \mu_1^{ftf}, \mu_2^{ftf}, \mu_3^{ftf})$. In this way, each structure can be described by the 12 numbers, and the similarity of two structures i and k can be calculated as:

$$S_{ik} = \frac{1}{\left(1 + \frac{1}{12}\sum_{l=1}^{12}\left(\left|M_l^i - M_l^k\right|\right)\right)}$$

where M_l^i, M_l^k are the lth USR descriptors of the ith and kth structures, respectively. The value of S_{ik} is limited between 0 and 1. A high value of S_{ik} indicates that the two isomers have close geometries, and a threshold can be selected in the program to distinguish two structures.

For the randomly constructed structure sets, the xTB method was applied to perform structural optimization and energy calculation. The parametrization in the method covers all spd-block elements and the lanthanides up to Z = 86 and it has been considered as a suitable method for dealing with various clusters with complex electronic structures (Grimme et al., 2017). The BH algorithm was then applied for the selected isomers based on their energies after the xTB optimization. Considering the BH method is one of the individual-based methods (Zhang and Glezakou, 2020), an initialized population with suitable size is applied here

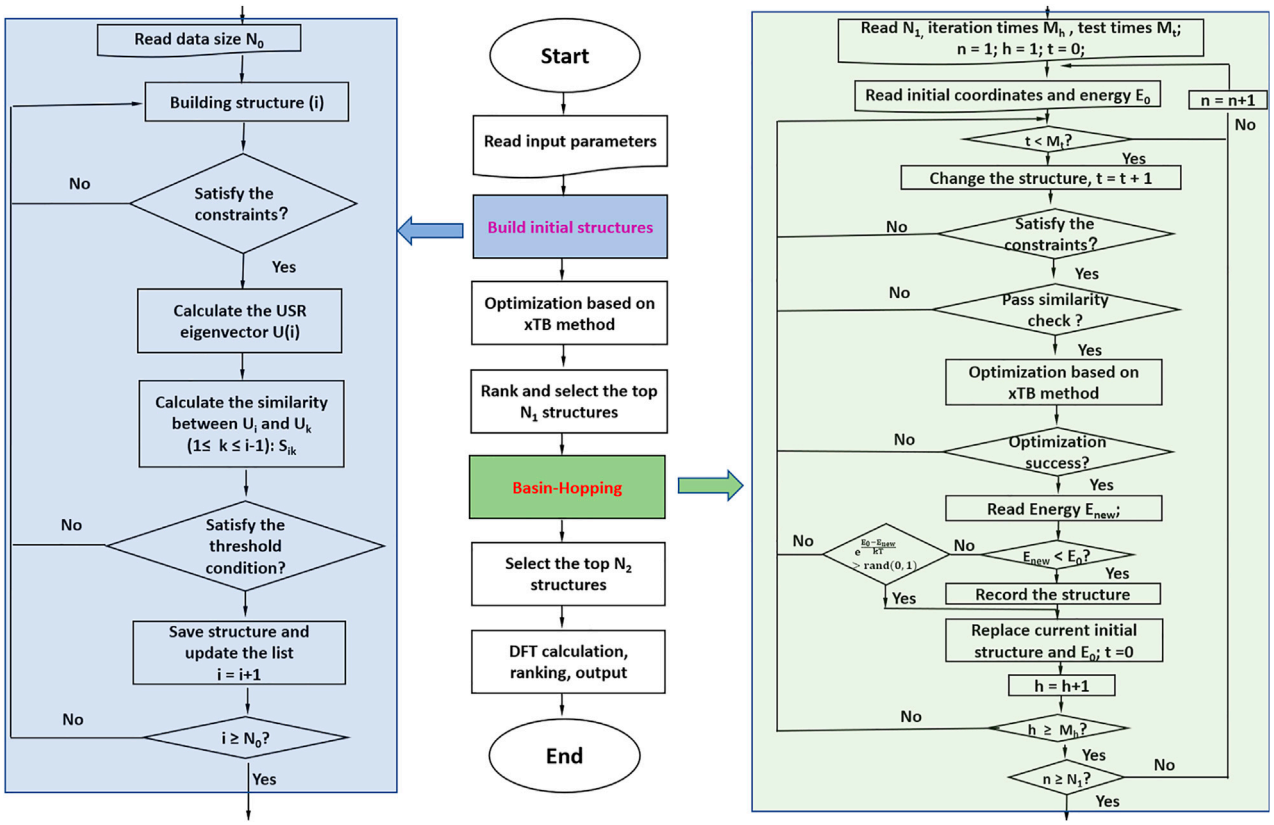

FIGURE 1 | The procedure of the whole program is shown in the middle. The left side shows the process of building initial structures, and the right side shows the detail of the basin-hopping algorithm applied here.

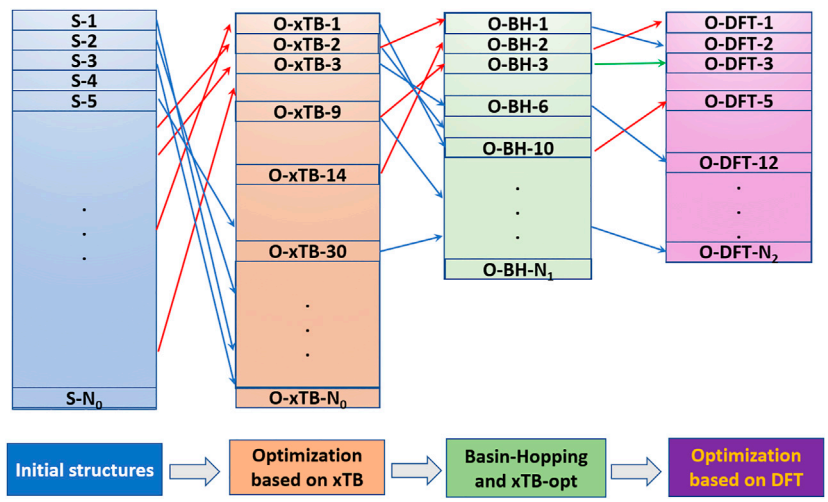

FIGURE 2 | The process for searching the global minimum by the NKCS program.

to improve its performance in the global optimization. After the selection of initial seed structures for BH algorithm based on their energies calculated by the xTB method, distorted structures are generated from the seeds by the displacement. The reasonability and similarity of the new structure should be checked and then optimized by the xTB method. For the acceptance of the newly

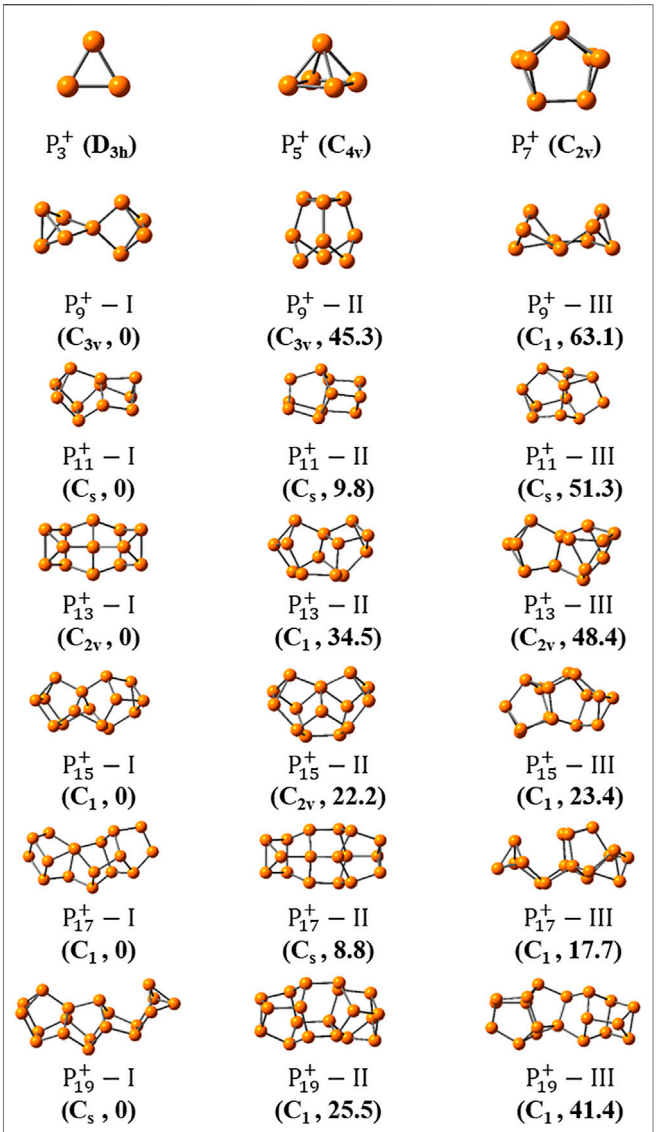

FIGURE 3 | The most stable isomers of P_{2n+1}^+ (n = 1–9) searched by the NKCS program. The three most stable isomers are identified as P_{2n+1}^+ – I, P_{2n+1}^+ – II, and P_{2n+1}^+ – III, in turn. Their symmetries and relative energies (in kJ/mol) to corresponding global minima are shown below.

distorted structure, the previously suggested criteria by Zhou et al. are applied here (Zhou et al., 2019). And the NKCS program also integrates the interface of Gaussian computing software (Frisch et al., 2009) to perform high-level structure optimization and frequency calculation for the selected isomers by the BH algorithm.

RESULTS AND DISCUSSION

The NKCS program has been tested with the odd-numbered phosphorus cluster cations here. In order to make the process clear, an example for searching the global minimum of P_{15}^+ is displayed in **Figure 2**. The initial population size for clusters (N_0) with N atoms is set as ~ $N^{2.8}$ for all the phosphorus clusters studied here. For P_{15}^+, after the reasonability and similarity check, 2000 structures were generated randomly. The distance between two adjacent phosphorus atoms is limited between 2 and 3 Å, and the USR threshold was selected to be 0.98. These 2000 structures were optimized by the xTB method and the top N_1 (30 in this case) structures were selected as seeds for BH processes. During the process, structural check for the new distorted isomers were also performed. If a new structure is more favorable in energy than the seed, it will be recorded and accepted as the new seed. Otherwise, the probability of accepting the structure, $e^{\frac{E_0-E_{new}}{kT}}$, would be compared with a random number located in (0,1) to decide whether it should be taken as a new seed. For all the phosphorus cluster cations here, the temperature T was set at 273 K. After the BH process, the top N_2 (30 in this case) structures were further selected for DFT calculation. These isomers would be optimized and ranked at the level of B3LYP/6–311+G(d) by the Gaussian 09 program.

Figures 3, **4** show the optimized global minimum geometries of P_{2n+1}^+ (n = 1 ~ 15). To make sure that the results obtained are indeed global minima, the program has been run three times for each phosphorus cluster. For all reported cationic phosphorus clusters, frequency calculations are preformed to ensure that they are true minima on the potential energy surfaces. For small

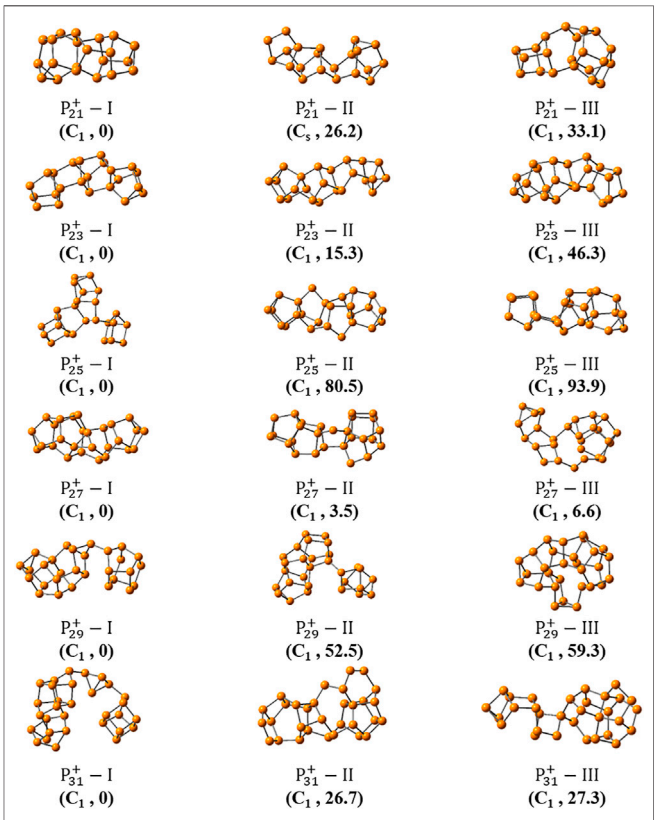

FIGURE 4 | The three most stable isomers of P_{2n+1}^+ (n = 10–15) searched by the NKCS program. Their symmetries and relative energies (in kJ/mol) to corresponding global minima are shown below.

cationic clusters of P_3^+, P_5^+ and P_7^+, the most stable isomers with D_{3h}, C_{4v} and C_{2v} symmetries in turn, have been revealed by Guo et al. (2004), Xue et al. (2010) previously. These structures have also been reproduced here and are shown in **Figure 3**. For P_9^+, the previously suggested lowest-energy geometry with D_{2d} symmetry was reproduced too (Xue et al., 2010). The second stable isomer of P_9^+ – II, has an energy 45.3 kJ/mol higher than that of the former one. It consists of a P_6 unit with a chair-like structure below and a triangle of P_3 unit above, characterized by its C_{3v} symmetry. For P_{11}^+, besides the previously reported structure (P_{11}^+ – II) (Xue et al., 2010), a new isomer of P_{11}^+ – I with a C_s symmetry, was found to be more stable by 9.8 kJ/mol than the former. For clusters with larger sizes, more stable isomers were found. To make them clear, the top eight isomers of P_{2n+1}^+ (n = 6–15) were all shown in **Supplementary Figures S1, S2**. For P_{13}^+, the previously suggested most stable isomer (P_{13}^+ – II) was found to be accompanied with a more stable isomer, P_{13}^+ – I. The latter is characterized by its C_{2v} symmetry and has an energy 34.5 kJ/mol lower than that of P_{13}^+ – II. For P_{15}^+, the found most stable isomer is the same as the one reported by Xue et al. (2020) previously. Another isomer of P_{15}^+ – II with C_{2v} symmetry was also found by the program, which has an energy 22.2 kJ/mol higher than P_{15}^+ – I. Interestingly, this isomer P_{15}^+ – II can be formed by adding two P atoms in the middle of P_{13}^+ – II. For ions of P_{17}^+, the previously reported isomer was found as the 10th most stable isomer (Xue et al., 2010). Nine more stable isomers have been identified and the three most stable isomers of P_{17}^+ – I, II and III are shown in **Figure 3**. The isomer P_{17}^+ – I, which has an energy 59.6 kJ/mol lower than the previously reported one, can be regarded as a P_8 cuneate unit connected with a P_7 norbornane though a P_2 unit, which has no symmetry. For P_{19}^+, 20 new isomers were found to have lower energies than the one previously reported. The top three isomers are shown in **Figure 3**, in which the most stable one has an energy 140.9 kJ/mol lower than the one reported before. And it is also characterized by a plane of symmetry.

As the size increased, the symmetry of the cluster ions decreases. The newly found most stable isomer of P_{21}^+ (P_{21}^+ – I), is more energy favorable than the previously reported one by 84.3 kj/mol. For P_{23}^+, the discovered isomer of P_{23}^+ – I has an energy 15.3 kJ/mol lower than the previously reported isomer of P_{23}^+ – II (Xue et al., 2010). Unlike other cluster ions of P_{2n+1}^+ (n = 7–11), the new isomer of P_{25}^+ – I does not has the chain-like geometry. There is a P_6 trigonal prism unit on the right side, suspended in the middle of the long P_{18} unit on the left by a single bond. This isomer is energetically more preferred by 80.5 kJ/mol than the previously suggested one (P_{25}^+ – II in **Figure 4**).

And the most stable isomers of P_{27}^+, P_{29}^+ and P_{31}^+ were suggested here for the first time. These structures are more complicated and show no symmetry (**Figure 4**). The most stable isomer of P_{27}^+ – I has a typical linear structure that likes that of P_{23}^+ – I or P_{25}^+ – II. The structure of P_{29}^+ – I, can be regarded as that its left and right sides are connected by a single P-P bond. The left side of the cluster ion has a compact unit of P_{16}, and right side has a unit of P_{11} that can be regarded as a six-member ring connected with a five-member ring directly. For the second stable isomer P_{29}^+ – II, the two units of P_{20} and P_9 are also linked by a single bond. Interestingly, the structure of P_{31}^+ – I includes three parts of P_{19}, P_4, and P_9, in which the first and the latter two parts are both connected though P-P bonds, respectively. And the whole ion has a curved linear structure. In order to make the results more reliable, calculation based on the level of MP2/6–311+G(d)// B3LYP/6–311+G(d) were performed for the top three isomers of P_{2n+1}^+ (n = 12–15). Although the values of their relative energies are some different, their orders in energies keep unchanged (**Supplementary Table S1** in the supporting information).

Briefly, the BH algorithm based on the xTB method has been developed for searching global minima of clusters. Considering the parametrization of xTB method covers all spd-block elements and the functional form of the xTB mostly avoids element-pair-specific parameters, the program developed here has a very wide range of applications. And compared with DFT-based methods, it significantly saves computing time. Medium-sized phosphorus cluster cations were studied here, and new energetically favored structures were identified. Based on these results, some structural rules of these cationic clusters should be further discussed, since it might be helpful to get some general pictures about these energetically preferred structures and structural tendency about large-sized clusters.

For one thing, it is interesting to find that symmetric structures are very important for small-sized clusters of P_{2n+1}^+ (n = 1–6). For P_{19}^+, the most stable isomer also has a C_s symmetry. For P_{15}^+, P_{17}^+, and P_{21}^+, although none of their most stable isomers have symmetry, their second most stable isomers have C_{2v}, C_s, and C_s symmetry, in turn. For clusters with larger size of P_{2n+1}^+ (n = 11–15), all their top three stable isomers show no symmetry. Although this, the symmetry of local unit in the large-size clusters still exists. For example, both units in P_{29}^+ – I linked by a single bond have rough C_s symmetry. These results also suggest the importance of an unbiased method in searching the global minima of large-sized clusters, which can cannot be directly replaced by simple intuitions.

For the second point, most medium-sized globe minima of P_{2n+1}^+ (n = 5–15) exhibit chain-like configurations, expect that of P_{25}^+. And the common building units include P_7, P_8, and P_9 building blocks. For clusters with larger sizes, the chains become curved. A statistical view on the size of the energetically preferred structures may provide some clues. The USR parameter *ftf* that indicates the distance between the farthest atom from *fct* can be applied as an indicator of the length of the cluster. Based on the xTB calculation results of the initial population built up in the second step of **Figure 2**, a general picture descripting the relationship between energy and length can be obtained. **Figure 5** shows the relative energy-*fct* diagrams for the xTB-optimized structures of the randomly generated populations of P_9^+, P_{19}^+, and P_{31}^+. It can be found that the most of energetically preferred structures for P_9^+ have a distribution of *fct* in the range of 4–6 Å. For P_{19}^+ and P_{31}^+, the lengths of energetically preferred structures were concentrated in the range of 7–10 and 8–12 Å, respectively. The results indicate that the lengths of the clusters grow with their sizes, but not linearly, and the curved structures will be more general for large-size clusters.

For the third point, it is interesting to found that both isomers of P_{29}^+ – I and P_{31}^+ – I are characterized by single P-P bonds

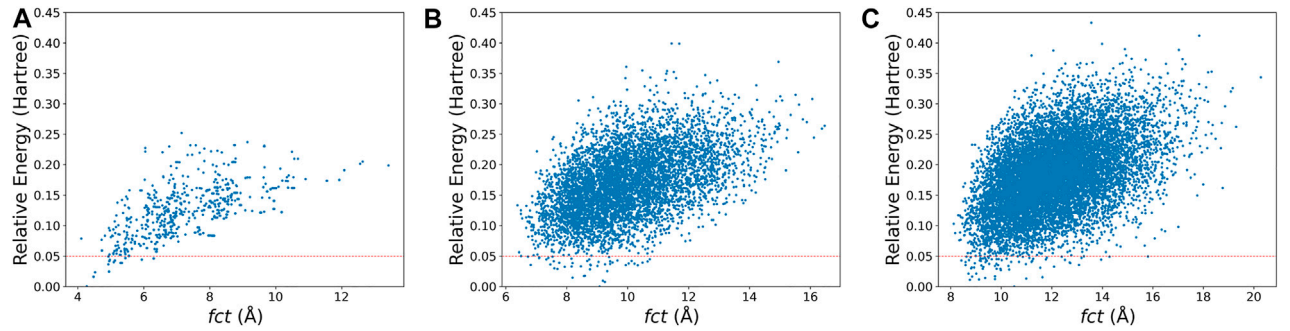

FIGURE 5 | The relative energy-*fct* diagrams for the xTB-optimized structures of the randomly generated populations of **(A)** P_9^+, **(B)** P_{19}^+ and **(C)** P_{31}^+. Every dot in the picture corresponds one structure and the dots below the red line indicates the isomers have relative energies less than 0.05 hartree compared to the corresponding global minimum in each subgraph.

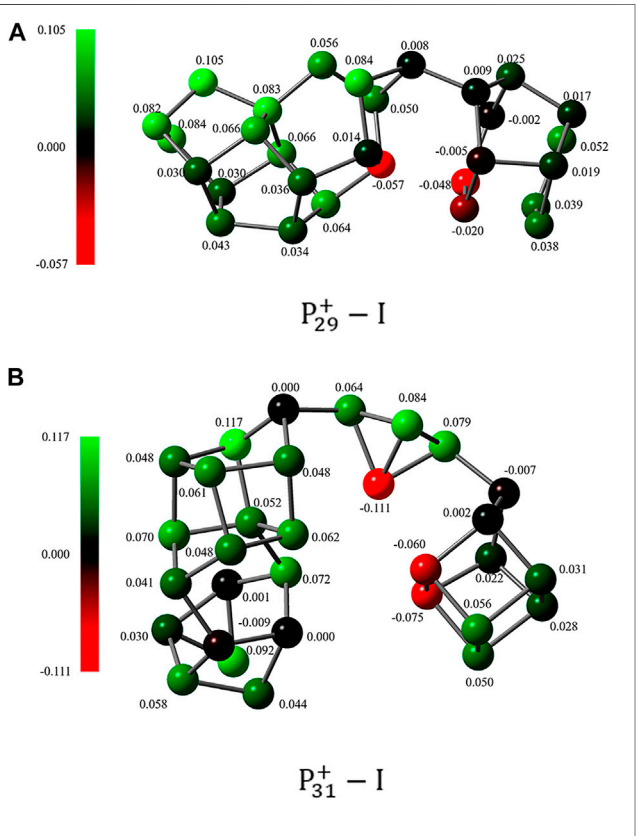

FIGURE 6 | The NBO charge distribution of **(A)** $P_{29}^+ - I$ and **(B)** $P_{31}^+ - I$.

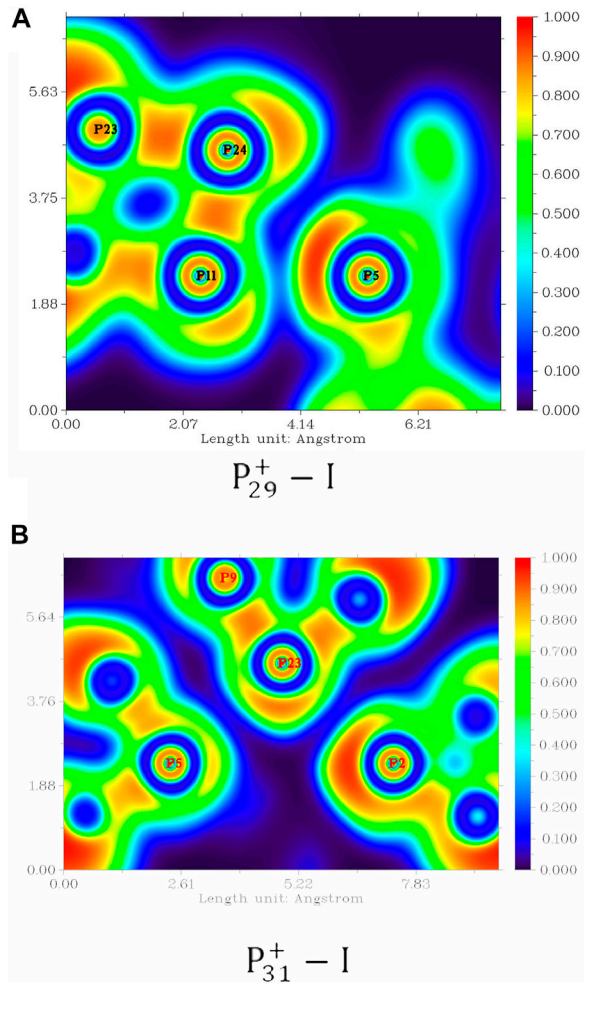

FIGURE 7 | ELFs of **(A)** $P_{29}^+ - I$ and **(B)** $P_{31}^+ - I$.

bridging units inside the clusters. Although this kind of bridging bonds is reasonable in forming one- or two-dimensional phosphorus nanomaterials, it is lesser-known for middle- or large-size homoatomic clusters. For homoatomic clusters, it is usually to suggest that the clusters are inclined to take compact structures with high symmetry or consistent linear structures. So why these clusters are so different? A possible explanation is that the weak polarities of these intra-cluster covalent bonds are distributed in a way to stabilize the whole cluster by enhancing their charge-charge, charge-dipole, or dipole-dipole interactions. However, the natural bond orbital (NBO) charge distribution (Carpenter and Weinhold, 1988; Reed et al., 1988) of these clusters shows although this interaction may help to

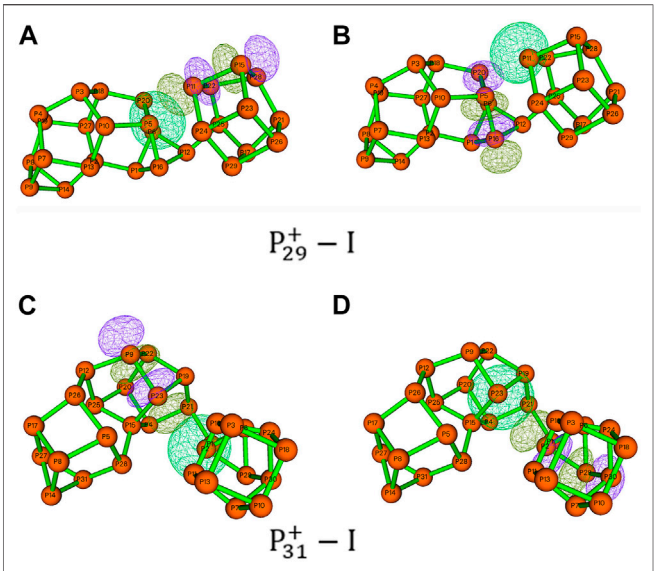

FIGURE 8 | Hyperconjugation of LP(P) → σ*(P–P). The natural bonding orbits were obtained by NBO analysis of **(A,B)** P_{29}^{+} – I and **(C,D)** P_{31}^{+} – I.

stabilize the isomer in some extent, it should not be the main reason (**Figure 6**).

On the other hand, the short distances between the nonbonding phosphorus atoms indicate that the pnicogen bonds (Zahn, et al., 2011; Scheiner, 2013) inside the clusters may play a very important role. In P_{29}^{+} – I, the distances of P5···P11 is 294 pm, which is below the sum of their van der Waals radii of 380 pm. Similarly, the distances of P2···P23 in P_{31}^{+} – I is 333 pm. These attractive P···P interactions are very similar to those previously reported pnicogen bonds in carbaboranes. Chemical bonding analyses were also examined by electron localization function (ELF) analysis with the program of Multiwfn (Lu and Chen, 2012). As shown in **Figure 7**, regions between P11 and P5 in P_{29}^{+} – I, and between P2 and P23 in P_{31}^{+} – I, are both characterized by their electron-pair densities. The pnicogen interaction can be further investigated by the second-order perturbation approach. As the example of P_{29}^{+} – I shown in **Figure 8A and B**, the interactions of LP(P5) →σ*(P11-P15) and LP(P11) →σ*(P5-P16) in P_{29}^{+} – I have the stabilization energies of 9.34 and 3.70 kcal/mol, respectively, showing a very strong pnicogen bond. The second example of P_{31}^{+} – I is shown in **Figure 8C and D**. The hyperconjugation of the lone pair of electrons at P2 with the adjacent phosphorus–phosphorus bond P23-P9 (LP(P2) →σ*(P23-P9)) was observed with a second-order perturbation stabilization energy of 2.66 kcal/mol. At the same time, the interaction of LP(P23) →σ*(P2-P29) also contributes 0.87 kcal/mol in stabilization the pnicogen bond.

Both Wiberg bond index (WBI) and QTAIM topological analysis were employed to analyze the bonding nature of these bonds. The calculated total WBI values of the bonds P5···P11 in P_{29}^{+} – I, P2···P23 in P_{31}^{+} – I are 0.14 and 0.04, respectively, supporting the existence of the pnicogen bonds. **Table 1**; **Supplementary Table S2**, show the results of AIM topology parameters, including electron density (ρ_e) at the pnicogen bond critical points and Laplacian ($\nabla^2\rho_e$). The results suggest that intracluster pnicogen bonds play a very important role for their structural stabilization and isomerization. It is also found that the pnicogen bond is important for other curved clusters with small sizes (shown in **Figure 4**). For example, the structure of P_{27}^{+} – I is characterized by a strong pnicogen bond with a P1 . . . P4 distance of 297 pm (with a WBI of 0.26). The NBO and QTAIM analysis also support the interaction (**Supplementary Figures S3, S4**; **Table 1** and **Supplementary Table S2**).

Although pnicogen bonds have been previously reported and studied for different species by many research groups, this is still the first study showing that the pnicogen bonds can exist and play important roles in homoatomic phosphorus clusters without the help of other ligands or heteroatoms. By comparing the pnicogen bonds reported herein with other previously reported pnicogen bonds, the important roles of these interactions in phosphorus clusters can be further reflected. Thus, some typical pnicogen bonds were selected from relative references (Zahn, et al., 2011; Del Bene et al., 2017; Esrafili and Sadr-Mousavi, 2017; Esrafili and Mousavian, 2018; Mokrai, and Benko, 2019; Wu, et al., 2019) and were compared with those bonds reported here. Results were shown in **Table 1**. The P . . . P pnicogen bonds reported here have similar bond distances and WBIs with those previously reported (Zahn, et al., 2011) and similar to other type pnicogen bonds including PN, P . . . Bi and P . . . Cl interactions. And the bond of P1 . . . P4 in P_{27}^{+} – I even has the highest WBI except to the special case of P . . . Cl in the ternary complex of FCl . . . PH_3 . . . NCH, in which the P . . . N pnicogen-bond was enhanced by the P . . . Cl halogen bond through the σ-hole (Del Bene, et al., 2017).

Briefly, these results reflected that the intracluster pnicogen bonds can greatly stabilize the cluster, thus play important roles in large-size phosphorus clusters and phosphorus-related materials. On the other hand, the ELF analysis shown in **Figure 7** also indicates the possibility of the existence of multiple pnicogen bonds in large-size phosphorus clusters. And a very interesting topic is how the introduce of heteroatom can affect the pnicogen bonds and their most stable structures. So, we hope the result reported here can attract more researchers to focus on this issue.

CONCLUSION

A combined algorithm of BH and xTB to locate global minima in potential energy surface of atomic clusters has been developed here. Several strategies, including the similarity check, are considered in the algorithm. The P_{2n+1}^{+} cluster cations are selected to be studied using the program due to their structural varieties and complexities. For cluster cations of P_{2n+1}^{+} (n = 1–4) and P_{15}^{+}, the program reproduced the lowest-energy structures reported previously. For P_{2n+1}^{+} (n = 5, 6, 8–12), new isomers with energies 10 ~ 80 kJ/mol lower than those previously reported have been identified on the level of B3LYP/6–311+G(d). The most stable isomers of P_{2n+1}^{+} (n =

TABLE 1 | Electron densities (ρ_e, a.u.), Laplacian of the electron densities ($\nabla^2\rho_e$, a.u.), Pnicogen bond distances (Å), and Wiberg Bond Indexes (WBI) of the pnicogen bonds in P_{27}^+ – I, P_{29}^+ – I and P_{31}^+ – I, compared with those of some pnicogen bonds previously reported.[a]

Bonds	ρ_e	$\nabla^2\rho_e$	Pnicogen bond distances (Å)	WBI	Ref
P1 … P4 (P_{27}^+ – I)	0.0258	0.0415	2.97	0.26	This study
P5 … P11 (P_{29}^+ – I)	0.0280	0.0419	2.94	0.14	This study
P2 … P23 (P_{31}^+ – I)	0.0137	0.0282	3.33	0.04	This study
P … P (PH_2Cl···PCl_3)	–	–	3.40	0.04	Zahn et al. (2011)
P … P (PH_2Cl···PH_2F)	–	–	2.99	0.12	Zahn et al. (2011)
P … N (FH_2P···NCCl)	0.0170	0.0590	2.80	0.04	Esrafili and Mousavian (2018)
P … N (ClH_2P···NCH)	0.0126	0.0513	2.89	–	Esrafili and Sadr-Mousavi (2017)
P … N (ClH_2P···NCH···C_2H_2)	0.0133	0.0468	2.87	–	Esrafili and Sadr-Mousavi (2017)
P … Bi (structure **2a**)	0.0131	0.0267	3.58(T), 3.37 (E)[b]	0.09	Mokrai and Benko (2019)
P … Cl (PH_3-BrCl)	0.0051	0.0176	3.68	–	Wu et al. (2019)
P … Cl (PH_2F-BrCl)	0.0091	0.0316	3.26	–	Wu et al. (2019)
P … Cl (FCl···PH_3···NCH)	–	–	2.22	0.78	Del Bene et al. (2017)

[a]*The AIM topology analysis of pnicogen bonds reported here is performed using Multiwfn program (Lu and Chen, 2012), while other results were taken from references directly.*
[b]*T and E indicate theoretical and experimental values, respectively.*

13–5) are also reported here. Although symmetric structures dominate the most stable isomers of all small-sized clusters of P_{2n+1}^+ (n = 1–6), their importance decrease for the clusters of P_{2n+1}^+ (n = 7–10). And for clusters with larger sizes, no symmetry has been observed for all their top three isomers. The lengths of the clusters grow with their sizes, but only distinct for clusters up to P_{23}^+. Curved structures with single P-P bonds are found to be important for P_{29}^+ and P_{31}^+. Further analysis shows that the pnicogen bonds play important roles in these phosphorus clusters. The results show that the new developed xTB-based BH program is effective and robust in searching global minimum structures for atomic clusters. And for large-size phosphorus clusters, a systemic study for a better understanding about the pnicogen bonds is needed very much.

DATA AVAILABILITY STATEMENT

The raw data supporting the conclusions of this article will be made available by the authors, without undue reservation.

AUTHOR CONTRIBUTIONS

MZ and YX designed the program and performed the calculations. YC participated in the calculation. XZ and XK directed the work, contributed to the interpretation of the data and wrote the paper. All authors have read and approved the content of the manuscript.

FUNDING

This work was supported by the National Natural Science Foundation of China (21627810, 11704004).

SUPPLEMENTARY MATERIAL

The Supplementary Material for this article can be found online at: https://www.frontiersin.org/articles/10.3389/fchem.2021.694156/full#supplementary-material

REFERENCES

Bai, J., Cui, L.-F., Wang, J., Yoo, S., Li, X., Jellinek, J., et al. (2006). Structural Evolution of Anionic Silicon Clusters SiN(20 ≤N≤ 45). *J. Phys. Chem. A.* 110, 908–912. doi:10.1021/jp055874s

Ballester, P. J., Finn, P. W., and Richards, W. G. (2009). Ultrafast Shape Recognition: Evaluating a New Ligand-Based Virtual Screening Technology. *J. Mol. Graphics Model.* 27, 836–845. doi:10.1016/j.jmgm.2009.01.001

Ballester, P. J., and Richards, W. G. (2007a). Ultrafast Shape Recognition for Similarity Search in Molecular Databases. *Proc. R. Soc. A.* 463, 1307–1321. doi:10.1098/rspa.2007.1823

Ballester, P. J., and Richards, W. G. (2007b). Ultrafast Shape Recognition to Search Compound Databases for Similar Molecular Shapes. *J. Comput. Chem.* 28, 1711–1723. doi:10.1002/jcc.20681

Bannwarth, C., Ehlert, S., and Grimme, S. (2019). GFN2-xTB-An Accurate and Broadly Parametrized Self-Consistent Tight-Binding Quantum Chemical Method with Multipole Electrostatics and Density-dependent Dispersion Contributions. *J. Chem. Theor. Comput.* 15, 1652–1671. doi:10.1021/acs.jctc.8b01176

Bulusu, S., and Zeng, X. C. (2006). Structures and Relative Stability of Neutral Gold Clusters: Aun (N=15-19). *J. Chem. Phys.* 125 (125), 154303. doi:10.1063/1.2352755

Carpenter, J. E., and Weinhold, F. (1988). Analysis of the Geometry of the Hydroxymethyl Radical by the "Different Hybrids for Different Spins" Natural Bond Orbital Procedure. *J. Mol. Struct. THEOCHEM* 169, 41–62. doi:10.1016/0166-1280(88)80248-3

Castleman, A. W., and Jena, P. (2006). Clusters: a Bridge between Disciplines. *Proc. Natl. Acad. Sci.* 103, 10552–10553. doi:10.1073/pnas.0601783103

Chen, X., Zhao, Y.-F., Wang, L.-S., and Li, J. (2017). Recent Progresses of Global Minimum Searches of Nanoclusters with a Constrained Basin-Hopping Algorithm in the TGMin Program. *Comput. Theor. Chem.* 1107, 57–65. doi:10.1016/j.comptc.2016.12.028

Chen, X., Zhao, Y. F., Zhang, Y. Y., and Li, J. (2019). TGMin: An Efficient Global Minimum Searching Program for Free and Surface-supported Clusters. *J. Comput. Chem.* 40, 1105–1112. doi:10.1002/jcc.25649

Choi, T. H., Liang, R., Maupin, C. M., and Voth, G. A. (2013). Application of the SCC-DFTB Method to Hydroxide Water Clusters and Aqueous Hydroxide Solutions. *J. Phys. Chem. B* 117, 5165–5179. doi:10.1021/jp400953a

Cooks, R. G., Zhang, D., Koch, K. J., Gozzo, F. C., and Eberlin, M. N. (2001). Chiroselective Self-Directed Octamerization of Serine: Implications for Homochirogenesis. *Anal. Chem.* 73, 3646–3655. doi:10.1021/ac010284l

Daven, D. M., Tit, N., Morris, J. R., and Ho, K. M. (1996). Structural Optimization of Lennard-Jones Clusters by a Genetic Algorithm. *Chem. Phys. Lett.* 256, 195–200. doi:10.1016/0009-2614(96)00406-X

Deaven, D. M., and Ho, K. M. (1995). Molecular Geometry Optimization with a Genetic Algorithm. *Phys. Rev. Lett.* 75, 288–291. doi:10.1103/PhysRevLett.75.288

Del Bene, J. E., Alkorta, I., Elguero, J., and Sánchez-Sanz, G. (2017). Lone-Pair Hole on P: P···N Pnicogen Bonds Assisted by Halogen Bonds. *J. Phys. Chem. A.* 121 (6), 1362–1370. doi:10.1021/acs.jpca.6b12553

Du, Y., Sheng, H., Astruc, D., and Zhu, M. (2020). Atomically Precise Noble Metal Nanoclusters as Efficient Catalysts: A Bridge between Structure and Properties. *Chem. Rev.* 120, 526–622. doi:10.1021/acs.chemrev.8b00726

Esrafili, M. D., and Mousavian, P. (2018). The Strengthening Effect of a Halogen, Chalcogen or Pnicogen Bonding on Halogen-π Interaction: a Comparative Ab Initio Study. *Mol. Phys.* 116, 526–535. doi:10.1080/00268976.2017.1406166

Esrafili, M. D., and Sadr-Mousavi, A. (2017). Modulating of the Pnicogen-Bonding by a H···π Interaction: An Ab Initio Study. *J. Mol. Graphics Model.* 75, 165–173. doi:10.1016/j.jmgm.2017.04.017

Fehlner, T., Halet, J. F., and Saillard, J. Y. (2007). *Molecular Clusters: A Bridge to Solid-State Chemistry*. Cambridge: Cambridge University Press.

Ferrando, R. (2015). Symmetry Breaking and Morphological Instabilities in Core-Shell Metallic Nanoparticles. *J. Phys. Condens. Matter* 27, 013003. doi:10.1088/0953-8984/27/1/013003

Frisch, M. J., Trucks, G. W., Schlegel, H. B., Scuseria, G. E., Robb, M. A., Cheeseman, J. R., et al. (2009). "Gaussian 09," in *Revision D.01* (Wallingford, CT: Gaussian, Inc).

Grimme, S., Bannwarth, C., and Shushkov, P. (2017). A Robust and Accurate Tight-Binding Quantum Chemical Method for Structures, Vibrational Frequencies, and Noncovalent Interactions of Large Molecular Systems Parametrized for All Spd-Block Elements (Z = 1-86). *J. Chem. Theor. Comput.* 13, 1989–2009. doi:10.1021/acs.jctc.7b00118

Guo, L., Wu, H., and Jin, Z. (2004). First Principles Study of the Evolution of the Properties of Neutral and Charged Phosphorus Clusters. *J. Mol. Struct. THEOCHEM* 677, 59–66. doi:10.1016/j.theochem.2004.02.014

Ha, M., Kim, J.-H., You, M., Li, Q., Fan, C., and Nam, J.-M. (2019). Multicomponent Plasmonic Nanoparticles: From Heterostructured Nanoparticles to Colloidal Composite Nanostructures. *Chem. Rev.* 119, 12208–12278. doi:10.1021/acs.chemrev.9b00234

Hartke, B. (1995). Global Geometry Optimization of Clusters Using a Growth Strategy Optimized by a Genetic Algorithm. *Chem. Phys. Lett.* 240, 560–565. doi:10.1016/0009-2614(95)00587-T

Hartke, B. (1993). Global Geometry Optimization of Clusters Using Genetic Algorithms. *J. Phys. Chem.* 97, 9973–9976. doi:10.1021/j100141a013

Huang, W., Sergeeva, A. P., Zhai, H.-J., Averkiev, B. B., Wang, L.-S., and Boldyrev, A. I. (2010). A Concentric Planar Doubly π-aromatic B19− Cluster. *Nat. Chem* 2, 202–206. doi:10.1038/nchem.534

Jäger, M., Schäfer, R., and Johnston, R. L. (2019). GIGA: a Versatile Genetic Algorithm for Free and Supported Clusters and Nanoparticles in the Presence of Ligands. *Nanoscale* 11, 9042–9052. doi:10.1039/C9NR02031D

Jana, G., Mitra, A., Pan, S., Sural, S., and Chattaraj, P. K. (2019). Modified Particle Swarm Optimization Algorithms for the Generation of Stable Structures of Carbon Clusters, Cn (N = 3-6, 10). *Front. Chem.* 7, 65–77. doi:10.3389/fchem.2019.00485

Jena, P., and Sun, Q. (2018). Super Atomic Clusters: Design Rules and Potential for Building Blocks of Materials. *Chem. Rev.* 118, 5755–5870. doi:10.1021/acs.chemrev.7b00524

Jiang, M., Zeng, Q., Zhang, T., Yang, M., and Jackson, K. A. (2012). Icosahedral to Double-Icosahedral Shape Transition of Copper Clusters. *J. Chem. Phys.* 136, 104501. doi:10.1063/1.3689442

Johnstom, R. L. (2002). *Atomic and Molecular Clusters*. London: CRC Press.

Kanters, R. P. F., and Donald, K. J. (2014). Cluster: Searching for Unique Low Energy Minima of Structures Using a Novel Implementation of a Genetic Algorithm. *J. Chem. Theor. Comput.* 10, 5729–5737. doi:10.1021/ct500744k

Kong, X., Mu, L., Zhou, M., and Yang, S. (2019). "Phosphorus Clusters and Quantum Dots," in *Fundamentals and Applications of Phosphorous Nanomaterial*. Editor H.-F. Ji (New York: ACS Symposium Series volume ACS Books), 79–102. doi:10.1021/bk-2019-1333.ch005

Kong, X., Tsai, I.-A., Sabu, S., Han, C.-C., Lee, Y. T., Chang, H.-C., et al. (2006). Progressive Stabilization of Zwitterionic Structures in [H(Ser)2-8]+ Studied by Infrared Photodissociation Spectroscopy. *Angew. Chem. Int. Ed.* 45, 4130–4134. doi:10.1002/anie.200600597

Kroto, H. W., Heath, J. R., O'Brien, S. C., Curl, R. F., and Smalley, R. E. (1985). C60: Buckminsterfullerene. *Nature* 318, 162–163. doi:10.1038/318162a0

Lazauskas, T., Sokol, A. A., and Woodley, S. M. (2017). An Efficient Genetic Algorithm for Structure Prediction at the Nanoscale. *Nanoscale* 9, 3850–3864. doi:10.1039/C6NR09072A

Li, J., Li, X., Zhai, H. J., and Wang, L. S. (2003). Au20: A Tetrahedral Cluster. *Science* 299, 864–867. doi:10.1126/science.1079879

Li, W.-L., Chen, X., Jian, T., Chen, T.-T., Li, J., and Wang, L.-S. (2017). From Planar boron Clusters to Borophenes and Metalloborophenes. *Nat. Rev. Chem.* 1, 0071. doi:10.1038/s41570-017-0071

Liu, L., and Corma, A. (2018). Metal Catalysts for Heterogeneous Catalysis: From Single Atoms to Nanoclusters and Nanoparticles. *Chem. Rev.* 118, 4981–5079. doi:10.1021/acs.chemrev.7b00776

Lu, T., and Chen, F. (2012). Multiwfn: A Multifunctional Wavefunction Analyzer. *J. Comput. Chem.* 33, 580–592. doi:10.1002/jcc.22885

Luo, Z., Castleman, A. W., and Khanna, S. N. (2016). Reactivity of Metal Clusters. *Chem. Rev.* 116, 14456–14492. doi:10.1021/acs.chemrev.6b00230

Martin, T. P. (1986). Compound Clusters. *Z. Phys. D - Atoms, Mol. Clusters* 3, 211–217. doi:10.1007/BF01384809

Mokrai, R., Barrett, J., Apperley, D. C., Batsanov, A. S., Benkő, Z., and Heift, D. (2019). Weak Pnictogen Bond with Bismuth: Experimental Evidence Based on Bi−P Through-Space Coupling. *Chem. Eur. J.* 25, 4017–4024. doi:10.1002/chem.201900266

Mu, L., Yang, S., Bao, X., Yin, H., and Kong, X. (2015). Medium-sized Phosphorus Cluster cationsP+2m+1(6 ≤ M ≤ 32) Studied by Collision-Induced Dissociation Mass Spectrometry. *J. Mass. Spectrom.* 50, 1352–1357. doi:10.1002/jms.3705

Paz-Borbón, L. O., Mortimer-Jones, T. V., Johnston, R. L., Posada-Amarillas, A., Barcaro, G., and Fortunelli, A. (2007). Structures and Energetics of 98 Atom Pd-Pt Nanoalloys: Potential Stability of the Leary Tetrahedron for Bimetallic Nanoparticles. *Phys. Chem. Chem. Phys.* 9, 5202–5208. doi:10.1039/b707136a

Piazza, Z. A., Hu, H.-S., Li, W.-L., Zhao, Y.-F., Li, J., and Wang, L.-S. (2014). Planar Hexagonal B36 as a Potential Basis for Extended Single-Atom Layer boron Sheets. *Nat. Commun.* 5, 3113. doi:10.1038/ncomms4113

Rabanal-León, W. A., Tiznado, W., Osorio, E., and Ferraro, F. (2018). Exploring the Potential Energy Surface of Small lead Clusters Using the Gradient Embedded Genetic Algorithm and an Adequate Treatment of Relativistic Effects. *RSC Adv.* 8, 145–152. doi:10.1039/C7RA11449D

Reed, A. E., Curtiss, L. A., and Weinhold, F. (1988). Intermolecular Interactions from a Natural Bond Orbital, Donor-Acceptor Viewpoint. *Chem. Rev.* 88, 899–926. doi:10.1021/cr00088a005

Rogan, J., Varas, A., Valdivia, J. A., and Kiwi, M. (2013). A Strategy to Find Minimal Energy Nanocluster Structures. *J. Comput. Chem.* 34, 2548–2556. doi:10.1002/jcc.23419

Scheiner, S. (2013). The Pnicogen Bond: Its Relation to Hydrogen, Halogen, and Other Noncovalent Bonds. *Acc. Chem. Res.* 46, 280–288. doi:10.1021/ar3001316

Scutelnic, V., Perez, M. A. S., Marianski, M., Warnke, S., Gregor, A., Rothlisberger, U., et al. (2018). The Structure of the Protonated Serine Octamer. *J. Am. Chem. Soc.* 140, 7554–7560. doi:10.1021/jacs.8b02118

Shayeghi, A., Götz, D., Davis, J. B. A., Schäfer, R., and Johnston, R. L. (2015). Pool-BCGA: a Parallelised Generation-free Genetic Algorithm for the Ab Initio Global Optimisation of Nanoalloy Clusters. *Phys. Chem. Chem. Phys.* 17, 2104–2112. doi:10.1039/C4CP04323E

VanGelder, L. E., Kosswattaarachchi, A. M., Forrestel, P. L., Cook, T. R., and Matson, E. M. (2018). Polyoxovanadate-alkoxide Clusters as Multi-Electron Charge Carriers for Symmetric Non-aqueous Redox Flow Batteries. *Chem. Sci.* 9, 1692–1699. doi:10.1039/c7sc05295b

VanGelder, L. E., Pratt, H. D., Anderson, T. M., and Matson, E. M. (2019). Surface Functionalization of Polyoxovanadium Clusters: Generation of Highly Soluble Charge Carriers for Nonaqueous Energy Storage. *Chem. Commun.* 55, 12247–12250. doi:10.1039/C9CC05380H

Wales, D. J., and Doye, J. P. K. (1997). Global Optimization by Basin-Hopping and the Lowest Energy Structures of Lennard-Jones Clusters Containing up to 110 Atoms. *J. Phys. Chem. A.* 101, 5111–5116. doi:10.1021/jp970984n

Wales, D. J., and Scheraga, H. A. (1999). Global Optimization of Clusters, Crystals, and Biomolecules. *Science* 285, 1368–1372. doi:10.1126/science.285.5432.1368

Wang, Y., Lv, J., Zhu, L., and Ma, Y. (2012). CALYPSO: A Method for crystal Structure Prediction. *Comput. Phys. Commun.* 183, 2063–2070. doi:10.1016/j.cpc.2012.05.008

Wu, J., Yan, H., Zhong, A., Chen, H., Jin, Y., and Dai, G. (2019). Theoretical and Conceptual DFT Study of Pnicogen- and Halogen-Bonded Complexes of PH2X---BrCl. *J. Mol. Model.* 25, 28. doi:10.1007/s00894-018-3905-3

Xue, T., Luo, J., Shen, S., Li, F., and Zhao, J. (2010). Lowest-energy structures of cationic P2m+1+ (m=1-12) clusters from first-principles simulated annealing. *Chem. Phys. Lett.* 485, 26–30. doi:10.1016/j.cplett.2009.12.019

Yañez, O., Báez-Grez, R., Inostroza, D., Rabanal-León, W. A., Pino-Rios, R., Garza, J., et al. (2019). AUTOMATON: A Program That Combines a Probabilistic Cellular Automata and a Genetic Algorithm for Global Minimum Search of Clusters and Molecules. *J. Chem. Theor. Comput.* 15, 1463–1475. doi:10.1021/acs.jctc.8b00772

Yang, S., Mu, L., and Kong, X. (2016). Collision-induced dissociation mass spectrometry of phosphorus cluster anionsP2m+1−(3 ≤ m ≤ 20). *Int. J. Mass Spectrom.* 399-400, 27–32. doi:10.1016/j.ijms.2016.02.006

Yoo, S., Zhao, J., Wang, J., and Zeng, X. C. (2004). Endohedral Silicon Fullerenes SiN(27 ≤N≤ 39). *J. Am. Chem. Soc.* 126, 13845–13849. doi:10.1021/ja046861f

Zahn, S., Frank, R., Hey-Hawkins, E., and Kirchner, B. (2011). Pnicogen Bonds: A New Molecular Linker?. *Chem. Eur. J.* 17, 6034–6038. doi:10.1002/chem.201002146

Zhai, H.-J., Zhao, Y.-F., Li, W.-L., Chen, Q., Bai, H., Hu, H.-S., et al. (2014). Observation of an all-boron fullerene. *Nat. Chem* 6, 727–731. doi:10.1038/NCHEM.1999

Zhan, L., Chen, J. Z. Y., Liu, W.-K., and Lai, S. K. (2005). Asynchronous multicanonical basin hopping method and its application to cobalt nanoclusters. *J. Chem. Phys.* 122, 244707. doi:10.1063/1.1940028

Zhang, J., and Glezakou, V. A. (2020). Global optimization of chemical cluster structures: Methods, applications, and challenges. *Int. J. Quan. Chem.* 121, e26553. doi:10.1002/qua.26553

Zhao, Y., Chen, X., and Li, J. (2017). TGMin: A global-minimum structure search program based on a constrained basin-hopping algorithm. *Nano Res.* 10, 3407–3420. doi:10.1007/s12274-017-1553-z

Zhou, C., Ieritano, C., and Hopkins, W. S. (2019). Augmenting Basin-Hopping With Techniques From Unsupervised Machine Learning: Applications in Spectroscopy and Ion Mobility. *Front. Chem.* 7, 519. doi:10.3389/fchem.2019.00519

Zhou, T., Ma, L., and Chen, H. (2020). Electronic structure and stability of Al6CMn (M = Li, Na, k; n = 2, 4, 6) clusters. *Comput. Theor. Chem.* 1178, 112780. doi:10.1016/j.comptc.2020.112780

Conflict of Interest: The authors declare that the research was conducted in the absence of any commercial or financial relationships that could be construed as a potential conflict of interest.

Publisher's Note: All claims expressed in this article are solely those of the authors and do not necessarily represent those of their affiliated organizations, or those of the publisher, the editors and the reviewers. Any product that may be evaluated in this article, or claim that may be made by its manufacturer, is not guaranteed or endorsed by the publisher.

frontiers in Chemistry

REVIEW
published: 16 August 2021
doi: 10.3389/fchem.2021.730548

Atomic Clusters: Structure, Reactivity, Bonding, and Dynamics

Ranita Pal[1], *Arpita Poddar*[2] *and Pratim Kumar Chattaraj*[2,3]*†

[1]*Advanced Technology Development Centre, Indian Institute of Technology Kharagpur, Kharagpur, India,* [2]*Department of Chemistry, Indian Institute of Technology Kharagpur, Kharagpur, India,* [3]*Department of Chemistry, Indian Institute of Technology Bombay, Mumbai, India*

Atomic clusters lie somewhere in between isolated atoms and extended solids with distinctly different reactivity patterns. They are known to be useful as catalysts facilitating several reactions of industrial importance. Various machine learning based techniques have been adopted in generating their global minimum energy structures. Bond-stretch isomerism, aromatic stabilization, Rener-Teller effect, improved superhalogen/superalkali properties, and electride characteristics are some of the hallmarks of these clusters. Different all-metal and nonmetal clusters exhibit a variety of aromatic characteristics. Some of these clusters are dynamically stable as exemplified through their fluxional behavior. Several of these cluster cavitands are found to be agents for effective confinement. The confined media cause drastic changes in bonding, reactivity, and other properties, for example, bonding between two noble gas atoms, and remarkable acceleration in the rate of a chemical reaction under confinement. They have potential to be good hydrogen storage materials and also to activate small molecules for various purposes. Many atomic clusters show exceptional opto-electronic, magnetic, and nonlinear optical properties. In this Review article, we intend to highlight all these aspects.

Keywords: aromaticity, Electrides, Particle swarm optimization, Firefly algorithm, Confinement, Hydrogen storage, Fluxionality

OPEN ACCESS

Edited by:
Ambrish Kumar Srivastava,
Deen Dayal Upadhyay Gorakhpur University, India

Reviewed by:
Santanab Giri,
Haldia Institute of Technology, India
Shamoon Ahmad Siddiqui,
Najran University, Saudi Arabia

****Correspondence:***
Pratim Kumar Chattaraj
pkc@chem.iitkgp.ac.in

†ORCID:
Pratim Kumar Chattaraj
orcid.org/0000-0002-5650-7666

Specialty section:
This article was submitted to Physical Chemistry and Chemical Physics, a section of the journal Frontiers in Chemistry

Received: *25 June 2021*
Accepted: *13 July 2021*
Published: *16 August 2021*

Citation:
Pal R, Poddar A and Chattaraj PK (2021) Atomic Clusters: Structure, Reactivity, Bonding, and Dynamics. Front. Chem. 9:730548. doi: 10.3389/fchem.2021.730548

INTRODUCTION

A cluster is defined as a finite aggregation of atoms, starting with as low as two atoms and extending up to an upper bound of some hundred thousand atoms (Herr, 1993; Corrigan and Dehnen, 2017). A theoretical study elucidates that cluster properties strongly depend on the geometry of the isolated cluster and the topology of the cluster sample. F. A. Cotton first used the term cluster for compounds with metal–metal bonds. Nonmetallic atomic clusters came into the limelight later, from both theoretical and experimental studies. The unique size-dependent properties of clusters are distinct from the molecules and bulk solids (Sergeeva et al., 2014). Experimental and theoretical methods on cluster research have seen substantial amount of improvement over the years in discovering a diversity of size-specific phenomena and physicochemical cluster properties (Jena and Castleman, 2010). Various physicochemical properties of metal clusters such as optical, magnetic, thermal, chemical properties differ remarkably from their bulk counterparts (Tsukuda and Hakkinen, 2015). In the last few decades, several studies have been reported on the ligand protected metal clusters, *viz.* phosphine-protected small Au cluster, thiolate (RS)-protected Au nanoparticles (Brust et al., 1994), *etc.* For small metal clusters (<~100 atoms), the electronic structures are not continuous as in the bulk metals, but rather discretized, which is the primary reason for different physicochemical properties and functionalities in small clusters and bulk metal (Sharma et al., 2017). Studies have

shown that clusters made of atoms with appropriate size and composition could potentially mimic the chemistry of elemental atoms in periodic table, and hence are known as superatoms (Li et al., 2008). Various experimental techniques such as laser ablation coupled with mass spectrometry, photoelectron spectroscopy have been employed to get insights into the atomic clusters. Along with experimental studies, theoretical investigations are required to get a better understanding of their geometric arrangement and corresponding properties (Srivastava, 2021).

A large number of theoretical studies have been reported dealing with finding the minimum energy structures of pure elemental clusters by using different optimization algorithms. The potential energy surface (PES) of various atomic clusters is explored to minimize their energy functional with the final objective of locating their global minimum (GM). Different optimization methods such as genetic algorithm (Holland, 1992) (GA), basin hopping (BH) algorithm (Wales and Doye, 1997), particle swarm optimization (PSO) algorithm (Bai, 2010), adaptive particle swarm optimization (APSO) (Zhan and Zhang, 2008), simulated annealing (SA) (Woodley et al., 1999), artificial bee colony optimization (ABC) (Karaboga and Basturk, 2007), honey bee mating optimization (HBMO) (Pham et al., 2005), ant colony optimization (ACO) (Colorni et al., 1991), heuristic algorithm combined with the surface and interior operators (HA-SIO), fast annealing evolutionary algorithm (FAEA), firefly algorithm (FA) (Yang, 2010). *etc*. are increasingly being used to solve the optimization problem in a time- and cost-efficient manner. Various models/empirical potentials (EPs) such as Lennard–Jones (LJ), Born–Mayer, Sutton–Chen, Gupta and Murrell–Mottram potentials can effectively explain the bonding within various clusters. A number of studies performed by Chattaraj *et al.* reveal that PSO is more efficient than commonly used techniques such as GA, SA, and BH for finding the GM of small clusters (Mitikiri et al., 2018; Jana et al., 2019). Further developments over PSO algorithm have been accomplished. Global optimization of boron clusters (B_5 and B_6) has been studied using an advanced PSO approach by Mitikiri et al. (2018). Jana et al. (2019) performed a similar study on carbon clusters, C_n (n = 3–6,10) by using a modified PSO algorithm. Mitra et al. (2020) reported the global optimization of Al_4^{2-} clusters by using firefly algorithm along with DFT.

The concept of trapping atoms and small molecules into the hollow cavity of clusters has shown several applications in biology (Cagle et al., 1996; Thrash et al., 1999; Wilson et al., 1999) and electrical engineering (Cioslowski and Nanayakkara, 1992). Pan et al. (2018) reported the encapsulation of noble gas (Ng) atoms into the B_{40} host moiety, which is shown to have a fluxional character (Moreno et al., 2014). The dynamical study of the aforementioned system showed that the fluxional character persists even after the encapsulation. Smaller cages such as $C_{20}H_{20}$ (Cross et al., 1999; Jiménez-Vázquez et al., 2001), $C_{10}H_{16}$ (Haaland et al., 2004), BN cages ($B_{12}N_{12}$ and $B_{16}N_{16}$) (Khatua et al., 2014a), Pb_{12}^{2-}, and Sn_{12}^{2-} (Sekhar et al., 2017) can act as host molecules to endohedrally trapped noble gas atoms. Cucurbit[n]urils, abbreviated as CB[n]s, n being the number of gycoluril units, can also act as host for different guest molecules including metal cations, organic dyes, drugs, halide ions, *etc.* (Lagona et al., 2005; Pan et al., 2013a). CB[7] was also reported to bind different guest compounds such as organic dyes (*e.g.*, Stilbenes, naphthalene), viologens, and metal complexes (*e.g.*, Oxaliplatin) applicable in cancer treatment (Wagner et al., 2003). In 2017, Pan et al. (2017) have reported the adsorption of 14 molecules, *viz*., CH_4, C_2H_2, C_2H_4, C_2H_6, F_2, Cl_2, NO_2, NO, CO, CO_2, SO_2, H_2S, N_2, H_2 endohedrally within the hydrophobic inner cavity of CB[7]. CB[6] is also known to encapsulate noble gas atoms (Pan et al., 2015). Chakraborty *et al.* (Chakraborty and Chattaraj, 2015) reported the accommodation of noble gas atoms within the BN-doped (3, 3) single-walled carbon nanotubes. The Ng binding ability of BeX (X = SO_4, CO_3, O) has been reported by Saha et al. (2015). Pan et al. (2014) have explored the stability of Ng-bound SiH_3^+ cluster ions. An emerging host molecule is the basket-shaped octa acid (OA) cavitand that can encapsulate different gas molecules (Chakraborty et al., 2016). Various steroids (Liu and Gibb, 2008), hydrophobic moieties such as ethane, ethylene, acetylene (Stang and Diederich, 2008; Hu et al., 2009; Florea and Nau, 2011; Zhang et al., 2011; Yang et al., 2015; Chong et al., 2016) have been confined inside OA. The encapsulation of gas molecules, especially the hazardous ones, by the cluster cavity has great applications in environmental chemistry. Encapsulation of greenhouse gases (CO_2) (Zhang and Chen, 2009; Jin et al., 2010; Kim et al., 2010; Jin et al., 2011; Mastalerz et al., 2011; Lü et al., 2014), air pollutants (NO_2) (Pan et al., 2017), and poisonous gases (CO, NO) using molecular cages has applications in reducing their negative impact on the atmosphere. N_2 encapsulation (Msayib et al., 2009; Akhtar et al., 2012; Schneider et al., 2012) is yet another important research topic in environmental chemistry. Chakraborty et al. (2016) reported a set of small gaseous molecules (C_2H_2, C_2H_4, C_2H_6, CO, CO_2, NO_2, NO, N_2, H_2^-), and rare gas atoms as guest molecules for the OA host system. In fact, OA is a very efficient reaction vessel for accommodating various different guest molecules. Li^+, Na^+, K^+, Be^{2+}, Mg^{2+}, Ca^{2+}, Li_3O^+, Na_3O^+, K_3O^+ and various nucleobases can occupy the basket-shaped octa acid cavitand as reported by Chakraborty and Chattaraj (2018).

In recent days, the conservation of the atmosphere and the desire to save up fuel for the upcoming generations has been a major concern in the scientific community that led to the search for alternatives of fossil fuel. Hydrogen, being renewable, recyclable, environment friendly, and abundantly available in nature, is now a globally acceptable fuel source with the potential to replace fossil fuels in the near future. The challenge, however, is designing compatible storage and transport materials. To that end, hydrogen-storing capacity of metal-organic-frameworks (MOF) (Rosi et al., 2003; Rowsell and Yaghi, 2005), covalent-organic-frameworks (COF) (Kuc et al., 2007; Cabria et al., 2008), clathrate hydrates (Lee et al., 2005; Chattaraj et al., 2011), polymers (McKeown et al., 2006), carbon nanotubes, BN cages, fullerene, grapheme-like materials (Froudakis, 2001; Deng et al., 2004; Heine et al., 2004; Sun et al., 2005; Wu et al., 2008), metal hydrides (Lee et al., 2005) have been explored. Pan et al. (2012a) performed a theoretical study on the H_2-storing capability of some Li-doped clusters and super-

alkalis. Zhu et al. (2010) have shown cucurbiturils acting as a promising candidate for hydrogen storage. Pan et al. (2013a) have discussed the hydrogen storage capability of the CB[7] system. A different class of compound, alkali-doped carbon materials (graphene sheet and single-walled carbon nanotubes), have been designed for reversible hydrogen storage for transportation purposes by Wei-Qiao Deng et al. (2004). On the other hand, very explosive acetylene can be stored within the porous MOF-505 analogue as reported by Yunxia Hu et al. (2009).

The confinement effect on atoms and molecules has intrigued both theoreticians and experimentalists alike. It brings out interesting changes in the energy levels of the confined systems, their bonding, reactivity, and properties (Grochala et al., 2007; Schettino and Bini, 2007; Sabin and Brandas, 2009; Gubbins et al., 2011; Chakraborty and Chattaraj, 2019; Pal and Chattaraj, 2021). Khatua et al. (2014b) have performed a theoretical investigation on the entrapment of $(HF)_2$ in C_n (n = 60, 70, 80, 90) cages. Although CO and N_2 are isoelectric species, the latter is known to be pretty inert owing to its high ionization potential, low electron affinity, and high frontier orbital energy gap ($\Delta E_{\text{HOMO-LUMO}}$). Thus, N_2 capture in various transition metal complexes has proven to induce bond activation that has various industrial applications (Chatt and Leigh, 1972; Yandulov and Schrock, 2003; Latysheva et al., 2012; Bergman et al., 2013; Hoffman et al., 2013). In this regard, Saha et al. (2017) reported the CO and N_2 bound metal supported boron clusters (MB_{12}^-, M = Co, Rh, Ir) which form a spinning umbrella-like structure and activate the bound molecules. Boron clusters have found profound applications in material science owing to their ability to act as nanomaterial building blocks. Their property to act as such is due to a bowl-like structure with an outer rim (B_9) and an inner well (B_3).

Along with the coordination and inorganic cages, various organic cavitands can also be considered host system for encapsulation. One such class of compounds is the cucurbiturils. Chemical reactions catalyzed by host–guest interactions are comparable to those catalyzed by enzymes (Dong et al., 2012). Hennig et al. (2007) successfully induced protease inhibition using the host–guest interaction with CB[7]. In addition to CB[7], $ExBox^{+4}$ (Barnes et al., 2013) can also act as an organic host molecule that can encapsulate a wide array of guest moieties. Chakraborty et al. (2017) performed a theoretical study on [4+2] cycloaddition reaction confined within CB[7] and $ExBox^{+4}$ host systems.

In recent times, low dimensional materials are being given more and more attention to be used as host moiety. Graphene has provided us with a plethora of highly efficient devices such as gas sensors, spintronic devices, nanoelectronics, and optoelectronic devices (Chakraborty and Chattaraj, 2017). An inorganic counterpart of graphene is the boron nitride doped system that can be functionalized with OLi_4, CLi_6, NLi_5, BLi_7, $Al_{12}Be$ to achieve some interesting properties (Chakraborty and Chattaraj, 2017). The M_3O^+ (M = Li, Na, K) functionalized graphene nanoflakes (Chakraborty and Chattaraj, 2016a) are known to sequestrate various polar molecules such as CO, NO, and CH_3OH. Sequestration of gas molecules such as H_2, O_2, O_3, CO, NO, and H_2O through bare boron nitride flakes (BNF) and metal oxide, MO (M = Cu, Ag, Au) functionalized BNF are also reported (Chakraborty and Chattaraj, 2016b). In this review we report some optimization techniques for the generation of minimum energy structures of some selected clusters and also the bonding, reactivity, and different properties of some selected confined systems. Aromatic behavior and electride properties of some clusters are also investigated.

THEORETICAL BACKGROUND AND COMPUTATIONAL DETAILS

Before optimizing the geometry of any system, we carefully ponder over the requirement of the study and select the level of theory maintaining a parity between the level of accuracy required and the computational cost to be incurred. Most often, the easiest way is to take into consideration the experimental data (if available) and select accordingly. The systems discussed in this article are optimized using the computational chemistry software package, Gaussian 09 (Frisch et al., 2009). We have used B3LYP (Lee et al., 1988; Becke, 1992), BP86 (Perdew, 1986a; Perdew, 1986b; Becke, 1988), ωb97X-D (Chai and Head-Gordon, 2008), PBE (Perdew et al., 1996; Perdew et al., 1997), TPSSTPSS (Staroverov and Scuseria, 2003; Tao et al., 2003), M06, M06-2X (Zhao and Truhlar, 2008), and M05-2X (Zhao et al., 2006) functionals for carrying out DFT calculations of various systems. The exact level of theory (method and basis set) chosen for the individual case studies is mentioned in the Results and Discussion section. Relativistic effects for heavier atoms are taken care of by effective core potentials (ECPs). The stationary states are better understood from the harmonic vibrational frequencies. The minimum energy structure and the transition state (TS) are identified with the presence of zero and one imaginary frequency, respectively.

The atomic charges, nature of interactions present within the systems, and the possible bond formation are analyzed with the help of natural population analysis (NPA) (Reed et al., 1985), Wiberg bond indices (WBI) (Wiberg, 1968) in the NBO scheme (Reed et al., 1988). The electron density topology is mapped using Bader's quantum theory of atoms-in-molecules (QTAIM) (Bader, 1985) in Multiwfn (Lu and Chen, 2012). Parameters such as electron density [$\rho(r_c)$], total electron energy density [$H(r_c)$], local kinetic energy density [$G(r_c)$], local potential energy density [$V(r_c)$], and Laplacian of electron density [$\nabla^2\rho(r)$] are computed at the bond critical points (BCPs) and they help analyze the extent of covalent or ionic character present along that bond path. The NCI index reveals the localized binding interaction in a system, and the plot can be visualized as red, blue, or green regions in the NCIPLOT program (Contreras-García et al., 2011) depending on whether the interaction is repulsive, H-bond, or van der Waals, respectively. The nonlinear optical (NLO) properties are evaluated in terms of average linear polarizability ($\overline{\alpha}$), first (β) and second ($\gamma_{\parallel}$) hyperpolarizabilities.

ADF 2013.01 software (Baerends et al., 2013) is utilized to perform the energy decomposition analysis (EDA) (Morokuma,

1971) with the natural orbitals for chemical valence (NOCV) (Mitoraj et al., 2009). The interaction between two selected fragments of the studied system is represented in terms of three attractive and one repulsive energy terms. The attractive term includes electrostatic energy (ΔE_{elstat}), orbital interaction energy (ΔE_{orb}), dispersion interaction energy (ΔE_{disp}), while the repulsive term is known as Pauli repulsion energy (ΔE_{Pauli}).

$$\Delta E_{\text{int}} = \Delta E_{\text{elstat}} + \Delta E_{\text{orb}} + \Delta E_{\text{disp}} + \Delta E_{\text{Pauli}} \quad (1)$$

In NOCV, the orbital term is represented as the sum of ΔE^k_{orb} (pairwise orbital energies) which is related to $\Delta\rho^k$(r) (pairwise charge contributions).

$$\Delta E_{orb} = \sum_k \Delta E^k_{orb} \quad (2)$$

Atom-centered density matrix propagation (ADMP) (Iyengar et al., 2001; Schlegel et al., 2001; Schlegel et al., 2002) in Gaussian 09, and Born-Oppenheimer molecular dynamics (BOMD) in deMon2K software (Koster et al., 2011) are used to perform the dynamic study of the systems under discussion in this article.

For the global optimization study using PSO, ADMP-CNN-PSO, and FA, the algorithms are written in Python 3.7 programming language (Van Rossum and Drake, 2009). The single point energies (SPEs) are calculated using Gaussian 09 at the post-processing step. The calculations for all the clusters are performed using the B3LYP (Lee et al., 1988; Becke, 1992) functional of DFT. The basis set 6-311+G(d,p) (McLean and Chandler, 1980; Raghavachari et al., 1980) is used for the boron clusters, 6-311+G(d) for Al_4^{2-}, C_5, and N_4^{2-}, 6-311G(d) for N_6^{4-}, and LANL2DZ (Dunning and Hay, 1977; Wadt and Hay, 1985; Hay and Wadt, 1985a; Hay and Wadt, 1985b) with ECPs for Au_n (n = 2–8) and Au_nAg_m ($2 \le (n+m) \le 8$). The algorithms are executed in a server with two Intel 2.70 GHz Xeon E5-2697 v2 processors (each with 12 cores and 30 threads) and a 256 GB RAM. The software Keras (Chollet, 2015) is used for interfacing with Python 3.7 with convolution neural networks (CNN).

RESULTS AND DISCUSSION

Global Optimization Using Machine Learning Techniques

Minimization of a system's energy functional is the most fundamental step in the determination of its ground state. Reaching the global minimum (GM) geometry, however, poses a number of challenges, the most important being the high probability of getting stuck in local minima in the PES. Swarm intelligence (SI)-based algorithms have turned out to be very effective in searching for optimal solutions in a given search space. Here we discuss three different techniques, PSO combined with DFT, PSO with CNN, and DFT-integrated FA. They do not need to implement any symmetry constraint, or consider bond characterization. DFT-PSO adjusts each particle's trajectory at every time stamp while following the convergence criteria. We have successfully implemented these techniques to find the GM configurations for small-sized nonmetallic clusters such as Boron (B_5 and B_6) (Yuan et al., 2014), Carbon (C_5) (Jana et al., 2019), and polynitrogen clusters (N_4^{2-} and N_6^{4-}) (Mitra et al., 2021), and metallic clusters such as Al_4^{2-} (Mitra et al., 2020), Au_n (n = 2–8), and Au_nAg_m ($2 \le n+m \le 8$) (Mitra et al., 2021).

PSO Combined With DFT (DFT-PSO)

We start off with 14 and 15 random structures for B_5 and B_6 (**Figure 1**), respectively, with velocity set at zero and maximum number of iterations set at 1,000. No significant change in bond length is detected after reaching the global best configuration at the end of the PSO run. Following this, the optimization is performed at the B3LYP/6-311+G(d,p) level as the post-processing step that helps align the symmetry of the PSO-obtained final structure and obtain the corresponding exact energy. The post-processing in this case takes only 20 s to complete, and the final geometry obtained is energetically very close (0.0015 eV difference) to that obtained at the end of the PSO run. The zero-point energy (ZPE) corrected energy, free energy, and enthalpy for B_5 (C_{2v}) are −123.9873, −124.0135, and −123.9821 a.u., respectively, while those for B_6 (C_{2h}) are −148.8100, −148.8381, and −148.8038 a.u., respectively. A comparison drawn between our method and other popular algorithms such as DFT-SA and DFT-BH reveals that while these two require a CPU time of 369.64 and 455.43 min to locate the minimum energy structure of B_5, respectively, our method takes only 80.50 min. It is also observed that while the BH and the SA require 600 (unconverged) and 324 number of iterations, respectively, our modified PSO converges after only 138 number of iterations.

For the carbon clusters, 10 random configurations are chosen with initial velocity zero and 1,000 number of iterations. For the C_n (n = 3–6) clusters, linear geometries are obtained with $D_{\infty h}$ point group as the GM. For n = 4–6, a cyclic isomer for each of them is also obtained with point groups D_{2h}, C_{2v}, and D_{3h} for C_4, C_5, and C_6, respectively, whereas for the relatively larger C_{10} cluster, the GM geometry is a D_{10h} ring structure. It is to be noted that the geometries and corresponding energies reported here match with those obtained from the experimental reports (Raghavachari and Binkley, 1987; Watts et al., 1992; Hutter and Lüthi, 1994; Pless et al., 1994; Martin and Taylor, 1996; Van Orden and Saykally, 1998). Again, comparing with DFT-SA and DFT-BH, we get encouraging results for our modified PSO approach. The total execution time for our technique is 143.30 min versus 215.98 and 5085.67 min for DFT-SA and DFT-BH, respectively.

For N_4^{2-} and N_6^{4-} clusters, convergence takes place after 483 and 627 numbers of iterations with 228 and 323 min of execution time, respectively. The geometries obtained before and after the post-processing step are energetically very close (**Figure 2**). The N_6^{4-} cluster, however, shows a higher order saddle point at the post-processing symmetry constrained optimization with point group D_{6h}. In case of the binary gold–silver clusters (Au_nAg_m), $AuAg_2$ has a ring (C_s) doublet GM, those with $n+m$ = 5 have trapezoidal GM, $n+m$ = 6, 7 have triangular 3D geometry (C_1), and $n+m$ = 8 failed to converge within the initial coordinates range of [−4, 4].

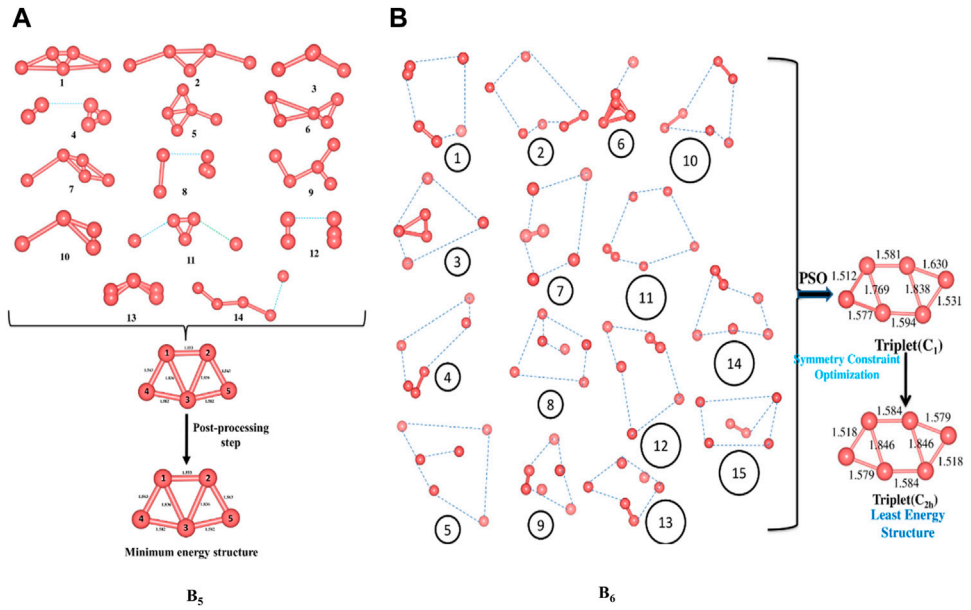

FIGURE 1 | Randomly generated configurations of **(A)** B_5 and **(B)** B_6 and their convergence to their respective global minimum energy structures (Bond lengths are provided in Å). (Adapted with permission from Mitikiri et al., 2018. Copyright© 2021, John Wiley & Sons, Inc.).

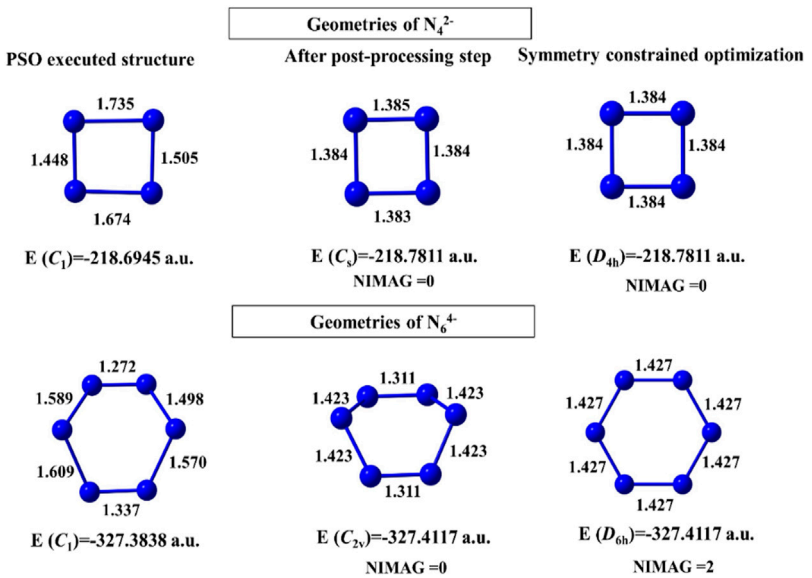

FIGURE 2 | Structures of N_4^{2-} and N_6^{4-} clusters obtained at the end of the PSO run, post-processing step, and geometry-constrained optimization computed at the B3LYP/6-311 + G(d) level. (Reprinted from Mitra et al., 2021 with permission from Theoretical Chemistry Accounts, Springer Nature. Copyright© 2021, Springer-Verlag GmbH, DE.).

CNN With PSO (CNN-PSO)

Supervised learning (CNN) is performed on an initial guess set generated with the help of (ADMP) simulation. Their corresponding single point energies (SPEs) are calculated and stored to be read by the PSO to search for the GM geometry. Statistically relevant analysis is derived by making the method 8-fold (each with 30 files containing number of iterations and the SPEs). Remarkably high success rate (~77–90%) is observed for this combined ADMP, CNN, PSO technique, indicating its efficiency in finding GMs. This technique is tested with the C_5 cluster and we have obtained the previously reported (Van Orden and Saykally, 1998) linear geometry as the GM with a higher convergence rate. However, two local minima are also detected due to a premature convergence (**Figure 3**).

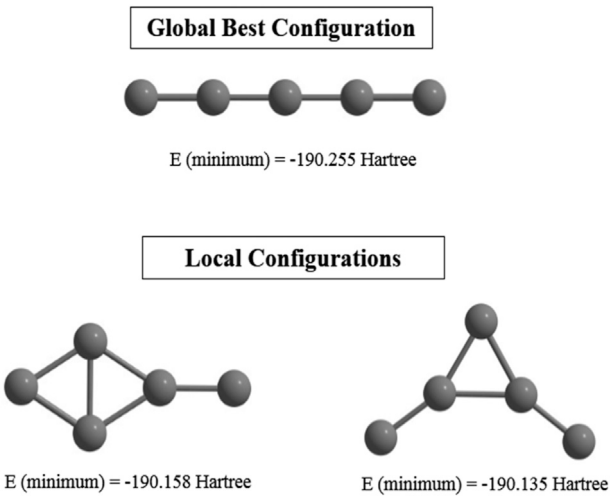

FIGURE 3 | Global and local minimum energy structures of C_5 cluster obtained at the end of the post-processing step computed at the B3LYP/6-311+G(d,p) level. (Reprinted from Mitra et al., 2021 with permission from Theoretical Chemistry Accounts, Springer Nature. Copyright© 2021, Springer-Verlag GmbH, DE.).

FA With DFT (DFT-FA)

A comparative study of the DFT-integrated FA algorithm with PSO is performed on Al_4^{2-} cluster considering planar and nonplanar structures, and it turns out that the former performs better than the PSO. The mean convergence times for the PSO and FA are 68.22 and 61.25 min for the planar, and 85.13 and 74.40 min for the nonplanar approach, respectively. The corresponding success rates are also higher for the FA. Since we know that the GM of Al_4^{2-} is planar, we have also investigated the search space of only the planar geometry to get a faster convergence since the number of variables decreases in this problem. Again, the modified FA performs better. A relation is also drawn between the stabilization energy of the system and the change in its aromaticity and number of iteration steps it takes to converge to the GM. The energy functional optimization and the NICS (0) value of Al_4^{2-} are scanned and depicted in **Figure 4**. It is observed that the aromaticity increases with the decrease in the energy, *i.e.*, with the increase in the stability of the system.

Aromaticity of Clusters From a CDFT Perspective

It is well known from Hückel's (4n+2) π electron theory (Hückel, 1931) and Pauling's quantum mechanical description (Pauling and Sherman, 1933) that aromaticity of conjugated systems with cyclic and planar geometry is associated with their increased stability. Various structural, energetic, electronic, and magnetic behavior-based parameters are considered to analyze the aromaticity of the systems, among which the Nucleus-Independent Chemical Shift (NICS) (Schleyer et al., 1996) is, perhaps, the most widely used criterion for aromaticity. CDFT also plays an important role in aromaticity determination (Chattaraj et al., 2005; Chattaraj et al., 2006; Chattaraj et al., 2007), and it does so with the help of reactivity descriptors and associated electronic structure principles (Chattaraj et al., 1993; Chattaraj and Maiti, 2001; Pan et al., 2013b; Chakraborty and Chattaraj, 2021). The relative aromaticity index ΔX, where X could be energy (E), polarizability (α), electrophilicity (ω), or hardness (η), is defined as the difference between the respective indices in the cyclic and open (or localized) systems, *i.e.*, $\Delta X = X_{\text{CYCLIC}} - X_{\text{OPEN(/LOCALIZED)}}$. They are observed to show a similar performance as those of the NICS and MCI values. They also provide valuable insights into the stability, reactivity, and electronic properties of the associated cluster.

All-metal aromatic Al_4^{2-} (Li et al., 2001) and antiaromatic Al_4^{4-} (Kuznetsov et al., 2003) clusters are investigated at the B3LYP/6-311G(d, p) level of theory to analyze their aromaticity from a CDFT perspective (Chattaraj et al., 2005; Chattaraj et al., 2006; Chattaraj et al., 2007). While $\Delta\eta > 0$ represents aromaticity and $\Delta\eta < 0$ represents antiaromaticity, the reverse is true in the cases of E, α, and ω indices. Their values for the aluminum clusters are compared with those of benzene (C_6H_6) and cyclobutadiene (C_4H_4). While Al_4^{2-} and C_6H_6 show positive $\Delta\eta$ and negative ΔE, $\Delta\alpha$, and $\Delta\omega$ values indicating an aromatic behavior, C_4H_4 shows an exact opposite trend to account for its antiaromaticity. For the Al_4^{4-} cluster, however, we have obtained somewhat contradictory results. ΔE and $\Delta\alpha$ values indicate the cluster's antiaromatic nature, whereas $\Delta\eta$, $\Delta\omega$, and NICS values reflect its aromatic nature. It is in conformity with the current knowledge that this cluster exhibits conflicting aromaticity. Experimental synthesis and theoretical studies reported along with ELF analysis (Li et al., 2001; Santos et al., 2005) suggest the cluster to be antiaromatic. Its σ-aromaticity directs the overall aromaticity by dominating over its π-counterpart as studied through NICS (Chen et al., 2003) and magnetic field induced current density (Havenith et al., 2004) analyses. Such conflicting aromaticity, along with other varieties of multiple aromaticity and antiaromaticity, δ- and Φ-aromaticity, bond stretch isomerism, *etc.* are exhibited by several other all-metal clusters (Zubarev et al., 2009; Zubarev and Boldyrev, 2011). Be_3^{2-}, Ca_3^{2-}, and Mg_3^{2-} clusters are classified as aromatic in terms of the ΔX indices (Roy and Chattaraj, 2008; Giri et al., 2010). Other applications of aromatic clusters are studied by our group through molecular electronic transport (Khatua et al., 2008), hydrogen storage (Havenith et al., 2005; Giri et al., 2011a; Giri et al., 2011b; Das and Chattaraj, 2012; Srinivasu et al., 2012; Pan et al., 2012b), and Zn–Zn and Be–Be bond stabilization (Chattaraj et al., 2008; Roy and Chattaraj, 2008) in the domain of CDFT. The ΔX and NICS parameters show their versatility in quantifying the aromaticity of not just planar and cyclic systems, but also any other nonplanar closed structure. They are both easily computable and ΔX also has a conceptual lucidity since it originates from the electronic structure principles of CDFT.

Structure, Bonding, and Reactivity of Various Molecular Electrides

Certain chemical entities contain loosely bound electrons not directly connected to any atom(s) within the cluster, but trapped

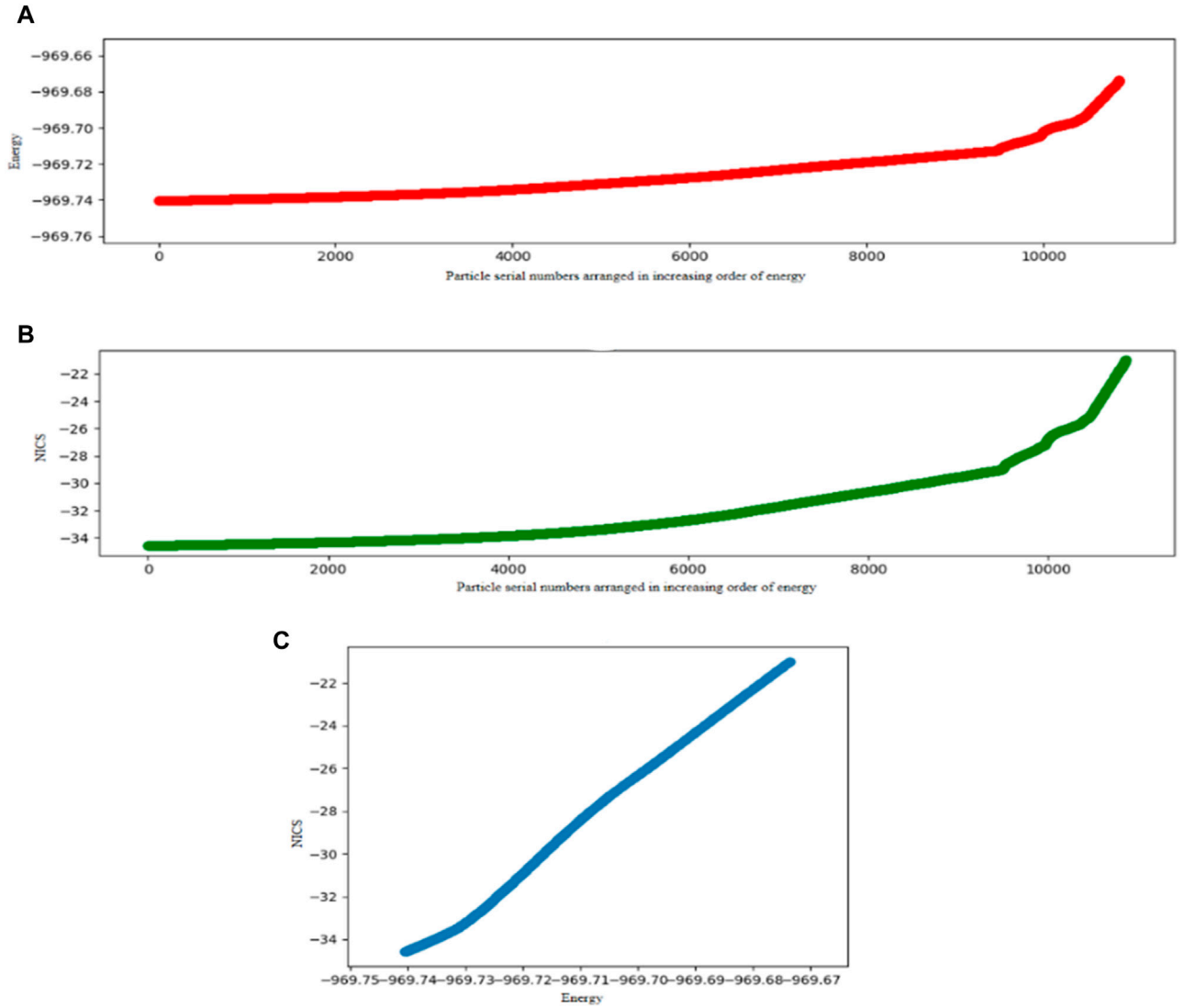

FIGURE 4 | Energy profiles (in a.u.) and Nucleus-Independent Chemical Shift (NICS) values on Al_4^{2-} where 4**(A)**, 4**(B),** and 4**(C)** represent plots of Energy vs. Particle serial numbers arranged in an increasing order of energy, NICS *vs*. Particle serial numbers arranged in an increasing order of energy and NICS vs. Energy, respectively. (Reprinted from Mitra et al., 2020 with permission from Theoretical Chemistry Accounts, Springer Nature. Copyright© 2020, Springer-Verlag GmbH Germany.).

within a hollow space (cavity of cage compounds or packing void in crystals) that act as anions. Such entities are known as electrides and they are known for their nonlinear optical (NLO) properties. Besides showing NLO properties, which is considered to be an identifiable character of an electride, it is also widely applicable in electron emission, catalysis, reversible hydrogen storage, super conductivity, *etc.* (Toda et al., 2007; Xu et al., 2007; Kitano et al., 2012). Organic electrides of crown ethers and cryptands (Ellaboudy et al., 1983; Ward et al., 1988; Dawes et al., 1991; Xie et al., 2000), and inorganic electrides such as $[Ca_{24}Al_{28}O_{64}]^{4+}(4e^-)$ (Matsuishi et al., 2003), Y_5Si_3 (Lu et al., 2016), $[Ba_2N_2](e^-)$, $[Li_2Ca_3N_6](2e^-)$ (Qu et al., 2019), $[Ca_2N]^+(e^-)$ (Lee et al., 2013), $[Y_2C]^{1.8+}\cdot 1.8e^-$ (Zhang et al., 2014), Sr_5P_3 (Wang et al., 2017), and Yb_5Sb_3 (Lu et al., 2018) are well reported in the literature. A different class of electrides, known as molecular electrides, are basically guest@host complexes containing a significant amount of localized electron cloud within the void of the host. Cavity-containing molecular structures such as decaborane (Muhammad et al., 2009; Muhammad et al., 2011), pyrrole (Chen et al., 2005), tetracyanoquinodimethane (TCNQ) (Li et al., 2009), fullerene cages (Das et al., 2020), $C_{20}F_{20}$ (Wang et al., 2012), $C_{60}F_{60}$, extended (3.1.3.1) porphyrin (EP) (Saha and Chattaraj, 2018), and many more are utilized for this purpose. The guest atoms are usually alkali and alkaline earth metals. For a guest@host complex to be characterized as a molecular or cluster electride, certain criteria need to be fulfilled such as the presence of a non-nuclear attractor/maximum (NNA/NNM) (a non-nuclear critical point with a local maximum of electron density), a negative Laplacian of electron density $[\nabla^2\rho(r_c)]$, presence of an ELF basin near the

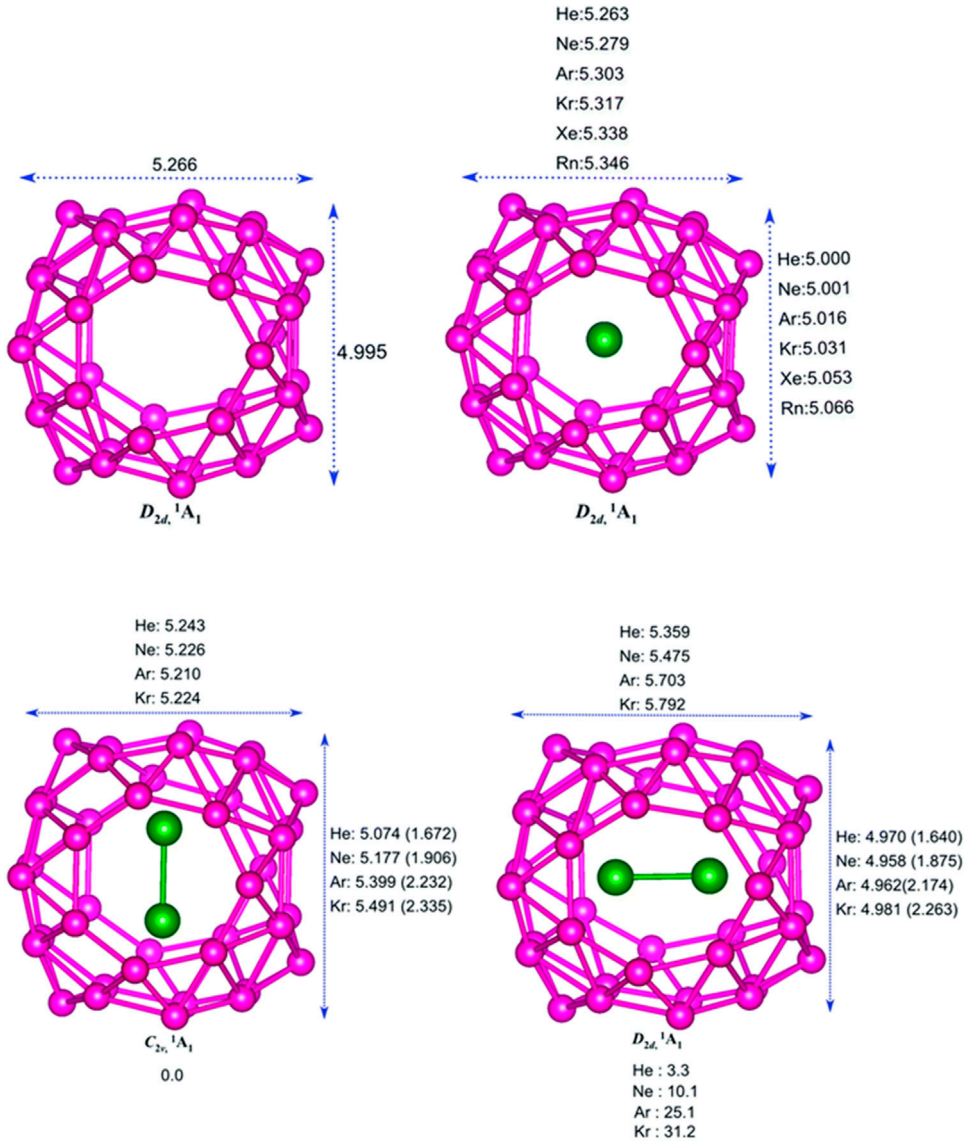

FIGURE 5 | Optimized structures of B_{40}, $Ng@B_{40}$, C_{2v}, and D_{2d} isomers of $Ng_2@B_{40}$ optimized at the ωB97X-D/def2-TZVP level. (Adapted from Pan et al., 2018 with permission from the PCCP Owner Societies.).

NNM, high NLO properties, and a green region in the NCI plot showing accumulation of electron density.

The Mg_2EP complex studied at the M06-2X-D3/6-311G(d,p) level of theory (Saha and Chattaraj, 2018) shows the presence of NNA in between the two Mg atoms where the value of $\nabla^2\rho(r_c) < 0$, with an ELF basin nearby. The electron population at said NNA is 1.02 *e* with 46% localization. The NLO properties in terms of $\overline{\alpha}$, β, and $\gamma_{\parallel}$ are calculated and compared with other electride systems that show that $\overline{\alpha}$ is higher while β and $\gamma_{\parallel}$ are lower in the studied systems. The donation of the loosely trapped electron to antibonding MOs of certain bonds in small molecules (H-H in H_2, C-O in CO_2, N-O in N_2O, and C-H in CH_4 and C_6H_6) results in the activation followed by the dissociation of the respective bonds (Saha and Chattaraj, 2018). Another study (Saha et al., 2019) performed by our group utilizes the modified form of β-diketiminate ligand (^{Dipp}Nacnac) to hold four Mg atoms with two equivalent Mg(I)-Mg(I) bonds ($[Mg_4(^{Dipp}_{H}L)_2]^{2-}$) in its lower energy singlet state. Two NNAs are found to be present at the center of each Mg(I)-Mg(I) bond with an electron population of 1.18 $|e|$ and 52% localization. The calculated values of $\overline{\alpha}$, β, and $\gamma_{\parallel}$ are 891.7, 0.0, and 8.9 × 10^5 a.u., respectively, which clearly indicate the system to be classified as an electride. This system is further stabilized by sandwiching it between two K@crown-6-ether$^+$ $[K@CE]^+$ counter cations. Again, the C_{60} cage trapping a magnesium dimer ($Mg_2@C_{60}$) (Das et al., 2020) and a lithium trimer ($Li_3@C_{60}$) (Das and Chattaraj, 2021a) act as electrides as indicated by the presence of NNA at the center of the Mg-Mg bond path and Li_3 cluster in the respective complexes. The Li_3

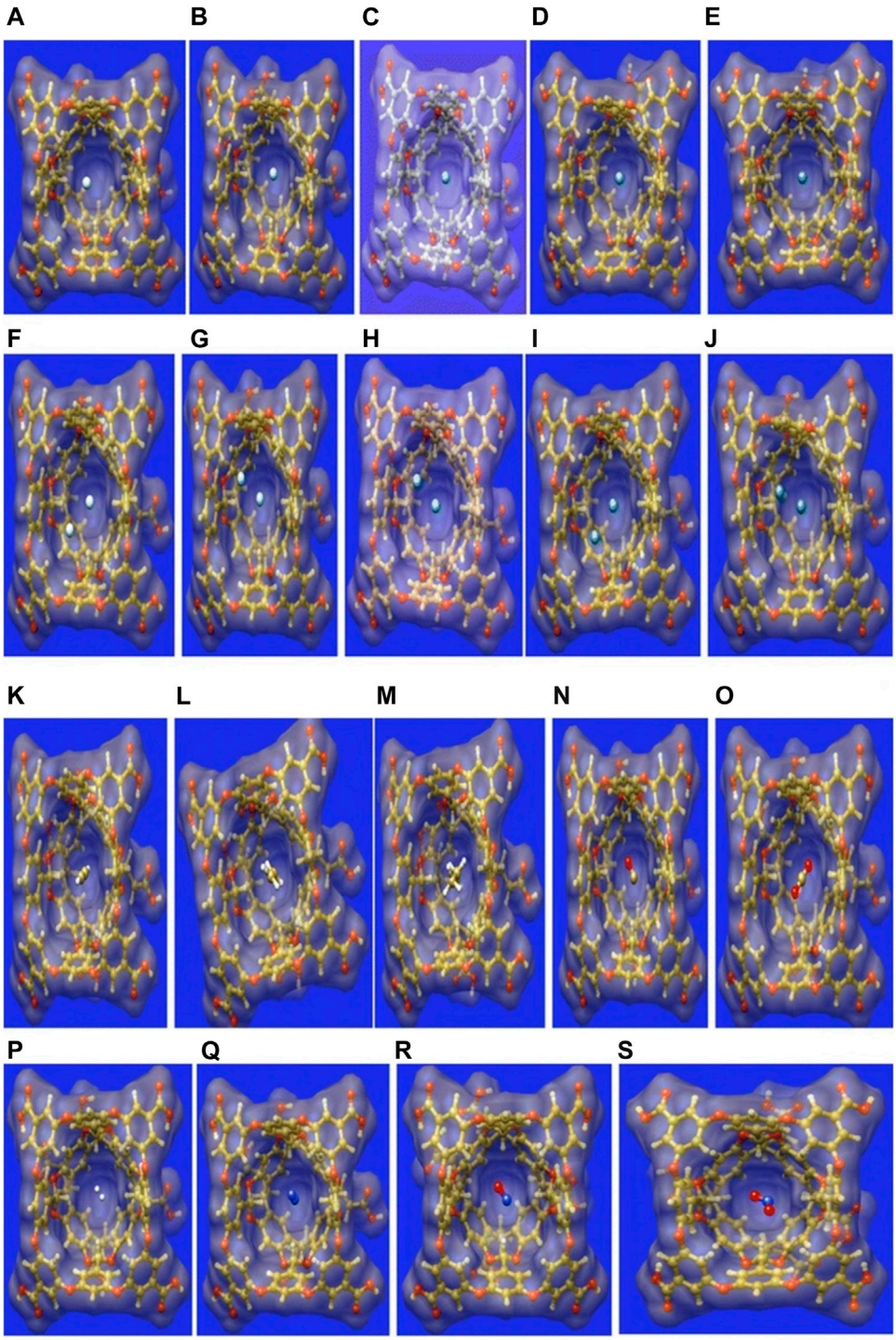

FIGURE 6 | The surface representation of the optimized geometries of the guest encapsulated OA, where the guests are: **(A)** He, **(B)** Ne, **(C)** Ar, **(D)** Kr, **(E)** Xe, **(F)** He_2, **(G)** Ne_2, **(I)** Ar_2, **(J)** Kr_2, **(K)** Xe_2, **(L)** C_2H_2, **(M)** C_2H_4, **(N)** C_2H_6, **(O)** CO, **(P)** CO_2, **(Q)** H_2, **(R)** N_2, **(S)** NO, and **(T)** NO_2. (Adapted from Chakraborty et al., 2016 with permission from Theoretical Chemistry Accounts, Springer Nature. Copyright© 2016, Springer-Verlag Berlin Heidelberg.).

cluster encapsulated within a B_{40} cage ($Li_3@B_{40}$) (Das and Chattaraj, 2020) shows a similar behavior with a lower electron population at the corresponding NNA owing to the electron deficiency in the B cage atoms. Binuclear sandwich complexes formed with Be and Mg dimers with $C_5H_5^-$, N_5^-, P_5^-, and As_5^- ligands forming $M_2(\eta^5\text{-L})_2$ complexes (Das and

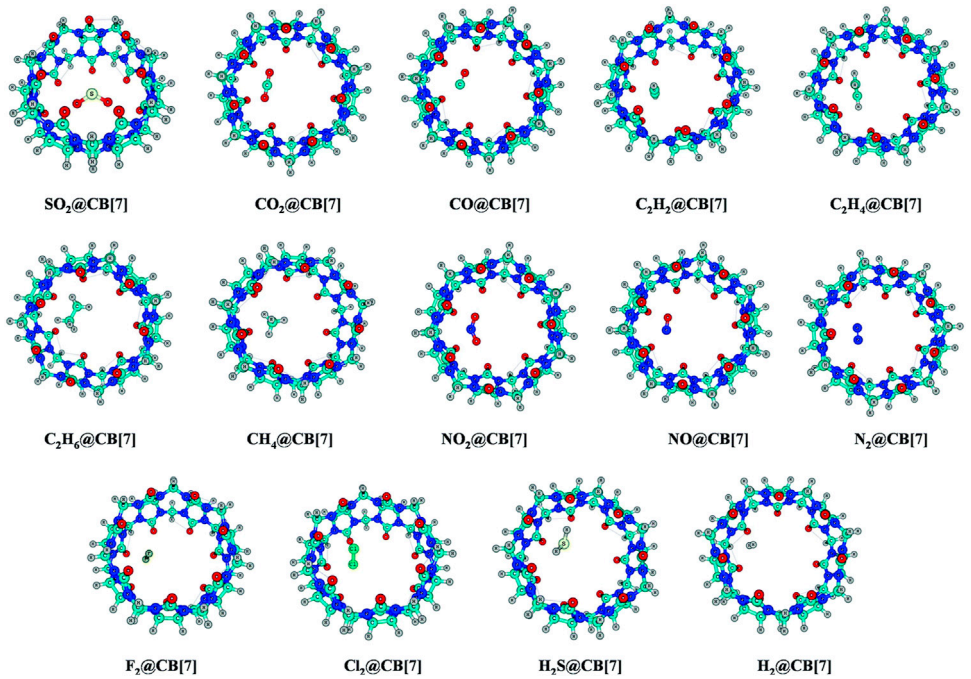

FIGURE 7 | Optimized geometries of the guest encapsulated CB[7] systems at the ωB97X-D/6-311+G(d,p) level of theory. (Reproduced from Pan et al., 2017 with permission from the PCCP Owner Societies.).

Chattaraj, 2020) contain NNAs at the center of the M-M bonds with population varying between 0.95 and 1.39 and percentage localization ranging within 43–62%. Discernible substituent effects on electride characterizers have also been reported (Das and Chattaraj, 2021b).

Noble Gas Encapsulated B_{40} Cage

The encapsulation of noble gas (Ng) atoms in B_{40} cavitand along with their structure and interactions of Ng with the Ng and B atoms in the host–guest complex is discussed with the help of DFT-based computations (Pan et al., 2018). Dissociation energy (ΔE_{diss}) and Gibbs free energy change (ΔG_{diss}) are calculated to study the stability of the encapsulated complexes. NBO, EDA, and NOCV calculations have been done for studying the nature of bonding. The optimized structure of the B_{40} cage along with the $Ng@B_{40}$ and $Ng_2@B_{40}$ systems (at ωB97X-D/def2-TZVP level) are depicted in **Figure 5**. The size of the B_{40} cage is suitable to accommodate He and Ne atoms at its center, whereas for heavier atom (Ar-Rn) encapsulation, the cavity diameter expands with the help of a certain amount of energy (preparation energy, ΔE_{prep}). Although these complexes are thermochemically unstable, they remain in their encapsulated form on account of their high kinetic barrier. Despite that, the lighter Ng encapsulated complexes have very low ΔE_{diss} (−1.8 kcal mol^{-1} for He and −7.1 kcal mol^{-1} for Ne) as compared with the experimentally identified $He@C_{20}H_{20}$ complex (−33.8 kcal mol^{-1}). For the heavier Ng atom-encapsulated $Ng@B_{40}$ systems (Ng = Kr-Rn), the ΔE_{diss} increases with the size of Ng. The possibility of releasing Ng atoms in the dissociation process is either through B_7 or B_6 holes for the lighter He-Ar atoms, whereas the heavier ones can only escape through the B_7 holes due to their larger size. Decapsulation through the B_7 hole has $\Delta G^{\neq}$ values ranging within 84.7–206.3 kcal mol^{-1}. The rate constant (k) calculated at 298 K for the dissociation through either the B_7 or the B_6 hole comes out to be pretty low suggesting that all the $Ng@B_{40}$ systems are kinetically stable.

In the case of two Ng atoms encapsulation, the inter atomic distance decreases from that of their free state. For $Ar_2@B_{40}$ and $Kr_2@B_{40}$, larger repulsion results in the exergonic dissociation of $Ng_2@B_{40}$ into Ng and $Ng@B_{40}$. Along with this, large ΔE_{prep} indicates the nonviability of Ar_2B_{40} and Kr_2B_{40}. For even heavier Ng atoms (Xe and Rn), no minimum energy structures are obtained for the corresponding dimer encapsulation. The corresponding transition states of the Ng release process of $Ng_2@B_{40}$ (Ng = He-Ar) suggest that one Ng atom approaches and leaves through the B_7 rings, while the other remains near the center of the cavity. The associated $\Delta G^{\neq}$ values for the He and Ne dimer encapsulated complexes are high enough for them to be kinetically viable.

The B_{40} cage exhibits a fluxional behavior due to the continuous interconversion between the B_6 and B_7 rings caused by the transfer of one B center from B_7 to B_6. The encapsulated system, $Ng@B_{40}$, also shows similar dynamic behavior as that of the bare B_{40}. The Ng atom inside the cage does not have any substantial influence on the fluxionality of the cage which is reflected in the free energy barrier values (16.4 kcal mol^{-1} for the bare cage, and a range of 16–18.9 kcal mol^{-1} for $Ng@B_{40}$). Topological analysis of $Ng@B_{40}$ explains the nature of the interactions therein. $\nabla^2\rho(r_c)$ and $H(r_c)$ values being positive at the BCPs of Ng-B bond suggest the presence of noncovalent character in most of the complexes except for $Rn@B_{40}$, Ar_2B_{40}, and Kr_2B_{40}, where $H(r_c) < 0$. For the encapsulation of Ng_2 (Ng =

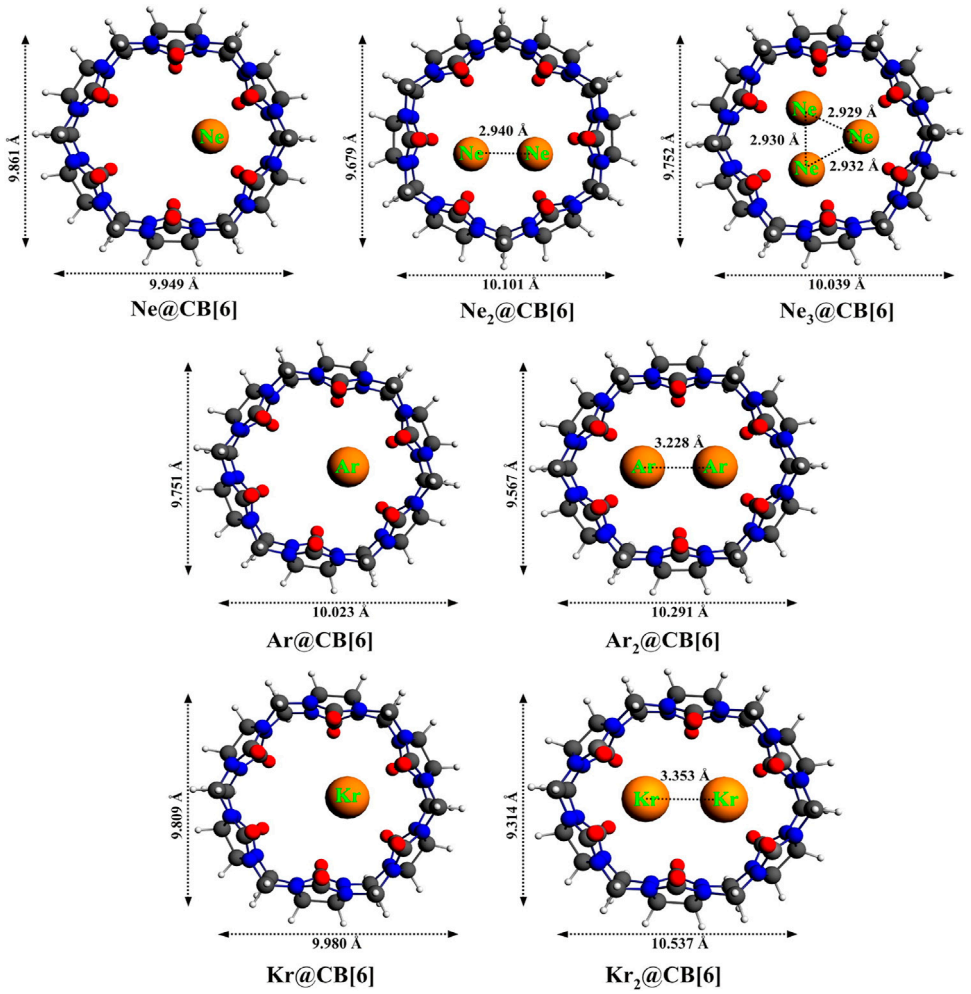

FIGURE 8 | Optimized geometries of noble gas encapsulated CB[6] complexes at the ωB97X-D/6-311G(2d,p) level. (Reprinted with permission from Pan et al., 2015. Copyright© 2015, American Chemical Society.).

Ar_2 & Kr_2) the Ng-Ng bond becomes partially covalent in contrast to their noncovalent character in the free state, except in the cases of $He_2@B_{40}$ and $Ne_2@B_{40}$ where no covalency is imparted. From NBO analysis it has been shown that Ng → B_{40} charge transfer increases with increasing the size of the Ng atoms. The electron transfer further increases in the case of Ng_2 encapsulation. Along He–Rn, an increase in WBI values indicates that the increasing size of Ng atoms increases the degree of covalency between the Ng and B centers. EDA analysis reveals a high positive ΔE_{pauli} which leads to positive ΔE_{int} suggesting the interaction to be repulsive in case of the heavier noble gas encapsulated B_{40} systems. Also, both the attractive terms, ΔE_{elstat} and ΔE_{orb}, increase with the increasing size of Ng atoms.

Small Gas Molecule Encapsulation Within Octa Acid Cavitand

Small gas molecules such as C_2H_2, C_2H_4, C_2H_6, CO, CO_2, NO_2, NO, N_2, H_2, and Ng atoms (He_n-Xe_n, n = 1,2) are selected as guest molecules encapsulated in OA cavitand (**Figure 6**) and analyzed via DFT approach (Chakraborty et al., 2016). The systems under study are optimized at the ωB97X-D/6-311G(*d*,*p*) level of theory (LanL2DZ basis set with ECP is used for Xe). There are two possible cavities for the accommodation of the guest atoms, the inner cavity of OA is more suitable as it increases the host–guest interaction. In the case of Ng@OA, due to encapsulation of Ng atoms, no notable distortion is observed in the OA. For Ng_2@OA systems, one guest atom can occupy the center of the host cavity, whereas the other one remains in the outer cavity. The Ng–Ng bond distances inside OA are 3.6, 3.7, 3.8, 3.9, and 4.1 Å, respectively, for He_2, Ne_2, Ar_2, Kr_2, and Xe_2. In the cases of CO@OA and NO@OA, the guest molecules prefer to stay in the inner cavity of OA. Their orientation with respect to the two nearest benzene-like fragments is almost perpendicular, whereas it is parallel to the rest of the benzene fragments of OA. The presence of these π electron clouds close to the encapsulated guests is expected to have a significant impact on the stability of the complexes, the nature of interaction, and dynamical behavior

as well. For N_2@OA and H_2@OA, N_2 and H_2 remain well inside the inner cavity. Thermochemical study reveals that except for He@OA, in all cases, D_0 value is positive indicating the stability of the host–guest complexes concerning their dissociation into the corresponding individual components. Going from lighter to heavier Ng atoms (also for Ng_2@OA), D_0 value increases, *i.e.*, the host–guest interaction increases. This could most likely be due to the increasing polarizability of the Ng atoms down the group. The dissociation channels for all the encapsulated complexes have positive D_0 values. Most of them, however, dissociate spontaneously at room temperature except in the cases of Kr, Kr_2, Xe, C_2H_2, C_2H_4, C_2H_6, and N_2 guest molecules. Thus, the encapsulation of the mentioned guest molecules is favorable at 298 K. In the cases of NO/NO_2@OA and CO/CO_2@OA, an increase in D_0 value is observed from NO to NO_2 and from CO to CO_2. It can thus be deduced that the encapsulation of NO_2 and CO_2 inside OA forms more stable complexes compared with NO and CO, respectively. Having said that, it is to be noted that all the four complexes have favorable dissociation channels at room temperature. The hydrocarbons have better interaction with the OA and hence are not prone to dissociation at ambient temperatures.

The interaction between the host and guest moieties is analyzed with the help of NBO, NCI, and EDA. All the Ng atoms acquire some positive charges, *i.e.*, transfer of electron density occurs from the Ng atoms to the host OA surface. The donation primarily occurs from the lone pair (LP) of Ng to the C-H antibonding orbital of OA for all the Ng atoms [except Ne where it takes place from LP to antibonding Rydberg state (Ry*)] and for CO, NO, N_2, and CO_2 molecules. WBI values for Ng–Ng and Ng–OA interactions indicate a purely noncovalent character therein. From this discussion it is clear that the confinement brings about an increase in the reactivity of all the guest atoms/molecules within the OA. NCI isosurfaces show the presence of green surface around the guest molecules indicating van der Waals interaction that stabilizes the host–guest complexes. EDA results show that there exists closed shell type of interaction between guest Ng/H_2 and OA. The ΔE_{disp} and ΔE_{orb} are the largest and the smallest contributors toward the total attractive interaction, respectively. The former increases in magnitude with increasing size of the encapsulated Ng atoms. For the guest hydrocarbons, the contribution from ΔE_{disp} increases and ΔE_{elstat} decreases with the increasing number of H atoms. This is because the molecules such as C_2H_2 and C_2H_4 containing labile electron cloud can accumulate enough positive charge to favorably interact with the electron-rich fragments of the OA. This makes the contribution from ΔE_{elstat} very important in stabilizing these complexes. The contribution from charge transfer and polarization are very less toward ΔE_{tot} as indicated by the very low values of ΔE_{orb}. A similar type of situation is observed for CO/CO_2@OA complexes. For nitrogen-containing guests, the ΔE_{orb} outweighs the ΔE_{elstat} contribution toward ΔE_{tot}. Since the main stabilizing factor for all the complexes is ΔE_{disp}, the nitrogen-containing guest molecules are prone to be affected by the polarization or charge transfer by OA, in comparison with the other guest molecules. ADMP simulation performed at 298 K shows that all the Ng atoms (except Ne) are prone to leaving the cavity, whereas at 50 K they remain within the OA. Polar molecules such as CO, CO_2, NO, and NO_2 have a higher tendency to stay within the OA than the nonpolar H_2. Again, C_2H_2, C_2H_4, and N_2 containing π electron cloud also prefer to stay inside OA. From the above thermochemical, kinetic, and dynamical analyses, it can be said that OA makes a reasonably good choice for accommodating gas molecules.

Cucurbit[*n*]urils as a Host Moiety

Cucurbiturils are methylene-linked macrocyclic molecules having glycoluril unit [=$C_4H_2N_4O_2$=] as a building block. This repeating glycoluril unit can bind with hydrogen with sufficient amount of binding energy. Thus CB[*n*] can be designed as an effective hydrogen storage compound. The nitrogen and the oxygen centers are found to be the most active centers to bind with hydrogen with positive binding energy. It was found that $(CH_3)_2C_4H_2N_4O_2(CH_3)_2$ unit can interact with total 13H_2 atoms (Pan et al., 2013a). Since hydrogen has an electric quadrupole moment, a charge–quadrupole interaction plays a pivotal role in binding the hydrogen with the host. NPA charge analysis reveals that the charge transfer occurs from the N and O centers to the σ^* orbital of H_2 molecule.

Among the CB[*n*] family, CB[7] can accommodate five H_2 molecules endohedrally. The O centers can adsorb a total of 28 H_2 molecules (two per O atom) and 19 H_2 molecules get adsorbed at the N centers exohedrally, making it a total of 52 hydrogen molecules. The binding energy and adsorption enthalpy are positive and negative, respectively, indicating CB[7] to be a potentially promising H_2 storage material. The gravimetric wt % of hydrogen for the CB[7] adsorbing 52 H_2 molecules comes out to be 8.3 with an average binding energy of 7.8 kJ mol^{-1}. These values are very encouraging when compared with various other potential hydrogen storage materials such as α-cyclodextrin (Zhu et al., 2010), COFs (Klontzas et al., 2008; Li et al., 2010), MOFs (Bhatia and Myers, 2006; Vitillo et al., 2008), Li-doped nanotubes (Wu et al., 2008), and polyacetylenes (Li and Jena, 2008), with average binding energies ranging within 5–8 kJ mol^{-1}.

The endohedral adsorption of gas molecules such as C_2H_2, C_2H_4, C_2H_6, CH_4, CO, CO_2, NO_2, NO, N_2, H_2, F_2, Cl_2, H_2S, and SO_2 into the CB[7] cavitand is depicted in **Figure 7**. Geometry optimizations are performed at the ωB97X-D/6-31G(d,p) and ωB97XD/6-311+G(d,p) levels (Pan et al., 2017). Both the CB[7] cage and the encapsulated gas molecules remain unaffected by the encapsulation. For SO_2 encapsulation, the binding enthalpy shows the highest value (14.3 kcal mol^{-1}) followed by Cl_2 and C_2H_2 (11.6 and 10.4 kcal mol^{-1}, respectively). CB[7] also encapsulates C_2H_4 and C_2H_6 more favorably than CO_2, NO_2, and H_2S. The binding enthalpies for NO/F_2/N_2/CO/CH_4@CB[7] systems vary from 4.7 to 5.8 kcal mol^{-1}, the highest value corresponding to CH_4. From the enthalpy values it is clear that CB[7] can selectively adsorb SO_2 among various gas molecules, and hence can be applicable in the SO_2 separation process from gas mixtures. ΔG value suggests that C_2H_6 is less prone to be encapsulated than CO_2 inside CB[7]. SO_2, Cl_2, and C_2H_2 adsorb with negative ΔG values, whereas those of C_2H_4 and CO_2 are slightly endergonic (0.6–0.7 kcal mol^{-1}). The corresponding ΔG values for the adsorption of C_2H_6, N_2, F_2, NO_2, NO, and H_2S vary

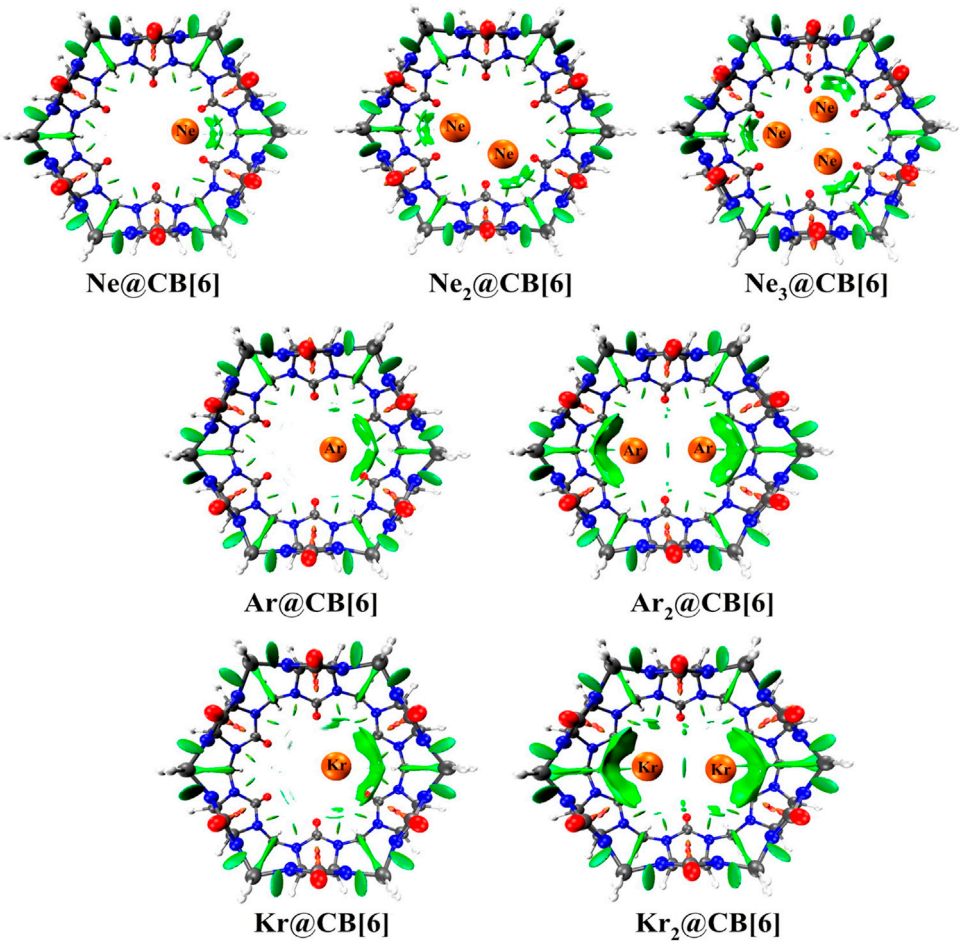

FIGURE 9 | NCI plots of Ng_n@CB[6] complexes. (Reprinted with permission from Pan et al., 2015. Copyright© 2015, American Chemical Society.).

within 1.3–2.8 kcal mol^{-1} at 298 K temperature. EDA results show that for all the discussed complexes, ΔE_{disp} contributes more toward the stabilization of the host–guest systems. ΔE_{elstat} term also plays an important role here. In the hydrocarbons, as the number of H atoms increases, ΔE_{elstat} decreases gradually due to the reduction in the acidic character of the H atoms. Higher ΔE_{elstat} and lower ΔE_{pauli} values in the SO_2 encapsulated complex make the interaction between the host and the guest stronger than for C_2H_4 and C_2H_6 analogues. This again validates the higher SO_2 selectivity of CB[7].

Cucurbit[6]uril, among the CB[*n*] family, is found to be a compatible host for the encapsulation of Ngs within its cavity (Pan et al., 2015). The optimized geometries at the ωB97X-D/6-311G(2*d*,*p*) level of theory of the Ng_n@CB[6] complexes are provided in **Figure 8**. CB[6] effectively accommodates three Ne atoms, but can only trap two of the large Ar and Kr atoms. No significant distortion in the cage is observed for trapping all the three Ne atoms or for the first atom of Ar and Kr, whereas inserting a second atom deforms the shape of the host. The Ng dissociation process becomes more endothermic as we move from Ne to Kr. At 298 K, the dissociations of all Ng_n@CB[6] are exergonic except Kr@CB[6]. At 77 K, apart from the second Ng (Ar and Kr) atom dissociation from Ng_2 encapsulated CB[6], all dissociations become endergonic. Kr encapsulation at 298 K and 1 atm pressure is thermochemically favorable, whereas for Ne and Ar encapsulation, high pressure and moderately low temperature are preferred.

NPA charge analysis reveals N and O to be negatively charged in Ng_n@CB[6], while C and H have positive charges. Slight charge transfer (~0.01 e^-) occurs from Ng→CB[6] moiety. Small $\rho(r_c)$ value and positive $\nabla^2\rho(r_c)$ and $H(r_c)$ values from topological analysis suggest the interaction to be of closed shell type. ELF analysis shows an absence of electron localization between the Ng-Ng and Ng-cage atoms, corroborating the result obtained from AIM. EDA analysis reveals the contribution from ΔE_{disp} to be the largest, followed by ΔE_{elstat}, and the smallest contribution is from ΔE_{orb}, all of which gradually increases going from Ne to Kr. The green surfaces observed between the Ng and CB[6] units in the NCI isosurface (**Figure 9**) are an indication of a small van der Waals interaction, which increases with the size of the Ng atoms. The dynamical study (*ab initio* MD) for 1 ps and at 298 K reveals that Ne and Ar remain inside the cavity, whereas Kr and all the Ng_2 in Ng_2@CB[6] move toward the open end but do not leave the cage. At 77 K, all guests stay inside the host.

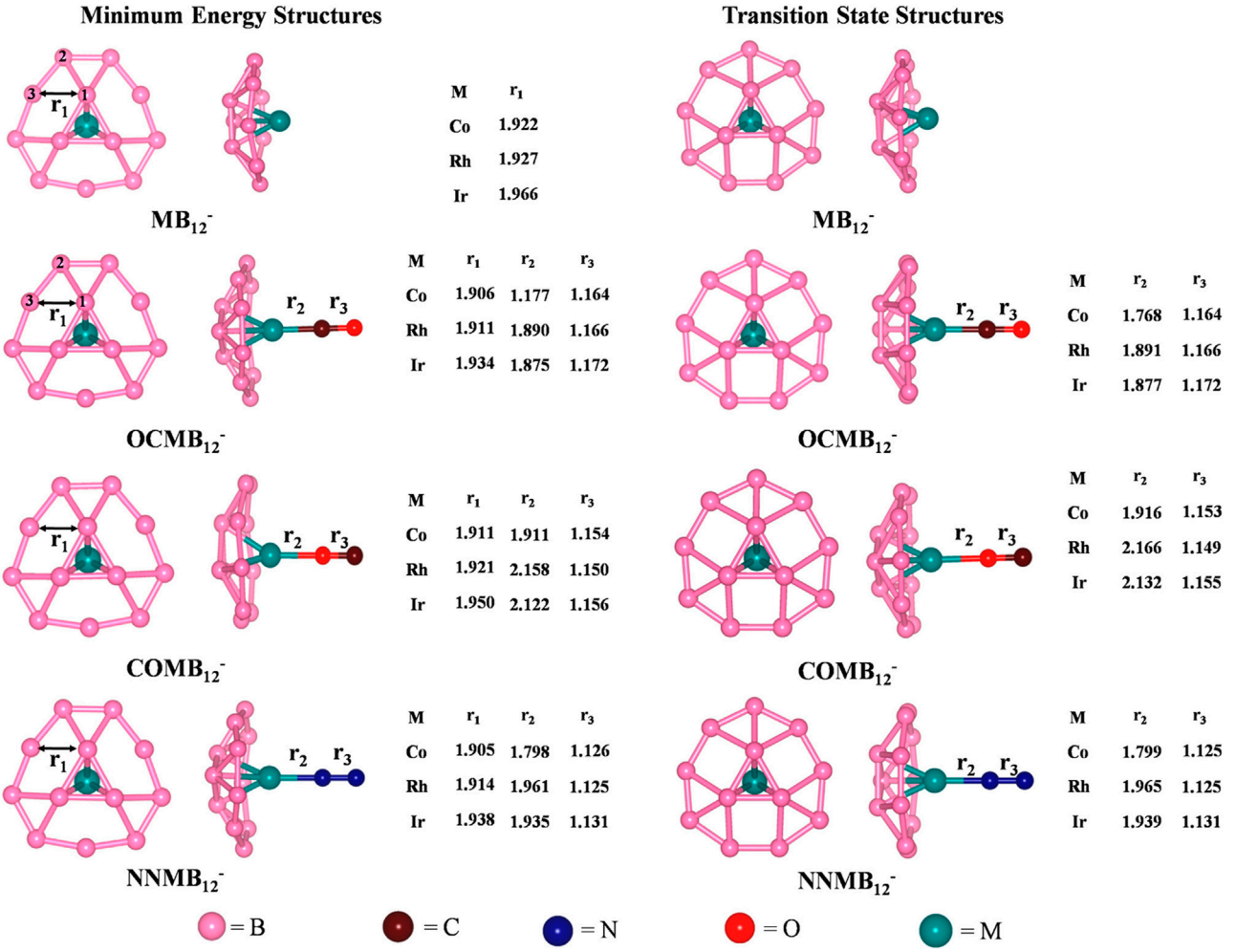

FIGURE 10 | Optimized geometries of MB_{12}^- and ligand bound MB_{12}^- at the PBE/def2-TZVPPD level, and their transition state structures for the internal rotation of the B_3 ring. Bond distances are provided in Angstrom unit. (Reprinted with permission from Saha et al., 2017. Copyright© 2017, American Chemical Society.).

Small Molecules Bound Metal Coordinated Boron Cluster

The activation of small molecules by a metal-supported boron cluster is studied through DFT calculations (Saha et al., 2017). They are known to be applicable in nanomaterial building blocks, automobiles (Norbye, 1971; Jiménez-Halla et al., 2010) *etc.* The global minimum energy structures calculated at PBE/def2-TZVPPD (Perdew et al., 1996; Weigend and Ahlrichs, 2005) level of MB_{12}^-, $CO@MB_{12}^-$, $N_2@MB_{12}^-$ clusters and their corresponding TSs for the internal rotation of the B_3 ring are provided in **Figure 10**. The coordination of the small molecules with the MB_{12}^- cluster forms an umbrella-shaped structure in which the M-L bonds act like the stick of the umbrella. The coordination of CO with the metal center can take place through both the C and O ends, the former producing a more stable isomer. For both $OCMB_{12}^-$ and $NNMB_{12}^-$, the Ir-L bond has the highest strength, followed by Co and Rh, while for a particular M center, CO forms a stronger bond than N_2. ΔG values of these complexes are highly positive which suggest that the corresponding complexes are thermodynamically stable concerning the dissociation process. The O-side bound isomers, however, have low positive ΔG for Co and Ir, and become slightly negative for Rh. They can be made viable by lowering the temperature. The N–N and C–O bonds get lengthened due to complexation in the order $COMB_{12}^-$ < $N_2MB_{12}^-$ < $OCMB_{12}^-$ causing a red shift in their bond stretching frequencies which is the highest for the Ir analogues.

NBO analysis reveals that upon complexation, the metal centers get more negatively charged, apart from $COIrB_{12}^-$ and $NNIrB_{12}^-$, where Ir still contains positive charge (less than that in IrB_{12}^-). L→M and M→L back transfers take place, and in certain complexes the latter completely compensates (or overcompensates) the former which is indicated by the zero (or negative) charge on the ligand. The Wiberg bond indices suggest that the covalent character follows the order M-C in $OCMB_{12}^-$ > M-N in $N_2MB_{12}^-$ > M-C in $COMB_{12}^-$. From EDA-NOCV, it is seen that the bonding between the metal and the ligand is predominantly orbital and electrostatic interactions

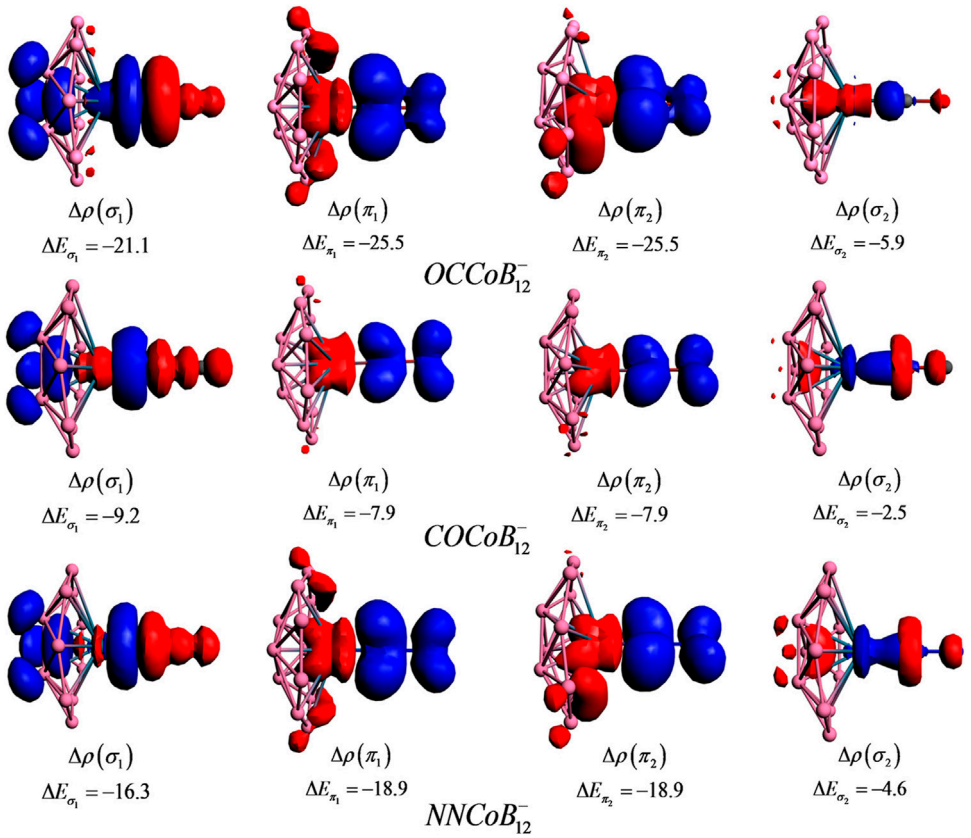

FIGURE 11 | Deformation density plots of the pairwise orbital interactions in $LCoB_{12}^-$ (OC, CO, and NN) systems at the revPBED3/TZ2P//PBE/def2-TZVPPD level. Energies are provided in kcal/mol. (Reprinted with permission from Saha et al., 2017. Copyright© 2017, American Chemical Society.).

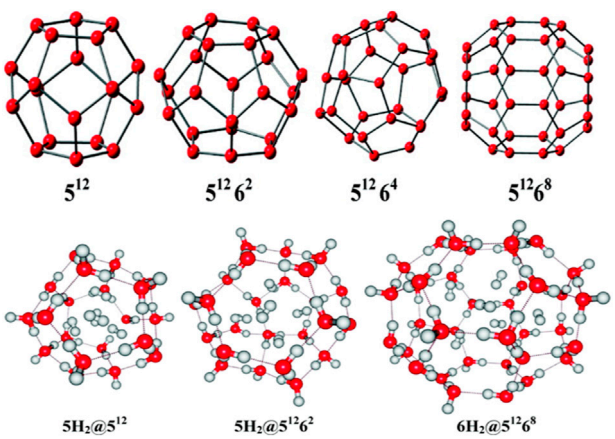

FIGURE 12 | Optimized geometries of the clathrate hydrates along with their maximum possible H_2 molecule encapsulated complexes. (Adapted with permission from Chattaraj et al., 2011. Copyright© 2011, American Chemical Society.).

(in more or less equal contributions), indicating the L-M bonds to have both covalent and ionic characters. For $OCMB_{12}^-$, however, the contribution from ΔE_{elstat} is higher than ΔE_{orb}. **Figure 11** shows the deformation densities [$\Delta\rho(r)$] for the pairwise orbital interactions for the LMB_{12}^- complexes, where a shift in the electron density occurs from the red to the blue region. The $\Delta\rho(\sigma_1)$ plot reveals that the shift of electron density occurs through the L→M→B scheme. $\Delta\rho(\pi_1)$ and $\Delta\rho(\pi_2)$ explain the π electron density shift from the $d_{L\rightarrow M}$. The extent of L←M π-back-donation is greater than the L→M σ-donation, causing a red-shift in its stretching frequency. The σ-donation occurs from the $HOMO_{(CO)}$ to the $LUMO_{(LMB_{12}^-)}$ fragment and π-back-donations occur from the degenerate $HOMO_{(MB_{12}^-)}$ to the degenerate π* $LUMO_{(CO)}$.

An internal rotation of the inner B_3 ring with respect to the outer B_9 ring occurs within the MB_{12}^- cluster. The energy barrier associated with this rotation is reported (Popov et al., 2014; Liu et al., 2016) to follow the order Co > Rh > Ir. BOMD simulation at 800 K shows the L-M bonds to be intact during the rotation. This makes the complex seem like a spinning umbrella with the L-M bond as the stick.

Hydrogen Storage in Clathrate Hydrates, Li-Doped Clusters, and Super Alkalis

Clathrate hydrates, a class of inclusion compounds, are known to encapsulate guest compounds within its hydrogen bonded polyhedral cage (Mao et al., 2002; Mao

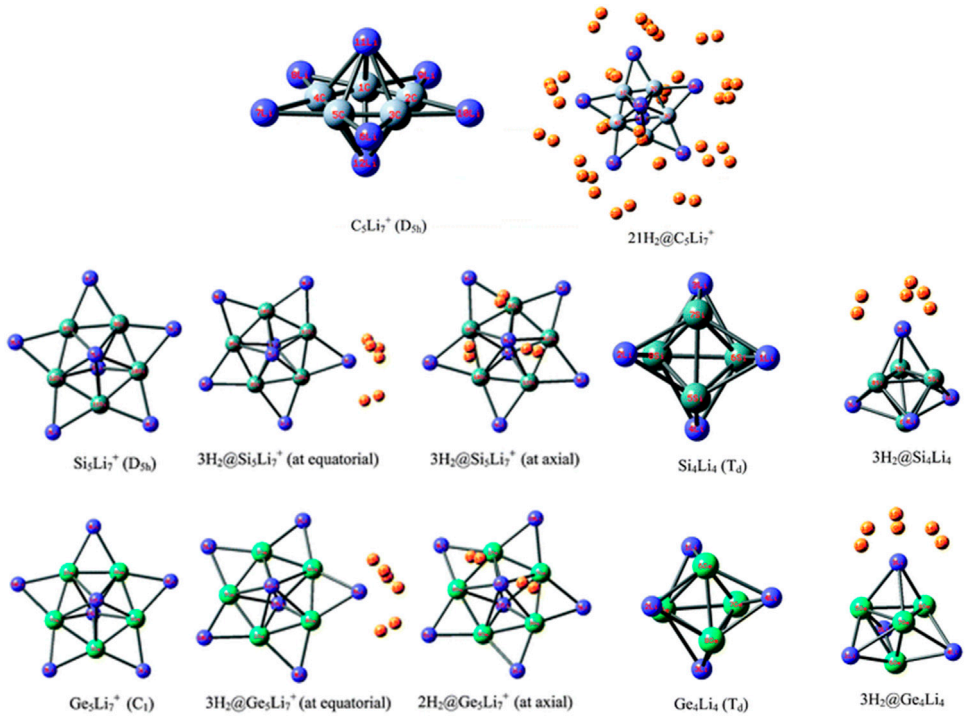

FIGURE 13 | Optimized structures of $C_5Li_7^+$, $M_5Li_7^+$, M_4Li_4 (M = Si, Ge) and their H_2-trapped analogues at the M06/6-311+G(d,p) level. (Adapted from Pan et al., 2012b with permission from the PCCP Owner Societies.).

and Mao, 2004; Lee et al., 2010). They constitute a very effective host for hydrogen storage. Four types of clathrate hydrates and their maximum possible hydrogen-encapsulated complexes studied at B3LYP/6-31G(d) level (Chattaraj et al., 2011) are depicted in **Figure 12**. 5^{12} represents the cavity having 12 pentagonal faces, whereas $5^{12}6^k$ (k = 2,4,8) represents 12 pentagonal faces along with k hexagonal faces. Here we discuss the structure, bonding, and stability of the bare and hydrogen-encapsulated complexes from a density functional theory perspective. For $nH_2@5^{12}$ complexes it is seen that for the first H_2 encapsulation, the process is energetically favorable although the overall nH_2 encapsulation is method dependent. Owing to the small size of 5^{12} cavity, it can accommodate a maximum of five H_2 molecules, after which a deformation in the cavity is observed. The GM for H_2 confinement in the 5^{12} cavity occurs endohedrally. The H_2 molecules favor the inside of 5^{12} more than the outside. In the case of $5^{12}6^2$ cage, it can also take up a maximum of five H_2 molecules. Slight distortion is observed in the system that becomes more noticeable during the third H_2 encapsulation which slowly decreases for the fourth and the fifth hydrogen molecule encapsulation. This is reflected in the slightly conflicting trend in the corresponding interaction energies. Now in the case of $5^{12}6^4$ clathrate, obtaining the minimum energy structure was difficult. It is fascinating to note that the encapsulation of one H_2 into the cage stabilizes the structure although it could not provide with the minimum energy structure. Further incorporation of guest molecules deforms the structure of the system. For $5^{12}6^8$, the interaction energy for all the six H_2 encapsulation is negative making the process favorable. The large size of the host cavity makes it feasible to accommodate all the six guest molecules efficiently. Positive ΔG value suggests that the complexes are kinetically stable. Finally, it can be concluded that the 5^{12} and $5^{12}6^2$ clathrates can encapsulate up to two hydrogen molecules without undergoing any structural distortions, whereas the $5^{12}6^8$ clathrate may entrap up to six H_2 molecules depending upon the level of theory used. Calculation of CDFT-based reactivity descriptors of the complexes with and without H_2 encapsulation suggests that for most of the systems, stability increases with the increase in number of trapped hydrogen molecules. This is concluded from the increasing hardness and decreasing electrophilicity values.

Li ion is popularly known to bind well with hydrogen molecule owing to its positive charge (Pan et al., 2012a). Inspired by this, a number of efforts have been made to effectively polarize the Li center of various clusters to increase its hydrogen adsorbing ability. Here we study the H_2 storage potential of the Li-doped clusters, $M_5Li_7^+$ (M = C, Si, Ge), M_4Li_4 (M = Si, Ge) at the M06/6-311+G(d,p) level, and some super-alkali ions at the M052X/6-311+G(d) level (**Figures 13**, **14**). The Li centers attain a net positive charge due to the high polarizability of the clusters, facilitating electrostatic interactions to bind with the H_2 molecules. The negative values of interaction energies and enthalpies

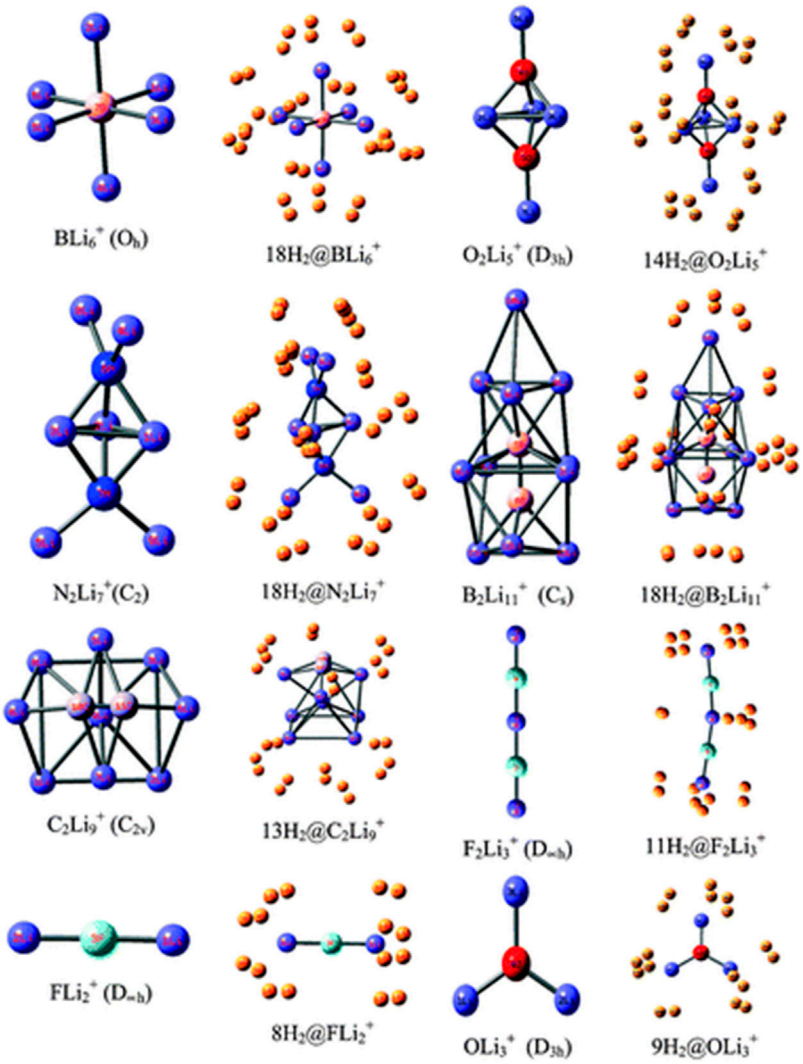

FIGURE 14 | Optimized structures of studied super-alkali ions and their hydrogen-trapped analogues at the M052X/6-311+G(d) level. (Adapted from Pan et al., 2012b with permission from the PCCP Owner Societies.).

indicate the efficacy of these clusters to be good H_2 storage materials. The gravimetric wt% of adsorbed H_2 are 28.0, 18.3, 9.3, 14.7, and 7.1 for $C_2Li_7^+$, $Si_5Li_7^+$, $Ge_5Li_7^+$, Si_4Li_4, and Ge_4Li_4, respectively. For the super-alkali ions, the values range from 13.2 to 40.9%, with the highest being that for BLi_6^+. On applying electric field, a gradual improvement is observed in the interaction energy value. Thus, in terms of gravimetric wt%, BLi_6^+ is preferable whereas the interaction energy per H_2 molecule suggests $B_2Li_{11}^+$ to be the preferred choice for hydrogen storage.

$(HF)_2$ Confinement in Fullerene Cages

The influence of encapsulation on the hydrogen bond strength in $(HF)_2$ within the fullerene cages is studied using DFT and *ab initio* MD (Khatua et al., 2014b). The optimized geometries of $(HF)_2@C_n$ (n = 60, 70, 80, 90) complexes wB97X-D/6-31G are depicted in **Figure 15**. The dissociation energy, enthalpy, and change in free energy are negative for the $(HF)_2@C_{60}$ system which indicates that the encapsulation process is thermodynamically unfavorable, whereas positive values for the rest of the HF encapsulated C_n cages imply them to be favorable (highest being for the C_{80} cage). Owing to the smaller size of the C_{60}, the HF units orient themselves antiparallelly to reduce repulsion at the cost of hydrogen bond strength. Thus, the energy associated with the HF-HF interaction is observed to be highest in the C_{60} cage (positive, and hence repulsive in nature). For all the studied cases, upon encapsulation, the hydrogen bond distance reduces from that in the free state, the least being inside the C_{70} cage. The EDA study reveals that the contribution from ΔE_{pauli} increases and the ΔE_{int} value decreases with decreasing the C_n cage cavity except for C_{80} cage. For the C_{60} cage, a very large value of ΔE_{pauli} makes the overall ΔE_{int} value positive. On account of the smaller H-bond distance within the C_{70} and C_{90} cages compared to the same within the C_{80} cavity,

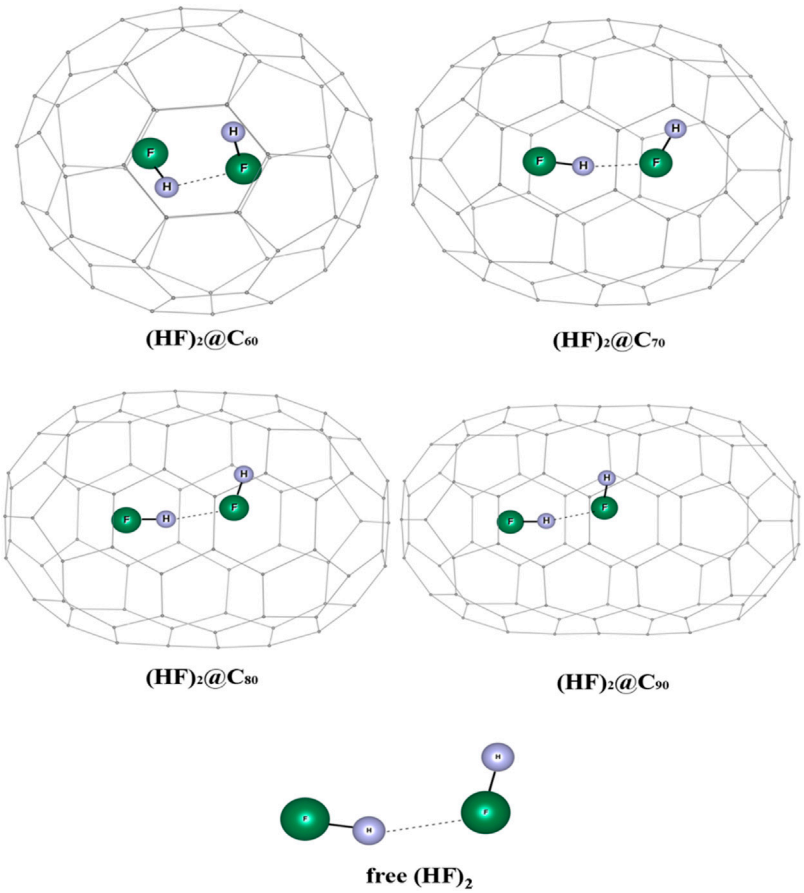

FIGURE 15 | Optimized structures of $(HF)_2@C_n$ (n = 60, 70, 80, 90) and free $(HF)_2$ at ωB97X-D/6-31G level. (Reprinted from Khatua et al., 2014b with permission from Elsevier. Copyright© 2014, Elsevier B.V.).

both the ΔE_{elstat} and ΔE_{orb} contribute more to the attractive interaction than those in C_{80}. AIM analysis reveals that for all these confined systems, $\nabla^2\rho(r_c) > 0$ and $H(r_c) < 0$ implying the partial covalent nature of the hydrogen bonds. The hydrogen bond is mostly covalent in case of $(HF)_2@C_{70}$ ELF analysis that also supports this observation.

CONCLUDING REMARKS

There exists an appreciable amount of interest in the field of cluster chemistry, especially in the gas-phase and surface-adsorbed studies, and for good reasons. Common curiosities in this area include the difference between the properties exhibited by the bulk and individual clusters, how the cluster size affects the overall behavior of the bulk, *etc*. Other important branches of this cluster chemistry include solving their global optimization problem in a fast and cost-effective way, and investigating the effect of confinement on the cluster-encapsulated systems.

The global optimizers discussed in this review are shown to locate the global minimum configurations for small metallic and nonmetallic clusters with less execution time and higher success rate than commonly used optimization algorithms, without having the need to impose any symmetry constraint or any other external restrictions. The only requirement is to adjust the local and global best parameters at each iteration. Comparisons made between our modified PSO with other DFT-integrated BH and SA reveal the superiority of the former with respect to the total execution time and number of iterations the program takes to converge. Again, the DFT-integrated FA turns out to be more efficient than the modified PSO. Furthermore, the ADMP-CNN-PSO technique is well suited for locating the global solution from a huge dataset of initial configurations.

The effect of adsorption and confinement of hydrogen, noble gas atoms, and various other small molecules on their stability, reactivity, nature of interactions, and dynamics are studied from a DFT perspective. The concept of aromaticity is analyzed in terms of CDFT-based descriptors such as E, α, ω, and η, where a lower value of the first three parameters and a higher value of hardness in comparison with that of a reference system characterize an aromatic molecule. The reverse is true for antiaromatic compounds. Certain guest@host complexes containing loosely bound electrons acting as anions and showing high NLO

properties, known as molecular electrides, are capable of bond activation in small molecules. Other host–guest complexes exhibit fluxionality. One such example is the B_{40} cage whose fluxional property remains unaltered even after Ng atoms encapsulation. The complexation ability of the B_{40} cage is also studied in some sandwich complexes and it is seen than the presence of Xe within the cage enhances its complexation ability. The gas molecules accommodated within the Octa acid cavitand become slightly more reactive compared to their free state. Most of the OA-guest complexes are stable with respect to dissociation. OA can thus be designated as a reasonably good storage material for a variety of small gas molecules. Cucurbiturils form another class of compounds which is well known for its hosting capabilities. CB[6] can act as an efficient noble gas carrier and CB[7] can bind up to 52 hydrogen molecules (8.3 wt%). CB[7] is also found to be highly selective toward the adsorption of SO_2 and hence can be used in separating SO_2 from a gas mixture. It is also known to accelerate the otherwise slow [4+2] cycloaddition reaction. The binding ability of the transition metal boron cluster (MB_{12}^-) with isoelectronic species, CO and N_2, is studied along with its fluxionality. Bond activation in both CO and N_2 is observed, and the rotation of the ligand-bound complex makes it look like a spinning umbrella. Hydrogen storage capabilities of clathrate hydrates, Li-doped clusters, and super alkali are investigated and it is found that the former can accommodate 2–6 hydrogen molecules, whereas the Li systems show a gravimetric wt% range of 7.1–28.0% for the star-like clusters and 13.2–40.9% for the super-alkali systems. The $(HF)_2$ encapsulation by the fullerene cages describes the confinement effect on the H-bond therein. Apart from C_{60}, all the cages form the complexes in a thermodynamically favorable process. Also, a partial covalent character is observed in the H-bonds upon confinement.

AUTHOR CONTRIBUTIONS

PKC came up with the concept and design of the review, wrote the abstract, reviewed the final manuscript. RP and AP contributed towards the literature survey, writing the manuscript. All authors contributed to manuscript revision, read, and approved the submitted version.

ACKNOWLEDGMENTS

PKC would like to thank Ambrish Kumar Srivastava for kindly inviting him to contribute an article to the research topic "Atomic Clusters: Theory & Experiments" in the journal, Frontiers in Chemistry. He also thanks DST, New Delhi, for the J. C. Bose National Fellowship, grant number SR/S2/JCB-09/2009, and his students whose work is presented in this article. RP and AP thank CSIR and IIT Kharagpur, respectively, for their fellowships.

REFERENCES

Akhtar, F., Liu, Q., Hedin, N., and Bergström, L. (2012). Strong and Binder Free Structured Zeolite Sorbents with Very High CO2-over-N2 Selectivities and High Capacities to Adsorb CO2 Rapidly. *Energy Environ. Sci.* 5, 7664–7673. doi:10.1039/C2EE21153J

Bader, R. F. W. (1985). Atoms in Molecules. *Acc. Chem. Res.* 18, 9–15. doi:10.1021/ar00109a003

Baerends, E. J., Ziegler, T., Autschbach, J., Bashford, D., Bérces, A., Bickelhaupt, F. M., and Ellis, D. E. (2013). "ADF2013. 01. SCM," in *Theo. Chem* (Amsterdam, Netherlands: Vrije Universiteit).

Bai, Q. (2010). Analysis of Particle Swarm Optimization Algorithm. *Cis* 3, 180. doi:10.5539/cis.v3n1p180

Barnes, J. C., Juríček, M., Strutt, N. L., Frasconi, M., Sampath, S., Giesener, M. A., et al. (2013). ExBox: a Polycyclic Aromatic Hydrocarbon Scavenger. *J. Am. Chem. Soc.* 135, 183–192. doi:10.1021/ja307360n

Becke, A. D. (1988). Density-functional Exchange-Energy Approximation with Correct Asymptotic Behavior. *Phys. Rev. A.* 38, 3098–3100. doi:10.1103/PhysRevA.38.3098

Becke, A. D. (1992). Density-functional Thermochemistry. I. The Effect of the Exchange-only Gradient Correction. *J. Chem. Phys.* 96, 2155–2160. doi:10.1063/1.462066

Bergman, B., Sandh, G., Lin, S., Larsson, J., and Carpenter, E. J. (2013). Trichodesmium- a Widespread marine Cyanobacterium with Unusual Nitrogen Fixation Properties. *FEMS Microbiol. Rev.* 37, 286–302. doi:10.1111/j.1574-6976.2012.00352.x

Bhatia, S. K., and Myers, A. L. (2006). Optimum Conditions for Adsorptive Storage. *Langmuir* 22, 1688–1700. doi:10.1021/la0523816

Brust, M., Walker, M., Bethell, D., Schiffrin, D. J., and Whyman, R. (1994). Synthesis of Thiol-Derivatised Gold Nanoparticles in a Two-phase Liquid-Liquid System. *J. Chem. Soc. Chem. Commun.* 7, 801–802. doi:10.1039/C39940000801

Cabria, I., López, M. J., and Alonso, J. A. (2008). Hydrogen Storage Capacities of Nanoporous Carbon Calculated by Density Functional and Møller-Plesset Methods. *Phys. Rev. B* 78, 075415. doi:10.1103/PhysRevB.78.075415

Cagle, D. W., Thrash, T. P., Alford, M., Chibante, L. P. F., Ehrhardt, G. J., and Wilson, L. J. (1996). Synthesis, Characterization, and Neutron Activation of Holmium Metallofullerenes. *J. Am. Chem. Soc.* 118, 8043–8047. doi:10.1021/ja960841z

Chai, J.-D., and Head-Gordon, M. (2008). Long-range Corrected Hybrid Density Functionals with Damped Atom-Atom Dispersion Corrections. *Phys. Chem. Chem. Phys.* 10, 6615–6620. doi:10.1039/B810189B

Chakraborty, D., and Chattaraj, P. K. (2019). Bonding, Reactivity, and Dynamics in Confined Systems. *J. Phys. Chem. A.* 123, 4513–4531. doi:10.1021/acs.jpca.9b00830

Chakraborty, D., and Chattaraj, P. K. (2021). Conceptual Density Functional Theory Based Electronic Structure Principles. *Principles. Chem. Sci.* 12, 6264–6279. doi:10.1039/D0SC07017C

Chakraborty, D., and Chattaraj, P. K. (2015). Confinement Induced Binding in noble Gas Atoms within a BN-Doped Carbon Nanotube. *Chem. Phys. Lett.* 621, 29–34. doi:10.1016/j.cplett.2014.12.053

Chakraborty, D., and Chattaraj, P. K. (2017). Effect of Functionalization of boron Nitride Flakes by Main Group Metal Clusters on Their Optoelectronic Properties. *J. Phys. Condens. Matter* 29, 425201. doi:10.1088/1361-648X/aa8651

Chakraborty, D., and Chattaraj, P. K. (2018). Host-guest Interactions between Octa Acid and Cations/nucleobases. *J. Comput. Chem.* 39, 161–175. doi:10.1002/jcc.25097

Chakraborty, D., and Chattaraj, P. K. (2016a). Optical Response and Gas Sequestration Properties of Metal Cluster Supported Graphene Nanoflakes. *Phys. Chem. Chem. Phys.* 18, 18811–18827. doi:10.1039/C6CP02134D

Chakraborty, D., and Chattaraj, P. K. (2016b). Sequestration and Activation of Small Gas Molecules on BN-Flakes and the Effect of Various Metal Oxide Molecules Therein. *J. Phys. Chem. C* 120, 27782–27799. doi:10.1021/acs.jpcc.6b08404

Chakraborty, D., Das, R., and Chattaraj, P. K. (2017). Does Confinement Always Lead to Thermodynamically And/or Kinetically Favorable Reactions? A Case Study Using Diels-Alder Reactions within ExBox+4 and CB[7]. *ChemPhysChem* 18, 2162–2170. doi:10.1002/cphc.201700308

Chakraborty, D., Pan, S., and Chattaraj, P. K. (2016). Encapsulation of Small Gas Molecules and Rare Gas Atoms inside the Octa Acid Cavitand. *Theor. Chem. Acc.* 135, 119. doi:10.1007/s00214-016-1876-y

Chatt, J., and Leigh, G. J. (1972). Nitrogen Fixation. *Chem. Soc. Rev.* 1, 121–144. doi:10.1039/cs9720100121

Chattaraj, P. K., Bandaru, S., and Mondal, S. (2011). Hydrogen Storage in Clathrate Hydrates. *J. Phys. Chem. A.* 115, 187–193. doi:10.1021/jp109515a

Chattaraj, P. K., and Maiti, B. (2001). Electronic Structure Principles and the Atomic Shell Structure. *J. Chem. Educ.* 78, 811–813. doi:10.1021/ed078p811

Chattaraj, P. K., Nath, S., and Sannigrahi, A. (1993). Ab Initio SCF Study of Maximum Hardness and Maximum Molecular Valency Principles. *Chem. Phys. Lett.* 212, 223–230. doi:10.1016/0009-2614(93)89318-C

Chattaraj, P. K., Roy, D. R., and Duley, S. (2008). Bonding and Aromaticity in an All-Metal sandwich-like Compound, Be_8^{2-}. *Chem. Phys. Lett.* 460, 382–385. doi:10.1016/j.cplett.2008.06.005

Chattaraj, P. K., Roy, D. R., Elango, M., and Subramanian, V. (2006). Chemical Reactivity Descriptor Based Aromaticity Indices Applied to and Systems. *J. Mol. Struct. THEOCHEM* 759, 109–110. doi:10.1016/j.theochem.2005.10.041

Chattaraj, P. K., Roy, D. R., Elango, M., and Subramanian, V. (2005). Stability and Reactivity of All-Metal Aromatic and Antiaromatic Systems in Light of the Principles of Maximum Hardness and Minimum Polarizability. *J. Phys. Chem. A.* 109, 9590–9597. doi:10.1021/jp0540196

Chattaraj, P. K., Sarkar, U., and Roy, D. R. (2007). Electronic Structure Principles and Aromaticity. *J. Chem. Educ.* 84, 354. doi:10.1021/ed084p354

Chen, W., Li, Z.-R., Wu, D., Li, Y., Sun, C.-C., and Gu, F. L. (2005). The Structure and the Large Nonlinear Optical Properties of Li@Calix[4]pyrrole. *J. Am. Chem. Soc.* 127, 10977–10981. doi:10.1021/ja050601w

Chen, Z., Corminboeuf, C., Heine, T., Bohmann, J., and Schleyer, P. V. R. (2003). Do all-metal Antiaromatic Clusters Exist? *J. Am. Chem. Soc.* 125, 13930–13931. doi:10.1021/ja0361392

Chollet, F. (2015). Keras. GitHub. Available at: https://github.com/fchollet/keras. doi:10.2210/pdb4trn/pdb

Chong, Z. R., Yang, S. H. B., Babu, P., Linga, P., and Li, X.-S. (2016). Review of Natural Gas Hydrates as an Energy Resource: Prospects and Challenges. *Appl. Energ.* 162, 1633–1652. doi:10.1016/j.apenergy.2014.12.061

Cioslowski, J., and Nanayakkara, A. (1992). Endohedral Fullerites: a New Class of Ferroelectric Materials. *Phys. Rev. Lett.* 69, 2871–2873. doi:10.1103/PhysRevLett.69.2871

Colorni, A., Dorigo, M., and Maniezzo, V. (1991). "Distributed Optimization by Ant Colonies," in Proceedings of the first European conference on artificial life. 142. Paris, France: Elsevier Publishing, 134–142.

Contreras-García, J., Johnson, E. R., Keinan, S., Chaudret, R., Piquemal, J.-P., Beratan, D. N., et al. (2011). NCIPLOT: a Program for Plotting Noncovalent Interaction Regions. *J. Chem. Theor. Comput.* 7, 625–632. doi:10.1021/ct100641a

Cross, R. J., Saunders, M., and Prinzbach, H. (1999). Putting Helium inside Dodecahedrane. *Org. Lett.* 1, 1479–1481. doi:10.1021/ol991037v

Das, P., and Chattaraj, P. K. (2021a). Comparison between Electride Characteristics of Li3@B40 and Li3@C60. *Front. Chem.* 9, 638581. doi:10.3389/fchem.2021.638581

Das, P., and Chattaraj, P. K. (2020). Electride Characteristics of Some Binuclear Sandwich Complexes of Alkaline Earth Metals, M2(η5-L)2 (M = Be, Mg; L = C5H5-, N5-, P5-, As5-). *J. Phys. Chem. A.* 124, 9801–9810. doi:10.1021/acs.jpca.0c08306

Das, P., Saha, R., and Chattaraj, P. K. (2020). Encapsulation of Mg2 inside a C60 Cage Forms an Electride. *J. Comput. Chem.* 41, 1645–1653. doi:10.1002/jcc.26207

Das, P., and Chattaraj, P. K. (2021b). Substituent Effects on Electride Characteristics of $Mg_2(\eta5\text{-}C_5H_5)2$: A Theoretical Study. *J. Phys. Chem. A.* 125,6207–6220. doi:10.1021/acs.jpca.1c04605

Das, R., and Chattaraj, P. K. (2012). A (T-P) Phase Diagram of Hydrogen Storage on (N4C3H)6Li6. *J. Phys. Chem. A.* 116, 3259–3266. doi:10.1021/jp212472u

Dawes, S. B., Eglin, J. L., Moeggenborg, K. J., Kim, J., and Dye, J. L. (1991). Cesium(+1)(15-crown-5)2.cntdot.e-. A Crystalline Antiferromagnetic Electride. *J. Am. Chem. Soc.* 113, 1605–1609. doi:10.1021/ja00005a025

Deng, W.-Q., Xu, X., and Goddard, W. A. (2004). New Alkali Doped Pillared Carbon Materials Designed to Achieve Practical Reversible Hydrogen Storage for Transportation. *Phys. Rev. Lett.* 92, 166103. doi:10.1103/PhysRevLett.92.166103

Dong, Z., Luo, Q., and Liu, J. (2012). Artificial Enzymes Based on Supramolecular Scaffolds. *Chem. Soc. Rev.* 41 (23), 7890–7908. doi:10.1039/C2CS35207A

Dunning, T. H., Jr., and Hay, P. J. (1977). "Gaussian Basis Sets for Molecular Calculations," in *Modern Theoretical Chemistry*. Editor H. F. Schaefer, III (New York: Plenum), Vol. 3, 1–27. doi:10.1007/978-1-4757-0887-5_1

Ellaboudy, A., Dye, J. L., and Smith, P. B. (1983). Cesium 18-crown-6 Compounds. A Crystalline Ceside and a Crystalline Electride. *J. Am. Chem. Soc.* 105, 6490–6491. doi:10.1021/ja00359a022

Florea, M., and Nau, W. M. (2011). Strong Binding of Hydrocarbons to Cucurbituril Probed by Fluorescent Dye Displacement: A Supramolecular Gas-Sensing Ensemble. *Angew. Chem.* 123, 9510–9514. doi:10.1002/ange.201104119

Frisch, M. J., Trucks, G. W., Schlegel, H. B., Scuseria, G. E., Robb, M. A., Cheeseman, J. R., et al. (2009). *Gaussian 09*. Wallingford CT: Gaussian, Inc.

Froudakis, G. E. (2001). Hydrogen Interaction with Single-Walled Carbon Nanotubes: A Combined Quantum-Mechanics/molecular-Mechanics Study. *Nano Lett.* 1, 179–182. doi:10.1021/nl015504p

Giri, S., Bandaru, S., Chakraborty, A., and Chattaraj, P. K. (2011a). Role of Aromaticity and Charge of a System in its Hydrogen Trapping Potential and Vice Versa. *Phys. Chem. Chem. Phys.* 13, 20602–20614. doi:10.1039/C1CP21752F

Giri, S., Chakraborty, A., and Chattaraj, P. K. (2011b). Potential Use of Some Metal Clusters as Hydrogen Storage Materials-A Conceptual DFT Approach. *J. Mol. Model.* 17, 777–784. doi:10.1007/s00894-010-0761-1

Giri, S., Roy, D. R., Duley, S., Chakraborty, A., Parthasarathi, R., Elango, M., et al. (2009). Bonding, Aromaticity, and Structure of Trigonal Dianion Metal Clusters. *J. Comput. Chem.* 31, 1815–1821. doi:10.1002/jcc.21452

Grochala, W., Hoffmann, R., Feng, J., and Ashcroft, N. W. (2007). The Chemical Imagination at Work inVery Tight Places. *Angew. Chem. Int. Ed.* 46 (20), 3620–3642. doi:10.1002/anie.200602485

Gubbins, K. E., Liu, Y.-C., Moore, J. D., and Palmer, J. C. (2011). The Role of Molecular Modeling in Confined Systems: Impact and Prospects. *Phys. Chem. Chem. Phys.* 13, 58–85. doi:10.1039/C0CP01475C

Haaland, A., Shorokhov, D. J., and Tverdova, N. V. (2004). Topological Analysis of Electron Densities: Is the Presence of an Atomic Interaction Line in an Equilibrium Geometry a Sufficient Condition for the Existence of a Chemical Bond? *Chem. Eur. J.* 10, 4416–4421. doi:10.1002/chem.200400663

Havenith, R. W. A., Fowler, P. W., Steiner, E., Shetty, S., Kanhere, D., and Pal, S. (2004). Aromaticity and Antiaromaticity of LixAl4clusters: Ring Current Patterns versus Electron Counting. *Phys. Chem. Chem. Phys.* 6, 285–288. doi:10.1039/B311559N

Havenith, R. W., Proft, F. De., Fowler, P. W., and Geerlings, P. (2005). σ-Aromaticity in H_3^+ and Li_3^+: Insights from Ring-Current Maps. *Chem. Phys. Lett.* 407, 391–396. doi:10.1016/j.cplett.2005.03.099

Hay, P. J., and Wadt, W. R. (1985b). Ab Initio effective Core Potentials for Molecular Calculations. Potentials for K to Au Including the Outermost Core Orbitals. *J. Chem. Phys.* 82, 299–310. doi:10.1063/1.448975

Hay, P. J., and Wadt, W. R. (1985a). Ab Initio effective Core Potentials for Molecular Calculations. Potentials for the Transition Metal Atoms Sc to Hg. *J. Chem. Phys.* 82, 270–283. doi:10.1063/1.448799

Heine, T., Zhechkov, L., and Seifert, G. (2004). Hydrogen Storage by Physisorption on Nanostructured Graphite plateletsElectronic Supplementary Information (ESI) Available: Fig. 1S: Potential Energy Surface of H2 Parallel to Benzene at the MP2 Level. See. *Phys. Chem. Chem. Phys.* 6, 980–984. doi:10.1039/B316209E

Hennig, A., Ghale, G., and Nau, W. M. (2007). Effects of Cucurbit[7]uril on Enzymatic Activity. *Chem. Commun.* 16, 1614–1616. doi:10.1039/B618703J

Herr, W. A. D. (1993). The Physics of Simple Metal Clusters: Experimental Aspects and Simple Models. *Rev. Mod. Phys.* 65, 611. doi:10.1103/RevModPhys.65.611

Hoffman, B. M., Lukoyanov, D., Dean, D. R., and Seefeldt, L. C. (2013). Nitrogenase: a Draft Mechanism. *Acc. Chem. Res.* 46, 587–595. doi:10.1021/ar300267m

Holland, J. H. (1992). Genetic Algorithms. *Sci. Am.* 267, 66–72. doi:10.1038/scientificamerican0792-66

Hu, Y., Xiang, S., Zhang, W., Zhang, Z., Wang, L., Bai, J., et al. (2009). A New MOF-505 Analog Exhibiting High Acetylene Storage. *Chem. Commun.* 48, 7551–7553. doi:10.1039/B917046D

Hückel, E. (1931). Quantentheoretische Beiträge Zum Benzolproblem. *Z. Phys.* 70, 204–286. doi:10.1007/BF01339530

Hutter, J., and Lüthi, H. P. (1994). The Molecular Structure of C6: A Theoretical Investigation. *J. Chem. Phys.* 101, 2213–2216. doi:10.1063/1.467661

Iyengar, S. S., Schlegel, H. B., Millam, J. M., A. Voth, G. G., Scuseria, G. E., and Frisch, M. J. (2001). Ab Initio molecular Dynamics: Propagating the Density Matrix with Gaussian Orbitals. II. Generalizations Based on Mass-Weighting, Idempotency, Energy Conservation and Choice of Initial Conditions. *J. Chem. Phys.* 115, 10291–10302. doi:10.1063/1.1416876

Jana, G., Mitra, A., Pan, S., Sural, S., and Chattaraj, P. K. (2019). Modified Particle Swarm Optimization Algorithms for the Generation of Stable Structures of Carbon Clusters, Cn (N = 3-6, 10). *Front. Chem.* 7, 485. doi:10.3389/fchem.2019.00485

Jena, P., and Castleman, A. W. (2010). Introduction to Atomic Clusters. *Sci. Technol. At. Mol. Condensed Matter Biol. Syst.* 1, 1–36. doi:10.1016/B978-0-444-53440-8.00001-X

J. F. Corrigan and S. Dehnen (Editors) (2017). *Clusters-contemporary Insight in Structure and Bonding* (Cham: Springer), 174.

Jiménez-Halla, J. O., Islas, R., Heine, T., and Merino, G. (2010). B19-: an Aromatic Wankel Motor. *Angew. Chem. Int. Ed. Engl.* 49, 5668–5671. doi:10.1002/anie.201001275

Jiménez-Vázquez, H. A., Tamariz, J., and Cross, R. J. (2001). Binding Energy in and Equilibrium Constant of Formation for the Dodecahedrane Compounds He@C20H20 and Ne@C20H20. *J. Phys. Chem. A.* 105, 1315–1319. doi:10.1021/jp0027243

Jin, Y., Voss, B. A., Jin, A., Long, H., Noble, R. D., and Zhang, W. (2011). Highly CO2-Selective Organic Molecular Cages: What Determines the CO2Selectivity. *J. Am. Chem. Soc.* 133, 6650–6658. doi:10.1021/ja110846c

Jin, Y., Voss, B. A., Noble, R. D., and Zhang, W. (2010). A Shape-Persistent Organic Molecular Cage with High Selectivity for the Adsorption of CO2 over N2. *Angew. Chem.* 122, 6492–6495. doi:10.1002/ange.201001517

Karaboga, D., and Basturk, B. (2007). A Powerful and Efficient Algorithm for Numerical Function Optimization: Artificial Bee Colony (ABC) Algorithm. *J. Glob. Optim.* 39, 459–471. doi:10.1007/s10898-007-9149-x

Khatua, M., Pan, S., and Chattaraj, P. K. (2014a). Confinement Induced Binding of noble Gas Atoms. *J. Chem. Phys.* 140, 164306. doi:10.1063/1.4871800

Khatua, M., Pan, S., and Chattaraj, P. K. (2014b). Confinement of (HF)2 in Cn (n= 60, 70, 80, 90).... Cages. *Chem. Phys. Lett.* 616-617, 49–54. doi:10.1016/j.cplett.2014.10.025

Khatua, S., Roy, D. R., Bultinck, P., Bhattacharjee, M., and Chattaraj, P. K. (2008). Aromaticity in Cyclic Alkali Clusters. *Phys. Chem. Chem. Phys.* 10, 2461–2474. doi:10.1039/B718176K

Kim, H., Kim, Y., Yoon, M., Lim, S., Park, S. M., Seo, G., et al. (2010). Highly Selective Carbon Dioxide Sorption in an Organic Molecular Porous Material. *J. Am. Chem. Soc.* 132, 12200–12202. doi:10.1021/ja105211w

Kitano, M., Inoue, Y., Yamazaki, Y., Hayashi, F., Kanbara, S., Matsuishi, S., et al. (2012). Ammonia Synthesis Using a Stable Electride as an Electron Donor and Reversible Hydrogen Store. *Nat. Chem* 4, 934–940. doi:10.1038/nchem.1476

Klontzas, E., Tylianakis, E., and Froudakis, G. E. (2008). Hydrogen Storage in 3D Covalent Organic Frameworks. A Multiscale Theoretical Investigation. *J. Phys. Chem. C* 112, 9095–9098. doi:10.1021/jp711326g

Koster, A. M., Geudtner, G., Calaminici, P., Casida, M. E., Dominguez, V. D., Flores-Moreno, R., and Salahub, D. R. (2011). *DeMon2K, Version 3*. Cinvestav, México: The deMon Developers.

Kuc, A., Zhechkov, L., Patchkovskii, S., Seifert, G., and Heine, T. (2007). Hydrogen Sieving and Storage in Fullerene Intercalated Graphite. *Nano Lett.* 7, 1–5. doi:10.1021/nl0619148

Kuznetsov, A. E., Birch, K. A., Boldyrev, A. I., Li, X., Zhai, H. J., and Wang, L. S. (2003). All-Metal Antiaromatic Molecule: Rectangular Al44- in the Li3Al4- Anion. *Science* 300, 622–625. doi:10.1126/science.1082477

Lagona, J., Mukhopadhyay, P., Chakrabarti, S., and Isaacs, L. (2005). The Cucurbit [n]uril Family. *Angew. Chem. Int. Ed.* 44 (31), 4844–4870. doi:10.1002/anie.200460675

Latysheva, N., Junker, V. L., Palmer, W. J., Codd, G. A., and Barker, D. (2012). The Evolution of Nitrogen Fixation in Cyanobacteria. *Bioinformatics* 28 (5), 603–606. doi:10.1093/bioinformatics/bts008

Lee, C., Yang, W., and Parr, R. G. (1988). Development of the Colle-Salvetti Correlation-Energy Formula into a Functional of the Electron Density. *Phys. Rev. B* 37, 785–789. doi:10.1103/PhysRevB.37.785

Lee, H., Lee, J.-w., Kim, D. Y., Park, J., Seo, Y.-T., Zeng, H., et al. (2005). Tuning Clathrate Hydrates for Hydrogen Storage. *Nature* 434, 743–746. doi:10.1038/nature03457

Lee, H., Lee, J.-w., Kim, D. Y., Park, J., Seo, Y.-T., Zeng, H., Moudrakovski, I. L., Ratcliffe, C. I., and Ripmeester, J. A. (2010). "Tuning Clathrate Hydrates for Hydrogen Storage," in Materials For Sustainable Energy: A Collection of Peer-Reviewed Research and Review Articles from Nature Publishing Group, 285–288. doi:10.1142/9789814317665_0042

Lee, K., Kim, S. W., Toda, Y., Matsuishi, S., and Hosono, H. (2013). Dicalcium Nitride as a Two-Dimensional Electride with an Anionic Electron Layer. *Nature* 494, 336–340. doi:10.1038/nature11812

Li, F., Zhao, J., Johansson, B., and Sun, L. (2010). Improving Hydrogen Storage Properties of Covalent Organic Frameworks by Substitutional Doping. *Int. J. Hydrogen Energ.* 35, 266–271. doi:10.1016/j.ijhydene.2009.10.061

Li, S., and Jena, P. (2008). Li-and B-Decorated Cis-Polyacetylene: A Computational Study. *Phys. Rev. B.* 77, 193101. doi:10.1103/physrevb.77.193101

Li, X., Kuznetsov, A. E., Zhang, H. F., Boldyrev, A. I., and Wang, L. S. (2001). Observation of All-Metal Aromatic Molecules. *Science* 291, 859–861. doi:10.1126/science.291.5505.859

Li, Y., Wu, D., and Li, Z.-R. (2008). Compounds of Superatom Clusters: Preferred Structures and Significant Nonlinear Optical Properties of the BLi6-X (X = F, LiF2, BeF3, BF4) Motifs. *Inorg. Chem.* 47, 9773–9778. doi:10.1021/ic800184z

Li, Z.-J., Wang, F.-F., Li, Z.-R., Xu, H.-L., Huang, X.-R., Wu, D., et al. (2009). Large Static First and Second Hyperpolarizabilities Dominated by Excess Electron Transition for Radical Ion Pair Salts M2+TCNQ−(M = Li, Na, K). *Phys. Chem. Chem. Phys.* 11, 402–408. doi:10.1039/B809161G

Liu, L., Moreno, D., Osorio, E., Castro, A. C., Pan, S., Chattaraj, P. K., et al. (2016). Structure and Bonding of IrB12−: Converting a Rigid boron B12 Platelet to a Wankel Motor. *RSC Adv.* 6, 27177–27182. doi:10.1039/C6RA02992B

Liu, S., and Gibb, B. C. (2008). High-definition Self-Assemblies Driven by the Hydrophobic Effect: Synthesis and Properties of a Supramolecular Nanocapsule. *Chem. Commun.* 32, 3709–3716. doi:10.1039/B805446K

Lü, J., Perez-Krap, C., Suyetin, M., Alsmail, N. H., Yan, Y., Yang, S., et al. (2014). A Robust Binary Supramolecular Organic Framework (SOF) with High CO2 Adsorption and Selectivity. *J. Am. Chem. Soc.* 136, 12828–12831. doi:10.1021/ja506577g

Lu, T., and Chen, F. (2012). Multiwfn: a Multifunctional Wavefunction Analyzer. *J. Comput. Chem.* 33, 580–592. doi:10.1002/jcc.22885

Lu, Y., Li, J., Tada, T., Toda, Y., Ueda, S., Yokoyama, T., et al. (2016). Water Durable Electride Y5Si3: Electronic Structure and Catalytic Activity for Ammonia Synthesis. *J. Am. Chem. Soc.* 138, 3970–3973. doi:10.1021/jacs.6b00124

Lu, Y., Wang, J., Li, J., Wu, J., Kanno, S., Tada, T., et al. (2018). Realization of Mott-insulating Electrides in Dimorphic Yb5Sb3. *Phys. Rev. B* 98, 125128. doi:10.1103/PhysRevB.98.125128

Mao, W. L., and Mao, H.-k. (2004). Hydrogen Storage in Molecular Compounds. *Proc. Natl. Acad. Sci.* 101, 708–710. doi:10.1073/pnas.0307449100

Mao, W. L., Mao, H. K., Goncharov, A. F., Struzhkin, V. V., Guo, Q., Hu, J., and Zhao, Y. (2002). Hydrogen Clusters in Clathrate Hydrate. *Science* 297, 2247–2249. doi:10.1126/science.1075394

Martin, J. M. L., and Taylor, P. R. (1996). Structure and Vibrations of Small Carbon Clusters from Coupled-Cluster Calculations. *J. Phys. Chem.* 100, 6047–6056. doi:10.1021/jp952471r

Mastalerz, M., Schneider, M. W., Oppel, I. M., and Presly, O. (2011). A Salicylbisimine Cage Compound with High Surface Area and Selective CO2/CH4 Adsorption. *Angew. Chem. Int. Ed.* 50, 1046–1051. doi:10.1002/anie.201005301

Matsuishi, S., Toda, Y., Miyakawa, M., Hayashi, K., Kamiya, T., Hirano, M., et al. (2003). High-Density Electron Anions in a Nanoporous Single Crystal: [Ca24Al28O64]4+(4e-). *Science.* 301, 626–629. doi:10.1126/science.1083842

McKeown, N. B., Gahnem, B., Msayib, K. J., Budd, P. M., Tattershall, C. E., Mahmood, K., et al. (2006). Towards Polymer-Based Hydrogen Storage

Materials: Engineering Ultramicroporous Cavities within Polymers of Intrinsic Microporosity. *Angew. Chem. Int. Ed.* 45, 1804–1807. doi:10.1002/anie.200504241

McLean, A. D., and Chandler, G. S. (1980). Contracted Gaussian Basis Sets for Molecular Calculations. I. Second Row Atoms, Z=11-18. *J. Chem. Phys.* 72, 5639–5648. doi:10.1063/1.438980

Mitikiri, P., Jana, G., Sural, S., and Chattaraj, P. K. (2018). A Machine Learning Technique toward Generating Minimum Energy Structures of Small boron Clusters. *Int. J. Quan. Chem.* 118, e25672. doi:10.1002/qua.25672

Mitoraj, M. P., Michalak, A., and Ziegler, T. (2009). A Combined Charge and Energy Decomposition Scheme for Bond Analysis. *J. Chem. Theor. Comput.* 5, 962–975. doi:10.1021/ct800503d

Mitra, A., Jana, G., Agrawal, P., Sural, S., and Chattaraj, P. K. (2020). Integrating Firefly Algorithm with Density Functional Theory for Global Optimization of Al42− Clusters. *Theor. Chem. Acc.* 139, 1–12. doi:10.1007/s00214-020-2550-y

Mitra, A., Jana, G., Pal, R., Gaikwad, P., Sural, S., and Chattaraj, P. K. (2021). Determination of Stable Structure of a Cluster Using Convolutional Neural Network and Particle Swarm Optimization. *Theor. Chem. Acc.* 140, 1–12. doi:10.1007/s00214-021-02726-z

Moreno, D., Pan, S., Zeonjuk, L. L., Islas, R., Osorio, E., Martínez-Guajardo, G., et al. (2014). B182−: a Quasi-Planar Bowl Member of the Wankel Motor Family. *Chem. Commun.* 50, 8140–8143. doi:10.1039/C4CC02225D

Morokuma, K. (1971). Molecular Orbital Studies of Hydrogen Bonds. III. C=O···H-O Hydrogen Bond in H2CO···H2O and H2CO···2H2O. *J. Chem. Phys.* 55, 1236–1244. doi:10.1063/1.1676210

Msayib, K. J., Book, D., Budd, P. M., Chaukura, N., Harris, K. D. M., Helliwell, M., et al. (2009). Nitrogen and Hydrogen Adsorption by an Organic Microporous Crystal. *Angew. Chem.* 121, 3323–3327. doi:10.1002/ange.200900234

Muhammad, S., Xu, H., Liao, Y., Kan, Y., and Su, Z. (2009). Quantum Mechanical Design and Structure of the Li@B10H14 Basket with a Remarkably Enhanced Electro-Optical Response. *J. Am. Chem. Soc.* 131, 11833–11840. doi:10.1021/ja9032023

Muhammad, S., Xu, H., and Su, Z. (2011). Capturing a Synergistic Effect of a Conical Push and an Inward Pull in Fluoro Derivatives of Li@B10H14Basket: Toward a Higher Vertical Ionization Potential and Nonlinear Optical Response. *J. Phys. Chem. A.* 115, 923–931. doi:10.1021/jp110401f

Norbye, J. P. (1971). *The Wankel Engine: Design, Development, Applications*. 1st Ed. Philadelphia, PA: Chilton Book Company.

Pal, R., and Chattaraj, P. K. (2021). Possible Effects of Fluxionality of a Cavitand on its Catalytic Activity through Confinement. *Phys. Chem. Chem. Phys.* 23, 15817–15834. doi:10.1039/D1CP01826D

Pan, S., Ghara, M., Kar, S., Zarate, X., Merino, G., and Chattaraj, P. K. (2018). Noble Gas Encapsulated B40 Cage. *Phys. Chem. Chem. Phys.* 20, 1953–1963. doi:10.1039/C7CP07890K

Pan, S., Giri, S., and Chattaraj, P. K. (2012a). A Computational Study on the Hydrogen Adsorption Capacity of Various Lithium-Doped boron Hydrides. *J. Comput. Chem.* 33, 425–434. doi:10.1002/jcc.21985

Pan, S., Jana, G., Gupta, A., Merino, G., and Chattaraj, P. K. (2017). Endohedral Gas Adsorption by Cucurbit[7]uril: a Theoretical Study. *Phys. Chem. Chem. Phys.* 19, 24448–24452. doi:10.1039/C7CP03984K

Pan, S., Mandal, S., and Chattaraj, P. K. (2015). Cucurbit[6]uril: a Possible Host for noble Gas Atoms. *J. Phys. Chem. B* 119, 10962–10974. doi:10.1021/acs.jpcb.5b01396

Pan, S., Merino, G., and Chattaraj, P. K. (2012b). The Hydrogen Trapping Potential of Some Li-Doped star-like Clusters and Super-alkali Systems. *Phys. Chem. Chem. Phys.* 14, 10345–10350. doi:10.1039/C2CP40794A

Pan, S., Mondal, S., and Chattaraj, P. K. (2013a). Cucurbiturils as Promising Hydrogen Storage Materials: a Case Study of Cucurbit[7]uril. *New J. Chem.* 37, 2492–2499. doi:10.1039/C3NJ00399J

Pan, S., Moreno, D., Merino, G., and Chattaraj, P. K. (2014). Stability of Noble-Gas-Bound SiH3+Clusters. *ChemPhysChem* 15, 3554–3564. doi:10.1002/cphc.201402370

Pan, S., Solà, M., and Chattaraj, P. K. (2013b). On the Validity of the Maximum Hardness Principle and the Minimum Electrophilicity Principle During Chemical Reactions. *J. Phys. Chem. A* 117, 1843–1852. doi:10.1021/jp312750n

Pauling, L., and Sherman, J. (1933). The Nature of the Chemical Bond. VI. The Calculation from Thermochemical Data of the Energy of Resonance of Molecules Among Several Electronic Structures. *J. Chem. Phys.* 1, 606–617. doi:10.1063/1.1749335

Perdew, J. P., Burke, K., and Ernzerhof, M. (1996). Generalized Gradient Approximation Made Simple. *Phys. Rev. Lett.* 77, 3865–3868. doi:10.1103/PhysRevLett.77.3865

Perdew, J. P., Burke, K., and Ernzerhof, M. (1997). Generalized Gradient Approximation Made Simple [Phys. Rev. Lett. 77, 3865 (1996)]. *Phys. Rev. Lett.* 78, 1396. doi:10.1103/PhysRevLett.78.1396

Perdew, J. P. (1986a). Density-functional Approximation for the Correlation Energy of the Inhomogeneous Electron Gas. *Phys. Rev. B* 33, 8822–8824. doi:10.1103/PhysRevB.33.8822

Perdew, J. P. (1986b). Erratum: Density-Functional Approximation for the Correlation Energy of the Inhomogeneous Electron Gas. *Phys. Rev. B* 34, 7406. doi:10.1103/PhysRevB.34.7406

Pham, D. T., Ghanbarzadeh, A., Koc, E., Otri, S., Rahim, S., and Zaidi, M. (2005). "The Bees Algorithm," in *Technical Note* (UK: Manufacturing Engineering Centre, Cardiff University).

P. J. Stang and F. Diederich (Editors) (2008). *Modern Acetylene Chemistry* (Hoboken, New Jersey, USA: John Wiley & Sons).

Pless, V., Suter, H. U., and Engels, B. (1994). Ab Initio study of the Energy Difference between the Cyclic and Linear Forms of the C6 Molecule. *J. Chem. Phys.* 101, 4042–4048. doi:10.1063/1.467521

Popov, I. A., Li, W.-L., Piazza, Z. A., Boldyrev, A. I., and Wang, L.-S. (2014). Complexes between Planar Boron Clusters and Transition Metals: A Photoelectron Spectroscopy and Ab Initio Study of CoB12- and RhB12-. *J. Phys. Chem. A.* 118, 8098–8105. doi:10.1021/jp411867q

Qu, J., Zhu, S., Zhang, W., and Zhu, Q. (2019). Electrides with Dinitrogen Ligands. *ACS Appl. Mater. Inter.* 11, 5256–5263. doi:10.1021/acsami.8b18676

Raghavachari, K., Binkley, J. S., Seeger, R., and Pople, J. A. (1980). Self-Consistent Molecular Orbital Methods. 20. Basis Set for Correlated Wave-Functions. *J. Chem. Phys.* 72, 650–654. doi:10.1063/1.438955

Raghavachari, K., and Binkley, J. S. (1987). Structure, Stability, and Fragmentation of Small Carbon Clusters. *J. Chem. Phys.* 87, 2191–2197. doi:10.1063/1.453145

Reed, A. E., Curtiss, L. A., and Weinhold, F. (1988). Intermolecular Interactions from a Natural Bond Orbital, Donor-Acceptor Viewpoint. *Chem. Rev.* 88, 899–926. doi:10.1021/cr00088a005

Reed, A. E., Weinstock, R. B., and Weinhold, F. (1985). Natural Population Analysis. *J. Chem. Phys.* 83, 735–746. doi:10.1063/1.449486

Rosi, N. L., Eckert, J., Eddaoudi, M., Vodak, D. T., Kim, J., O'Keeffe, M., et al. (2003). Hydrogen Storage in Microporous Metal-Organic Frameworks. *Science* 300, 1127–1129. doi:10.1126/science.1083440

Rowsell, J. L. C., and Yaghi, O. M. (2005). Strategies for Hydrogen Storage in Metal-Organic Frameworks. *Angew. Chem. Int. Ed.* 44, 4670–4679. doi:10.1002/anie.200462786

Roy, D. R., and Chattaraj, P. K. (2008). Reactivity, Selectivity, and Aromaticity of Be32- and its Complexes. *J. Phys. Chem. A.* 112, 1612–1621. doi:10.1021/jp710820c

Sabin, J. R., and Brandas, E. J. (2009). *Advances in Quantum Chemistry: Theory of Confined Quantum Systems-Part One*. Cambridge: Academic Press.

Saha, R., and Chattaraj, P. K. (2018). Activation of Small Molecules (H2, CO2, N2O, CH4, and C6H6) by a Porphyrinoid-Based Dimagnesium(I) Complex, an Electride. *ACS Omega* 3, 17199–17211. doi:10.1021/acsomega.8b03006

Saha, R., Das, P., and Chattaraj, P. K. (2019). A Complex Containing Four Magnesium Atoms and Two Mg-Mg Bonds Behaving as an Electride. *Eur. J. Inorg. Chem.* 2019, 4105–4111. doi:10.1002/ejic.201900813

Saha, R., Kar, S., Pan, S., Martínez-Guajardo, G., Merino, G., and Chattaraj, P. K. (2017). A Spinning Umbrella: Carbon Monoxide and Dinitrogen Bound MB12- Clusters (M = Co, Rh, Ir). *J. Phys. Chem. A.* 121, 2971–2979. doi:10.1021/acs.jpca.6b12232

Saha, R., Pan, S., Merino, G., and Chattaraj, P. K. (2015). Comparative Study on the Noble-Gas Binding Ability of BeX Clusters (X = SO4, CO3, O). *J. Phys. Chem. A.* 119, 6746–6752. doi:10.1021/acs.jpca.5b03888

Santos, J. C., Andres, J., Aizman, A., and Fuentealba, P. (2005). An Aromaticity Scale Based on the Topological Analysis of the Electron Localization Function Including σ and π Contributions. *J. Chem. Theor. Comput.* 1, 83–86. doi:10.1021/ct0499276

Schettino, V., and Bini, R. (2007). Constraining Molecules at the Closest Approach: Chemistry at High Pressure. *Chem. Soc. Rev.* 36, 869–880. doi:10.1039/B515964B

Schlegel, H. B., Iyengar, S. S., Li, X., Millam, J. M., Voth, G. A., Scuseria, G. E., et al. (2002). Ab Initio molecular Dynamics: Propagating the Density Matrix with Gaussian Orbitals. III. Comparison with Born-Oppenheimer Dynamics. *J. Chem. Phys.* 117, 8694–8704. doi:10.1063/1.1514582

Schlegel, H. B., Millam, J. M., Iyengar, S. S., Voth, G. A., Daniels, A. D., Scuseria, G. E., et al. (2001). Ab Initiomolecular Dynamics: Propagating the Density Matrix with Gaussian Orbitals. *J. Chem. Phys.* 114, 9758–9763. doi:10.1063/1.1372182

Schleyer, P. v. R., Maerker, C., Dransfeld, A., Jiao, H., and van Eikema Hommes, N. J. R. (1996). Nucleus-independent Chemical Shifts: A Simple and Efficient Aromaticity Probe. *J. Am. Chem. Soc.* 118, 6317–6318. doi:10.1021/ja960582d

Schneider, M. W., Oppel, I. M., Ott, H., Lechner, L. G., Hauswald, H.-J. S., Stoll, R., et al. (2012). Periphery-Substituted [4+6] Salicylbisimine Cage Compounds with Exceptionally High Surface Areas: Influence of the Molecular Structure on Nitrogen Sorption Properties. *Chem. Eur. J.* 18, 836–847. doi:10.1002/chem.201102857

Sekhar, P., Ghosh, A., Joshi, M., and Ghanty, T. K. (2017). Noble Gas Encapsulated Endohedral Zintl Ions Ng@Pb122- and Ng@Sn122- (Ng = He, Ne, Ar, and Kr): A Theoretical Investigation. *J. Phys. Chem. C* 121, 11932–11949. doi:10.1021/acs.jpcc.7b03294

Sergeeva, A. P., Popov, I. A., Piazza, Z. A., Li, W.-L., Romanescu, C., Wang, L.-S., et al. (2014). Understanding Boron through Size-Selected Clusters: Structure, Chemical Bonding, and Fluxionality. *Acc. Chem. Res.* 47, 1349–1358. doi:10.1021/ar400310g

Sharma, S., Kurashige, W., Niihori, Y., and Negishi, Y. (2017). Nanocluster Science. *Supra-materials Nanoarchitectonics*, 3–32. doi:10.1016/B978-0-323-37829-1.00001-8

Srinivasu, K., Ghosh, S. K., Das, R., Giri, S., and Chattaraj, P. K. (2012). Theoretical Investigation of Hydrogen Adsorption in All-Metal Aromatic Clusters. *RSC Adv.* 2, 2914–2922. doi:10.1039/C2RA00643J

Srivastava, R. (2021). Application of Optimization Algorithms in Clusters. *Front. Chem.* 9, 637286. doi:10.3389/fchem.2021.637286

Staroverov, V. N., Scuseria, G. E., Tao, J., and Perdew, J. P. (2003). Comparative Assessment of a New Nonempirical Density Functional: Molecules and Hydrogen-Bonded Complexes. *J. Chem. Phys.* 119, 12129–12137. doi:10.1063/1.1626543

Sun, Q., Wang, Q., and Jena, P. (2005). Storage of Molecular Hydrogen in B–N Cage: Energetics and Thermal Stability. *Nano Lett.* 5, 1273–1277. doi:10.1021/nl050385p

Tao, J., Perdew, J. P., Staroverov, V. N., and Scuseria, G. E. (2003). Climbing the Density Functional Ladder: Nonempirical Meta-Generalized Gradient Approximation Designed for Molecules and Solids. *Phys. Rev. Lett.* 91, 146401. doi:10.1103/PhysRevLett.91.146401

Tsukuda, T., and Hakkinen, H. (2015). "Protected Metal Clusters: From Fundamentals to Applications," in *Frontiers of Nanoscience*. 1st Ed. Editors R. E. Palmer (Amsterdam: Elsevier), Vol. 9.

Thrash, T. P., Cagle, D. W., Alford, J. M., Wright, K., Ehrhardt, G. J., Mirzadeh, S., et al. (1999). Toward Fullerene-Based Radiopharmaceuticals: High-Yield Neutron Activation of Endohedral 165Ho Metallofullerenes. *Chem. Phys. Lett.* 308, 329–336. doi:10.1016/S0009-2614(99)00581-3

Toda, Y., Yanagi, H., Ikenaga, E., Kim, J. J., Kobata, M., Ueda, S., et al. (2007). Work Function of a Room-Temperature, Stable Electride [Ca24Al28O64]4+(e-)4. *Adv. Mater.* 19, 3564–3569. doi:10.1002/adma.200700663

Van Orden, A., and Saykally, R. J. (1998). Small Carbon Clusters: Spectroscopy, Structure, and Energetics. *Chem. Rev.* 98, 2313–2358. doi:10.1021/cr970086n

Van Rossum, G., and Drake, F. L. (2009). *Python 3 Reference Manual*. Scotts Valley, CA: CreateSpace. doi:10.1201/9781420049114.ch23

Vitillo, J. G., Regli, L., Chavan, S., Ricchiardi, G., Spoto, G., Dietzel, P. D. C., et al. (2008). Role of Exposed Metal Sites in Hydrogen Storage in MOFs. *J. Am. Chem. Soc.* 130, 8386–8396. doi:10.1021/ja8007159

Wadt, W. R., and Hay, P. J. (1985). Ab Initio effective Core Potentials for Molecular Calculations. Potentials for Main Group Elements Na to Bi. *J. Chem. Phys.* 82, 284–298. doi:10.1063/1.448800

Wagner, B. D., Stojanovic, N., Day, A. I., and Blanch, R. J. (2003). Host Properties of Cucurbit[7]uril: Fluorescence Enhancement of Anilinonaphthalene Sulfonates. *J. Phys. Chem. B* 107, 10741–10746. doi:10.1021/jp034891j

Wales, D. J., and Doye, J. P. K. (1997). Global Optimization by basin-hopping and the Lowest Energy Structures of Lennard-Jones Clusters Containing up to 110 Atoms. *J. Phys. Chem. A.* 101, 5111–5116. doi:10.1021/jp970984n

Wang, J.-J., Zhou, Z.-J., Bai, Y., Liu, Z.-B., Li, Y., Wu, D., et al. (2012). The Interaction between Superalkalis (M3O, M = Na, K) and a C20F20 Cage Forming Superalkali Electride Salt Molecules with Excess Electrons inside the C20F20 Cage: Dramatic Superalkali Effect on the Nonlinear Optical Property. *J. Mater. Chem.* 22, 9652–9657. doi:10.1039/C2JM15405F

Wang, J., Hanzawa, K., Hiramatsu, H., Kim, J., Umezawa, N., Iwanaka, K., et al. (2017). Exploration of Stable Strontium Phosphide-Based Electrides: Theoretical Structure Prediction and Experimental Validation. *J. Am. Chem. Soc.* 139, 15668–15680. doi:10.1021/jacs.7b06279

Ward, D. L., Huang, R. H., and Dye, J. L. (1988). Structures of Alkalides and Electrides. I. Structure of Potassium cryptand[2.2.2] Electride. *Acta Crystallogr. C* 44, 1374–1376. doi:10.1107/s0108270188002847

Watts, J. D., Gauss, J., Stanton, J. F., and Bartlett, R. J. (1992). Linear and Cyclic Isomers of C4. A Theoretical Study with Coupled-cluster Methods and Large Basis Sets. *J. Chem. Phys.* 97, 8372–8381. doi:10.1063/1.463407

Weigend, F., and Ahlrichs, R. (2005). Balanced Basis Sets of Split Valence, Triple Zeta Valence and Quadruple Zeta Valence Quality for H to Rn: Design and Assessment of Accuracy. *Phys. Chem. Chem. Phys.* 7, 3297–3305. doi:10.1039/B508541A

Wiberg, K. B. (1968). Application of the Pople-Santry-Segal CNDO Method to the Cyclopropylcarbinyl and Cyclobutyl Cation and to Bicyclobutane. *Tetrahedron* 24, 1083–1096. doi:10.1016/0040-4020(68)88057-3

Wilson, L. J., Cagle, D. W., Thrash, T. P., Kennel, S. J., Mirzadeh, S., Alford, J. M., et al. (1999). Metallofullerene Drug Design. *Coord. Chem. Rev.* 190–192, 199–207. doi:10.1016/S0010-8545(99)00080-6

Woodley, S. M., Battle, P. D., Gale, J. D., and Richard A. Catlow, C. (1999). The Prediction of Inorganic crystal Structures Using a Genetic Algorithm and Energy Minimisation. *Phys. Chem. Chem. Phys.* 1, 2535–2542. doi:10.1039/A901227C

Wu, X., Gao, Y., and Zeng, X. C. (2008). Hydrogen Storage in Pillared Li-Dispersed boron Carbide Nanotubes. *J. Phys. Chem. C* 112, 8458–8463. doi:10.1021/jp710022y

Xie, Q., Huang, R. H., Ichimura, A. S., Phillips, R. C., Pratt, W. P., and Dye, J. L. (2000). Structure and Properties of a New Electride, Rb+(cryptand[2.2.2])e-. *J. Am. Chem. Soc.* 122, 6971–6978. doi:10.1021/ja9943445

Xu, H.-L., Li, Z.-R., Wu, D., Wang, B.-Q., Li, Y., Gu, F. L., et al. (2007). Structures and Large NLO Responses of New Electrides: Li-Doped Fluorocarbon Chain. *J. Am. Chem. Soc.* 129, 2967–2970. doi:10.1021/ja068038k

Yandulov, D. V., and Schrock, R. R. (2003). Catalytic Reduction of Dinitrogen to Ammonia at a Single Molybdenum center. *Science* 301, 76–78. doi:10.1126/science.1085326

Yang, C.-J., Leveen, L., and King, K. (2015). Ethane as a Cleaner Transportation Fuel. *Environ. Sci. Technol.* 49, 3263–3264. doi:10.1021/acs.est.5b00575

Yang, X. S. (2010). Firefly Algorithm, Stochastic Test Functions and Design Optimisation. *Int. J. Bio-Inspired Comput.* 2, 78–84. doi:10.1504/IJBIC.2010.032124

Yuan, G.-N., Zhang, L.-N., Liu, L.-Q., and Wang, K. (2014). Passengers' Evacuation in Ships Based on Neighborhood Particle Swarm Optimization. *Math. Probl. Eng.* 2014, 1–10. doi:10.1155/2014/939723

Zhan, Z.-h., and Zhang, J. (2008). "Adaptive Particle Swarm Optimization," in International Conference on Ant Colony Optimization and Swarm Intelligence (Berlin, Germany: Springer), 227–234. doi:10.1007/978-3-540-87527-7_21

Zhang, J.-P., and Chen, X.-M. (2009). Optimized Acetylene/carbon Dioxide Sorption in a Dynamic Porous crystal. *J. Am. Chem. Soc.* 131, 5516–5521. doi:10.1021/ja8089872

Zhang, X., Xiao, Z., Lei, H., Toda, Y., Matsuishi, S., Kamiya, T., et al. (2014). Two-Dimensional Transition-Metal Electride Y2C. *Chem. Mater.* 26, 6638–6643. doi:10.1021/cm503512h

Zhang, Z., Xiang, S., and Chen, B. (2011). Microporous Metal-Organic Frameworks for Acetylene Storage and Separation. *CrystEngComm* 13 (20), 5983–5992. doi:10.1039/C1CE05437F

Zhao, Y., Schultz, N. E., and Truhlar, D. G. (2006). Design of Density Functionals by Combining the Method of Constraint Satisfaction with Parametrization for

Thermochemistry, Thermochemical Kinetics, and Noncovalent Interactions. *J. Chem. Theor. Comput.* 2, 364–382. doi:10.1021/ct0502763

Zhao, Y., and Truhlar, D. G. (2008). The M06 Suite of Density Functionals for Main Group Thermochemistry, Thermochemical Kinetics, Noncovalent Interactions, Excited States, and Transition Elements: Two New Functionals and Systematic Testing of Four M06-Class Functionals and 12 Other Functionals. *Theor. Chem. Account.* 120, 215–241. doi:10.1007/s00214-007-0310-x

Zhu, H., Liu, Y., Chen, Y., and Wen, Z. (2010). Cyclodextrins: Promising Candidate media for High-Capacity Hydrogen Adsorption. *Appl. Phys. Lett.* 96, 054101. doi:10.1063/1.3294631

Zubarev, D. Y., and Boldyrev, A. I. (2011). "Multiple Aromaticity, Multiple Antiaromaticity, and Conflicting Aromaticity in Inorganic Systems," in Encyclopedia of Inorganic and Bioinorganic Chemistry (Hoboken, NY, USA: John Wiley & Sons). doi:10.1002/9781119951438.eibc0396

Zubarev, D. Y., Sergeeva, A. P., and Boldyrev, A. I. (2009). "Multifold Aromaticity, Multifold Antiaromaticity, and Conflicting Aromaticity: Implications for Stability and Reactivity of Clusters," in Chemical Reactivity Theory (Boca Raton, FL, USA: CRC Press), 456–469.

Conflict of Interest: The authors declare that the research was conducted in the absence of any commercial or financial relationships that could be construed as a potential conflict of interest.

The reviewer (SG) declared a past co-authorship with one of the authors (PKC) to the handling Editor.

frontiers in Chemistry

ORIGINAL RESEARCH
published: 10 September 2021
doi: 10.3389/fchem.2021.751482

OsB_9^-: An Aromatic Osmium-Centered Monocyclic Boron Ring

Rui Yu[1], *Sudip Pan*[*,2,3] *and Zhong-hua Cui*[*,1,4]

[1]Institute of Atomic and Molecular Physics, Key Laboratory of Physics and Technology for Advanced Batteries (Ministry of Education), Jilin University, Changchun, China, [2]Wilhelm Ostwald Institute for Physical and Theoretical Chemistry, Leipzig University, Leipzig, Germany, [3]Fachbereich Chemie, Philipps-Universität Marburg, Marburg, Germany, [4]Beijing National Laboratory for Molecular Sciences, Beijing, China

Transition-metal-centered monocyclic boron wheels are important candidates in the family of planar hypercoordinate species that show intriguing structure, stability and bonding situation. Through the detailed potential energy surface explorations of MB_9^- (M = Fe, Ru, Os) clusters, we introduce herein OsB_9^- to be a new member in the transition-metal-centered borometallic molecular wheel gallery. Previously, FeB_9^- and RuB_9^- clusters were detected by photoelectron spectroscopy and the structures were reported to have singlet D_{9h} symmetry. Our present results show that the global minimum for FeB_9^- has a molecular wheel-like structure in triplet spin state with C_s symmetry, whereas its heavier homologues are singlet molecular wheels with D_{9h} symmetry. Chemical bonding analyses show that RuB_9^- and OsB_9^- display a similar type of electronic structure, where the dual σ + π aromaticity, originated from three delocalized σ bonds and three delocalized π bonds, accounts for highly stable borometallic molecular wheels.

Keywords: molecular wheel, bonding, electron delocalization, dual aromaticity, electronic structure calculation

OPEN ACCESS

Edited by:
Ambrish Kumar Srivastava,
Deen Dayal Upadhyay Gorakhpur University, India

Reviewed by:
Hong-Guang Xu,
Chinese Academy of Sciences (CAS), China
Jifu Sun,
Shandong University of Science and Technology, China
Jin-Chang Guo,
Shanxi University, China

***Correspondence:**
Sudip Pan
pans@chemie.uni-marburg.de
Zhong-hua Cui
zcui@jlu.edu.cn

Specialty section:
This article was submitted to Theoretical and Computational Chemistry, a section of the journal Frontiers in Chemistry

Received: *01 August 2021*
Accepted: *24 August 2021*
Published: *10 September 2021*

Citation:
Yu R, Pan S and Cui Z (2021) OsB_9^-: An Aromatic Osmium-Centered Monocyclic Boron Ring. Front. Chem. 9:751482. doi: 10.3389/fchem.2021.751482

INTRODUCTION

The pure and doped boron clusters have attracted great attentions because of their novel structures, intriguing chemical bonds and promising building blocks for boron-based nanomaterials (Alexandrova et al., 2006; Jian et al., 2019). Up to date, great achievements of boron-based clusters have been attained by extensive experimental and theoretical studies (Albert and Hillebrecht, 2009). They show a zoo of structural diversity ranging from planar (Pan et al., 2008; Piazza et al., 2014; Bai et al., 2019) or quasi-planar (Popov et al., 2013) configurations, tubular nanostructures (Kiran et al., 2005; Yang et al., 2008) to all-boron borospherenes/borophenes (Wang 2016; Li et al., 2017) with the increasing B_n size. On the other hand, the striking electronic properties, i.e., multiple aromaticity, nuclear dynamics, hydrocarbon analogues strongly enrich our knowledge of electronic theory. These unusual structural and electronic properties can be regarded as a consequence of the electron deficiency of boron atom, which gives rise to the extraordinary ability of boron to form delocalized multi-center bonds with itself and other elements. Indeed, the introduction of heteroatoms in boron clusters has created a variety of intriguing doped boron clusters, including metal-centered monocyclic ring/tubular/cage structures, (Romanescu et al., 2011; Jian et al., 2016; Dong et al., 2018; Liang et al., 2018; Chen et al., 2019; Lu et al., 2021), half-sandwich structures, (Chen et al., 2018; Ren et al., 2019), inverse sandwich structures, (Cui et al., 2020; Jiang et al., 2021), metallo-borophenes (Li et al., 2016; Zhang et al., 2016) and metallo-borospherenes, (Chen et al., 2020; Zhang et al., 2021), strongly leading to a new direction of research on boron

chemistry and pushing the limit of structural chemistry as well as the record of coordination number in 2D and 3D environments for central metal atoms. (Islas et al., 2007; Liu et al., 2007; Miao et al., 2009; Li et al., 2012; Popov et al., 2014; Pan et al., 2018; Chen et al., 2019).

Amongst, the metal-centered monocyclic wheels represent a family of fascinating planar double aromatic borometallic compounds (Luo 2008; Pu et al., 2009; Romanescu et al., 2013; Romanescu et al., 2013). Such species were firstly found in the global minimum of CoB_8^- and FeB_9^- predicted by computational studies (Ito et al., 2008; Pu et al., 2009). After that, a set of MB_n^- monocyclic wheels (CoB_8^-, FeB_8^-, FeB_9^-, RuB_9^-, RhB_9^- and IrB_9^-) (Ito et al., 2008; Luo 2008; Romanescu et al., 2011; Li et al., 2012; Yang et al., 2015) have been characterized by the photoelectron spectroscopy supported by the computational studies. Thereafter, TaB_{10}^- and NbB_{10}^-, the largest member setting the new limit of maximum coordination number in planar form, were also experimentally detected (Galeev et al., 2012; Li et al., 2013). The extraordinary stability in planar structures in all these metal-centered monocyclic wheels can be rationalized by the presence of σ and π double aromaticity, making it an effective electronic design principle.

We noted that MB_n^- (M = group 8 and 9 elements) clusters have been detected and characterized to be the global monocyclic wheels except for M = Os. Thus, the question remains as to whether OsB_9^- is a real exception. To address this issue, the detailed potential energy surfaces (PESs) of MB_9^- (M = Fe, Ru, Os) were explored herein, and structural and electronic properties of the lowest-energy structures were systematically analyzed by coupling with various chemical bonding approaches. Interestingly, we found a new global minimum for FeB_9^-. A molecular wheel-like structure in triplet spin state with C_s symmetry is lower in energy than the previously reported singlet molecular wheel form with D_{9h} symmetry (Romanescu et al., 2012). On the other hand, OsB_9^- is a singlet global monocyclic wheel that behaves similarly to RuB_9^-, where σ and π double aromaticity (three delocalized σ bonds and three delocalized π bonds) gives rise to their high stability, making it a suitable target for future experimental detection. (Romanescu et al., 2011).

COMPUTATIONAL METHODS

The CALYPSO (Wang et al., 2016) (Crystal structure AnaLYsis by Particle Swarm Optimization) code was used for the detailed structural explorations of MB_9^- (M = Fe, Ru, Os) in their singlet, triplet, and quintet spin states at the PBE0/def2-SVP level. For the low-lying energy isomers, further reoptimization followed by harmonic vibrational frequency calculation were done at the PBE0/def2-TZVPP level. For comparison, another level of theory, TPSSh/def2-TZVPP was also chosen. For further energetic refinement, singlet point calculations were further done at the CCSD(T) (Pople et al., 1987)/def2-TZVPP//PBE0/def2-TZVPP level. Total energies were corrected by the zero-point corrected energies (ZPE) of PBE0/def2-TZVPP level. The natural bond orbital (NBO), (Glendening et al., 2019), nucleus-independent chemical shift (NICS), (Mitchell 2001), adaptive natural density partitioning (AdNDP), (Zubarev and Boldyrev, 2008), quantum theory of atoms in molecules (QTAIM) and electron localization (ELF) analyses (Fuster et al., 2000) were performed for these global monocyclic molecular wheels using Multiwfn code (Lu and Chen, 2012). To facilitate future experimental characterization, the simulated photoelectron spectra of RuB_9^- and OsB_9^- were calculated at the BP86/def2-TZVPP level based on generalized Koopmans' theorem (Tsuneda et al., 2010). The aromaticity was understood by the gauge including magnetically induced current (GIMIC) analysis (Fliegl et al., 2011) and the anisotropy of the current induced density (ACID) (Geuenich et al., 2005). All the calculations were performed using the Gaussian 09 package. (Frisch et al., 2016).

Structures and Energetics

The singlet PES of FeB_9^- was explored in 2008, (Ito et al., 2008), where the singlet D_{9h}-symmetry planar nonacoordinate Fe-centered monocyclic boron wheel (isomer **d** in **Figure 1**) was reported to be the lowest-energy structure that lies 14.9 kcal/mol more stable than the second alternative at the BP86/TZVPP level. In 2012, the photoelectron spectroscopy of FeB_9^- was explained based on the singlet wheel isomer (Romanescu et al., 2012). However, by the detailed structural searches of singlet, triplet, and quintet states, we found that the triplet molecular wheel with C_s symmetry (**a**) is 19.5 kcal/mol lower in energy than **d** at the PBE0/def2-TZVPP level. Meanwhile, large T1 diagnostic values obtained with the coupled-cluster wave function indicate that FeB_9^- system is a multireference problem. Note that the broken-symmetry spin-unrestricted approach was used for the monocyclic boron wheel, which is still 2.1 kcal/mol lower in energy relative to the closed-shell one. Thus, the coexistence of triplet global state of the molecular wheel FeB_9^- could be the reason of the observed broad features in photoelectron spectrum, as assumed by the authors. (Romanescu et al., 2012).

Figure 2 displays the low-lying energy isomers of RuB_9^- and OsB_9^-. The monocyclic boron wheel with D_{9h} symmetry and $^1A_1'$ electronic state is predicted to be a real global minimum having the lowest vibrational frequencies of 62.2 and 17.2 cm^{-1} for RuB_9^- and OsB_9^-, respectively. At the CCSD(T)/def2-TZVPP level, the monocyclic boron wheel is a global minimum that lies 30.4 and 37.1 kcal/mol more stable than the second alternative for RuB_9^- and OsB_9^-, respectively. The triplet monocyclic boron wheels are also located, but unlike FeB_9^-, they are significantly high-energy isomers. Note that the results at the TPSSh/def2-TZVPP level are very similar to the PBE0/def2-TZVPP level, except for the relative energy between isomer **a** and **d** of FeB_9^- (see **Supplementary Figure S1**). This is presumably because of the multireference character in these systems. The T1 diagnostic factors of RuB_9^- and OsB_9^- are within 0.05, suggesting that the single-reference method can be safely used for these two clusters. Given the fact that RuB_9^- was detected earlier by photoelectron spectroscopy, we believe that the monocyclic boron wheel OsB_9^- cluster is also a suitable target for the gas-phase experimental study.

To understand the high stability of the MB_9^- monocyclic wheels, their detailed structural parameters are given in **Figure 2**. We found the MB_9^- (M = Ru, Os) clusters possess similar structural properties. In the case of OsB_9^-, like all other metal-centered monocyclic boron wheels, the B-B bonds show

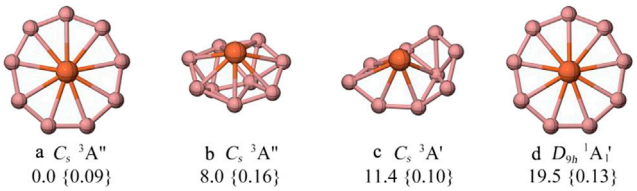

FIGURE 1 | The low-lying energy isomers of FeB_9^- computed at the PBE0/def2-TZVPP level and T1 diagnostic values obtained with coupled-cluster wavefunction are given in curly braces. All energies are corrected from zero-point energies (ZPE) at the PBE0/def2-TZVPP level.

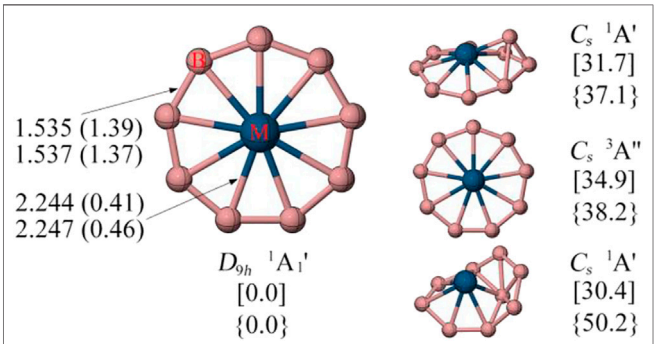

FIGURE 2 | The minimum energy geometries and the corresponding bond distances in Å and WBI values in parentheses of RuB_9^- **(top)** and OsB_9^- **(bottom)** are given at the PBE0/def2-TZVPP level. Relative energies in kcal/mol of the low-lying energy isomers of [RuB_9^-] and {OsB_9^-} are given at the CCSD(T)/def2-TZVPP//PBE0/def2-TZVPP level with ZPE correction of PBE0. The T1 diagnostic are less than 0.05.

strong multiple bonding characteristic as indicated by the short bond distance of 1.54 Å and Wiberg bond indices (WBIs) value of 1.37, which is clearly shorter than the single B-B bond (1.70 Å) using the self-consistent covalent radius of Pyykkö (Pyykko and Atsumi, 2009). The strong peripheral B-B bonds is because each boron atom fully participate in the two-center two electron (2c-2e) B-B σ bonds and two sets of the delocalized σ and π bonds (see discussed below). The M-B bonds of OsB_9^- have the bond distance of 2.247 Å (WBI = 0.46), which is slightly longer than the M-B single bond using the self-consistent covalent radius of Pyykkö, a common characteristic for the multicentered bonds. (Pyykko and Atsumi, 2009).

Electronic Delocalization

The adaptive natural density partitioning (AdNDP) (Zubarev and Boldyrev, 2008) analyses were carried out for OsB_9^- to further understand its chemical bonding and electronic structure. As shown in **Figure 3A**, the first row displays three one center-two electrons (1c-2e) lone pair electrons associated with d orbitals of Os center, where the occupation number (ON) for the d_z^2 LP is 1.99 |e| and the same for others two are 1.49 |e|. Somewhat lower ON for these LPs are because of partial delocalization to boron rings. An alternative 10c-2e description gives ideal 2.00 |e| ON, but we continue it as 1c-2e LPs for similarity since in the previously reported AdNDP results for RuB_9^- the authors describe them as LPs (Romanescu et al., 2011). Nevertheless, even consideration of them as 10c-2e delocalized σ-bonds would not change the nature of aromaticity drawn based on the number of delocalized electrons. Nine 2c-2e bonds with ONs of 1.96 |e| account for the peripheral B-B bonds. The second row presents three delocalized 10c-2e σ bonds (left) and three delocalized 10c-2e π bonds (right), and they vividly satisfy the σ + π double aromaticity. The electron localization function (ELF) (Fuster et al., 2000) as shown in **Figure 3B** further confirms AdNDP results. The plot of ELF shows that the strong electron density is localized in the peripheral boron ring, but relatively lower electron density between M center and boron ring because of the delocalized σ and π clouds.

We performed quantum theory of atom in molecules (QTAIM) analysis to shed additional light into the nature of Os-B interaction. The contour plot of Laplacian of the electron density ($\nabla^2\rho(\mathbf{r})$) at the molecular plane is given in **Figure 3C**. There are nine bond paths and bond critical points (indicated by the small blue spheres) between Os and boron centers. The plot also shows that there are electron density accumulated regions (indicated by blue dotted lines) in between B and Os centers but BCPs just lie outside of the blue dotted regions because of polar nature of the bond giving positive $\nabla^2\rho(\mathbf{r_c})$ value at BCP. This is a very usual feature for the bonds involving heavier elements where the criterion of negative $\nabla^2\rho(\mathbf{r_c})$ value at BCP for covalent bond does not satisfy. For these cases, the total energy density $H(\mathbf{r_c})$ is more suitable descriptor for such cases which is negative for covalent bonds (Cremer and Kraka, 1984).[55] The corresponding value of $H(\mathbf{r_c})$ at the BCP of Os-B bonds is −0.04 au, showing their covalent nature. On the other hand, for B-B bonds as expected both $\nabla^2\rho(\mathbf{r_c})$ and $H(\mathbf{r_c})$ are negative. Similar electron topology is noted in case of RuB_9^- as well (see **Supplementary Figure S2** in supporting information).

Aromaticity

The dual σ + π aromaticity was further confirmed in the following discussion. The nucleus-independent chemical shift (NICS) (Mitchell 2001) is a key method to quantify aromaticity, where $NICS_{zz}$ values (the out-of-plane ("zz") shielding tensor component of NICS). As shown in **Figure 4A**, the grids of $NICS_{zz}$ points are created at the center of wheels, the center of B-M-B ring and out of the ring associated with 1.0 Å vertical spacings from the wheel plane. The considerable negative $NICS_{zz}$ values vividly show aromatic boron wheels, especially the big $NICS(1)_{zz}$ of the wheel centers (−123.6 ppm) is consistent with

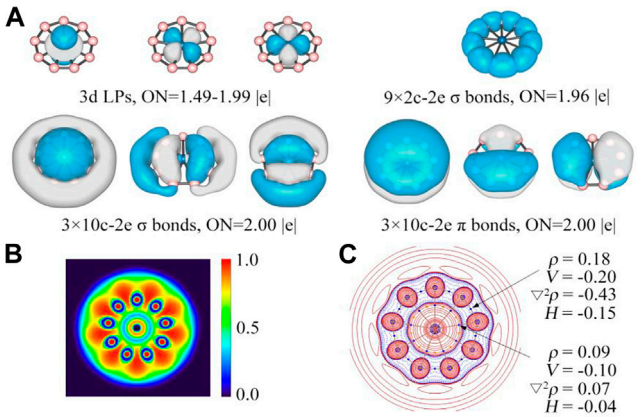

FIGURE 3 | (A) AdNDP results, and **(B)** color-filled map of ELF and **(C)** contour plot of Laplacian of electron density of OsB_9^-. In c, the contour line map of Laplacian of electron density, red solid lines and blue dotted lines represent positive and negative regions, respectively. Blue and orange points correspond to position of bond critical points (BCPs) and ring critical point (RCP), respectively. Values of some real space functions at the BCP are given, including ρ (electron density), *V* (potential energy density), $\nabla^2\rho$, *H* (energy density).

the reported transition-metal-centered borometallic molecular wheel family. **Figure 4B** displays a gauge including magnetically induced current (GIMIC) map, (Fliegl et al., 2011), where the induced ring current is generated by employing an external magnetic field perpendicular to the molecular plane. The diatropic (clockwise) current comply with the left-handed rule. It is worthy of note that the inner and outside of the peripheral ring both show a diatropic and unidirectional current. This current behavior is similar to the C_{18} clusters with double aromaticity (σ + π) but sharply different from the benzene (π aromaticity only), where the ring current show a diatropic inside but paratropic outside of benzene ring. The induced current density ($\mathbf{J}^{ind}$) is integrated into a specific area, which starts at the center of the ring and intersects the B-B bond ending about 4 Å away for the current system. The ring-current strength of RuB_9^- (25.4 nA/T) and OsB_9^- (26.4 nA/T) is similar to C_{18} (Lu et al., 2020) (25.3 and 21.2 nA/T), and stronger than the benzene (11.5 nA/T) at the wB97XD/def2-TZVP level, which could be another indicator of dual σ + π aromaticity. The anisotropy of the current induced density (ACID) is able to describe the σ and π contribution for aromaticity as given in **Figure 4C**. Overall, the σ and π dual aromaticity is strongly confirmed by these analyses in **Figure 4** and **Supplementary Figure S3** for OsB_9^- and RuB_9^-, respectively.

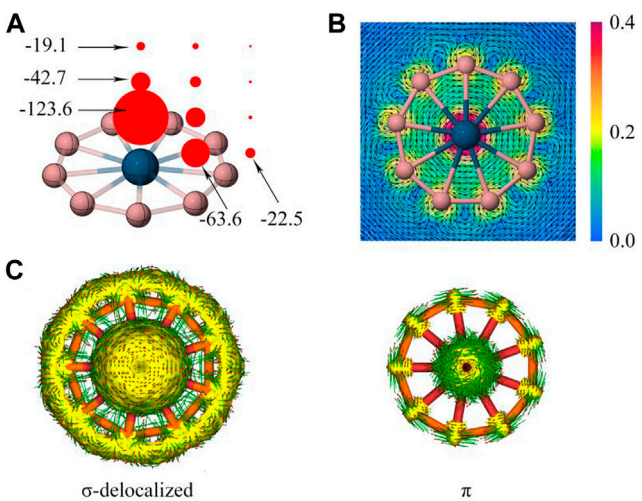

FIGURE 4 | (A) $NICS_{zz}$, and **(B)** GIMIC map and **(C)** induced ring current of the delocalized σ and π electrons based on ACID values of OsB_9^-. In b), the arrows indicate direction of induced current, the color correspond to magnitude of induced current.

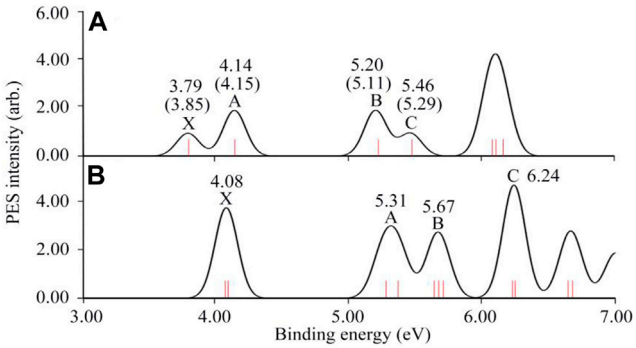

FIGURE 5 | The simulated photoelectron spectrums of **(A)** RuB_9^- and **(B)** OsB_9^- were calculated at the BP86/def2-TZVPP level based on generalized Koopmans' theorem. The experimental results of RuB_9^- are given in parenthesis.

Simulated Photoelectron Spectra

The simulated photoelectron spectra of RuB_9^- and OsB_9^- are given in **Figure 5** based on the generalized Koopmans' theorem (Tsuneda et al., 2010). The simulated spectrum for RuB_9^- is in good agreement with the experimental data as shown in **Figure 5A**. Thus, to facilitate the experimental confirmation, the simulated photoelectron spectrum of OsB_9^- cluster is illustrated in **Figure 5B**, where the well-resolved detachment transitions at the lower-binding-energy side, are labeled as X (4.08), A (5.31), B (5.67), C (6.24) in eV.

CONCLUSION

The OsB_9^- cluster was found to be a new member of transition-metal-centered borometallic molecular wheel family. The detailed electronic structure analyses including the AdNDP, ELF, NICS, and ACID approaches all suggested that the dual σ + π aromaticity (three delocalized σ bonds and three delocalized π bonds) occurs in RuB_9^- and OsB_9^-, and it is a key factor to design highly stable borometallic molecular wheels. Additionally, we found a different picture relative to the previous work for FeB_9^-. The present results show that the global minimum for FeB_9^- has a molecular wheel-like structure in triplet spin state with C_s symmetry, whereas previously reported singlet molecular wheels with D_{9h} symmetry is higher energy isomer.

DATA AVAILABILITY STATEMENT

The original contributions presented in the study are included in the article/**Supplementary Material**, further inquiries can be directed to the corresponding authors.

AUTHOR CONTRIBUTIONS

RY performed all the calculations, SP and Z-HC designed the work, validated the results, and wrote the draft.

FUNDING

This work was funded by the National Natural Science Foundation of China (No. 11874178, 11922405, 91961204). This work was supported by Beijing National Laboratory for Molecular Sciences (BNLMS201910). The partial calculations in this work supported by High Performance Computing Center of Jilin University, China.

SUPPLEMENTARY MATERIAL

The Supplementary Material for this article can be found online at: https://www.frontiersin.org/articles/10.3389/fchem.2021.751482/full#supplementary-material

REFERENCES

Albert, B., and Hillebrecht, H. (2009). Boron: Elementary Challenge for Experimenters and Theoreticians. *Angew. Chem. Int. Ed.* 48, 8640–8668. doi:10.1002/anie.200903246

Alexandrova, A. N., Boldyrev, A. I., Zhai, H.-J., and Wang, L.-S. (2006). All-boron Aromatic Clusters as Potential New Inorganic Ligands and Building Blocks in Chemistry. *Coord. Chem. Rev.* 250, 2811–2866. doi:10.1016/j.ccr.2006.03.032

Bai, H., Chen, T.-T., Chen, Q., Zhao, X.-Y., Zhang, Y.-Y., Chen, W.-J., et al. (2019). Planar B41− and B42− Clusters with Double-Hexagonal Vacancies. *Nanoscale* 11, 23286–23295. doi:10.1039/c9nr09522e

Chen, B. L., Sun, W. G., Kuang, X. Y., Lu, C., Xia, X. X., Shi, H. X., et al. (2018). Structural Stability and Evolution of Medium-Sized Tantalum-Doped Boron Clusters: A Half-Sandwich-Structured TaB12 - Cluster. *Inorg. Chem.* 57, 343–350. doi:10.1021/acs.inorgchem.7b02585

Chen, T.-T., Li, W.-L., Bai, H., Chen, W.-J., Dong, X.-R., Li, J., et al. (2019). ReB8- and ReB9-: New Members of the Transition-Metal-Centered Borometallic Molecular Wheel Family. *J. Phys. Chem. A.* 123, 5317–5324. doi:10.1021/acs.jpca.9b03942

Chen, T. T., Li, W. L., Chen, W. J., Yu, X. H., Dong, X. R., Li, J., et al. (2020). Spherical Trihedral Metallo-Borospherenes. *Nat. Commun.* 11, 2766. doi:10.1038/s41467-020-16532-x

Cremer, D., and Kraka, E. (1984). Chemical Bonds without Bonding Electron Density - Does the Difference Electron-Density Analysis Suffice for a Description of the Chemical Bond?. *Angew. Chem. Int. Ed.* 23, 627–628. doi:10.1002/anie.198406271

Cui, Z.-h., Chen, C., Wang, Q., Zhao, L., Wang, M.-h., and Ding, Y.-h. (2020). Inverse sandwich Complexes of B7M2−, B8M2, and B9M2+ (M = Zr, Hf): the

Nonclassical M-M Bonds Embedded in Monocyclic boron Rings. *New J. Chem.* 44, 17705–17713. doi:10.1039/d0nj03999c

Dong, X., Jalife, S., Vásquez-Espinal, A., Ravell, E., Pan, S., Cabellos, J. L., et al. (2018). Li2 B12 and Li3 B12 : Prediction of the Smallest Tubular and Cage-like Boron Structures. *Angew. Chem. Int. Ed.* 57, 4627–4631. doi:10.1002/anie.201800976

Fliegl, H., Taubert, S., Lehtonen, O., and Sundholm, D. (2011). The Gauge Including Magnetically Induced Current Method. *Phys. Chem. Chem. Phys.* 13, 20500–20518. doi:10.1039/c1cp21812c

Frisch, M. J., Trucks, G. W., Schlegel, H. B., Scuseria, G. E., Robb, M. A., Cheeseman, J. R., et al. (2016). *Gaussian 09, Revision C.01*. Wallingford CT: Gaussian, Inc.

Fuster, F., Sevin, A., and Silvi, B., (2000). Topological Analysis of the Electron Localization Function (ELF) Applied to the Electrophilic Aromatic Substitution, *J. Phys. Chem. A.* 104, 852–858. doi:10.1021/jp992783k

Galeev, T. R., Romanescu, C., Li, W.-L., Wang, L.-S., and Boldyrev, A. I. (2012). Observation of the Highest Coordination Number in Planar Species: Decacoordinated TaB10− and NbB10− Anions. *Angew. Chem. Int. Ed.* 51, 2101–2105. doi:10.1002/anie.201107880

Geuenich, D., Hess, K., Köhler, F., and Herges, R. (2005). Anisotropy of the Induced Current Density (ACID), a General Method to Quantify and Visualize Electronic Delocalization. *Chem. Rev.* 105, 3758–3772. doi:10.1021/cr0300901

Glendening, E. D., Landis, C. R., and Weinhold, F. (2019). NBO 7.0 : New Vistas in Localized and Delocalized Chemical Bonding Theory. *J. Comput. Chem.* 40, 2234–2241. doi:10.1002/jcc.25873

Islas, R., Heine, T., Ito, K., Schleyer, P. V. R., and Merino, G. (2007). Boron Rings Enclosing Planar Hypercoordinate Group 14 Elements. *J. Am. Chem. Soc.* 129, 14767–14774. doi:10.1021/ja074956m

Ito, K., Pu, Z., Li, Q.-S., and Schleyer, P. V. R. (2008). Cyclic Boron Clusters Enclosing Planar Hypercoordinate Cobalt, Iron, and Nickel. *Inorg. Chem.* 47, 10906–10910. doi:10.1021/ic800993b

Jian, T., Chen, X., Li, S.-D., Boldyrev, A. I., Li, J., and Wang, L.-S. (2019). Probing the Structures and Bonding of Size-Selected boron and Doped-boron Clusters. *Chem. Soc. Rev.* 48, 3550–3591. doi:10.1039/c9cs00233b

Jian, T., Li, W.-L., Popov, I. A., Lopez, G. V., Chen, X., Boldyrev, A. I., et al. (2016). Manganese-centered Tubular boron Cluster - MnB16−: A New Class of Transition-Metal Molecules. *J. Chem. Phys.* 144, 154310. doi:10.1063/1.4946796

Jiang, Z.-Y., Chen, T.-T., Chen, W.-J., Li, W.-L., Li, J., and Wang, L.-S. (2021). Expanded Inverse-Sandwich Complexes of Lanthanum Borides: La2B10- and La2B11-. *J. Phys. Chem. A.* 125, 2622–2630. doi:10.1021/acs.jpca.1c01149

Kiran, B., Bulusu, S., Zhai, H.-J., Yoo, S., Zeng, X. C., and Wang, L.-S. (2005). Planar-to-tubular Structural Transition in boron Clusters: B20 as the Embryo of Single-Walled boron Nanotubes. *Proc. Natl. Acad. Sci.* 102, 961–964. doi:10.1073/pnas.0408132102

Li, W.-L., Romanescu, C., Galeev, T. R., Piazza, Z. A., Boldyrev, A. I., and Wang, L.-S. (2012). Transition-Metal-Centered Nine-Membered Boron Rings: M©B9 and M©B9- (M = Rh, Ir). *J. Am. Chem. Soc.* 134, 165–168. doi:10.1021/ja209808k

Li, W.-L., Romanescu, C., Piazza, Z. A., and Wang, L.-S. (2012). Geometrical Requirements for Transition-Metal-Centered Aromatic boron Wheels: the Case of VB10−. *Phys. Chem. Chem. Phys.* 14, 13663–13669. doi:10.1039/c2cp42218b

Li, W. L., Ivanov, A. S., Federič, J., Romanescu, C., Černušák, I., Boldyrev, A. I., et al. (2013). On the Way to the Highest Coordination Number in the Planar Metal-Centred Aromatic Ta©B10- Cluster: Evolution of the Structures of TaB(n)- (N = 3-8). *J. Chem. Phys.* 139, 104312–104313. doi:10.1063/1.4820401

Li, W. L., Chen, X., Jian, T., Chen, T. T., Li, J., and Wang, L. S. (2017). From Planar boron Clusters to Borophenes and Metalloborophenes. *Nat. Rev. Chem.* 1, 1–9. doi:10.1038/s41570-017-0071

Li, W. L., Jian, T., Chen, X., Chen, T. T., Lopez, G. V., Li, J., et al. (2016). The Planar CoB 18 − Cluster as a Motif for Metallo-Borophenes. *Angew. Chem. Int. Ed.* 55, 7358–7363. doi:10.1002/anie.201601548

Liang, W.-y., Das, A., Dong, X., and Cui, Z.-h. (2018). Lithium Doped Tubular Structure in LiB20 and LiB20−: a Viable Global Minimum. *Phys. Chem. Chem. Phys.* 20, 16202–16208. doi:10.1039/c8cp01376d

Liu, X., Zhao, G. F., Guo, L. J., Jing, Q., and Luo, Y. H. (2007). Structural, Electronic, and Magnetic Properties of MB_n (M = Cr, Mn, Fe, Co, Ni, N≤7) Clusters. *Phys. Rev. A.* 75, 063201. doi:10.1103/physreva.75.063201

Lu, T., and Chen, F. (2012). Multiwfn: A Multifunctional Wavefunction Analyzer. *J. Comput. Chem.* 33, 580–592. doi:10.1002/jcc.22885

Lu, T., Chen, Q., and Liu, Z. (2020). A Thorough Theoretical Exploration of Intriguing Characteristics of Cyclo[18]carbon: Geometry, Bonding Nature, Aromaticity, Weak Interaction, Reactivity, Excited States, Vibrations, Molecular Dynamics and Various Molecular Properties. *ChemRxiv*, 468–475. doi:10.26434/chemrxiv.11320130

Lu, X.-Q., Gao, C.-Y., Wei, Z., and Li, S.-D. (2021). Cage-like La4B24 and Core-Shell La4B290/+/− : Perfect Spherically Aromatic Tetrahedral Metallo-Borospherenes. *J. Mol. Model.* 27, 130. doi:10.1007/s00894-021-04739-8

Luo, Q. (2008). Boron Rings Containing Planar Octa-And Enneacoordinate Cobalt, Iron and Nickel Metal Elements. *Sci. China Ser. B-chem.* 51, 607–613. doi:10.1007/s11426-008-0073-9

Miao, C., Guo, J., and Li, S. (2009). M@B9 and M@B10 Molecular Wheels Containing Planar Nona- and Deca-Coordinate Heavy Group 11, 12, and 13 Metals (M=Ag, Au, Cd, Hg, in, Tl). *Sci. China Ser. B-chem.* 52, 900–904. doi:10.1007/s11426-009-0086-z

Mitchell, R. H. (2001). Measuring Aromaticity by NMR. *Chem. Rev.* 101, 1301–1316. doi:10.1021/cr990359+

Pan, L.-L., Li, J., and Wang, L.-S. (2008). Low-lying Isomers of the B9− boron Cluster: The Planar Molecular Wheel versus Three-Dimensional Structures. *J. Chem. Phys.* 129, 024302. doi:10.1063/1.2948405

Pan, S., Kar, S., Saha, R., Osorio, E., Zarate, X., Zhao, L., et al. (2018). Boron Nanowheels with Axles Containing Noble Gas Atoms: Viable Noble Gas Bound MB10 − Clusters (M=Nb, Ta). *Chem. Eur. J.* 24, 3590–3598. doi:10.1002/chem.201705790

Piazza, Z. A., Hu, H.-S., Li, W.-L., Zhao, Y.-F., Li, J., and Wang, L.-S. (2014). Planar Hexagonal B36 as a Potential Basis for Extended Single-Atom Layer boron Sheets. *Nat. Commun.* 5, 3113. doi:10.1038/ncomms4113

Pople, J. A., Head-Gordon, M., and Raghavachari, K. (1987). Quadratic Configuration Interaction. A General Technique for Determining Electron Correlation Energies. *J. Chem. Phys.* 87, 5968–5975. doi:10.1063/1.453520

Popov, I. A., Piazza, Z. A., Li, W. L., Wang, L. S., and Boldyrev, A. I. (2013). A Combined Photoelectron Spectroscopy and Ab Initio Study of the Quasi-Planar B24(-) Cluster. *J. Chem. Phys.* 139, 144307. doi:10.1063/1.4824156

Popov, I. A., Li, W.-L., Piazza, Z. A., Boldyrev, A. I., and Wang, L.-S. (2014). Complexes between Planar Boron Clusters and Transition Metals: A Photoelectron Spectroscopy and Ab Initio Study of CoB12- and RhB12-. *J. Phys. Chem. A.* 118, 8098–8105. doi:10.1021/jp411867q

Pu, Z., Ito, K., Schleyer, P. v. R., and Li, Q.-S. (2009). Planar Hepta-, Octa-, Nona-, and Decacoordinate First Row D-Block Metals Enclosed by Boron Rings. *Inorg. Chem.* 48, 10679–10686. doi:10.1021/ic901377h

Pyykkö, P., and Atsumi, M. (2009). Molecular Single-Bond Covalent Radii for Elements 1-118. *Chem. Eur. J.* 15, 186–197. doi:10.1002/chem.200800987

Ren, M., Jin, S., Wei, D., Jin, Y., Tian, Y., Lu, C., et al. (2019). NbB12−: a New Member of Half-sandwich Type Doped boron Clusters with High Stability. *Phys. Chem. Chem. Phys.* 21, 21746–21752. doi:10.1039/c9cp03496j

Romanescu, C., Galeev, T. R., Li, W.-L., Boldyrev, A. I., and Wang, L.-S. (2011). Aromatic Metal-Centered Monocyclic Boron Rings: CoB8− and RuB9−. *Angew. Chem. Int. Ed.* 50, 9334–9337. doi:10.1002/anie.201104166

Romanescu, C., Galeev, T. R., Li, W.-L., Boldyrev, A. I., and Wang, L.-S. (2013). Geometric and Electronic Factors in the Rational Design of Transition-Metal-Centered boron Molecular Wheels. *J. Chem. Phys.* 138, 134315. doi:10.1063/1.4798935

Romanescu, C., Galeev, T. R., Li, W.-L., Boldyrev, A. I., and Wang, L.-S. (2013). Transition-Metal-Centered Monocyclic Boron Wheel Clusters (MBn): A New Class of Aromatic Borometallic Compounds. *Acc. Chem. Res.* 46, 350–358. doi:10.1021/ar300149a

Romanescu, C., Galeev, T. R., Sergeeva, A. P., Li, W.-L., Wang, L.-S., and Boldyrev, A. I. (2012). Experimental and Computational Evidence of Octa- and Nona-Coordinated Planar Iron-Doped boron Clusters: FeB8− and FeB9−. *J. Organomet. Chem.* 721-722, 148–154. doi:10.1016/j.jorganchem.2012.07.050

Tsuneda, T., Song, J. W., Suzuki, S., and Hirao, K. (2010). On Koopmans' Theorem in Density Functional Theory. *J. Chem. Phys.* 133, 174101–174109. doi:10.1063/1.3491272

Wang, H., Wang, Y., Lv, J., Li, Q., Zhang, L., and Ma, Y. (2016). CALYPSO Structure Prediction Method and its Wide Application. *Comput. Mater. Sci.* 112, 406–415. doi:10.1016/j.commatsci.2015.09.037

Wang, L.-S. (2016). Photoelectron Spectroscopy of Size-Selected boron Clusters: from Planar Structures to Borophenes and Borospherenes. *Int. Rev. Phys. Chem.* 35, 69–142. doi:10.1080/0144235x.2016.1147816

Yang, L.-M., Ganz, E., Chen, Z., Wang, Z.-X., and Schleyer, P. v. R. (2015). Four Decades of the Chemistry of Planar Hypercoordinate Compounds. *Angew. Chem. Int. Ed.* 54, 9468–9501. doi:10.1002/anie.201410407

Yang, X. B., Ding, Y., and Ni, J. (2008). Ab Initio prediction of Stable boron Sheets and boron Nanotubes: Structure, Stability, and Electronic Properties. *Phys. Rev. B.* 77, 41402. doi:10.1103/physrevb.77.041402

Zhang, H., Li, Y., Hou, J., Tu, K., and Chen, Z. (2016). FeB6 Monolayers: The Graphene-like Material with Hypercoordinate Transition Metal. *J. Am. Chem. Soc.* 138, 5644–5651. doi:10.1021/jacs.6b01769

Zhang, Y., Lu, X.-Q., Yan, M., and Li, S.-D. (2021). Perfect Spherical Tetrahedral Metallo-Borospherene Ta4B18 as a Superatom Following the 18-Electron Rule. *ACS. Omega.* 6, 10991–10996. doi:10.1021/acsomega.1c00828

Zubarev, D. Y., and Boldyrev, A. I. (2008). "Developing Paradigms of Chemical Bonding: Adaptive Natural Density Partitioning. *Phys. Chem. Chem. Phys.* 10, 5207–5217. doi:10.1039/b804083d

Conflict of Interest: The authors declare that the research was conducted in the absence of any commercial or financial relationships that could be construed as a potential conflict of interest.

frontiers in Chemistry

ORIGINAL RESEARCH
published: 17 September 2021
doi: 10.3389/fchem.2021.753617

Theoretical Design of Novel Boron-Based Nanowires *via* Inverse Sandwich Clusters

Cailian Jiang[1], *Zhiwei Lv*[1], *Sudong Lv*[1], *Linwei Sai*[2]*, *Shukai Wang*[1]* and *Fengyu Li*[1]*

[1]School of Physical Science and Technology, Inner Mongolia University, Hohhot, China, [2]College of Science, Hohai University, Changzhou, China

Borophene has important application value, boron nanomaterials doped with transition metal have wondrous structures and chemical bonding. However, little attention was paid to the boron nanowires (NWs). Inspired by the novel metal boron clusters $Ln_2B_n^-$ (Ln = La, Pr, Tb, n = 7–9) adopting inverse sandwich configuration, we examined Sc_2B_8 and Y_2B_8 clusters in such novel structure and found that they are the global minima and show good stability. Thus, based on the novel structural moiety and first-principles calculations, we connected the inverse sandwich clusters into one-dimensional (1D) nanowires by sharing B–B bridges between adjacent clusters, and the 1D-Sc_4B_{24} and 1D-Y_2B_{12} were reached after structural relaxation. The two nanowires were identified to be stable in thermodynamical, dynamical and thermal aspects. Both nanowires are nonmagnetic, the 1D-Sc_4B_{24} NW is a direct-bandgap semiconductor, while the 1D-Y_2B_{12} NW shows metallic feature. Our theoretical results revealed that the inverse sandwich structure is the most energy-favored configuration for transition metal borides Sc_2B_8 and Y_2B_8, and the inverse sandwich motif can be extended to 1D nanowires, providing useful guidance for designing novel boron-based nanowires with diverse electronic properties.

Keywords: first-principles, clusters, inverse sandwich structure, boron-based nanowires, magnetic and electronic properties

OPEN ACCESS

Edited by:
Iwona Anusiewicz,
University of Gdansk, Poland

Reviewed by:
Ke-Qiu Chen,
Hunan University, China
Junjie He,
University of Bremen, Germany
Celina Sikorska,
The University of Auckland, New Zealand

***Correspondence:**
Linwei Sai
sailinwei@hhu.edu.cn
Shukai Wang
wangshukai0323@163.com
Fengyu Li
fengyuli@imu.edu.cn

Specialty section:
This article was submitted to Physical Chemistry and Chemical Physics, a section of the journal Frontiers in Chemistry

Received: *05 August 2021*
Accepted: *30 August 2021*
Published: *17 September 2021*

Citation:
Jiang C, Lv Z, Lv S, Sai L, Wang S and Li F (2021) Theoretical Design of Novel Boron-Based Nanowires via Inverse Sandwich Clusters. Front. Chem. 9:753617. doi: 10.3389/fchem.2021.753617

INTRODUCTION

Boron-based materials were found wide applications in the fileds of emissions, supercapacitors, optical absorptions, photodetectors, *etc.* (Xu et al., 2013; Sussardi et al., 2015; Akopov et al., 2017; Carenco et al., 2013; Tian et al., 2019). Unlike the extensive attention on carbon clusters such as fullerenes and carbon fibers, boron clusters and materials are relatively less studied by scientists. However, there is much space and potential to develop boron-based nanomaterials.

Boron shows a strong tendency to form multi-center-two-electron bonds (mc-2e) in both polyhedral molecules and bulk isotopes (Wang, 2016; Jian et al., 2019; Lipscomb, 1977; Alexandrova et al., 2006) due to its electron deficiency. Therefore, boron clusters have the characteristic of electron delocalization bonding with some delocalized electronic structures and unique aromaticity (Li et al., 2018). In the past two decades, the structure and chemical bonding of bare boron clusters have been studied by combining experimental and theoretical methods (Li et al., 2017; Li et al., 2017; Pan et al., 2019), and planar clusters, nanotube-like cluster structures, graphene-like boron spheres and fullerene-like boron spheres have been found (Kiran et al., 2005; Piazza et al., 2014; Li et al., 2014; Bai et al., 2019; Zhai et al., 2014). Also due to the characteristic of electron deficiency, boron can be doped with metal to form different kinds of metal boride structures. Boron

has formed a large number of important boride materials, ranging from superconducting MgB_2 and superhard transition metal borides to borides with extremely high thermal conductivity (Nagamatsu et al., 2001; Chung et al., 2007).

As the 5th element adjacent to carbon in the periodic table, ring and cage boron clusters have poor stability due to their electron-deficient properties. However, the introduction of transition metals can greatly improve the stability of boron clusters. Transition-metal-doped boron clusters have led to a new direction of boron nanomaterials, such as the metal-centered aromatic borometallic wheels and tubular metal-centered drums (Romanescu et al., 2011; Popov et al., 2015; Jian et al., 2016; Jian et al., 2016; Li et al., 2017). On the other hand, assembling boron clusters by doping them with different types of atoms is a potential way to change properties. For example, CoB_{18}^- and RhB_{18}^- planar clusters have been found, which makes it possible to dope metal with borographene (Li et al., 2016; Jian et al., 2016). Wang and Boldyrev's joint research group have reported a variety of neutral or charged planar wheel clusters centered on supercoordination transition metals M©B_n (M = Fe, Co, Nb, Ru, Rh, Ir, Ta; n = 8–10) (Romanescu et al., 2011).

Recently, Wang's experimental group and Li's theoretical group jointly observed several new metal boron clusters $Ln_2B_n^-$ (Ln = La, Pr, Tb; n = 7–9) with an inverse sandwich structure (Li et al., 2018; Chen et al., 2019). It is found that these clusters have the double aromatic properties of π and σ bonding contributions, showing high stability and symmetry, and the magnetization of B_8^- ring is high. The study provides a novel pattern for the design of new lanthanide borides, and a few inverse sandwich complexes were proposed (Wang et al., 2019; Cui et al., 2020; Shakerzadeh et al., 2020; Xiao et al., 2021). A few questions arise naturally: Would the transition metal borides adopt the inverse sandwich structure in a stable manner? Can the inverse sandwich structure motif be extended to periodic nanomaterials, like designing the super stable 1D-P_{10} nanowire and 2D-P_8N_2 nanosheet based on all pentagon containing P_8 clusters (Wang et al., 2020; Dong et al., 2021)? Thus, in this work, by means of first-principles calculations, we examined the stability of M_2B_8 (M = Sc and Y) clusters with the inverse sandwich structure, and extended the inverse sandwich moiety to design novel boron-based nanowires (NWs). The constructed 1D-Sc_4B_{24} and 1D-Y_2B_{12} NWs show good stability, and the former/later one is a semiconductor/metal. Our theoretical work successfully extended the inverse sandwich moiety to the 1D crystals, which is helpful to design novel boron-based nanowires with diverse electronic properties.

METHODS

The comprehensive genetic algorithm (CGA) (Zhao et al., 2016) combined with the DMol^3 program (Delley, 1990; Delley, 2000) was used to search the global minimum of Sc_2B_8 and Y_2B_8 clusters. The low-energy clusters generated by CGA were further optimized using density functional theory (DFT) implemented in the Vienna *Ab initio* Simulation Package (VASP) code (Kresse and Furthmuller, 1996; Kresse and Hafner, 1993; Kresse and Hafner, 1994). The exchange and correlation functional are defined by the generalized gradient approximation (GGA) with the Perdew–Burke–Ernzerhof (PBE) functional (Perdew et al., 1996). The k points of the geometric optimization and the molecular dynamics simulation were set to $1 \times 7 \times 1$ and $1 \times 3 \times 1$. The phonon spectra were calculated by VASP and Phonopy codes (Togo and Tanaka, 2015). Thermal stability was assessed at 300 and 500 K based on first-principles molecular dynamics [FPMD simulations conducted at the DFT level using a canonical ensemble having a constant number of atoms, volume with the temperature controlled by the Nosé-Hoover thermostat (Martyna et al., 1992; Kresse and Hafner, 1993)], and temperature (NVT) with 1 fs time steps for a total simulated time duration of 5 ps. The band structures of the designed nanowires were calculated by PBE and Heyd-Suseria-Ernzerhof (HSE06) hybrid functional (Heyd et al., 2003). To predict the clusters and nanowires in a more reliable manner, we also considered the PBE + D2 approach (Bučko et al., 2010). Almost no difference was found between the PBE-D2 and PBE structures and cohesive energies.

RESULTS

Structure, Stability and Magnetic Properties of Sc_2B_8 and Y_2B_8 Clusters

Based on the inverse sandwich structure of $La_2B_8^-$, we optimized the neutral transition metal boron clusters of the same configuration—Sc_2B_8 and Y_2B_8 clusters (the two Sc/Y atoms locate symmetrically to the two sides of the B_8 ring). In **Figure 1**, M–B (M = Sc and Y) and B–B bond lengths in two cluster structures are given. For the cluster Sc_2B_8, the bond lengths of Sc–B (d_{Sc-B}) and B–B (d_{B-B}) are 1.68 and 1.62 Å, respectively. For the cluster Y_2B_8, Y–B bond length (d_{Y-B}) is 2.81 Å and the bond length of B–B (d_{B-B}) is 1.62 Å. Both two optimized neutral clusters well preserve the inverse sandwich structure of D_{8h} symmetry.

As shown in **Supplementary Figure S1**, the two vibrational spectra have simple vibration modes due to the high symmetry, and no negative mode was found, indicating the stability of these two clusters. In the Sc_2B_8 cluster, the intensity peaks of 144 and 752 cm^{-1} can be assigned to Sc–B bond and B–B bond vibrations, respectively. The sharp asymmetric oscillations in the Y_2B_8 cluster are at 149 and 721 cm^{-1}, indicating the vibration modes of the Y–B bond and the B–B bond, respectively.

At the same time, a FPMD simulation lasting for 5 ps was performed for both clusters at room temperature (300 K). The annealed structures well remain the original inverse sandwich configuration, as shown in **Supplementary Figure S2**, which also suggests the good stability of the Sc_2B_8 and Y_2B_8 clusters adopting inverse sandwich structure.

Furthermore, CGA was used to generate low-energy isomers of Sc_2B_8 and Y_2B_8 clusters. The four low-lying structures, and an isomer, which can be viewed as the B-centered B_7 ring sandwiched by two Sc/Y atoms, were presented in **Supplementary Figure S3**, and the inverse sandwich configuration for both Sc_2B_8 and Y_2B_8 clusters is the most

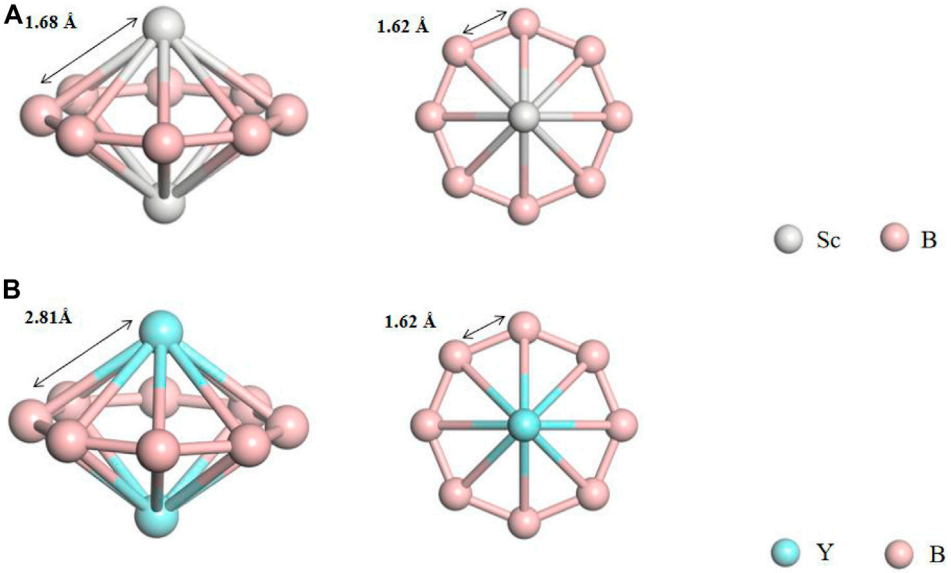

FIGURE 1 | Side and top views of the optimized Sc_2B_8 **(A)** and Y_2B_8 **(B)** clusters.

TABLE 1 | Relative energies of Sc_2B_8 and Y_2B_8 clusters with different magnetic configurations (in eV).

	NM	FM	AFM
Sc_2B_8	0.00	0.00	0.00
Y_2B_8	0.00	0.00	0.00

stable one (0.69–1.34 eV lower than the other four low-energy isomers at PBE-D2 level of theory). In particular, the CCSD(T) test computations also support the PBE-D2 results that the inverse sandwich structures are much lower in energy than other isomers. Thus it is feasible to synthesize the inverse sandwich Sc_2B_8 and Y_2B_8 clusters in experiments.

Additionally, we examined the dissociation of inverse sandwich M_2B_8 (M = Sc, Y) clusters. For the first M dissociation ($M_2B_8 \rightarrow M + MB_8$), the reaction is endothermic by 2.11 and 2.08 eV, respectively for M = Sc and Y; and for removing the second M ($MB_8 \rightarrow M + B_8$), it is also an endothermic reaction with the energy input of 2.37 and 2.17 eV for M = Sc and Y, respectively. The highly endothermic dissociations of M from B_8, indicate reaction barriers are >2 eV. Meanwhile, when the M atoms were put 5 Å from the B_8 center, it will be optimized to the energetically favored inverse sandwich structure. The above results as summarized in **Supplementary Figure S4** again confirmed that the M_2B_8 (M = Sc, Y) clusters with inverse sandwich configuration are highly stable.

Besides, we further explored magnetic properties of the global minimum structures. Three magnetic configurations were compared, namely, antiferromagnetic (AFM), ferromagnetic (FM) and nonmagnetic (NM) states. We set the energy value of NM as 0 eV and all other energy values as their relative differences. Our calculations revealed that both Sc_2B_8 and Y_2B_8 clusters are nonmagnetic (**Table 1**).

Structure and Stability of 1D Nanowires

Considering that the Sc_2B_8 and Y_2B_8 clusters of inverse sandwich configuration are the global minima, the inverse sandwich structural moiety might be extended to a periodic manner. Therefore, we connected the inverse sandwich clusters into 1D nanowires by sharing B–B bridges between adjacent clusters, similar to the observation of inverse triple-decker $La_3B_{14}^-$ (Chen et al., 2019). The 1D-Sc_4B_{24} and 1D-Y_2B_{12} nanowires were obtained after structural relaxation as displayed in **Figure 2**. For the optimized 1D-Sc_4B_{24} (**Figure 2A**), neither the inverse sandwich moiety of Sc_2B_8 nor the sharing B–B bonds was clearly observed, largely due to the formation of B_4 rhombus, which is regarded as a stable unit of boron analogs. The shared B–B (d_{B-B}) key length is ~1.59 Å, and the other B–B (d_{B-B}) lengths are in the range of 1.58–1.62 Å. The Sc–B bond lengths (d_{Sc-B}) are 2.41–2.49 Å. In contrast, for the 1D-Y_2B_{12} NW (**Figure 2B**), the unitcell is formed by two Y_2B_8 clusters of inverse sandwich moiety by sharing a B–B bond. The length of the shared B–B bond ($d_{B\_}B$) is 1.56 Å, the lengths of others B–B bonds are ranged from 1.56 to 1.60 Å. The Y–B bond lengths ($d_{Y\_}B$) are ranged in 2.56–2.72 Å. Compared to the free cluster structures, the $d_{Y\_}B$ were compressed in 1D-Y_2B_{12} nanowire, while the $d_{Sc\_}B$ were significantly stretched in the 1D-Sc_4B_{24}, indicating that although Sc_2B_8 and Y_2B_8 clusters have the same structure, they have different structural characteristics when forming one-dimensional nanowires.

In order to confirm the stability of the two nanowires, we first examined their thermodynamic stability by calculating the cohesive energy (E_{coh}). In our work, the cohesive energy is defined as equation 1, where, E_1/E_2 is the energy of an

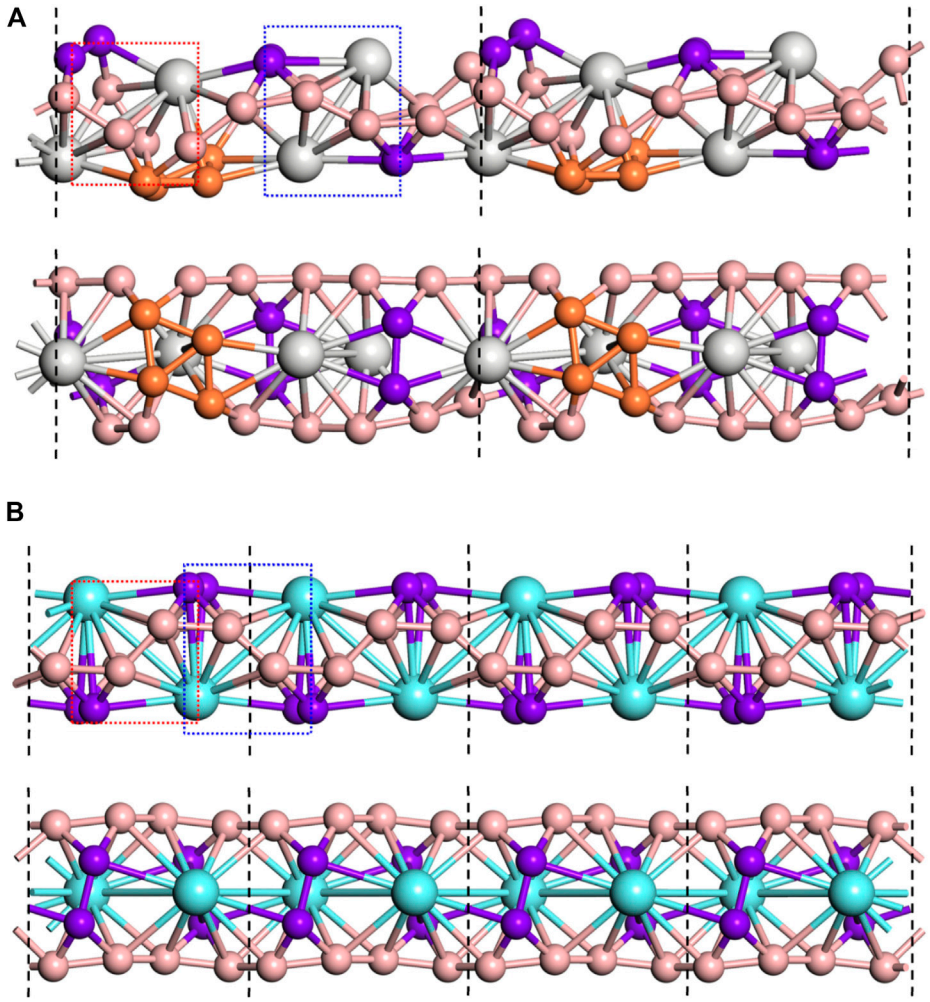

FIGURE 2 | Two views of the 1D-Sc_4B_{24} NW **(A)** and 1D-Y_2B_{12} NW **(B)**. The unitcell was marked by black dashed lines. The inverse sandwich unit M_2B_8 was marked by red and blue dashed rectangle. The sharing B–B bonds and the B rhombus were highlighted in purple and orange, respectively.

isolated transition metal atoms (Sc or Y)/B atom, E_{tot} is the total energy of nanowire, n/m is the number of transition metal/B atoms.

According to the above definition of cohesive energy, the larger the calculated value is, the more stable the structure is. The calculated cohesive energies of 1D-Sc_4B_{24} and 1D-Y_2B_{12} nanowires are 5.92 and 6.00 eV/atom, respectively, much larger than the E_{coh} values of the clusters (5.35 and 5.29 eV/atom, respectively for Sc_2B_8 and Y_2B_8). These high cohesion energies show that two 1D nanowires have good thermodynamic stability.

Then, we calculated the phonon dispersion to investigate their dynamic stability. In these phonon dispersions, no imaginary frequencies were observed (**Figure 3**), indicating that the two designed nanowires based on the inverse sandwich Sc_2B_8 and Y_2B_8 clusters are dynamically stable.

Finally, we performed FPMD simulations in order to access their thermal stability with the supercell of 112 atoms (16 transition metal atoms and 96 B atoms). The 1D-$Sc_{16}B_{96}$ was annealed at 300 K for 5 ps, and the final structure retained the original B_8 rings (**Supplementary Figure S5A**), and the structure obtained remains intact. For the one-dimensional nanowire structure constructed by Y_2B_8, we conducted two 5 ps simulation at room temperature of 300 K (**Supplementary Figure S5B**) and 500 K (**Supplementary Figure S5**), respectively. The 1D-$Y_{16}B_{96}$ structure still showed structural integrity under both simulation conditions. It also preserves structural integrity at 500 K in particular. The results of FPMD simulations confirm that two designed nanowires possess good thermal stability.

Magnetic and Electronic Properties

Through the above analysis of thermodynamic, dynamic and thermal stability, it is found that the two designed nanowires are stable. Therefore, we further explored the magnetic and electronic properties of the two nanowires. For the magnetic

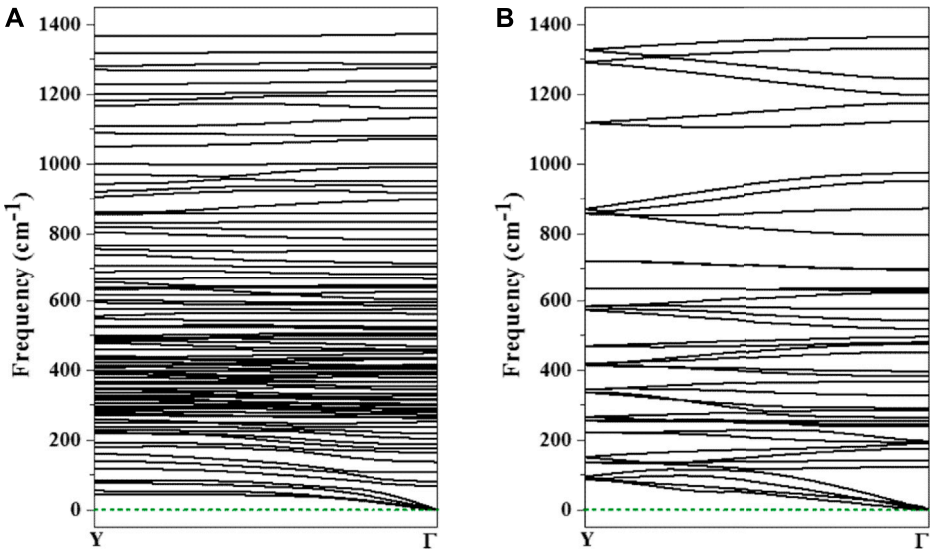

FIGURE 3 | The calculated phonon spectra of the designed 1D-Sc_4B_{24} **(A)** and 1D-Y_2 B_{12} **(B)**.

TABLE 2 | Relative energies of 1D- Sc_4B_{24} and 1D-Y_2B_{12} nanowires with various magnetic configurations (in eV).

	NM	FM	AFM1	AFM2	AFM3
1D-Sc_4B_{24}	0.00	0.00	0.00	0.00	0.00
1D- Y_2B_{12}	0.00	0.00	0.00	0.00	0.00

feature, five magnetic orderings were considered, namely AFM (including AFM1: − + − +, AFM2: + − − +, and AFM3: − − + +, **Supplementary Figure S7**, FM, and NM. Our computations showed that neither 1D-Sc_4B_{24} nor 1D-Y_2B_{12} is magnetic. The relative energies of examined magnetic configurations of the two structures were given in **Table 2**. In addition, through the analysis of charge transfer, we found that each Sc/Y atom transferred ~1.5/2.0 electrons to boron. The differential charge density diagrams of the two 2D nanostructures (**Figure 4**) showed that the electrons have delocalized bonding characteristics.

We used the PBE method to predict the electronic band structures of the two designed nanowires (**Figure 5**). Compared to the metallicity of teetotum cluster Li_2FeB_{14} based nanowire (Shakerzadeh et al., 2020), the 1D-Sc_4B_{24} nanowire is a direct-bandgap semiconductor with the bandgap of 0.51 eV, while the 1D-Y_2B_{12} NW is a metal, and the p orbital of B dominates the state near the Fermi level. The commonly used PBE method usually underestimates the bandgaps. Therefore, we also used HSE06 method to calculate the electronic band structure of 1D-Sc_4B_{24} nanowire, as shown in **Supplementary Figure S8**. The bandgap calculated by the HSE06 method is about 0.85 eV, 0.34 eV larger than the PBE value. The different electronic

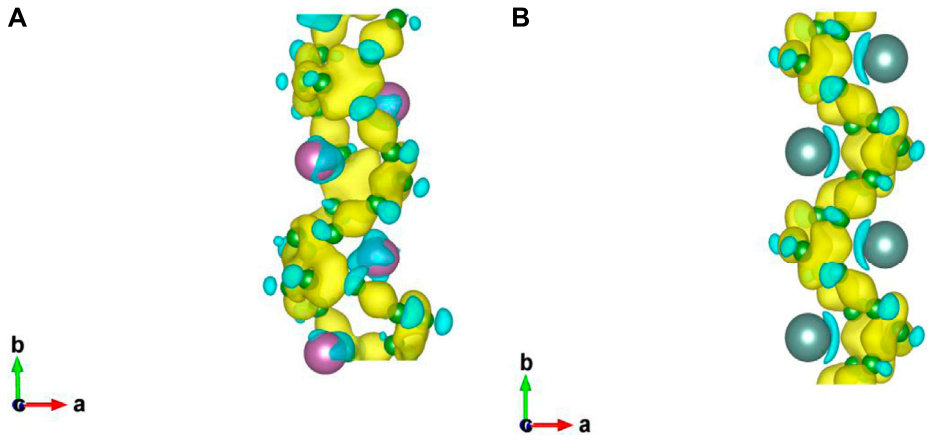

FIGURE 4 | Differential charge density diagrams of designed nanowires 1D-Sc_4B_{24} **(A)** and 1D-Y_2B_{12} **(B)**. The isosurface value was set to be 0.015 e/Bohr^3.

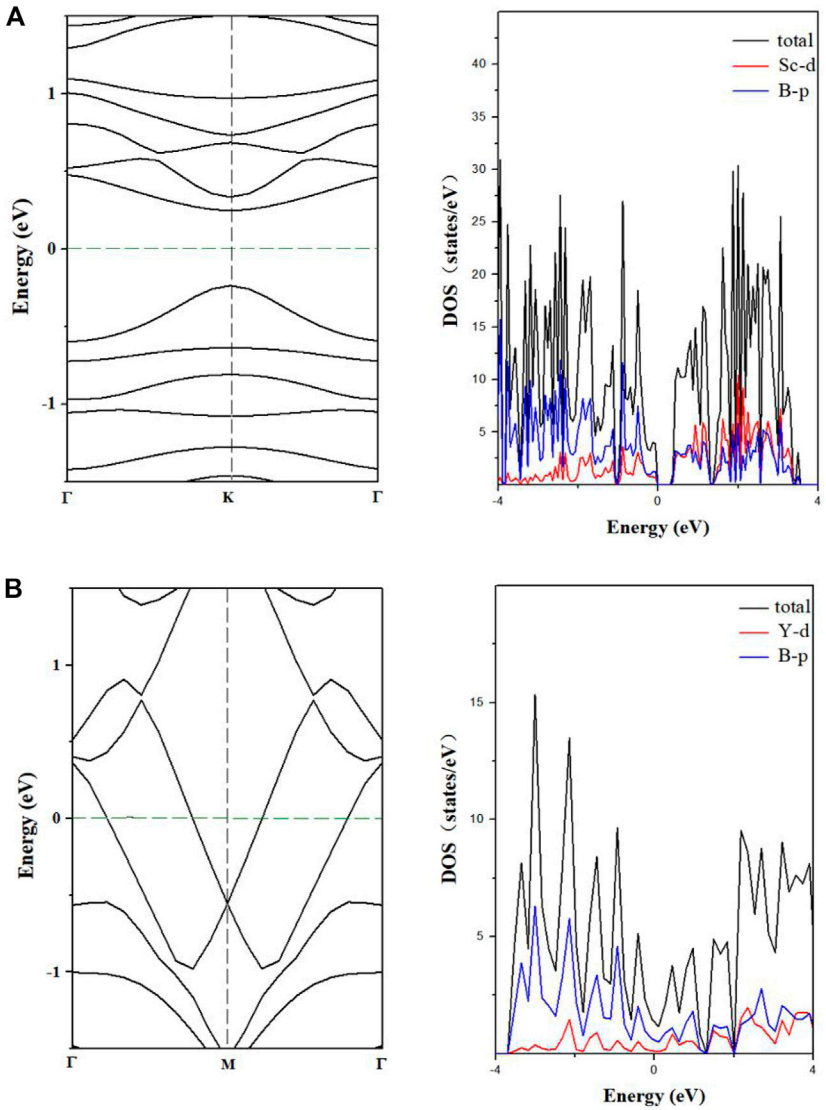

FIGURE 5 | Energy band and density of states of 1D-Sc_4B_{24} **(A)**, 1D-Y_2B_{12} **(B)** nanowires predicted by PBE.

behavior of the two designed nanowires may originate from the different structures (Zeng et al., 2019).

CONCLUSION

In summary, by means of first-principles calculations combined with CGA search, we found that Sc_2B_8 and Y_2B_8 clusters of inverse sandwich structure are the lowest-energy isomers and have good stability, and we constructed one-dimensional nanowires containing the structural moiety of the two clusters. The high stability of 1D-Sc_4B_{24} and 1D-Y_2B_{12} nanowires is confirmed by the investigation of thermodynamical, dynamical and thermal perspectives. Both 1D-Sc_4B_{24} and 1D-Y_2B_{12} nanowires are nonmagnetic; in terms of electronic behavior, the 1D-Sc_4B_{24} is semiconducting with the HSE06 bandgap of 0.85 eV, while the 1D-Y_2B_{12} is metallic. Our theoretical work not only identified the inverse sandwich configuration as the lowest-energy one for transition metal borides Sc_2B_8 and Y_2B_8 clusters, but also successfully extended the inverse sandwich moiety to 1D nanomaterials. Thus, it is helpful to design novel boron-based nanowires for both experimental and theoretical communities.

$$E_{coh} = (nE_1 + mE_2 - E_{tot})/(n + m)$$

Permission to Reuse and Copyright

licenses, to follow any citation instructions requested by third-party rights holders, and cover any supplementary charges.

DATA AVAILABILITY STATEMENT

The original contributions presented in the study are included in the article/**Supplementary Material**, further inquiries can be directed to the corresponding authors.

AUTHOR CONTRIBUTIONS

CJ contributed to calculations, methodology, formal analysis, writing—original draft, and funding acquisition. ZL performed formal analysis and writing—original draft. SL performed data curation and investigation. LS and SW performed methodology, investigation, writing—original draft, and supervision, and funding acquisition. FL contributed to conceptualization, methodology, writing—review and editing, funding acquisition, project administration, and supervision.

FUNDING

This work was supported by the National Natural Science Foundation of China (11964024, 1804076), the "Grassland Talents" project of Inner Mongolia autonomous region (12000-12102613), and the Training Program of Innovation and Entrepreneurship for Undergraduates of Inner Mongolia University (201810126056).

SUPPLEMENTARY MATERIAL

The Supplementary Material for this article can be found online at: https://www.frontiersin.org/articles/10.3389/fchem.2021.753617/full#supplementary-material

REFERENCES

Akopov, G., Yeung, M. T., and Kaner, R. B. (2017). Rediscovering the Crystal Chemistry of Borides. *Adv. Mater.* 29, 1604506. doi:10.1002/adma.201604506

Alexandrova, A. N., Boldyrev, A. I., Zhai, H.-J., and Wang, L.-S. (2006). All-boron Aromatic Clusters as Potential New Inorganic Ligands and Building Blocks in Chemistry. *Coord. Chem. Rev.* 250, 2811–2866. doi:10.1016/j.ccr.2006.03.032

Bai, H., Chen, T.-T., Chen, Q., Zhao, X.-Y., Zhang, Y.-Y., Chen, W.-J., et al. (2019). Planar B41− and B42− Clusters with Double-Hexagonal Vacancies. *Nanoscale* 11, 23286–23295. doi:10.1039/C9NR09522E

Bučko, T., Hafner, J., Lebègue, S., and Ángyán, J. G. (2010). Improved Description of the Structure of Molecular and Layered Crystals: Ab Initio DFT Calculations with van der Waals Corrections. *J. Phys. Chem. A.* 114, 11814–11824. doi:10.1021/jp106469x

Carenco, S., Portehault, D., Boissière, C., Mézailles, N., and Sanchez, C. (2013). Nanoscaled Metal Borides and Phosphides: Recent Developments and Perspectives. *Chem. Rev.* 113, 7981–8065. doi:10.1021/cr400020d

Chen, T.-T., Li, W.-L., Li, J., and Wang, L.-S. (2019). [La(ηx-Bx)La]− (X = 7-9): a New Class of Inverse sandwich Complexes. *Chem. Sci.* 10, 2534–2542. doi:10.1039/C8SC05443F

Chung, H.-Y., Weinberger, M. B., Levine, J. B., Kavner, A., Yang, J.-M., Tolbert, S. H., et al. (2007). Synthesis of Ultra-incompressible Superhard Rhenium Diboride at Ambient Pressure. *Science* 316, 436–439. doi:10.1126/science.1139322

Cui, Z.-H., Chen, C., Wang, Q., Zhao, L., Wang, M.-H., and Ding, Y.-h. (2020). Inverse sandwich Complexes of B7M2−, B8M2, and B9M2+ (M = Zr, Hf): the Nonclassical M-M Bonds Embedded in Monocyclic boron Rings. *New J. Chem.* 44, 17705–17713. doi:10.1039/D0NJ03999C

Delley, B. (1990). An All-electron Numerical Method for Solving the Local Density Functional for Polyatomic Molecules. *J. Chem. Phys.* 92, 508–517. doi:10.1063/1.458452

Delley, B. (2000). From Molecules to Solids with the DMol3 Approach. *J. Chem. Phys.* 113, 7756–7764. doi:10.1063/1.1316015

Dong, Y., Wang, S., Yu, C., Li, F., Gong, J., and Zhao, J. (2021). First-principles Explorations on P8 and N2 Assembled Nanowire and Nanosheet. *Nano Express* 2, 010004. doi:10.1088/2632-959X/abd899

Heyd, J., Scuseria, G. E., and Ernzerhof, M. (2003). Hybrid Functionals Based on a Screened Coulomb Potential. *J. Chem. Phys.* 118, 8207–8215. doi:10.1063/1.1564060

Jian, T., Chen, X., Li, S.-D., Boldyrev, A. I., Li, J., and Wang, L.-S. (2019). Probing the Structures and Bonding of Size-Selected Boron and Doped-boron Clusters. *Chem. Soc. Rev.* 48, 3550–3591. doi:10.1039/C9CS00233B

Jian, T., Li, W.-L., Chen, X., Chen, T.-T., Lopez, G. V., Li, J., et al. (2016). Competition between Drum and Quasi-Planar Structures in RhB18−: Motifs for Metallo-Boronanotubes and Metallo-Borophenes. *Chem. Sci.* 7, 7020–7027. doi:10.1039/C6SC02623K

Jian, T., Li, W.-L., Popov, I. A., Lopez, G. V., Chen, X., Boldyrev, A. I., et al. (2016). Manganese-centered Tubular boron Cluster - MnB16−: A New Class of Transition-Metal Molecules. *J. Chem. Phys.* 144, 154310. doi:10.1063/1.4946796

Kiran, B., Bulusu, S., Zhai, H.-J., Yoo, S., Zeng, X. C., and Wang, L.-S. (2005). Planar-to-tubular Structural Transition in boron Clusters: B20 as the Embryo of Single-Walled boron Nanotubes. *Proc. Natl. Acad. Sci.* 102, 961–964. doi:10.1073/pnas.0408132102

Kresse, G., and Furthmüller, J. (1996). Efficiency of Ab-Initio Total Energy Calculations for Metals and Semiconductors Using a Plane-Wave Basis Set. *Comput. Mater. Sci.* 6, 15–50. doi:10.1016/0927-0256(96)00008-0

Kresse, G., and Hafner, J. (1993). Ab Initiomolecular Dynamics for Liquid Metals. *Phys. Rev. B* 47, 558–561. doi:10.1103/PhysRevB.47.558

Kresse, G., and Hafner, J. (1994). Ab Initiomolecular-Dynamics Simulation of the Liquid-Metal-Amorphous-Semiconductor Transition in Germanium. *Phys. Rev. B.* 49, 14251–14269. doi:10.1103/physrevb.49.14251

Li, W.-L., Chen, Q., Tian, W.-J., Bai, H., Zhao, Y.-F., Hu, H.-S., et al. (2014). The B35 Cluster with a Double-Hexagonal Vacancy: A New and More Flexible Structural Motif for Borophene. *J. Am. Chem. Soc.* 136, 12257–12260. doi:10.1021/ja507235s

Li, W.-L., Chen, T.-T., Xing, D.-H., Chen, X., Li, J., and Wang, L.-S. (2018). Observation of Highly Stable and Symmetric Lanthanide Octa-boron Inverse Sandwich Complexes. *Proc. Natl. Acad. Sci. USA.* 115, E6972–E6977. doi:10.1073/pnas.1806476115

Li, W.-L., Chen, X., Jian, T., Chen, T.-T., Li, J., and Wang, L.-S. (2017). From Planar Boron Clusters to Borophenes and Metalloborophenes. *Nat. Rev. Chem.* 1, 0071. doi:10.1038/s41570-017-0071

Li, W.-L., Hu, H.-S., Zhao, Y.-F., Chen, X., Chen, T.-T., Jian, T., et al. (2018). Recent Progress on the Investigations of boron Clusters and boron-based Materials (I): Borophene. *Sci. Sin.-Chim.* 48, 98–107. doi:10.1360/N032017-00185

Li, W.-L., Jian, T., Chen, X., Li, H.-R., Chen, T.-T., Luo, X.-M., et al. (2017). Observation of a Metal-Centered B2-Ta@B18−tubular Molecular Rotor and a Perfect Ta@B20−boron Drum with the Record Coordination Number of Twenty. *Chem. Commun.* 53, 1587–1590. doi:10.1039/C6CC09570D

Li, W. L., Jian, T., Chen, X., Chen, T. T., Lopez, G. V., Li, J., et al. (2016). The Planar CoB 18 − Cluster as a Motif for Metallo-Borophenes. *Angew. Chem. Int. Ed.* 55, 7358–7363. doi:10.1002/anie.201601548

Lipscomb, W. N. (1977). The Boranes and Their Relatives. *Science* 196, 1047–1055. doi:10.1126/science.196.4294.1047

Martyna, G. J., Klein, M. L., and Tuckerman, M. (1992). Nosé-Hoover Chains: The Canonical Ensemble via Continuous Dynamics. *J. Chem. Phys.* 97, 2635–2643. doi:10.1063/1.463940

Nagamatsu, J., Nakagawa, N., Muranaka, T., Zenitani, Y., and Akimitsu, J. (2001). Superconductivity at 39 K in Magnesium Diboride. *Nature* 410, 63–64. doi:10.1038/35065039

Pan, S., Barroso, J., Jalife, S., Heine, T., Asmis, K. R., and Merino, G. (2019). Fluxional Boron Clusters: From Theory to Reality. *Acc. Chem. Res.* 52, 2732–2744. doi:10.1021/acs.accounts.9b00336

Perdew, J. P., Burke, K., and Ernzerhof, M. (1996). Generalized Gradient Approximation Made Simple. *Phys. Rev. Lett.* 77, 3865–3868. doi:10.1103/PhysRevLett.77.3865

Piazza, Z. A., Hu, H.-S., Li, W.-L., Zhao, Y.-F., Li, J., and Wang, L.-S. (2014). Planar Hexagonal B36 as a Potential Basis for Extended Single-Atom Layer boron Sheets. *Nat. Commun.* 5, 2014. doi:10.1038/ncomms4113

Popov, I. A., Jian, T., Lopez, G. V., Boldyrev, A. I., and Wang, L.-S. (2015). Cobalt-centred boron Molecular Drums with the Highest Coordination Number in the CoB16− Cluster. *Nat. Commun.* 6. doi:10.1038/ncomms9654

Romanescu, C., Galeev, T. R., Li, W.-L., Boldyrev, A. I., and Wang, L.-S. (2011). Aromatic Metal-Centered Monocyclic Boron Rings: CoB8− and RuB9−. *Angew. Chem. Int. Ed.* 50, 9334–9337. doi:10.1002/anie.201104166

Shakerzadeh, E., Duong, L. V., Pham-Ho, M. P., Tahmasebi, E., and Nguyen, M. T. (2020). The Teetotum Cluster Li2FeB14 and its Possible Use for Constructing boron Nanowires. *Phys. Chem. Chem. Phys.* 22, 15013–15021. doi:10.1039/D0CP02046J

Sussardi, A., Tanaka, T., Khan, A. U., Schlapbach, L., and Mori, T. (2015). Enhanced Thermoelectric Properties of Samarium Boride. *J. Materiomics* 1, 196–204. doi:10.1016/j.jmat.2015.07.007

Tian, Y., Guo, Z., Zhang, T., Lin, H., Li, Z., Chen, J., et al. (2019). Inorganic Boron-Based Nanostructures: Synthesis, Optoelectronic Properties, and Prospective Applications. *Nanomaterials* 9, 538. doi:10.3390/nano9040538

Togo, A., and Tanaka, I. (2015). First Principles Phonon Calculations in Materials Science. *Scripta Materialia* 108, 1–5. doi:10.1016/j.scriptamat.2015.07.021

Wang, L.-S. (2016). Photoelectron Spectroscopy of Size-Selected Boron Clusters: From Planar Structures to Borophenes and Borospherenes. *Int. Rev. Phys. Chem.* 35, 69–142. doi:10.1080/0144235X.2016.1147816

Wang, S., Gu, J., Dong, Y., Sai, L., and Li, F. (2020). A Super Stable Assembled P Nanowire with Variant Structural and Magnetic/Electronic Properties via Transition Metal Adsorption. *Nanoscale* 12, 12454–12461. doi:10.1039/D0NR02176H

Wang, Y.-J., Miao, C.-Q., Xie, J.-J., Wei, Y.-R., and Ren, G.-M. (2019). Be2B6 and Be2B7+: Two Double Aromatic Inverse sandwich Complexes with Spin-Triplet Ground State. *New J. Chem.* 43, 15979–15982. doi:10.1039/C9NJ02819F

Xiao, Y., Zhao, X.-K., Wu, T., Miller, J. T., Hu, H.-S., Li, J., et al. (2021). Distinct Electronic Structures and Bonding Interactions in Inverse-Sandwich Samarium and Ytterbium Biphenyl Complexes. *Chem. Sci.* 12, 227–238. doi:10.1039/D0SC03555F

Xu, J., Hou, G., Li, H., Zhai, T., Dong, B., Yan, H., et al. (2013). Fabrication of Vertically Aligned Single-Crystalline Lanthanum Hexaboride Nanowire Arrays and Investigation of Their Field Emission. *NPG Asia Mater.* 5, e53. doi:10.1038/am.2013.25

Zeng, Y. J., Wu, D., Cao, X. H., Zhou, W. X., Tang, L. M., and Chen, K. Q. (2019). Nanoscale Organic Thermoelectric Materials: Measurement, Theoretical Models, and Optimization Strategies. *Adv. Funct. Mater.* 30, 1903873. doi:10.1002/adfm.201903873

Zhai, H.-J., Zhao, Y.-F., Li, W.-L., Chen, Q., Bai, H., Hu, H.-S., et al. (2014). Observation of an All-Boron Fullerene. *Nat. Chem.* 6, 727–731. doi:10.1038/nchem.1999

Zhao, J., Shi, R., Sai, L., Huang, X., and Su, Y. (2016). Comprehensive Genetic Algorithm Forab Initioglobal Optimisation of Clusters. *Mol. Simulation* 42, 809–819. doi:10.1080/08927022.2015.1121386

Conflict of Interest: The authors declare that the research was conducted in the absence of any commercial or financial relationships that could be construed as a potential conflict of interest.

Publisher's Note: All claims expressed in this article are solely those of the authors and do not necessarily represent those of their affiliated organizations, or those of the publisher, the editors and the reviewers. Any product that may be evaluated in this article, or claim that may be made by its manufacturer, is not guaranteed or endorsed by the publisher.

frontiers in Chemistry

ORIGINAL RESEARCH
published: 12 November 2021
doi: 10.3389/fchem.2021.767421

Cluster Assembled Silicon-Lithium Nanostructures: A Nanowire Confined Inside a Carbon Nanotube

*Walter Orellana[1], Ricardo Pino-Rios[2], Osvaldo Yañez[3,4], Alejandro Vásquez-Espinal[5], Francesca Peccati[6], Julia Contreras-García[7], Carlos Cardenas[8,9] and William Tiznado[5]**

[1]Departamento de Ciencias Físicas, Universidad Andres Bello, Santiago, Chile, [2]Laboratorio de Química Teórica, Facultad de Química y Biología, Universidad de Santiago de Chile (USACH), Santiago, Chile, [3]Center of New Drugs for Hypertension (CENDHY), Santiago, Chile, [4]Department of Pharmaceutical Science and Technology, School of Chemical and Pharmaceutical Sciences, Universidad de Chile, Santiago, Chile, [5]Departamento de Ciencias Químicas, Computational and Theoretical Chemistry Group, Facultad de Ciencias Exactas, Universidad Andres Bello, Santiago, Chile, [6]Center for Cooperative Research in Biosciences (CIC bioGUNE), Basque Research and Technology Alliance (BRTA), Bizkaia Technology Park, Derio, Spain, [7]Sorbonne Universités, UPMC and CNRS, Laboratoire de Chimie Théorique (LCT), 75005, Paris, France, [8]Departamento de Física, Facultad de Ciencias, Universidad de Chile, Santiago, Chile, [9]Centro para el Desarrollo de la Nanociencias y Nanotecnologia, CEDENNA, Avenida Ecuador, Santiago, Chile

We computationally explore an alternative to stabilize one-dimensional (1D) silicon-lithium nanowires (NWs). The $Li_{12}Si_9$ Zintl phase exhibits the NW $^1_\infty[Li_6Si_5]$, combined with Y-shaped Si_4 structures. Interestingly, this NW could be assembled from the stacking of the Li_6Si_5 aromatic cluster. The $^1_\infty[Li_6Si_5]$@CNT nanocomposite has been investigated with density functional theory (DFT), including molecular dynamics simulations and electronic structure calculations. We found that van der Waals interaction between Li's and CNT's walls is relevant for stabilizing this hybrid nanocomposite. This work suggests that nanostructured confinement (within CNTs) may be an alternative to stabilize this free NW, cleaning its properties regarding $Li_{12}Si_9$ solid phase, i.e., metallic character, concerning the perturbation provided by their environment in the $Li_{12}Si_7$ compound.

Keywords: nanowire, density functional theory, silicon-lithium clusters, carbon nanotube, metallic character

OPEN ACCESS

Edited by:
Iwona Anusiewicz,
University of Gdansk, Poland

Reviewed by:
Fengyu Li,
Inner Mongolia University, China
Tanmoy Chakraborty,
Sharda University, India

****Correspondence:***
William Tiznado
wtiznado@unab.cl

Specialty section:
This article was submitted to Theoretical and Computational Chemistry, a section of the journal Frontiers in Chemistry

Received: *30 August 2021*
Accepted: *01 October 2021*
Published: *12 November 2021*

Citation:
Orellana W, Pino-Rios R, Yañez O, Vásquez-Espinal A, Peccati F, Contreras-García J, Cardenas C and Tiznado W (2021) Cluster Assembled Silicon-Lithium Nanostructures: A Nanowire Confined Inside a Carbon Nanotube. Front. Chem. 9:767421. doi: 10.3389/fchem.2021.767421

INTRODUCTION

The insertion of inorganic materials into single-walled carbon nanotubes (SWCNTs), hereinafter identified simply as CNT, enables the encapsulation of extreme nanowires (NWs) with diameters comparable to a unit cell of the parent material (Green, 1998; Sloan et al., 2002; Spencer et al., 2014). Although NWs of similar diameter can be produced using several templates, such as zeolites (Derouane, 1998), mesoporous phases (Alba-Simionesco et al., 2006; Ke et al., 2009), and metal-organic framework (MOF) (Lu et al., 2012) type materials, CNTs present many advantages as templates; they are atomically smooth, electron transparent, readily available, and can be filled by bulk infiltration to create milligram quantities of encapsulated nanowires, at least on a laboratory scale. Thus, encapsulated NW-CNT are scientifically interesting not only on their own but also as precursors to a wide range of other extreme nanowire materials.

In 2016, Ivanov et al. published a theoretical prediction of helix-shaped lithium-phosphorus nanowires encapsulated into single-walled carbon nanotubes (LiP@CNTs) (Ivanov et al., 2016). Note that helix-shaped Li_nP_n clusters (n = 5–9) had previously been reported as global minimum structures (Ivanov et al., 2012). Some solid phases consist of structural motifs like atomic clusters, i.e., in Zintl phases. This connection brings consistency to the use of models based on

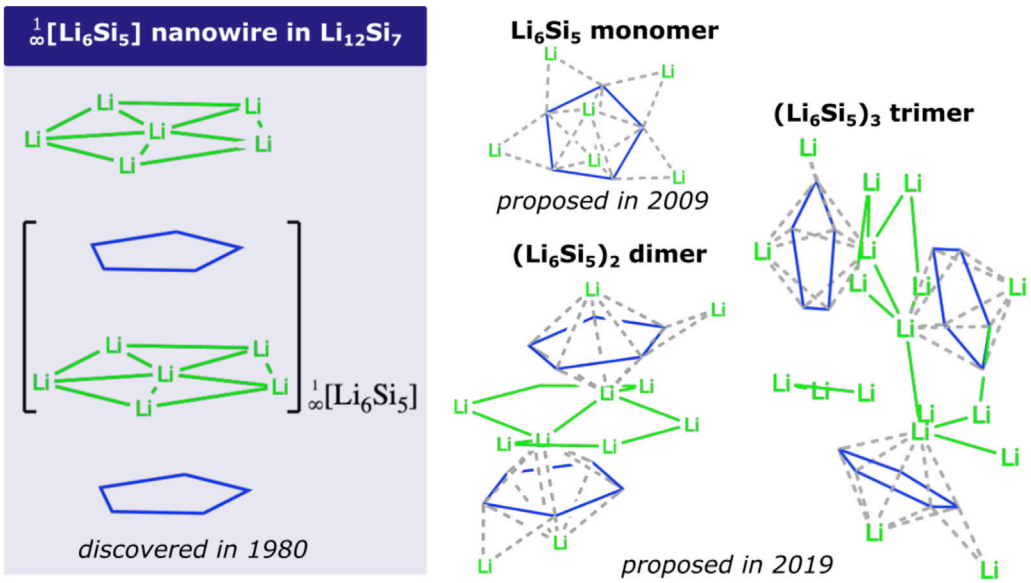

Scheme 1 | Structures of $^{1}_{\infty}[Li_6Si_5]$ NW, Li_6Si_5, $Li_{12}Si_{10}$, and $Li_{18}Si_{15}$ global minima structures, where the square brackets show a repeating unit.

stable clusters to generate NWs inside nanotubes, as proposed in Ivanov's work (Ivanov et al., 2012). The study of these clusters inside CNTs can provide relevant information about these hybrid materials, for example, about their viability (stability analysis), their structural characteristics (geometry analysis), their physical and chemical properties (analysis of their electronic structure).

Due to its excellent energy storage capacity, Si has been extensively studied experimentally as a negative electrode material for Li-ion batteries (Gao et al., 2001; Ryu et al., 2004; Li et al., 2006, Li et al., 2008, Li et al., 2009; Obrovac et al., 2007; Song et al., 2014; Shin et al., 2020). Hence, Si lithifies at high temperature (415°C) in a LiCl-KCl melt, identifying potential plateaus evidencing the crystalline phases $Li_{12}Si_7$, Li_7Si_3, $Li_{13}Si_4$, and $Li_{22}Si_5$ (Wen and Huggins, 1981). In particular, the binary (non-paramagnetic) Zintl-type $Li_{12}Si_7$ silicide contains semi-infinite sandwich-like $^{1}_{\infty}[Li_6Si_5]$ linear chains, consisting of Si_5 pentagons intercalated with Li atoms (see **Scheme 1**). Note that the unit cell of the Zintl $Li_{12}Si_7$ phase has been rationalized (Nesper, 1990; Chevrier et al., 2010; Köster et al., 2011; Kuhn et al., 2011a, Kuhn et al., 2011b) as $(Li_6{}^{6+}[Si_5]_6)_2$ $(Li_{12}{}^{10+}[Si_4]_{10})_2$, with two well-defined silicon moieties: planar Si_5 rings and the Y-shaped Si_4 moiety. Such a structural pattern is justified by assigning 26 electrons (20 from 6Si + 6 from 6Li) to the $Si_5{}^{6-}$ ring, favoring Hückel's aromaticity (Hückel, 1930, Hückel, 1931a, Hückel, 1931b; Zhao et al., 2017). This aromatic character is supported by experimental evidence of an upfield shift (to -17.2 ppm) of Li (at the center of the Li_6 fragment in **Scheme 1**) in the corresponding magic angle NMR (MAS) spectrum (Kuhn et al., 2011b; Köster et al., 2011). It is noteworthy that the $Si_5{}^{6-}$ structural motif is also present in the ternary compound Li_8MgSi_6 (Nesper et al., 1986a). On the other hand, at the cluster level, our group has identified that the global minimum (GM) of the Li_6Si_5 cluster, consists of an aromatic $Si_5{}^{6-}$ pentagon surrounded by 6 Li^+ counterions (Tiznado et al., 2009; Perez-Peralta et al., 2011; Contreras et al., 2013; Vásquez-Espinal et al., 2018). More recently, we have identified the GM structures of the oligomers $(Li_6Si_5)_2$ and $(Li_6Si_5)_3$ (Yañez et al., 2019b; Manrique-de-la-Cuba et al., 2021), which also consist of aromatic Si_5 rings surrounded by Li's (see **Scheme 1**). However, the stacking of Li_6Si_5 units does not tend to form the nanowire identified in $Li_{12}Si_7$, suggesting that $Li_{12}{}^{10+}[Si_4]^{10-}$ component (with the Y-shaped Si_4 moiety) contributes decisively to the stabilization of this NW. In mentioned cluster studies, explorations of the potential energy surface have been performed by hybrid methods, including genetic algorithms (Yañez et al., 2019a, Yañez et al., 2020).

To build new class of materials with desirable properties, using atomic clusters instead of atoms as building blocks, is a remarkable possibility. However, it requires that atomic clusters must retain their identity when assembled, as Khanna and Jena first outlined when they coined the word "cluster-assembled materials" (CAMs) (Khanna and Jena, 1992). These authors argued that the clusters' coupling would have a unique effect on both the assembled material's electronic structure and mechanical properties, which is not possible when the assembly blocks are atoms (Khanna and Jena, 1995; Jena et al., 1996; Jena and Khanna, 1996; Claridge et al., 2009; Jena and Sun, 2018). For a more detailed and timely overview of advances in the assembly of materials from clusters, please refer to the following reviews: (Chakraborty and Pradeep, 2017; Jena and Sun, 2018; Pinkard et al., 2018; Zheng et al., 2019; Doud et al., 2020).

Given the above background, here we evaluated, *in silico*, the stability of the isolated $^{1}_{\infty}[Li_6Si_5]$ NW, as well as its electronic properties. In addition, we studied the hybrid material consisting of the NW confined in a CNT. The latter focused on identifying alternative ways to stabilize this conformation and to evaluate the effect of this association on NW electronic properties. Our density functional theory (DFT) calculations demonstrate that Li-Si@CNTs hybrid systems have excellent stability and thus have potential for experimental realization.

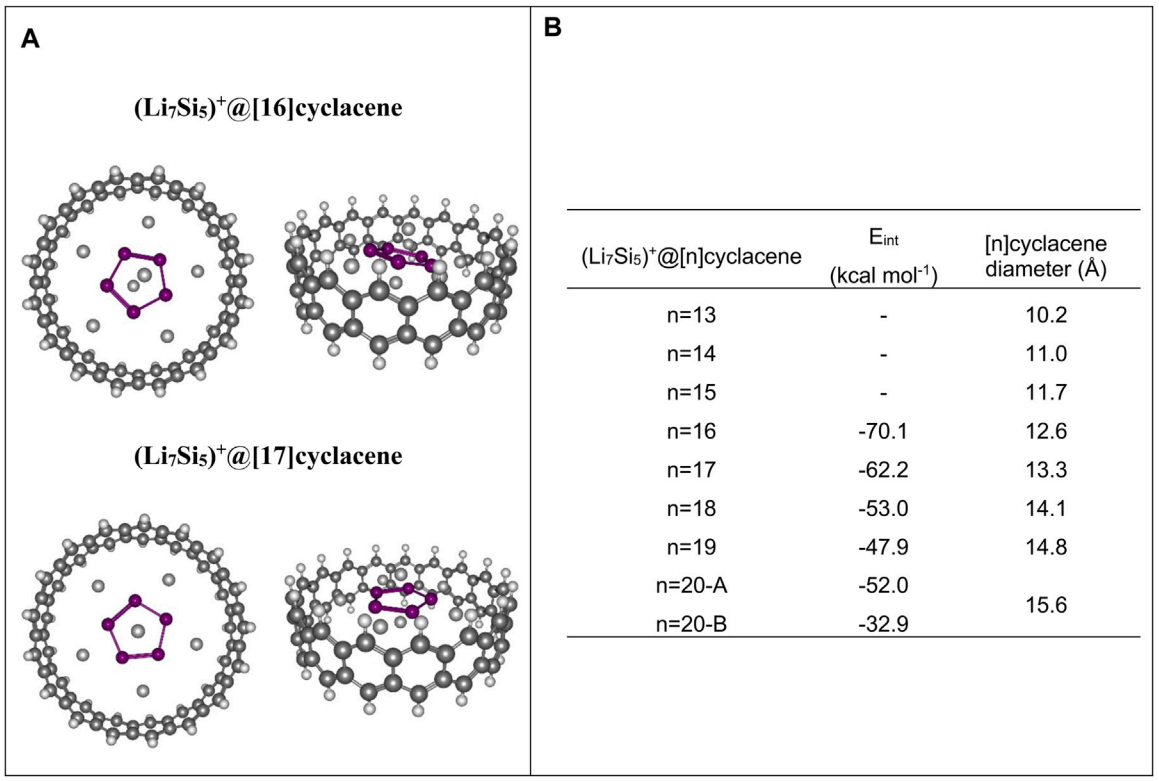

$(Li_7Si_5)^+$@[n]cyclacene	E_{int} (kcal mol^{-1})	[n]cyclacene diameter (Å)
n=13	-	10.2
n=14	-	11.0
n=15	-	11.7
n=16	-70.1	12.6
n=17	-62.2	13.3
n=18	-53.0	14.1
n=19	-47.9	14.8
n=20-A	-52.0	15.6
n=20-B	-32.9	

FIGURE 1 | (A) Top-and side-views of optimized structures of $Li_7Si_5^+$ inside both [16]cyclacene and [17]cyclacene at PBE0/def2-TZVP level. **(B)** $Li_7Si_5^+$ and [n] cyclacene interaction energy (E_{int}), number of hexagonal rings and diameter (in Å) of the [n]cyclacene.

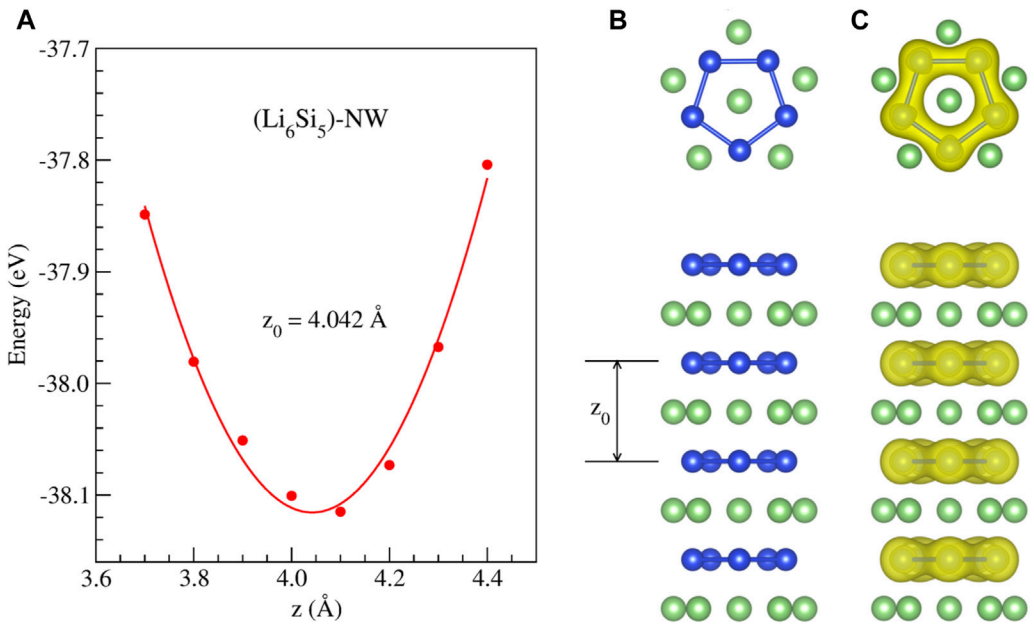

FIGURE 2 | Stability of the $^1_\infty[Li_6Si_5]$ isolated model (Li_6Si_5-NW) obtained from periodic DFT calculations: **(A)** Energy as a function of the distance between Li_6Si_5 units, **(B)** top and side views of the equilibrium geometry, **(C)** electronic density distribution for the isosurface at 0.05 $e/A^{\circ 3}$.

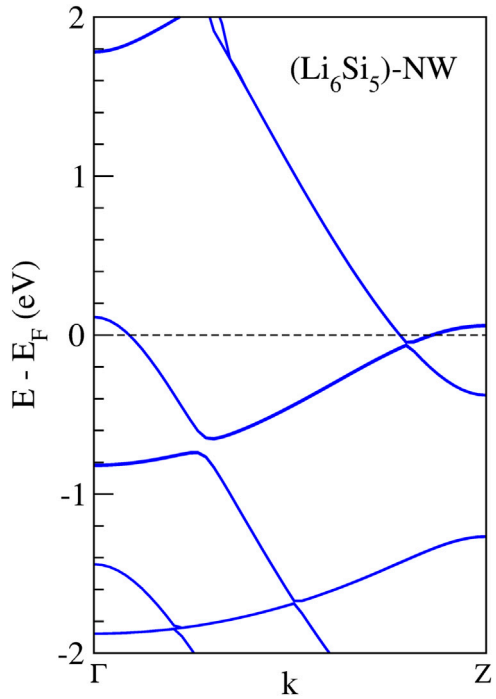

FIGURE 3 | Band structures calculation of the Li_6Si_5-NW in the unit cell. The dashed line indicates the Fermi energy.

COMPUTATIONAL METHODS

In the finite models (clusters), geometry optimizations and frequency calculations were performed at the PBE0 (Adamo and Barone, 1999)/Def2TZVP(Weigend and Ahlrichs, 2005) level with the Gaussian 16 program (M. J. Frisch, G. W. Trucks, H. B. Schlegel et al., 2016).

For the solid-state study, we performed first-principles calculations based on DFT (Sham and Kohn, 1966; Kohn et al., 1996) as implemented in the Vienna Ab Initio Simulation Package (VASP) (Kresse and Furthmüller, 1996). The exchange-correlation energies were calculated at PBE-D3 level (Ernzerhof and Perdew, 1998; Grimme et al., 2010). Plane-wave basis set with a kinetic energy cutoff of 400 eV, and the projector augmented-wave method for the core-valence interaction was employed (Blöchl et al., 1994). The $^{1}_{\infty}[Li_6Si_5]$ NWs were simulated in a large unit cell with volume $(20 \times 20 \times z_0)$ Å^3, considering periodic boundary conditions along the NW direction, where z_0 is the periodicity. Within this supercell, the lateral distance between NW images is set to 15 Å. We use a $(1 \times 1 \times 10)$ Monkhorst-Pack k-point mesh (Monkhorst and Pack, 1976). We also study finite $(Li_6Si_5)_4$ structures in the free space, also inside both an armchair and a zigzag single-walled carbon nanotube (SWCNTs). We consider armchair CNTs with chiral indexes (8,8), (9,9), and (10,10), which have diameters of 10.93, 12.27, and 13.63 Å, and zigzag CNTs with chiral indexes (14,0), (15,0), and (16,0) which have diameters of 11.04, 11.80, and 12.59 Å, respectively. For $(Li_6Si_5)_4$@CNT simulation, $(22 \times 22 \times z_0)$ Å^3 volume was used, where z_0 is the periodicity chosen for the CNTs. All studied structures were allowed to freely relax without any constraint until forces on each atom were smaller than 25 meV/Å. To gain insights on the stability of the NW models in the free space and inside the SWCNTs, we performed Born-Oppenheimer ab initio molecular dynamics (BO-AIMD) simulations within the NVT ensemble at different temperatures, over a total simulation time of 10 ps, considering a time step of 1 fs.

RESULTS AND DISCUSSION

Finite Model Tests to Estimate the Optimal Width of SWNTS

The first question that arises is which is the optimal SWCNT width to favor the $^{1}_{\infty}[Li_6Si_5]$ NW grown? This is a relevant question, considering that the electronic structure of group 1 elements, such as Li, is particularly sensitive to confinement

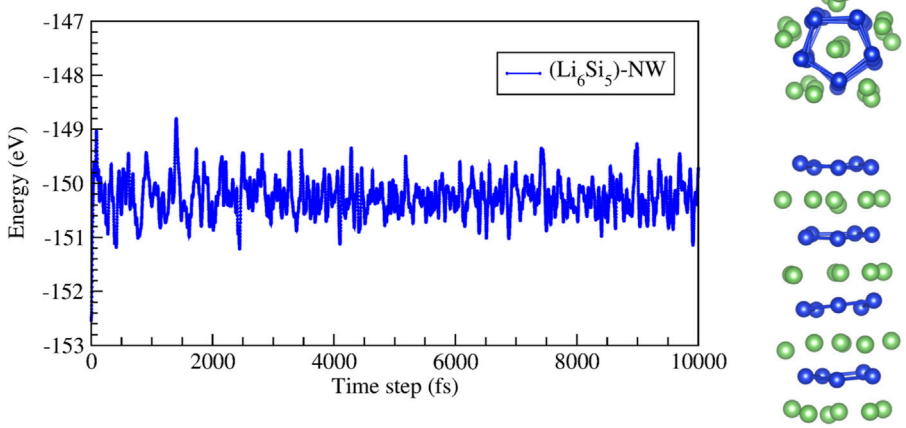

FIGURE 4 | Energy as a function of time for the molecular dynamic simulations at 500 K of the infinite Si_5Li_6 nanowire. The unit cell for this simulation considers four Si_5Li_6 units. The right images show top and side views of a snapshot taken at 10,000 fs

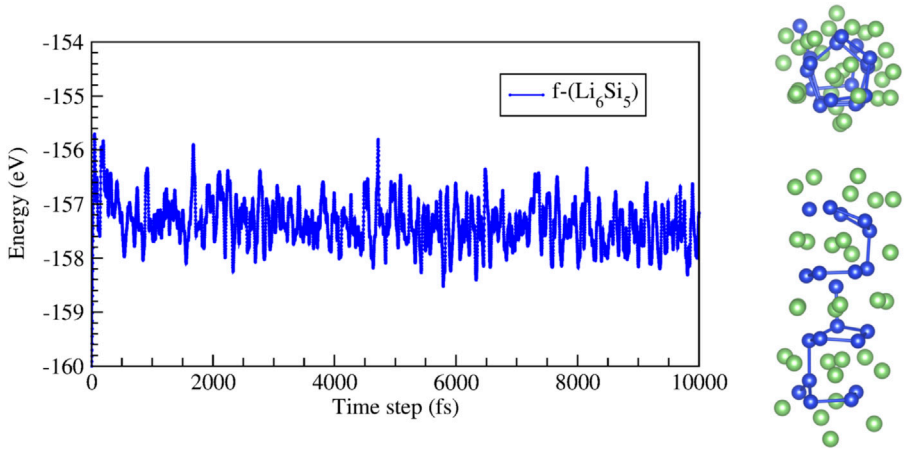

FIGURE 5 | Energy as a function of time for molecular dynamic simulations at 500 K for the finite Li_6Si_5 structure (f-Li_6Si_5). The right images show top and side views of a snapshot taken at 10,000 fs

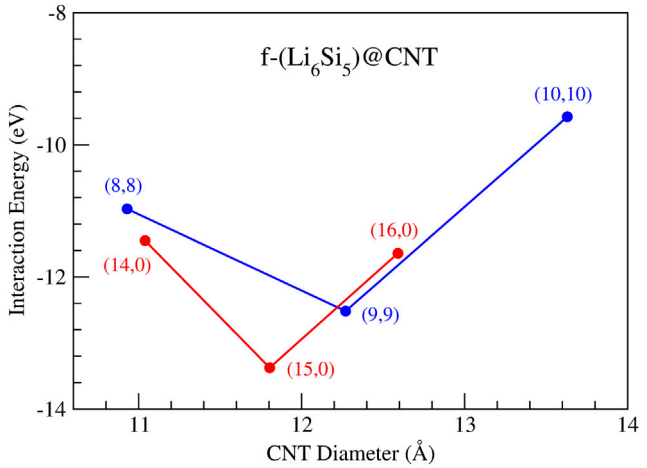

FIGURE 6 | Interaction energy as a function of the nanotube diameters for the finite Li_6Si_5 structures inside armchair CNTs with chiral indexes (8,8), (9,9), and (10,10) and zigzag CNTs with chiral indexes (14,0), (15,0), and (16,0).

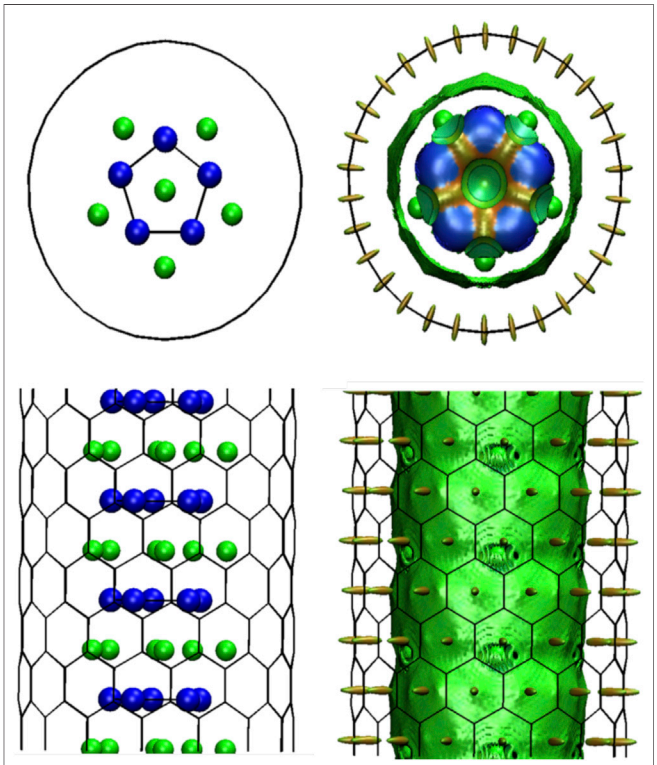

FIGURE 7 | f-Li_6Si_5@NTC optimized structure, for zigzag CNTs with chiral indexes (15,0), with NCI surfaces (s = 0.3, color range: −0.03 to 0.03 a.u.). Geometries and electron density were taken from solid state computations.

(Robles-Navarro et al., 2020). To get an idea of the nanotube widths to be considered in our study, we first performed a finite model analysis. This model consists of [n]cyclacenes (n = 13–20) in their optimal structure (at the PBE0/Def2TZVP level), covering the diameter range from 10.2 to 15.6 Å. Then the $Li_7Si_5^+$ cluster was placed, centering it on emulating the growth pattern towards the nanowire (see **Scheme 1**). We choose the star-shaped D_{5h}-$Li_7Si_5^+$ cluster as a suitable model for projecting the nanowire inside the CNT due to its high symmetry and its analogy in electronic structure with the Li_6Si_5 unit. In this study, we have kept the [n] cyclacene structure rigid, allowing only the optimization of the $Li_7Si_5^+$ structure (at the PBE0/Def2TZVP level).

In the case of small [n]cyclacenes (n = 13–15), $Li_7Si_5^+$ cluster undergoes noticeable changes in the optimization process due to the confinement effects. In contrast, when [n]cyclocenes with n = 16–20 are used, the $Li_7Si_5^+$ cluster maintains its structure at the end of the optimization process, leading to the best interaction energy, [E_{int} = E ($Li_7Si_5^+$at[n]cyclacene)-(E (Li_7Si_5)$^+$E ([n]cyclacene))], with [16] cyclacene (-70.1 kcal mol^{-1} at PBE0/Def2TZVP level). Since this

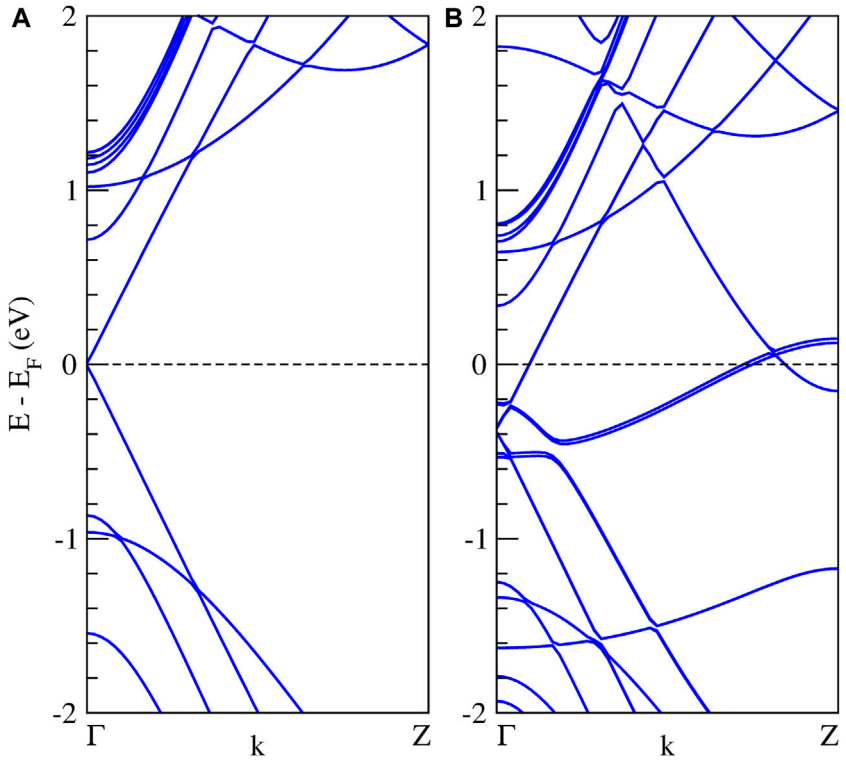

FIGURE 8 | Band structure calculations of the infinite Li_6Si_5-NW inside the zigzag carbon nanotubes, **(A)** the isolated (15,0) CNT, and **(B)** the Li_6Si_5-NW@CNT system. The dashed line indicates the Fermi energy.

analysis is only a reference for estimating the most suitable nanotube diameters to explore in the periodic calculations, we have not included basis set superposition error (BSSE) corrections. The most stable structures, as well as the E_{int}, are shown in **Figure 1**. The structures for the other complexes are shown in **Supplementary Figure S1** and their Cartesian coordinates in **Supplementary Table S1**. These results guided us to use CNTs with diameters in the range of 11–14 Å in next steps of our research.

Insights on the stability of free $^1_\infty[Li_6Si_5]$ NW.

We first studied the stability of periodically repeated Li_6Si_5 units (Li_6Si_5-NW), which are stacked along the *z* direction, forming a one-dimensional structure, as shown in **Figure 2**.

We found a stable structure with an equilibrium distance between Si_5 rings of 4.04 Å which is the periodicity of the Li_6Si_5 unit cell. In the equilibrium geometry, the distance between Li atoms of the border is 3.33 Å while the distance with respect to the center one is 2.83 Å. The Si-Si distance between neighboring atoms is 2.37 Å, very close to the ones in Li_6Si_5 monomer (between 2.30 and 2.35 Å). Our computations of the electronic band structure of the Li_6Si_5-NW in the primitive unit cell suggest a metallic character (see **Figure 3**). Note that the bandgaps of $Li_{12}Si_7$ was reported from conductivity-temperature experimental measurements and found to be 0.6 eV (Nesper et al., 1986b).

The stability of the Li_6Si_5-NW was also verified by BO-AIMD simulations at 300 K and 500K, during a simulation time of 10 ps. The simulation was performed by considering four Li_6Si_5 units in the periodic unit cell, as shown in **Figure 4**. We observe that at 500 K the Si_5Li_6 NW preserves its stability, showing energy fluctuations of around 2 eV. Supporting information contains short movies extracted from the BO-AIMD simulations.

Stability of the Li_6Si_5-NW Inside the CNTs

Next, we studied a finite Li_6Si_5 structure (f-Li_6Si_5) in the free space and encapsulated it inside both armchair and zigzag carbon nanotubes (f-Li_6Si_5@CNT). For the f-Li_6Si_5 structure, we consider four Si_5 rings surrounded by five Li_6 moieties. BO-AIMD simulations provide insights on the stability of the f-Li_6Si_5 system in the free space at 300 K and 500 K. We find that at 300 K, the f-Li_6Si_5 structure preserves its stability. Still, at 500 K, it tends to form Si-Si bonds between adjacent Si rings without losing its one-dimensional array, as shown in **Figure 5**. However, it is important to note that this model does not have the exact stoichiometry of NW because, to maintain symmetry, an extra Li_6 unit group is added, i.e., $[(Li_6)_5(Si_5)_4]$.

To study the f-Li_6Si_5 structure inside the CNTs, we consider three armchair CNTs with chiral indexes of (8,8), (9,9), and (10,10), and three zigzag CNTs with chiral indexes of (14,0), (15,0), and (16,0). With this choice, we seek to find the CNT size that best accommodates the Li_6Si_5-NW inside. Note that we selected these CNTs according to our preliminary findings from the $Li_7Si_5^+$@[n]cyclacene model, suggesting diameters between 12 and 15 Å. The CNTs were simulated with periodic boundary conditions along its axis with a periodicity of z_0 = 30 Å.

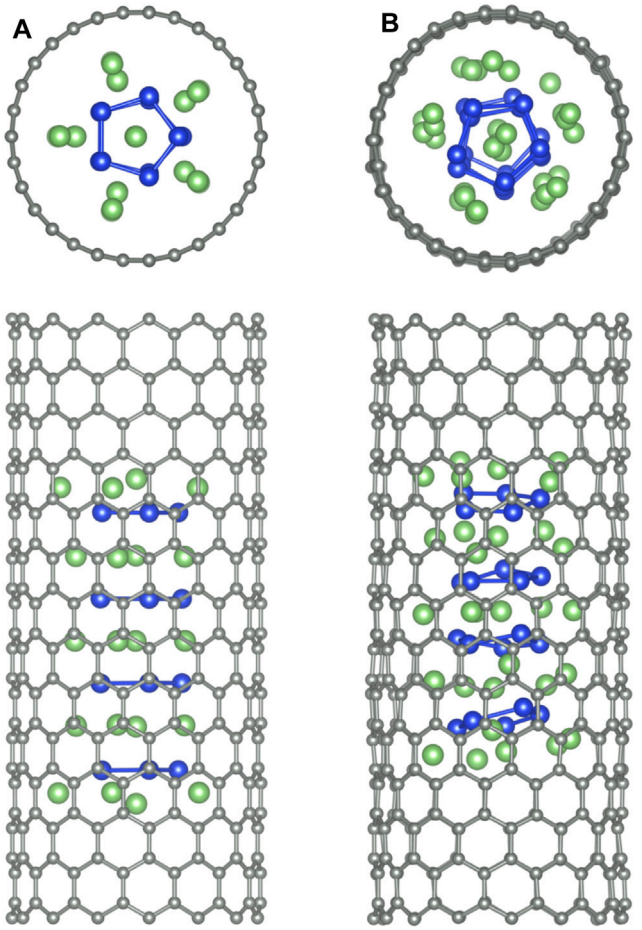

FIGURE 9 | The f-Li_6Si_5 structure inside a zigzag (15,0) CNT. **(A)** Top and side views of the equilibrium geometry at 0 K. **(B)** Top and side views of a snapshot taken at 2000 fs of BO-AIMD simulation at 300 K. The periodicity of the CNT along its axis is z_0 = 30 Å.

The latter allows a vacuum region for the encapsulated f-Li_6Si_5 structure of 14 Å, allowing the atomic movement inside the CNT. Next, we calculate the E_{int} between encapsulated f-Li_6Si_5 and the CNTs by the equation:

$$E_{\text{int}} = E_{tot}\left(f\text{–}Li_6Si_5@CNT\right) - E_{tot}\left(f\text{–}Li_6Si_5\right) - E_{\text{tot}}\left(CNT\right),$$

where $E_{tot}\,(f\text{–}Li_6Si_5)$ and $E_{\text{tot}}\,(\text{CNT})$ are the total energies of the isolated f-Li_6Si_5 and the CNT, respectively, and $E_{\text{tot}}\,(f\text{–}Li_6Si_5@\text{CNT})$ is the total energy of f-Li_6Si_5 unit inside the CNT. Our results for the E_{int} are shown in **Figure 6**. The armchair (9,9) and the zigzag (15,0) CNTs of 12.3 and 11.8 Å in diameter, respectively, exhibit the more stabilizing E_{int}, being the best candidates to accommodate the f-Li_6Si_5 inside. In addition, the f-Li_6Si_5 is better stabilized inside the zigzag (15,0) CNT than inside the armchair (9,9) CNT by 0.9 eV. Noteworthy, the larger-diameter CNTs are energetically less favorable to encapsulate the f-Li_6Si_5, as shown in **Figure 6**, in agreement with the $Li_7Si_5^+$@[n] cyclacene model. This behavior is presumable due to the van der Waals (vdW) interaction between the f-Li_6Si_5 and the CNT internal walls, stabilizing the system. The non-covalent interaction index (NCI) plots confirm the non-covalent character of f-Li_6Si_5 with the CNT [f-Li_6Si_5 inside the zigzag (15,0) CNT]. In the NCI method (Johnson et al., 2010; Contreras-García et al., 2011), an isosurface of the reduced density gradient (s) is colored with the density times the sign of the second eigenvalue of the electron density Hessian matrix, λ_2, to distinguish between attractive and repulsive interactions. The following color code is used: blue for attractive such as hydrogen bonds, green for very weak interactions such as vdW and red for steric repulsion. **Figure 7** depicts the second one (vdW) between f-Li_6Si_5 and the walls of the CNT.

We also calculate the band structure of the Li_6Si_5-NW inside the zigzag (15,0) CNT. It is important to note that the unit cells of the Li_6Si_5-NW and the CNT have a mismatch of 5.7%, which means that the Li_6Si_5-NW is not in its equilibrium geometry in the Li_6Si_5-NW@CNT unit cell, where the distance between the Si_5 rings increases by 0.23 Å. However, this mismatch is relatively small and should not affect the electronic properties of the system. For the isolated CNT we find a small bandgap of 0.02 eV as shown in **Figure 8A**, which is in good agreement with the measured value of 0.029 ± 0.004 eV (Ouyang et al., 2001). Whereas the Li_6Si_5-NW@CNT system exhibits metallic properties as shown **Figure 8B**, suggesting that the Li_6Si_5-NW would preserve its electronic properties inside the CNT as can be compared with **Figure 3**.

Finally, we study the stability of the f-Li_6Si_5 structure inside both zigzag (15,0) and armchair (9,9) CNTs by performing BO-AIMD simulations. **Figure 9A** shows the equilibrium geometry of the f-Si_5Li_6 structure inside the (15,0) CNT. We find that the structure remains almost unchanged with respect to f-Si_5Li_6 in the free space, showing that the CNT would have a small influence in the Li_6Si_5 NW stability. We only note a small displacement of the Li ions at the extreme of the f-Li_6Si_5 structure which move toward the CNT wall. The integrity of the f-Li_6Si_5 structure inside the (15,0) and (9,9) CNTs was investigated by BO-AIMD simulations at 300 K. We find that the f-Si_5Li_6 structure preserves its stability where the Li ions move around the Si_5 ring without detaching. Similar results are found for the f-Li_6Si_5 structure inside the armchair (9,9) CNT, indicating that the formation and stability of the Li_6Si_5 NW inside the CNTs is independent of its chirality. This result suggests that Li_6 Si_5-NW are likely to form inside CNTs in a compact form, which would allow efficient storage of Li ions into CNTs mediated by Si_5 rings. **Supplementary Figure S2** shows the variation of the total energy for the BO-AIMD simulation of f-Li_6Si_5 inside the (15,0) and (9,9) CNTs at 300 K. We observe energy fluctuation of around 5 eV in both CNTs, preserving the stability of the f-Li_6Si_5 structure.

CONCLUSION

Using periodic DFT calculations and Born-Oppenheimer *ab initio* molecular dynamic simulations, we have shown that Li_6Si_5 units can be stacked one above the other, forming a one-dimensional structure linked together by Coulomb interactions. This study complements previous findings, where we

demonstrated that Li_6Si_5, $(Li_6Si_5)_2$, and $(Li_6Si_5)_3$ lowest energy structures contain one, two, and three Si_5^{6-} aromatic rings stabilized by Li^+ counterions. Additionally, the $^1_\infty[Li_6Si_5]$ nanowire was identified in the Zintl $Li_{12}Si_7$ compound but coexisting with Y-shaped Si_4 moieties. In this case, we support the stability of the isolated Si-Li-nanowire—additionally, the relaxed structure (at room temperature) exhibits metallic characteristics.

We also found that finite $(Li_6Si_5)_4$ systems are stable inside both armchair and zigzag carbon nanotubes of around 12 Å in diameter, preserving its stability at room temperature, supporting the viable formation of Li_6Si_5-NW inside the CNTs. Interestingly, the Li_6Si_5-NW@CNTs hybrid nanocomposite maintains the metallic character. Finally, in the Li_6Si_5-NW, the Li_6Si_5 units are connected by strong electrostatic interactions (Si_5^{6-} aromatic pentagons intercalated with the Li_6^{6+} moiety) in agreement with the Zintl ion concept. In the [Li_6Si_5-NW]@CNTs, NCI predicts that Li_6Si_5-NW interacts with the CNT walls by van der Waals interactions Frisch et al., 2016.

DATA AVAILABILITY STATEMENT

The original contributions presented in the study are included in the article/**Supplementary Material**, further inquiries can be directed to the corresponding author.

AUTHOR CONTRIBUTIONS

All authors listed have made a substantial, direct, and intellectual contribution to the work and approved it for publication.

FUNDING

We thank the financial support of National Agency for Research and Development (ANID) through ECOS170045, FONDECYT projects 1211128 (W.T.), 1181121 (C.C.), and 1170480 (W.O.). FONDECYT Postdoctorado 3180119 (R.P.-R.), ANID/PIA ACT192144 (O.Y.). Powered@NLHPC: This research was partially supported by the supercomputing infrastructure of the NLHPC (ECM-02) of the Universidad de Chile. Computational resources for periodic DFT calculations and BO-AIMD simulations were provided by Fenix HCP of the Universidad Andres Bello. C.C. acknowledges Center for the Development of Nanoscience and Nanotechnology CEDENNA AFB180001.

SUPPLEMENTARY MATERIAL

The Supplementary Material for this article can be found online at: https://www.frontiersin.org/articles/10.3389/fchem.2021.767421/full#supplementary-material

REFERENCES

Adamo, C., and Barone, V. (1999). Toward Reliable Density Functional Methods without Adjustable Parameters: The PBE0 Model. *J. Chem. Phys.* 110, 6158–6170. doi:10.1063/1.478522

Alba-Simionesco, C., Coasne, B., Dosseh, G., Dudziak, G., Gubbins, K. E., Radhakrishnan, R., et al. (2006). Effects of Confinement on Freezing and Melting. *J. Phys. Condens. Matter* 18, R15–R68. doi:10.1088/0953-8984/18/6/r01

Blöchl, P. E., Jepsen, O., and Andersen, O. K. (1994). Improved Tetrahedron Method for Brillouin-Zone Integrations. *Phys. Rev. B* 49, 16223–16233. doi:10.1103/physrevb.49.16223

Chakraborty, I., and Pradeep, T. (2017). Atomically Precise Clusters of noble Metals: Emerging Link between Atoms and Nanoparticles. *Chem. Rev.* 117, 8208–8271. doi:10.1021/acs.chemrev.6b00769

Chevrier, V. L., Zwanziger, J. W., and Dahn, J. R. (2010). First Principles Study of Li-Si Crystalline Phases: Charge Transfer, Electronic Structure, and Lattice Vibrations. *J. Alloys Compd.* 496, 25–36. doi:10.1016/j.jallcom.2010.01.142

Claridge, S. A., Castleman, A. W., Jr, Khanna, S. N., Murray, C. B., Sen, A., and Weiss, P. S. (2009). Cluster-assembled Materials. *ACS Nano* 3, 244–255. doi:10.1021/nn800820e

Contreras, M., Osorio, E., Ferraro, F., Puga, G., Donald, K. J., Harrison, J. G., et al. (2013). Isomerization Energy Decomposition Analysis for Highly Ionic Systems: Case Study of Starlike E5Li7+Clusters. *Chem. Eur. J.* 19, 2305–2310. doi:10.1002/chem.201203329

Contreras-García, J., Johnson, E. R., Keinan, S., Chaudret, R., Piquemal, J.-P., Beratan, D. N., et al. (2011). NCIPLOT: A Program for Plotting Noncovalent Interaction Regions. *J. Chem. Theor. Comput.* 7, 625–632. doi:10.1021/ct100641a

Derouane, E. G. (1998). Zeolites as Solid solvents1Paper Presented at the International Symposium `Organic Chemistry and Catalysis' on the Occasion of the 65th Birthday of Prof. H. Van Bekkum, Delft, Netherlands, 2-3 October 1997.1. *J. Mol. Catal. A: Chem.* 134, 29–45. doi:10.1016/s1381-1169(98)00021-1

Doud, E. A., Voevodin, A., Hochuli, T. J., Champsaur, A. M., Nuckolls, C., and Roy, X. (2020). Superatoms in Materials Science. *Nat. Rev. Mater.* 5, 371–387. doi:10.1038/s41578-019-0175-3

Ernzerhof, M., and Perdew, J. P. (1998). Generalized Gradient Approximation to the Angle- and System-Averaged Exchange Hole. *J. Chem. Phys.* 109, 3313–3320. doi:10.1063/1.476928

Frisch, M. J., Trucks, G. W., Schlegel, H. B., Scalmani, G., Robb, M. A., Cheeseman, J. R., et al. (2016). *Gaussian 16, Inc.Revis. B.01*. (Wallingford CT: Gaussian).

Gao, B., Sinha, S., Fleming, L., and Zhou, O. (2001). Alloy Formation in Nanostructured Silicon. *Adv. Mater.* 13, 816–819. doi:10.1002/1521-4095(200106)13:11<816:aid-adma816>3.0.co;2-p

Green, M. H. (1998). The Opening and Filling of Single Walled Carbon Nanotubes (SWTs). *Chem. Commun.* (3), 347–348. doi:10.1039/a707632k

Grimme, S., Antony, J., Ehrlich, S., and Krieg, H. (2010). A Consistent and Accurate Ab Initio Parametrization of Density Functional Dispersion Correction (DFT-D) for the 94 Elements H-Pu. *J. Chem. Phys.* 132, 154104. doi:10.1063/1.3382344

Hückel, E. (1931a). Quanstentheoretische Beitrage Zum Benzolproblem. *Z. Physik* 72, 310–337. doi:10.1007/BF01341953

Hückel, E. (1931b). Quantentheoretische Beitrage Zum Benzolproblem. *Z. Physik* 70, 204–286. doi:10.1007/BF01339530

Hückel, E. (1930). Zur Quantentheorie der Doppelbindung. *Z. Physik* 60, 423–456. doi:10.1007/BF01341254

Ivanov, A. S., Kar, T., and Boldyrev, A. I. (2016). Nanoscale Stabilization of Zintl Compounds: 1D Ionic Li-P Double helix Confined inside a Carbon Nanotube. *Nanoscale* 8, 3454–3460. doi:10.1039/c5nr07713c

Ivanov, A. S., Morris, A. J., Bozhenko, K. V., Pickard, C. J., and Boldyrev, A. I. (2012). Inorganic Double-Helix Structures of Unusually Simple Lithium-Phosphorus Species. *Angew. Chem. Int. Ed.* 51, 8330–8333. doi:10.1002/anie.201201843

Jena, P., and Khanna, S. N. (1996). Physics of Cluster Assembled Materials. *Mater. Sci. Eng. A* 217-218, 218–222. doi:10.1016/s0921-5093(96)10361-0

Jena, P. K., Khanna, S. N., and Rao, B. K. (1996). Stability and Electronic Structure of Cluster Assembled Materials. *Msf* 232, 1–26. doi:10.4028/www.scientific.net/msf.232.1

Jena, P., and Sun, Q. (2018). Super Atomic Clusters: Design Rules and Potential for Building Blocks of Materials. *Chem. Rev.* 118, 5755–5870. doi:10.1021/acs.chemrev.7b00524

Johnson, E. R., Keinan, S., Mori-Sánchez, P., Contreras-García, J., Cohen, A. J., and Yang, W. (2010). Revealing Noncovalent Interactions. *J. Am. Chem. Soc.* 132, 6498–6506. doi:10.1021/ja100936w

Ke, J., Su, W., Howdle, S. M., George, M. W., Cook, D., Perdjon-Abel, M., et al. (2009). Electrodeposition of Metals from Supercritical Fluids. *Proc. Natl. Acad. Sci.* 106, 14768–14772. doi:10.1073/pnas.0901986106

Khanna, S. N., and Jena, P. (1992). Assembling Crystals from Clusters. *Phys. Rev. Lett.* 69, 1664–1667. doi:10.1103/physrevlett.69.1664

Khanna, S. N., and Jena, P. (1995). Atomic Clusters: Building Blocks for a Class of Solids. *Phys. Rev. B* 51, 13705–13716. doi:10.1103/physrevb.51.13705

Kohn, W., Becke, A. D., and Parr, R. G. (1996). Density Functional Theory of Electronic Structure. *J. Phys. Chem.* 100, 12974–12980. doi:10.1021/jp960669l

Köster, T. K.-J., Salager, E., Morris, A. J., Key, B., Seznec, V., Morcrette, M., et al. (2011). Resolving the Different Silicon Clusters in Li12Si7 by 29Si and 6,7Li Solid-State NMR Spectroscopy. *Angew. Chem. Int. Ed.* 50, 12591–12594. doi:10.1002/anie.201105998

Kresse, G., and Furthmüller, J. (1996). Efficient Iterative Schemes Forab Initiototal-Energy Calculations Using a Plane-Wave Basis Set. *Phys. Rev. B* 54, 11169–11186. doi:10.1103/physrevb.54.11169

Kuhn, A., Sreeraj, P., Pöttgen, R., Wiemhöfer, H.-D., Wilkening, M., and Heitjans, P. (2011a). Li Ion Diffusion in the Anode Material Li12Si7: Ultrafast quasi-1D Diffusion and Two Distinct Fast 3D Jump Processes Separately Revealed by 7Li NMR Relaxometry. *J. Am. Chem. Soc.* 133, 11018–11021. doi:10.1021/ja2020108

Kuhn, A., Sreeraj, P., Pöttgen, R., Wiemhöfer, H.-D., Wilkening, M., and Heitjans, P. (2011b). Li NMR Spectroscopy on Crystalline Li12Si7: Experimental Evidence for the Aromaticity of the Planar Cyclopentadienyl-Analogous Si56− Rings. *Angew. Chem. Int. Ed.* 50, 12099–12102. doi:10.1002/anie.201105081

Li, J., Christensen, L., Obrovac, M. N., Hewitt, K. C., and Dahn, J. R. (2008). Effect of Heat Treatment on Si Electrodes Using Polyvinylidene Fluoride Binder. *J. Electrochem. Soc.* 155, A234. doi:10.1149/1.2830545

Li, J., Lewis, R. B., and Dahn, J. R. (2006). Sodium Carboxymethyl Cellulose: A Potential Binder for Si Negative Electrodes for Li-Ion Batteries. *Electrochem. Solid State. Lett.* 10, A17. doi:10.1149/1.2398725

Li, J., Smith, A., Sanderson, R. J., Hatchard, T. D., Dunlap, R. A., and Dahn, J. R. (2009). *In Situ* [sup 119]Sn Mössbauer Effect Study of the Reaction of Lithium with Si Using a Sn Probe. *J. Electrochem. Soc.* 156, A283. doi:10.1149/1.3073879

Lu, G., Li, S., Guo, Z., Farha, O. K., Hauser, B. G., Qi, X., et al. (2012). Imparting Functionality to a Metal-Organic Framework Material by Controlled Nanoparticle Encapsulation. *Nat. Chem* 4, 310–316. doi:10.1038/nchem.1272

Manrique-de-la-Cuba, M. F., Leyva-Parra, L., Inostroza, D., Gomez, B., Vásquez-Espinal, A., Garza, J., et al. (2021). Li8Si8, Li10Si9, and Li12Si10: Assemblies of Lithium-Silicon Aromatic Units. *ChemPhysChem* 22 (10), 906–910. doi:10.1002/cphc.202001051

Monkhorst, H. J., and Pack, J. D. (1976). Special Points for Brillouin-Zone Integrations. *Phys. Rev. B* 13, 5188–5192. doi:10.1103/physrevb.13.5188

Nesper, R., Curda, J., and Von Schnering, H. G. (1986a). Li8MgSi6, a Novel Zintl Compound Containing Quasi-Aromatic Si5 Rings. *J. Solid State. Chem.* 62, 199–206. doi:10.1016/0022-4596(86)90232-x

Nesper, R. (1990). Structure and Chemical Bonding in Zintl-Phases Containing Lithium. *Prog. Solid State. Chem.* 20, 1–45. doi:10.1016/0079-6786(90)90006-2

Nesper, R., von Schnering, H. G., and Curda, J. (1986b). Li12Si7, eine Verbindung mit trigonal-planaren Si4-Clustern und isometrischen Si5-Ringen. *Chem. Ber.* 119, 3576–3590. doi:10.1002/cber.19861191207

Obrovac, M. N., Christensen, L., Le, D. B., and Dahn, J. R. (2007). Alloy Design for Lithium-Ion Battery Anodes. *J. Electrochem. Soc.* 154, A849. doi:10.1149/1.2752985

Ouyang, M., Huang, J.-L., Cheung, C. L., and Lieber, C. M. (2001). Energy Gaps in "Metallic" Single-Walled Carbon Nanotubes. *Science* 292, 702–705. doi:10.1126/science.1058853

Perez-Peralta, N., Contreras, M., Tiznado, W., Stewart, J., Donald, K. J., and Merino, G. (2011). Stabilizing Carbon-Lithium Stars. *Phys. Chem. Chem. Phys.* 13, 12975–12980. doi:10.1039/C1CP21061K

Pinkard, A., Champsaur, A. M., and Roy, X. (2018). Molecular Clusters: Nanoscale Building Blocks for Solid-State Materials. *Acc. Chem. Res.* 51, 919–929. doi:10.1021/acs.accounts.8b00016

Robles-Navarro, A., Fuentealba, P., Muñoz, F., and Cardenas, C. (2020). Electronic Structure of First and Second Row Atoms under Harmonic Confinement. *Int. J. Quan. Chem.* 120, e26132.

Ryu, J. H., Kim, J. W., Sung, Y.-E., and Oh, S. M. (2004). Failure Modes of Silicon Powder Negative Electrode in Lithium Secondary Batteries. *Electrochem. Solid-state Lett.* 7, A306. doi:10.1149/1.1792242

Sham, L. J., and Kohn, W. (1966). One-particle Properties of an Inhomogeneous Interacting Electron Gas. *Phys. Rev.* 145, 561–567. doi:10.1103/physrev.145.561

Shin, H.-J., Hwang, J.-Y., Kwon, H. J., Kwak, W.-J., Kim, S.-O., Kim, H.-S., et al. (2020). Sustainable Encapsulation Strategy of Silicon Nanoparticles in Microcarbon Sphere for High-Performance Lithium-Ion Battery Anode. *ACS Sustain. Chem. Eng.* 8, 14150–14158. doi:10.1021/acssuschemeng.0c04828

Sloan, J., Kirkland, A. I., Hutchison, J. L., and Green, M. L. H. (2002). Integral Atomic Layer Architectures of 1D Crystals Inserted into Single Walled Carbon Nanotubes. *Chem. Commun.* 2010, 1319–1332. doi:10.1039/b200537a

Song, T., Hu, L., and Paik, U. (2014). One-dimensional Silicon Nanostructures for Li Ion Batteries. *J. Phys. Chem. Lett.* 5, 720–731. doi:10.1021/jz4027979

Spencer, J. H., Nesbitt, J. M., Trewhitt, H., Kashtiban, R. J., Bell, G., Ivanov, V. G., et al. (2014). Raman Spectroscopy of Optical Transitions and Vibrational Energies of ~1 Nm HgTe Extreme Nanowires within Single Walled Carbon Nanotubes. *ACS Nano* 8, 9044–9052. doi:10.1021/nn5023632

Tiznado, W., Perez-Peralta, N., Islas, R., Toro-Labbe, A., Ugalde, J. M., and Merino, G. (2009). Designing 3-D Molecular Stars. *J. Am. Chem. Soc.* 131, 9426–9431. doi:10.1021/ja903694d

Vásquez-Espinal, A., Palacio-Rodríguez, K., Ravell, E., Orozco-Ic, M., Barroso, J., Pan, S., et al. (2018). E5M7+ (E= C–Pb, M= Li–Cs): A Source of Viable Star-Shaped Clusters. *Chem. Asian J.* 13, 1751–1755. doi:10.1002/asia.201800654

Weigend, F., and Ahlrichs, R. (2005). Balanced Basis Sets of Split Valence, Triple Zeta Valence and Quadruple Zeta Valence Quality for H to Rn: Design and Assessment of Accuracy. *Phys. Chem. Chem. Phys.* 7, 3297–3305. doi:10.1039/b508541a

Wen, C. J., and Huggins, R. A. (1981). Chemical Diffusion in Intermediate Phases in the Lithium-Silicon System. *J. Solid State. Chem.* 37, 271–278. doi:10.1016/0022-4596(81)90487-4

Yañez, O., Báez-Grez, R., Inostroza, D., Rabanal-León, W. A., Pino-Rios, R., Garza, J., et al. (2019a). AUTOMATON: a Program that Combines a Probabilistic Cellular Automata and a Genetic Algorithm for Global Minimum Search of Clusters and Molecules. *J. Chem. Theor. Comput.* 15, 1463–1475. doi:10.1021/acs.jctc.8b00772

Yañez, O., Garcia, V., Garza, J., Orellana, W., Vásquez-Espinal, A., and Tiznado, W. (2019b). (Li 6 Si 5) 2-5 : The Smallest Cluster-Assembled Materials Based on Aromatic Si 5 6− Rings. *Chem. Eur. J.* 25, 2467–2471. doi:10.1002/chem.201805677

Yañez, O., Inostroza, D., Usuga-Acevedo, B., Vásquez-Espinal, A., Pino-Rios, R., Tabilo-Sepulveda, M., et al. (2020). Evaluation of Restricted Probabilistic Cellular Automata on the Exploration of the Potential Energy Surface of Be6B11−. *Theor. Chem. Acc.* 139, 41. doi:10.1007/s00214-020-2548-5

Zhao, L., Grande-Aztatzi, R., Foroutan-Nejad, C., Ugalde, J. M., and Frenking, G. (2017). Aromaticity, the Hückel 4 N+2 Rule and Magnetic Current. *ChemistrySelect* 2, 863–870. doi:10.1002/slct.201602080

Zheng, X.-Y., Xie, J., Kong, X.-J., Long, L.-S., and Zheng, L.-S. (2019). Recent Advances in the Assembly of High-Nuclearity Lanthanide Clusters. *Coord. Chem. Rev.* 378, 222–236. doi:10.1016/j.ccr.2017.10.023

Conflict of Interest: The authors declare that the research was conducted in the absence of any commercial or financial relationships that could be construed as a potential conflict of interest.

Publisher's Note: All claims expressed in this article are solely those of the authors and do not necessarily represent those of their affiliated organizations, or those of the publisher, the editors and the reviewers. Any product that may be evaluated in this article, or claim that may be made by its manufacturer, is not guaranteed or endorsed by the publisher.

Advantages of publishing in Frontiers

OPEN ACCESS
Articles are free to read for greatest visibility and readership

FAST PUBLICATION
Around 90 days from submission to decision

HIGH QUALITY PEER-REVIEW
Rigorous, collaborative, and constructive peer-review

TRANSPARENT PEER-REVIEW
Editors and reviewers acknowledged by name on published articles

Frontiers
Avenue du Tribunal-Fédéral 34
1005 Lausanne | Switzerland

Visit us: www.frontiersin.org
Contact us: frontiersin.org/about/contact

REPRODUCIBILITY OF RESEARCH
Support open data and methods to enhance research reproducibility

DIGITAL PUBLISHING
Articles designed for optimal readership across devices

FOLLOW US
@frontiersin

IMPACT METRICS
Advanced article metrics track visibility across digital media

EXTENSIVE PROMOTION
Marketing and promotion of impactful research

LOOP RESEARCH NETWORK
Our network increases your article's readership